APPLICATION OF POLYOXOMETALATES AS EFFICIENT AND GREEN CATALYST FOR CATALYTIC UPGRADING OF CELLULOSIC BIOMASS

Thesis

Submitted in partial fulfillment of requirements for the degree of

DOCTOR OF PHILOSOPHY

by

RITESH TIWARI

Reg. No. 165081CY16F05

DEPARTMENT OF CHEMISTRY

NATIONAL INSTITUTE OF TECHNOLOGY KARNATAKA,

SURATHKAL, MANGALORE-575025

June, 2020

DECLARATION

By the Ph.D. Research Scholar

I hereby *declare* that the Research Thesis entitled **"Application of Polyoxometalates as efficient and green catalyst for catalytic upgrading of cellulosic biomass"** which is being submitted to the **National Institute of Technology Karnataka, Surathkal** in partial fulfillment of the requirements for the award of the degree of **Doctor of Philosophy** in Chemistry is a *bonafide report of the research work carried out by me*. The material contained in the Research Thesis has not been submitted to any University or Institution for the award of any degree.

RITESH TIWARI
Reg. No. 165081CY16F05
Department of Chemistry

Place: Lucknow, Uttar Pradesh

Date: 05-06-2020

CERTIFICATE

This is to *certify* that the Research Thesis **"Application of Polyoxometalates as efficient and green catalyst for catalytic upgrading of cellulosic biomass"** submitted by **Mr. Ritesh Tiwari (Reg. No. 165081CY16F05)** as a record of research work carried out by him, *is accepted as the Research Thesis submission* in partial fulfillment of the requirements for the award of degree of **Doctor of Philosophy**.

Sib Sankar Mal

Dr. Sib Sankar Mal
Research Guide
Date: 08/06/2020

Saikat Dutta

Dr. Saikat Dutta
Research Co Guide
Date: 08/06/2020

08/06/2020

Chairman - DPRC
Date:

Dr. ARUN M. ISLOOR
Professor & Head
DEPARTMENT OF CHEMISTRY
National Institute of Technology Karnataka
Surathkal, Srinivasnagar
MANGALORE - 575 025, D.K., INDIA

I dedicate this doctoral thesis to my beloved parents and family for his unconditional support and encouragement to pursue my interest in science.

ACKNOWLEDGMENT

"When faced with a challenge, look for a way, not a way out."

—David Weatherford

It has been a great experience in pursuing my doctoral degree at the National Institute of Technology Karnataka (NITK), Surathakal with proficient and unique individuals who have helped me to achieve what I aimed. I would like to express my most profound appreciation for the help of the kind people around me, to only some of whom it is possible to give a particular mention here.

I wholeheartedly express my deep sense of gratitude to my honored research supervisors Dr. Sib Sankar Mal (Guide) and Dr. Saikat Dutta (Co Guide), for their supportive guidance and above all their belief in me. Throughout my doctoral work, they have been a constant source of encouragement and fruitful advice. I thank them for having instilled in me the work ethic and determination to achieve this goal. Be it success or failure, they had shared my feelings. Their unstrained support throughout the course of my research work has made my thesis appear in the present form. I feel privileged and fortunate for being his student.

I sincerely thank Prof. K. Umamaheshwar Rao, Director, NITK, for providing the necessary facilities to carry out this research work. I express my earnest thanks to the RPAC members, Prof. Ampar Chitharanjan Hegde, Chemistry Department, and Dr. Saumen Mandal, Metallurgical and Materials Engineering Department, NITK for insightful comments and constructive criticism towards the improvement of research quality.

I owe a very important debt to Dr. Sanjay Kumar for his profound encouragement and showing me the right direction at the most crucial moment, which seems to be difficult to forget throughout my life.

I am also thankful to Prof. A. V. Adhikari, Prof. A.N. Shetty, Prof. B. R. Bhat, Prof. A.M. Isloor, Prof. D. K. Bhat, Dr. D. R. Trivedi, Dr. Udaya Kumar Dalimba, Dr. P. B. Beneesh, and Dr. Debashree Chakraborty, Department of Chemistry for their constant support and encouragement.

I am grateful to the non-teaching staff, namely, Mrs. Shamila, Mrs. Kasturi, Mrs. Deepa, Mrs. Sharmila, Mr. Pradeep, Mrs. Prashanth, Mr. Harish, and Mr. Santosh for their timely cooperation with laboratory and analysis work.

I am thankful to MIT Manipal, Central Instrumentation Facility unit, for the timely analytical support.

I sincerely thank Dr. Anukul Jana, Department of Chemistry, TIFR Hyderabad, for collecting the NMR data.

I am grateful to NITK for the research infrastructure and fellowship that allowed me to work at a smoother pace.

I would like to thank all my colleagues Sharath B. O., Anjana A.V., Navya Bhat, Nivedha Vinod, and Harshitha Anchan, for creating an enthusiastic and pleasant work atmosphere.

I extended my sincere thanks to all the research scholars of the Chemistry Department for their constant help and supports.

Most of all, I am indebted to my parents and siblings for their endless support and encouragement throughout this work and my whole life. You have been a constant source of strength and determination, and you have brought a great deal of happiness to my life. I wish to express my profound gratitude and sincerest thanks to my wife, Mrs. Manju Tiwari, and daughter, Avanika Tiwari, for giving me inspiration and for being with me through the difficult times. Finally, I thank God almighty for strengthening me during hardships to successfully complete this endeavor.

Thank you.

Ritesh Tiwari

ABSTRACT

In recent years, the research on the sustainable production of energy, transportation fuels, and materials has been incentivized. Non-food and preferably waste biomass has been identified as a commercially-feasible renewable alternative to fossilized carbons for producing fuels and chemicals. The chemocatalytic value addition of biomass, where the oxygen-rich biopolymers are selectively deconstructed into functionally-rich small organic molecules, is of particular interest. A new generation of robust, inexpensive, and environment-friendly catalysts are crucial for the chemocatalytic route.

Over the past years, heteropolyacids (HPAs) are increasingly being used as a catalyst in the chemistry of renewables and biomass value addition. HPAs have been used in the hydrolysis and dehydration of pentose and hexose sugars in biomass into furfural and 5-(hydroxymethyl)furfural (HMF), respectively. Furfural, levulinic acid, and HMF act as renewable chemical building blocks that can be converted into commodity chemicals and materials via chemical or catalytic transformations.

The proposed work is intended to explore the efficiency of various homogenous and heterogeneous HPA catalysts for the catalytic upgrading of biomass-derived chemical intermediates into value-added chemicals. HPA-based homogeneous and heterogeneous catalysts were used for the acetalization, esterification, and Baeyer-Villiger oxidation reactions of various biomass-derived chemical intermediates. The reaction conditions were optimized on various parameters such as temperature, duration, loading of reactant, and loading of catalyst. The cyclic acetals of biomass-derived furfural were prepared in high isolated yields in refluxing benzene in the presence of the phosphotungstic acid (PTA) catalyst. The PTA catalyst was successfully recovered and reused several times without significant loss in mass or activity. The esterification of saturated and unsaturated free fatty acids such as oleic acid and stearic acid were conducted in the presence of PTA catalyst as an efficient and recyclable catalyst. 2-Furanone was prepared by the selective oxidation of furfural using hydrogen peroxide as an inexpensive oxidant and PTA supported on ammonium zeolites as the catalyst. A scalable and high yielding preparation of alkyl benzoates and alkyl 2-furoates has also been reported.

Keywords: Acetalization, Biodiesel, Biomass, Catalysis, Esterification, Heteropoly acids, Renewable synthesis

CONTENTS

LIST OF FIGURES i

LIST OF SCHEMES vii

LIST OF TABLES viii

NOMENCLATURE ix

LIST OF SYMBOLS AND UNITS x

CHAPTER 1: INTRODUCTION

1.1 GENERAL INTRODUCTION 1

1.2 POLYOXOMETALATES 2

1.3 CLASSIFICATION OF HETEROPOLYOXOMETALATES (HPOMs) 3

1.3.1 Keggin heteropoly ion 3

1.4 PRIMARY, SECONDARY, AND TERTIARY STRUCTURES OF HETEROPOLYACIDS 5

1.5 POSITION OF PROTONS IN KEGGIN HETEROPOLYACIDS 6

1.6 ACIDIC PROPERTIES OF HETEROPOLYACIDS 7

1.7 CATALYTIC APPLICATIONS OF HETEROPOLYACIDS 8

1.8 PRESENT SCENARIO AND MOTIVATION OF WORK 9

1.8.1 Production of Chemicals and Fuels from Biomass 9

1.9 LITERATURE SURVEY 10

1.10 SCOPE AND OBJECTIVES OF THE PRESENT WORK 19

CHAPTER 2: A SCALABLE AND HIGH-YIELDING SYNTHESIS OF 2-(2-FURYL)-1,3-DIOXOLANE FROM BIOMASS-DERIVED FURFURAL AND ETHYLENE GLYCOL USING HETEROPOLYACIDS AS GREEN CATALYST

2.1 GENERAL INTRODUCTION 23

2.2 EXPERIMENTAL SECTION 25

2.2.1 Materials 25

2.2.2 Reaction procedure 26

2.2.3 Instrument used for the characterization of compounds 26

2.2.3.1 FTIR and NMR (^{1}H and ^{13}C) characterization of 2-(furan-2-yl)-1,3-dioxolane 2a 26

2.3 RESULTS AND DISCUSSIONS 29

2.4 CONCLUSION 34

CHAPTER 3: SOLVENT-FREE AND SCALABLE PREPARATION OF ALKYL STEARATES AND ALKYL OLEATES FROM FREE FATTY ACIDS USING HETEROPOLYACIDS AS EFFICIENT AND RECYCLABLE CATALYST

3.1 INTRODUCTION 35

3.2 EXPERIMENTAL SECTION 38

3.2.1 Materials 38

3.2.2 Catalytic reactions (A): Esterification of stearic acids over HPA catalysts 38

3.2.3 Instrument used for the characterization of compounds 39

3.2.3.1 FTIR and NMR (^{1}H and ^{13}C) characterization of methyl stearate 3a 39

3.2.3.2 FTIR and NMR (^{1}H and ^{13}C) characterization of ethyl stearate 3b 42

3.2.3.3 FTIR and NMR (^{1}H and ^{13}C) characterization of propyl stearate 3c 44

3.2.3.4 FTIR and NMR (^{1}H and ^{13}C) characterization of butyl stearate 3d 46

3.2.4 Catalytic reactions (B): Esterification of oleic acid over HPAs catalysts 48
3.2.5 Instrument used for the characterization of compounds 48
3.2.5.1 FTIR and NMR (^{1}H and ^{13}C) characterization of methyl oleate 3e..... 48
3.2.5.2 FTIR and NMR (^{1}H and ^{13}C) characterization of ethyl oleate 3f..... 51
3.2.5.3 FTIR and NMR (^{1}H and ^{13}C) characterization of propyl oleate 3g 54
3.2.5.4 FTIR and NMR (^{1}H and ^{13}C) characterization of butyl oleate 3h..... 56
3.2.5.5 FTIR and NMR (^{1}H and ^{13}C) characterization of pentyl oleate 3i..... 59
3.2.5.6 FTIR and NMR (^{1}H and ^{13}C) characterization of hexyl oleate 3j..... 61
3.3 RESULTS AND DISCUSSIONS..... 63
3.3.1 Esterification of stearic acid over Heteropolyacids (HPAs) 63
3.3.2 Effect of reaction temperature..... 64
3.3.3 Effect of mole ratio of SA to propanol..... 65
3.3.4 Efficiency of various HPA catalysts 65
3.3.5 Effect of catalyst loading..... 66
3.3.6 Effect of different alcohol 67
3.3.7 Recycling and recovery of catalysts..... 68
3.3.8 Characterization of recycled catalysts..... 69
3.3.9 Esterification of oleic acid (OA) over HPA catalysts 74
3.3.10 Effect of reaction temperature..... 74
3.3.11 Effect of mole ratio of OA to 1-butanol..... 75
3.3.12 Efficiency of different HPA in preparing alkyl oleates..... 76
3.3.13 Effect of catalyst loading..... 77
3.3.14 Effect of different alcohol 78
3.4 CONCLUSION..... 82

CHAPTER 4: OXIDATION OF BIOMASS DERIVED FURFURAL TO FURANONE BY USING HETEROPOLYACIDS SUPPORTED MOLECULAR SIEVES

4.1 INTRODUCTION 83

4.2 EXPERIMENTAL SECTION 85

4.2.1 Materials 85

4.2.2 Synthesis of HPA supported NH_4YZ catalysts 85

4.2.3 Characterization techniques 86

4.2.4 Catalyst reactions 86

4.2.5 Instrument used for the characterization of compounds 87

4.2.5.1 FTIR and NMR (^{1}H and ^{13}C) characterization of furanone 4a 87

4.3 RESULTS AND DISCUSSIONS 89

4.3.1 Characterization of heteropolyacids supported NH_4YZ catalysts 89

4.3.2 Catalytic study for selective oxidation of furfural 93

4.3.3 Effect of the catalyst type 94

4.3.4 The effect of PTA loading on NH_4YZ zeolites 94

4.3.5 Effect of catalyst loading 95

4.3.6 Effect of the amount of H_2O_2 96

4.3.7 Effect of the temperature 97

4.3.8 Catalyst recycling 97

4.4. CONCLUSIONS 98

CHAPTER 5: EFFICIENT PREPARATION OF ALKYL BENZOATES AND ALKYL 2-FUROATES BY HETEROPOLYACID-CATALYZED ESTERIFICATION OF BENZOIC ACID AND 2-FUROIC ACID

5.1 INTRODUCTION 99

5.2 EXPERIMENTAL SECTION 102

5.2.1 Materials 102

5.2.2 Catalytic reactions (A): Esterification of benzoic acid over HPA catalysts ... 103

5.2.3 Instrument used for the characterization of compounds 103

5.2.3.1 FTIR and NMR (^{1}H and ^{13}C) characterization of methyl benzoate 5a ... 104

5.2.3.2 FTIR and NMR (^{1}H and ^{13}C) characterization of ethyl benzoate 5b 106

5.2.3.3 FTIR and NMR (^{1}H and ^{13}C) characterization of propyl benzoate 5c ... 108

5.2.3.4 FTIR and NMR (^{1}H and ^{13}C) characterization of butyl benzoate 5d 110

5.2.3.5 FTIR and NMR (^{1}H and ^{13}C) characterization of pentyl benzoate 5e 112

5.2.3.6 FTIR and NMR (^{1}H and ^{13}C) characterization of hexyl benzoate 5f 115

5.2.3.7 FTIR and NMR (^{1}H and ^{13}C) characterization of propane-1,3-diyl dibenzoate 5g 117

5.2.3.8 FTIR and NMR (^{1}H and ^{13}C) characterization of butyl 4-chlorobenzoate 5h 119

5.2.3.9 FTIR and NMR (^{1}H and ^{13}C) characterization of butyl 4-methoxybenzoate 5i 121

5.2.10 FTIR and NMR (^{1}H and ^{13}C) characterization of butyl 4-nitrobenzoate 5j 123

5.2.11 FTIR and NMR (^{1}H and ^{13}C) characterization of butyl 4-methylbenzoate 5k 125

5.2.12 FTIR and NMR (^{1}H and ^{13}C) characterization of dibutyl phthalate 5l ... 127

5.2.13 FTIR and NMR (^{1}H and ^{13}C) characterization of dibutyl terephthalate 5m 129

5.2.14 FTIR and NMR (^{1}H and ^{13}C) characterization of butyl trans-cinnamate 5n 131

5.2.15 FTIR and NMR (^{1}H and ^{13}C) characterization of butyl 2-hydroxybenzoate 5o 133

5.2.16 FTIR and NMR (^{1}H and ^{13}C) characterization of butyl 2-bromobenzoate 5p 135

5.2.4 Catalytic reactions (B): Esterification of 2-furoic acid (FA) over HPA catalysts 137

5.2.5 Instrument used for the characterization of compounds 137

5.2.5.1 FTIR and NMR (^{1}H and ^{13}C) characterization of methyl 2-furoate 5q ... 137

5.2.5.2 FTIR and NMR (^{1}H and ^{13}C) characterization of ethyl 2-furoate 5r 140

5.2.5.3 FTIR and NMR (^{1}H and ^{13}C) characterization of propyl 2-furoate 5s 142

5.2.5.4 FTIR and NMR (^{1}H and ^{13}C) characterization of isopropyl 2-furoate 5t 144

5.2.5.5 FTIR and NMR (^{1}H and ^{13}C) characterization of butyl 2-furoate 5u 146

5.3 RESULTS AND DISCUSSIONS 148

5.3.1 Esterification of benzoic acid over HPAs 148

5.3.2 Efficiency of various HPA catalysts 149

5.3.3 Effect of catalyst loading 150

5.3.4 Effect of reaction temperature 151

5.3.5 Effect of mole ratio of benzoic acid to 1-butanol 152

5.3.6 Effect of different alcohol 153

5.3.7 Effect of different substituted benzoic acid 154

5.3.8 Recycling and regeneration of catalysts 156

5.3.9 Characterization of recycled catalysts 157

5.3.10 Esterification of furoic acid (FA) over HPA catalysts 160

5.3.11 Effect of reaction temperature 160
5.3.12 Effect of mole ratio of FA to 1-butanol 161
5.3.13 Efficiency of different HPA in preparing alkyl furoates 162
5.3.14 Effect of catalyst loading 165
5.3.15 Effect of different alcohol 166
5.4 CONCLUSION 167
CHAPTER 6: SUMMARY AND CONCLUSIONS
6.1 SUMMARY 169
6.2 CONCLUSIONS 170
6.3 SCOPE FOR THE FUTURE WORK 172
References 173

LIST OF FIGURES
CHAPTER 1

Figure 1.1 The ball and stick representation of Keggin polyanion. 4
Figure 1.2 Polyhedra representation of Keggin-type polyoxometalate. 5
Figure 1.3 Primary, secondary, and tertiary structures; the hierarchical structure of heteropolyacids in the solid-state. 6
Figure 1.4 Protonic species present in $H_3PW_{12}O_{40}.nH_2O$. 7
Figure 1.5 Block diagram showing applications of HPAs. 8

CHAPTER 2

Figure 2.1 FTIR spectrum of 2-(furan-2-yl)-1,3-dioxolane **2a.** 27
Figure 2.2 ^{1}H-NMR spectrum of 2-(furan-2-yl)-1,3-dioxolane **2a**. 28
Figure 2.3 ^{13}C-NMR spectrum of 2-(furan-2-yl)-1,3-dioxolane **2a**. 28
Figure 2.4 Effects of various HPAs catalysts on the yield of 2-(furan-2-yl)-1,3-dioxolane **2a**. 30
Figure 2.5 Effect of catalyst loading of PTA catalyst on the yield of 2-(furan-2-yl)-1,3-dioxolane **2a**. 31
Figure 2.6 Effect of the molar ratio between ethylene glycol and furfural on the isolated yield of 2-(furan-2-yl)-1,3-dioxolane **2a**. 32
Figure 2.7 Effect of solvent on the yield of 2-(furan-2-yl)-1,3-dioxolane **2a**. 33
Figure 2.8 Effect of varying quantity of benzene on the yield of 2-(furan-2-yl)-1,3-dioxolane **2a**. 34

CHPTER 3

Figure 3.1 FTIR spectrum of methyl stearate **3a**. 39
Figure 3.2 ^{1}H-NMR spectrum of methyl stearate **3a**. 40
Figure 3.3 ^{13}C-NMR spectrum of methyl stearate **3a**. 41

Figure 3.4 FTIR spectrum of ethyl stearate **3b**. 42
Figure 3.5 ^{1}H-NMR spectrum of ethyl stearate **3b**. 43
Figure 3.6 ^{13}C-NMR spectrum of ethyl stearate **3b**. 43
Figure 3.7 FTIR spectrum of propyl stearate **3c**. 44
Figure 3.8 ^{1}H-NMR spectrum of propyl stearate **3c**. 45
Figure 3.9 ^{13}C-NMR spectrum of propyl stearate **3c**. 45
Figure 3.10 FTIR spectrum of butyl stearate **3d**. 46
Figure 3.11 ^{1}H-NMR spectrum of butyl stearate **3d**. 47
Figure 3.12 ^{13}C-NMR spectrum of butyl stearate **3d**. 47
Figure 3.13 FTIR spectrum of methyl oleate **3e**. 49
Figure 3.14 ^{1}H-NMR spectrum of methyl oleate **3e**. 50
Figure 3.15 ^{13}C-NMR spectrum of methyl oleate **3e**. 50
Figure 3.16 FTIR spectrum of ethyl oleate **3f**. 51
Figure 3.17 ^{1}H-NMR spectrum of ethyl oleate **3f**. 52
Figure 3.18 ^{13}C-NMR spectrum of ethyl oleate **3f**. 53
Figure 3.19 FTIR spectrum of propyl oleate **3g**. 54
Figure 3.20 ^{13}C-NMR spectrum of propyl oleate **3g**. 55
Figure 3.21 FTIR spectrum of butyl oleate **3h**. 56
Figure 3.22 ^{1}H-NMR spectrum of butyl oleate **3h**. 57
Figure 3.23 ^{13}C-NMR spectrum of butyl oleate **3h**. 58
Figure 3.24 FTIR spectrum of pentyl oleate **3i**. 59
Figure 3.25 ^{1}H-NMR spectrum of pentyl oleate **3i**. 60
Figure 3.26 ^{13}C-NMR spectrum of pentyl oleate **3i**. 61
Figure 3.27 FTIR spectrum of Hexyl oleate **3j**. 62
Figure 3.28 ^{1}H-NMR spectrum of Hexyl oleate **3j**. 62
Figure 3.29 ^{13}C-NMR spectrum of Hexyl oleate **3j**. 63
Figure 3.30 Effect of reaction temperature on the yield of propyl stearates **3c**. 64
Figure 3.31 Effect of equivalence of 1-propanol with respect to SA on the isolated yield of propyl stearate **3c**. 65

Figure 3.32 Efficiency of various HPAs on the yield of propyl stearate **3c**. 66
Figure 3.33 Effect of loading of PTA catalyst on the isolated yield of propyl stearate **3c**. 67
Figure 3.34 Preparation of alkyl stearates (**3a-3d**) from stearic acid..... 68
Figure 3.35 Recovery and reuse of PTA catalyst in the preparation of propyl stearate **3c**. 69
Figure 3.36 FTIR spectra of the fresh PTA (dried) and recycled (5^{th} cycle) PTA. 70
Figure 3.37 ^{31}P-NMR spectra of fresh and recovered PTA catalyst. 71
Figure 3.38 TGA graph of the fresh and recycled PTA catalyst..... 71
Figure 3.39 Effect of reaction temperature on the yield of butyl oleates **3h**. 75
Figure 3.40 Effect of equivalence of 1-butanol with respect to OA on the isolated yield of butyl oleate **3h**. 76
Figure 3.41 The efficiency of various HPAs on the yield of butyl oleate **3h**. 77
Figure 3.42 Effect of loading of PTA catalyst on the isolated yield of butyl oleate **3h**. . 78
Figure 3.43 Preparation of alkyl oleates (**3e-3j**) from oleic acid. 79

CHAPTER 4

Figure 4.1 FTIR spectrum of 2-furanone **4a**. 87
Figure 4.2 ^{1}H-NMR spectrum of 2-furanone **4a**. 88
Figure 4.3 ^{13}C-NMR spectrum of 2-furanone **4a**. 89
Figure 4.4 XRD spectra of (a) NH_4YZ and (b) 20%PTA/NH_4YZ (c) Used catalyst after reaction. 90
Figure 4.5 FTIR spectra of (a) PTA (b) NH_4YZ and (c) 20%PTA/NH_4YZ. 91
Figure 4.6 SEM image of the catalysts for (a) NH_4YZ (b) 20%PTA/NH_4YZ (Fresh) (c) After reaction (Recovered). 92
Figure 4.7 Thermal analysis diagrams of 20%PTA/NH_4YZ catalyst. 92
Figure 4.8 The efficiency of different HPAs on the yield of 2-furanone **4a**..... 94
Figure 4.9 Effect of PTA loading over NH_4YZ zeolites. 95

Figure 4.10 Effect of the catalyst loading on yield of 2-furanone **4a**. 96
Figure 4.11 Effect of the H_2O_2 on the yield of 2-furanone **4a**. 97

CHAPTER 5

Figure 5.1 FTIR spectrum of methyl benzoate **5a**. 104
Figure 5.2 ^{1}H-NMR spectrum of methyl benzoate **5a**. 105
Figure 5.3 ^{13}C-NMR spectrum of methyl benzoate **5a**. 106
Figure 5.4 FTIR spectrum of ethyl benzoate **5b**. 107
Figure 5.5 ^{1}H-NMR spectrum of ethyl benzoate **5b**. 107
Figure 5.6 ^{13}C-NMR spectrum of ethyl benzoate **5b**. 108
Figure 5.7 FTIR spectrum of propyl benzoate **5c**. 109
Figure 5.8 ^{1}H-NMR spectrum of propyl benzoate **5c**. 109
Figure 5.9 ^{13}C-NMR spectrum of propyl benzoate **5c**. 110
Figure 5.10 FTIR spectrum of butyl benzoate **5d**. 111
Figure 5.11 ^{1}H-NMR spectrum of butyl benzoate **5d**. 111
Figure 5.12 ^{13}C-NMR spectrum of butyl benzoate **5d**. 112
Figure 5.13 FTIR spectrum of pentyl benzoate **5e**..... 113
Figure 5.14 ^{1}H-NMR spectrum of pentyl benzoate **5e**..... 114
Figure 5.15 ^{13}C-NMR spectrum of pentyl benzoate **5e**. 114
Figure 5.16 FTIR spectrum of hexyl benzoate **5f**. 115
Figure 5.17 ^{1}H-NMR spectrum of hexyl benzoate **5f**. 116
Figure 5.18 ^{13}C-NMR spectrum of hexyl benzoate **5f**. 116
Figure 5. 19 FTIR spectrum of propane-1,3-diyl dibenzoate **5g**. 117
Figure 5.20 ^{1}H-NMR spectrum of propane-1,3-diyl dibenzoate **5g**. 118
Figure 5.21 ^{13}C-NMR spectrum of propane-1,3-diyl dibenzoate **5g**. 118
Figure 5.22 FTIR spectrum of butyl 4-chlorobenzoate **5h**. 119
Figure 5.23 ^{1}H-NMR spectrum of butyl 4-chlorobenzoate **5h**. 120
Figure 5.24 ^{13}C-NMR spectrum of butyl 4-chlorobenzoate **5h**. 120
Figure 5.25 FTIR spectrum of butyl 4-methoxybenzoate **5i**..... 121

Figure 5.26 ^{1}H-NMR spectrum of butyl 4-methoxybenzoate **5i**. 122
Figure 5.27 ^{13}C-NMR spectrum of butyl 4-methoxybenzoate **5i**. 122
Figure 5.28 FTIR spectrum of butyl 4-nitrobenzoate **5j**. 123
Figure 5.29 ^{1}H-NMR spectrum of butyl 4-nitrobenzoate **5j**. 124
Figure 5.30 ^{13}C-NMR spectrum of butyl 4-nitrobenzoate **5j**. 124
Figure 5.31 FTIR spectrum of butyl 4-methylbenzoate **5k**. 125
Figure 5.32 ^{1}H-NMR spectrum of butyl 4-methylbenzoate **5k**. 126
Figure 5.33 ^{13}C-NMR spectrum of butyl 4-methylbenzoate **5k**. 126
Figure 5.34 FTIR spectrum of dibutyl phthalate **5l**. 127
Figure 5.35 ^{1}H-NMR spectrum of dibutyl phthalate **5l**. 128
Figure 5.36 ^{13}C-NMR spectrum of dibutyl phthalate **5l**. 128
Figure 5.37 FTIR spectrum of dibutyl terephthalate **5m**. 129
Figure 5.38 ^{1}H-NMR spectrum of dibutyl terephthalate **5m**. 130
Figure 5.39 ^{13}C-NMR spectrum of dibutyl terephthalate **5m**. 130
Figure 5.40 FTIR spectrum of butyl trans-cinnamate **5n**. 131
Figure 5.41 ^{1}H-NMR spectrum of butyl trans-cinnamate **5n**. 132
Figure 5.42 ^{13}C-NMR spectrum of butyl trans-cinnamate **5n**. 132
Figure 5.43 FTIR spectrum of butyl 2-hydroxybenzoate **5o**. 133
Figure 5.44 ^{1}H-NMR spectrum of butyl 2-hydroxybenzoate **5o**. 134
Figure 5.45 ^{13}C-NMR spectrum of butyl 2-hydroxybenzoate **5o**. 134
Figure 5.46 FTIR spectrum of butyl 2-bromobenzoate **5p**. 135
Figure 5.47 ^{1}H-NMR spectrum of butyl 2-bromobenzoate **5p**. 136
Figure 5.48 ^{13}C-NMR spectrum of butyl 2-bromobenzoate **5p**. 136
Figure 5.49 FTIR spectrum of methyl 2-furoate **5q**. 138
Figure 5.50 ^{1}H-NMR spectrum of methyl 2-furoate **5q**. 139
Figure 5.51 ^{13}C-NMR spectrum of methyl 2-furoate **5q**. 140
Figure 5.52 FTIR spectrum of ethyl 2-furoate **5r**. 141
Figure 5.53 ^{13}H-NMR spectrum of ethyl 2-furoate **5r**. 141
Figure 5.54 ^{13}C-NMR spectrum of ethyl 2-furoate **5r**. 142

Figure 5.55 FTIR spectrum of propyl 2-furoate **5s**. 143
Figure 5.56 ^{1}H-NMR spectrum of propyl 2-furoate **5s**. 143
Figure 5.57 ^{13}C-NMR spectrum of propyl 2-furoate **5s**. 144
Figure 5.58 FTIR spectrum of isopropyl 2-furoate **5t**. 145
Figure 5.59 ^{1}H-NMR spectrum of isopropyl 2-furoate **5t**. 145
Figure 5.60 ^{13}C-NMR spectrum of isopropyl 2-furoate **5t**. 146
Figure 5.61 FTIR spectrum of butyl 2-furoate **5u**. 147
Figure 5.62 ^{1}H-NMR spectrum of butyl 2-furoate **5u**. 147
Figure 5.63 ^{13}C-NMR spectrum of butyl 2-furoate **5u**. 148
Figure 5.64 The efficiency of various HPAs on the yield of butyl benzoate **5d**. 150
Figure 5.65 The effect of loading of PTA catalyst on the isolated yield of butyl benzoate **5d**. 151
Figure 5.66 Effect of reaction temperature on the yield of butyl benzoate **5d**. 152
Figure 5.67 Effect of 1-butanol: benzoic acid molar ratio on the isolated yield of butyl benzoate **5d**. 153
Figure 5.68 Recovery and reuse of PTA catalyst in the preparation of butyl benzoate **5d**. 157
Figure 5.69 FTIR spectra of the fresh PTA (dried) and recycled (3rd cycle) PTA. 158
Figure 5.70 The ^{31}P-NMR spectrum of fresh and recovered PTA catalyst. 159
Figure 5.71 The TGA graph of the fresh and recycled PTA catalyst. 159
Figure 5.72 Effect of reaction temperature on the yield of butyl furoate **5u**. 161
Figure 5.73 Effect of equivalence of 1-butanol with respect to FA on the isolated yield of butyl furoate **5u**. 162
Figure 5.74 Efficiency of various heteropolyacids on the yield of butyl furoate **5u**. 163
Figure 5.75 The efficiency of various supported HPA catalysts on the yield of butyl furoate **5u**. 164
Figure 5.76 Effect of loading of PTA catalyst on the isolated yield of butyl furoate **5u**. 165

Figure 5.77 Preparation of alkyl furoates (**5q**-**5u**) from 2-furoic acid..... 166

LIST OF SCHEMES

CHAPTER 2

Scheme 2.1 Preparation of **2a** from furfural using HPA catalysts. 24
Scheme 2.2 Reaction mechanism for the Acetalization of furfural with ethylene glycol. 25

CHAPTER 3

Scheme 3.1 Preparation of (a) alkyl stearates from stearic acid and b) alkyl oleates from oleic acid using the HPA catalysts. 37

CHAPTER 4

Scheme 4.1 Selective oxidation of furfural to 2-furanone **4a** using HPA catalysts. 84
Scheme 4.2 The reaction mechanism for furfural oxidation. 85

CHAPTER 5

Scheme 5.1 Esterification of (a) benzoic acid, and (b) 2-furoic acid using HPA catalysts. 101
Scheme 5.2 Probable reaction mechanism of the esterification of Benzoic acid. 101
Scheme 5.3 Probable reaction mechanism of the esterification of furoic acid. 101
Scheme 5.4 Chemical structure of the synthesized alkyl 2-furoates. 160

LIST OF TABLES

CHAPTER 3

Table 3.1 Esterification of stearic acid using PTA catalyst 72

Table 3.2 Esterification of oleic acid using PTA catalyst. 80

CHAPTER 4

Table 4.1 Comparison of catalytic activities for H_2O_2, oxidation of furfural among the various supported polyoxometalates over NH_4YZ 93

Table 4.2 Comparison with other identified catalysts of furfural oxidation 98

CHAPTER 5

Table 5.1 Esterification of benzoic acid with alkyl alcohols using PTA as the catalyst 154

Table 5.2 Esterification of various benzoic acid derivatives using PTA catalyst 155

Table 5.3 Esterification of furoic acid using PTA catalyst 167

NOMENCLATURE

^{13}C-NMR	Carbon Nuclear Magnetic Resonance
EtOH	Ethanol
Equiv.	Equivalence
FFA	Free fatty acid
FTIR	Fourier Transform Infrared
Fur	Furfural
HPAs	Heteropolyacids
HMF	5-(hydroxymethyl)furfural
^{1}H-NMR	Proton Nuclear Magnetic Resonance
PMA	Phosphomolybdic acid
PTA	Phosphotungstic acid
POMs	Polyoxometalates
^{31}P-NMR	Phosphorus Nuclear Magnetic Resonance
RT	Room Temperature
SEM	Scanning Electron Microscope
SMA	Silicomolybdic acid
STA	Silicotungstic acid
TGA	Thermo Gravimetric Analysis
TLC	Thin layer chromatography
TMS	Tetramethylsilane
TON	Turn over number
PXRD	Powder X-ray diffraction

LIST OF SYMBOLS AND UNITS

α	Alpha
β	Beta
cm	Centimeter
º	Degree
ºC	Degree Celsius
γ	Gamma
g	Gram
>	Greater than
h	Hour
Hz	Hertz
Δ	Delta
λ	Lambda
<	Less than
mL	Milliliter
mmol	Millimole
min	Minute
M	Molar
wt	Weight
θ	Theta

CHAPTER 1

INTRODUCTION

Abstract: *This chapter discusses the structural features, properties, and catalytic applications of polyoxometalates (POMs), with special emphasis on the Keggin structure. The chapter highlights heteropolyacids (HPAs), a subclass of POM, as an efficient and environment-friendly acid catalyst for green chemistry and biorenewable syntheses. A review of the current literature, the scope of research, and the objectives of the current work are also discussed in this chapter.*

1.1 GENERAL INTRODUCTION

Chemical industries in the 21st century must focus on renewable feedstock, greener technologies, sustainable processes, and safer products (Anastas and Warner 1998; Lancaster 2016). Catalysis is one of the tenets of green chemistry and increasingly being adopted by the academic community and chemical industry (Horvath and Anastas 2007). A catalyst is a substance that accelerates the reaction rate by providing a lower energy alternative mechanistic pathway. However, the catalyst gets regenerated at the end of the pathway, commonly referred to as the 'catalytic cycle'. Catalyst makes it possible to access unique products, increase the selectivity of a particular product, and allow the reactions to proceed under mild conditions. One or more catalytic processes produce a significant fraction of the inorganic and organic chemicals. The majority of the catalysts that have been developed, and fine-tuned are related to petrorefinery operations. However, new generations of more efficient and environment-friendly catalysts are being developed that can be used for sustainable but challenging feedstock such as terrestrial and algal biomass.

HPAs based organic transformation reactions are the most affluent areas in both traditional and fundamental catalysis, because of their profoundly changing physical and chemical properties through "goal-oriented" alteration of their dynamic structure from atomic to nano-level. The Keggin-type of HPA has dual catalytic properties with strong acidity and high oxidizing efficiency, which is a unique and functional solid acid catalysts for industrial applications (Okuhara et al. 2001). In the field of industrial

chemistry and technology by catalysis, HPAs are considered to be effective solid acid catalysts. Japan has started using HPAs as catalysts in several petrochemical processes that cover the process of direct hydration of alkenes such as propene, isobutene, and n-butenes. The HPA-based catalysts have also used to produce of methacrylic acid from methacrolein, and polymerize tetrahydrofuran. HPAs are therefore growing a new trend in material science and catalysis.

The primary goal of this thesis was to investigate the catalytic properties of Keggin type HPAs as an efficient and environmentally-friendly catalyst for the synthesis of fuels and specialty chemicals from biomass-derived renewable chemical building blocks. Various homogeneous and heterogeneous HPA-based catalysts were prepared and their reactivities were compared. The synthesized HPA-based heterogeneous catalysts were characterized by analytical techniques like Fourier transform infrared spectroscopy (FTIR), powder X-ray diffractometry (PXRD), thermogravimetric analysis (TGA), and scanning electron microscopy (SEM) analysis.

1.2 POLYOXOMETALATES

The first polyoxometalate (POM), ammonium 12-molybdophosphate, was isolated by Berzelius in 1826 by mixing ammonium molybdate and orthophosphoric acid (Berzelius 1826). In 1854 Struve reported a few more other heteroatoms (Al^{3+}, Cu^{+}, etc.) containing polyoxometalates (Struve 1854). It was Marignac (Marignac 1862) who was accelerated the filed of polyoxometalates chemistry when he identified the two isomers of $[SiW_{12}O_{40}]^{4-}$ by analytical techniques. Notably, the field of POMs were grown rapidly in the first decade of the twentieth century by reporting almost 700 POMs compounds by several scientists around the world. Almost a decade later, it was Keggin, in 1933, first solved the structure of 12:1 heteropoly anion of the formula $[H_3PW_{12}O_{40}].5H_2O$ by powder X-ray diffraction method (Keggin 1933, 1934).

POMs are a class of water-soluble metal-oxygen nano-clusters, composed of group V and VI addenda atoms in their respective highest oxidation states. The acidic

forms of POM's are known as heteropolyacids (HPAs). The POMs, further divided into two specific families based on their chemical composition, i.e. (a) isopolyoxometalates and (b) heteropolyoxometalates. The isopolyoxometalates involve merely the d^0 metal ions (e.g., W^{6+}, Mo^{6+}, V^{5+}, etc.) to form the metal-oxide cluster having the general formula as $[M_mO_y]^{n-}$, while the heteropolyoxometalates involves one as well as many other heteroatoms (e.g., P, Si, B, Mn, Co, Gd, etc.) of p/d/f-blocks, in various oxidation number to form metal-oxide frame with the general formula $[X_xM_mO_y]^{p-}$ with a condition of $x < m$.

The application of POMs in chemical catalysis is increased day by day due to their (i) strong Bronsted acidity, (ii) reversible multielectron redox reactions, (iii) higher mobility of proton and solubility in the polar solvents, (iv) higher thermal stability, and (v) intriguing design. The applications of POMs have been overgrowing in recent years, including optics, electrical materials, magnetic materials, medicine (antiviral, anti-HIV activity), electronics, and catalysis, etc. (Xie 2006; Kogerler and Tsukerblat 2010)

1.3 CLASSIFICATION OF HETEROPOLYOXOMETALATES (HPOMs)

Heteropolyoxometalates are with complex structure, which consists of metal-oxygen octahedral as basic structure unit. We will discuss here only the Keggin type POMs. The important features of each type of heteropoly ions are explained briefly,

1.3.1 Keggin heteropoly ion

The general formula of Keggin type heteropoly anion is $X^nM_{12}O_{40}{}^{(8-n)-}$, where X is the typically B^{3+}, Al^{3+}, P^{5+}, Si^{4+}, As $^{3+/5+}$ and transition metals also act as heteroatom and M represents the addenda atoms (W^{6+} or Mo^{6+}) (**Figure 1.1**). The ratio found in the formation of Keggin-type compounds between the addenda atom and heteroatom is 12, (M/X = 12). The Keggin form of the HPAs has been under considerable attention due to its versatile properties such as relatively high thermal stability, redox, and acidic

properties, among which catalytic applications are most significant and applicable as an industrial catalyst.

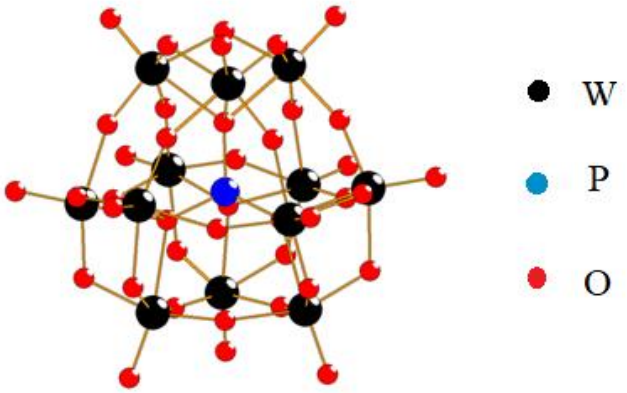

Figure 1.1 The ball and stick representation of Keggin polyanion.

The primary structure of Keggin $H_3PMo_{12}O_{40}$ is well-established, where a tetrahedral-coordinated central P atom (PO_4) is surrounded by 12 octahedral metal-oxygen (MO_6) units. The three acid protons neutralize the negative charge over Keggin POM. There are four types of oxygen atoms (**Figure 1.2**) presents in the basic Keggin type POMs, i) four central oxygen atoms (O_a) which are attached with the central heteroatom, ii) 12 oxygen atoms bridging two molybdenum atoms sharing a central oxygen atom (edge-sharing O_c), iii) 12 oxygen atoms bridging molybdenum atoms not sharing a central oxygen atom (O_b), and iv) 12 terminal oxygen atoms (O_d) bound to a single atom.

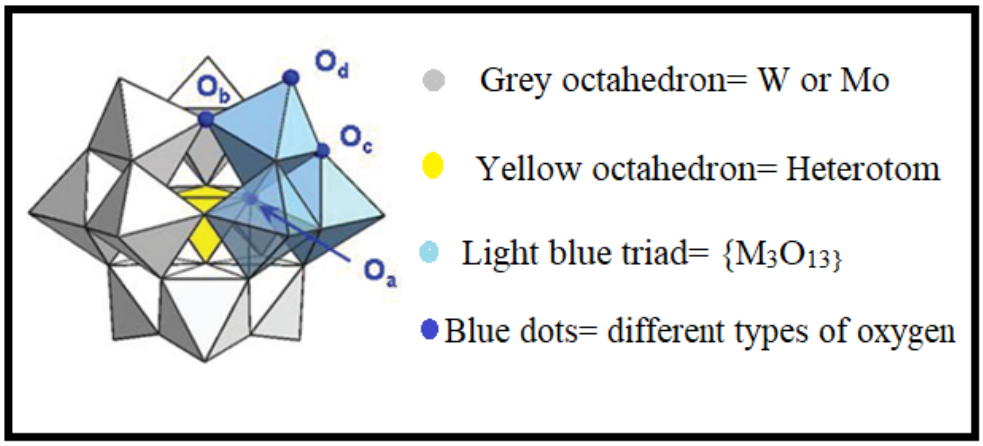

Figure 1.2 Polyhedra representation of Keggin-type polyoxometalate.

Other examples of Keggin types heteropolyacid are: i) Phosphomolybdic acid ($H_3PMo_{12}O_{40}$, PMA), ii) Phosphotungstic acid ($H_3PW_{12}O_{40}$, PTA), iii) Silicomolybdic acid ($H_4SiMo_{12}O_{40}$, SMA), iv) Silicotungstic acid ($H_4SiW_{12}O_{40}$, STA).

1.4 PRIMARY, SECONDARY, AND TERTIARY STRUCTURES OF HETEROPOLYACIDS

Generally, HPAs and their salts form ionic crystals composed of heteropoly anions (primary structure), counter cations (H^+, H_3O^+, $H_5O_2^+$), hydration water, and other molecules. The hierarchical structure of solid HPAs is essential for the understanding of their catalytic activity, and the substructures were denoted as primary, secondary, and tertiary (Misino et al. 1980). A schematic model for heteropolyacid microstructure is shown in **Figure 1.3**. The main structure is the heteropoly anion $[PW_{12}O_{40}]^{3-}$ i.e., the structure of Keggin ion. The secondary structure (e.g., $Cs_{2.5}H_{0.5}PW_{12}O_{40}$) is formed by arranging the primary structure with countercations. The secondary structure is flexible, depending on the amount of water for hydration, counter cation, and heteropoly anion. The aggregates of secondary structures in three-dimensional manners give the tertiary structure. It explains the formation of solid particles and relates to properties such as

particle size, surface area, pore structure, and distribution of protons in particles (Misono 1992).

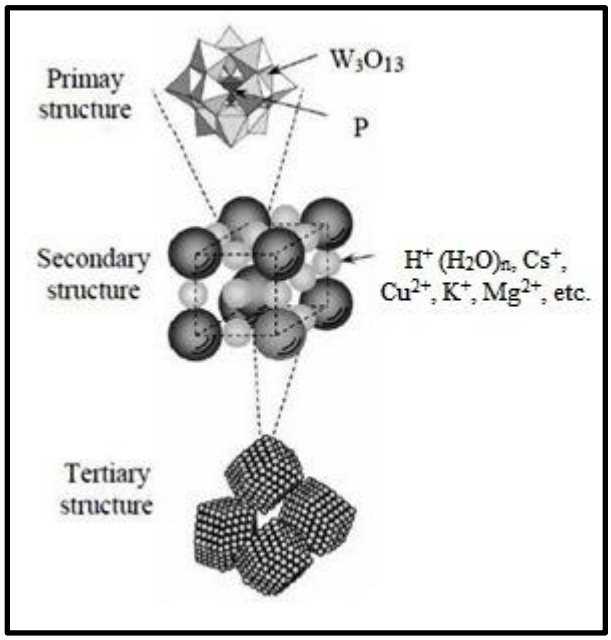

Figure 1.3 Primary, secondary, and tertiary structures; the hierarchical structure of heteropolyacids in the solid-state.

1.5 POSITION OF PROTONS IN KEGGIN HETEROPOLYACIDS

In the solid HPAs, two types of protons have found; hydrated protons $[H(H_2O)_n]^+$ and non-hydrated protons. Hydrated protons are highly mobile and are responsible for extremely high proton conductivity of hydrates of crystalline HPA. The Non-hydrated protons have much less mobility, and those protons are localized on the either on M=O or/and bridging oxygens of M-O-M (edge-sharing and corner-sharing) (Janik et al. 2004). Nevertheless, both hydrated or non-hydrated protons, participate in the formation of the crystal structure in the solid crystalline HPAs, connecting the adjacent HPAs. The bulk proton of $H_3PW_{12}O_{40}.nH_2O$ presents as a planer, quasi-symmetrical hydrogen-bonded diaquahydrogen ions ($H_5O_2^+$), which act as a linker to the other surrounded four units of

$H_3PW_{12}O_{40}.nH_2O$ through hydrogen bonds via terminal W=O oxygen atoms (**Figure 1.4**).

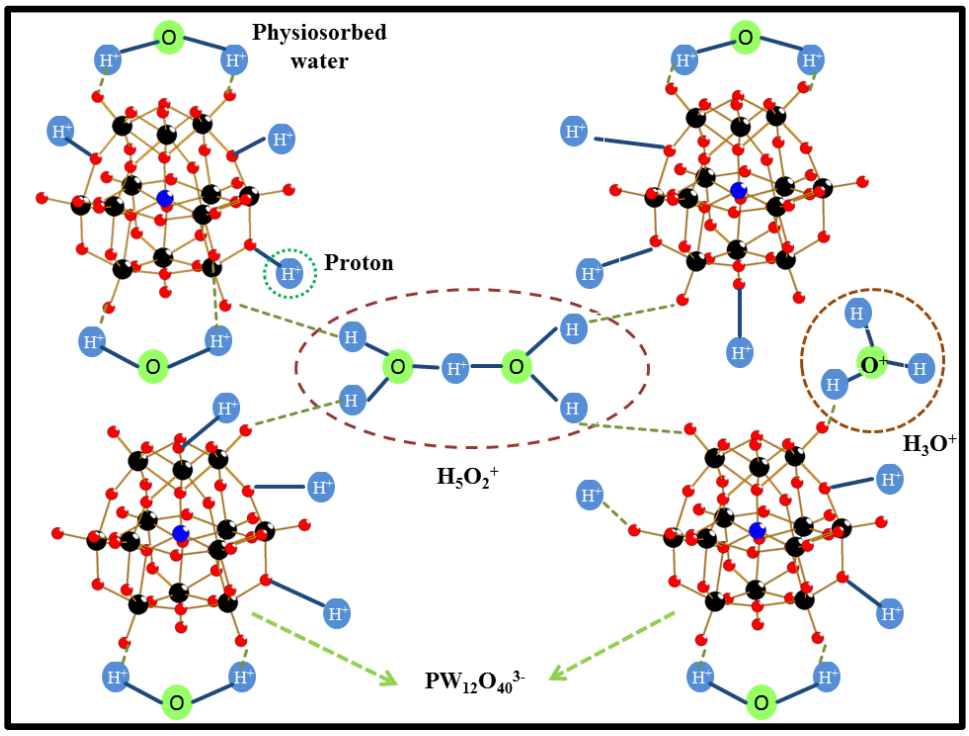

Figure 1.4 Protonic species present in $H_3PW_{12}O_{40}.nH_2O$.

1.6 ACIDIC PROPERTIES OF HETEROPOLYACIDS

HPAs are strong acids in aqueous solution. All HPAs are stronger than conventional mineral acids like H_2SO_4, HCl, HNO_3, etc., and sometimes called as superacids (Misono Okuhara 1993). The protons in the secondary HPAs structure are considered to be mobile protons. Thus, the high mobility of these protons made HPAs as superacids. The acid strength of HPAs varies in a wide range depending on the polyanion structure and its constituent elements (both hetero and addenda atoms), as well as on the extent of hydration and reduction. PTA ($H_3PW_{12}O_{40}.nH_2O$) is much stronger acid among the Keggin type HPAs, and acidity is similar to super acid. Crystalline HPAs strength decreases in the $H_3PW_{12}O_{40}$ > $H_4SiW_{12}O_{40}$ > $H_3PMo_{12}O_{40}$ > $H_4SiMo_{12}O_{40}$ series (Putluru

et al. 2011) because tungsten HPAs have a stronger acidity, higher thermal stability, and lower oxidation potential compared to molybdenum acids.

1.7 CATALYTIC APPLICATIONS OF HETEROPOLYACIDS

The applications of HPAs are based on their unique properties, including size, mass, electron and proton transfer/storage abilities, thermal stability, and mobility of lattice oxygen and high Bronsted acidity (Okuhara et al. 1996). HPAs have used both homogeneous and heterogeneous acid-catalyzed organic transformation reactions. HPAs have found significant contributions in different fields of science and technology after discovering the tremendous potential in the catalysis field. The area of HPA chemistry is more than two centuries old, but they are still a large and fast-growing class of compounds, mainly because of their wide range of applications. A block diagram shows the applications for HPAs (**Figure 1.5**). There are several patent and scientific reports claim to contribute to catalytic applications of HPAs (Katsoulis 1998).

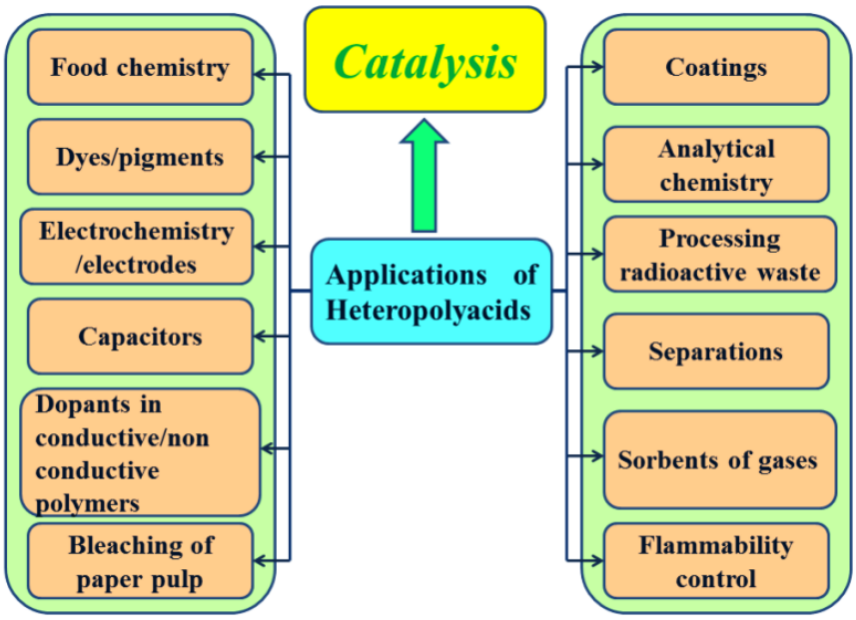

Figure 1.5 Block diagram showing applications of HPAs.

1.8 PRESENT SCENARIO AND MOTIVATION OF WORK

1.8.1 Production of Chemicals and Fuels from Biomass

Non-food, abundant biomass is a commercially-attractive source of carbon for the renewable production of liquid transportation fuels and value-added chemicals (Huber et al. 2006; Zhang et al. 2016c; Zhou et al. 2011). In a biorefinery concept, the highly functional and oxygen-rich biopolymers like cellulose and lignin are selectively converted into small organics by thermal, biotechnological, or chemocatalytic processes. The chemocatalytic value addition is of particular interest since they are fast, selective, biomass agnostic, and could potentially be integrated into the petrorefinery infrastructure. A handful of compounds are produced initially in a biorefinery, acting as renewable chemical building blocks, which are then synthetically or catalytically upgraded into fuels and commodity chemicals. A new generation of robust, inexpensive, selective, and environment-friendly catalysts are being developed for biorefinery operations. In this regard, HPAs have been considered as suitable candidates that can be used as catalysts for biomass value addition. Over the past years, HPAs are increasingly being used as a catalyst in the chemistry of renewables. HPAs have been used in the hydrolysis and dehydration of pentose and hexose sugars in biomass into furfural and 5-(hydroxymethyl)furfural (HMF), respectively. Furfural and HMF act as renewable chemical building blocks that can be converted into commodity chemicals and materials via chemical or catalytic transformations. However, the reports on the catalytic upgrading of furfural and HMF using HPA-based catalysts are scarce.

1.9 LITERATURE SURVEY

As discussed earlier, POMs are increasingly being used as the catalyst of choice in the chemocatalytic value addition of biomass and green chemistry in general. Hereby, the recent literature reports are discussed.

Li et al. (2018) synthesized a series of mesoporous catalysts by supporting acidic ionic liquids on SBA-15 and amorphous SiO_2. The characterization of the catalysts showed that the Brønsted ionic liquid [BSmim][HSO_4] was supported over the mesoporous materials and used as a catalyst for the ketalization of cyclohexanone with ethylene glycol. The conversion of cyclohexanone reached up to 85.2% (50 °C, 2 h) using only 1.3 wt% of the BAIL@SBA-15 catalyst. The supported ionic liquid catalyst was successfully recovered and recycled for five consecutive cycles (**Scheme 1.1**).

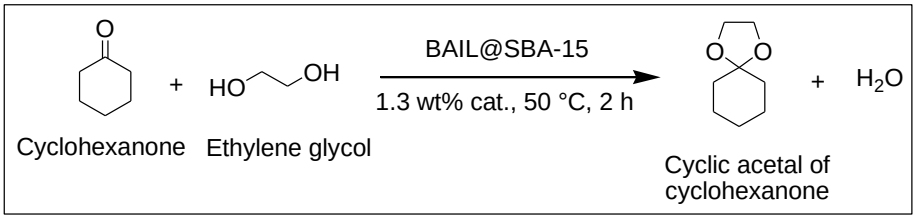

Scheme 1.1

Zhang et al. (2016a) developed a HPA-based ionic liquid immobilized on chitosan as a catalyst for the acetalization of ethyl acetoacetate with ethylene glycol. The catalyst was produced by a radical addition reaction of N-vinylimidazoliumpropane sulfonate and chitosan, followed by acidification. The water byproduct formed in the acetalization reaction was removed by distillation using cyclohexane. The acetal was obtained in excellent (83-96%) yields within 2 h at 80 °C using only 0.23 mol% (PTA content) of the catalyst. The catalyst was successfully recovered and recycled for eight consecutive cycles without significant loss of activity (**Scheme 1.2**).

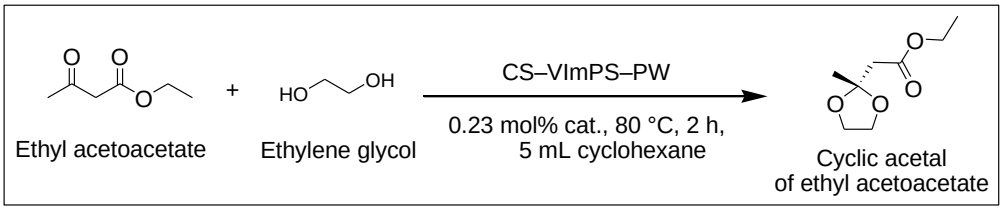

Scheme 1.2

Zhang et al. (2015) prepared mesoporous metal-organic framework MIL-100(Fe) by reacting ferric nitrate with trimesic acid (H_3BTC) under HF-free conditions. The catalyst exhibited excellent catalytic activity for the preparation of cyclic acetals (**Scheme 1.3**).

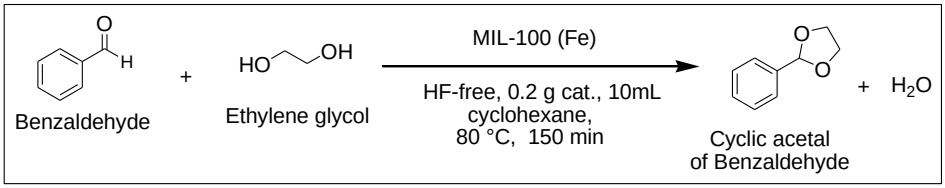

Scheme 1.3

Tropecêlo et al. (2010) examined the SBA-15 supported HPAs as catalyst for the preparation of methyl palmitate from palmitic acid. The reaction was performed at 60 °C using excess methanol. The catalytic efficiency was in the order PTA-SBA-15>STA-SBA-15>PMA-SBA-15, where methyl palmitate was isolated in 92%, 57%, and 45% yield, respectively. The deactivation of the PTA-SBA-15 catalyst was attributed to the leaching of PTA from the SBA-15 support (**Scheme 1.4**).

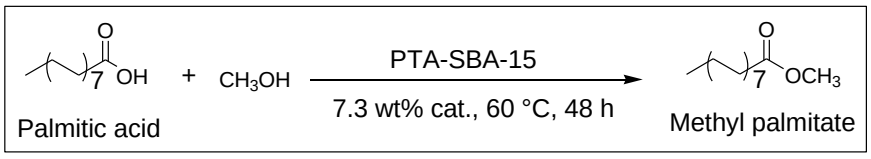

Scheme 1.4

Oliveira et al. (2010) prepared PTA (5-60 wt%) supported on ZrO_2 using the wet impregnation method. The catalytic efficiency of the synthesized catalysts was examined for the esterification of oleic acid in ethanol. The catalysts were characterized by FTIR, FT-Raman, XRD, ^{31}P-NMR, and BET surface area measurements. The Keggin-structure was found to be intact even after the calcination process at 200 °C. The 20%H_3PW-ZrO_2 was found to the most effective catalyst for the ethyl oleate, where a 88% conversion of oleic ester was achieved after 4 h at 100 °C six equivalents of ethanol and 10 wt% of the catalyst (**Scheme 1.5**).

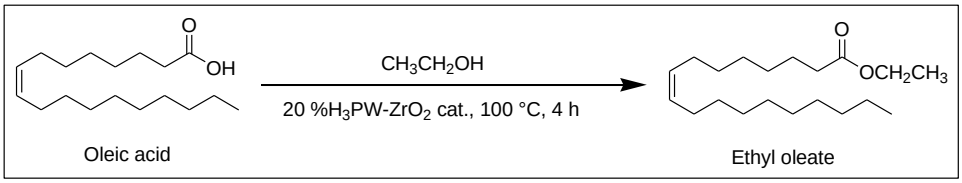

Scheme 1.5

Brahmkhatri and Patel (2011) reported that a series of PTA supported on SBA-15 catalysts for the biodiesel production from free fatty acids. Under optimized conditions, the conversion of oleic acid reached 90% within 4 h at 40 °C using a 1:40 molar ratio of oleic acid to alcohol, and 0.8 wt% of the catalyst. Newly synthesized mesoporous MCM-41 and SBA-15 that were impregnated with tungustophosphoric acid (TPA) and used as catalysts for the same biodiesel production from oleic acid. This time, they have achieved 98% conversion keeping the same reaction condition (**Scheme 1.6**).

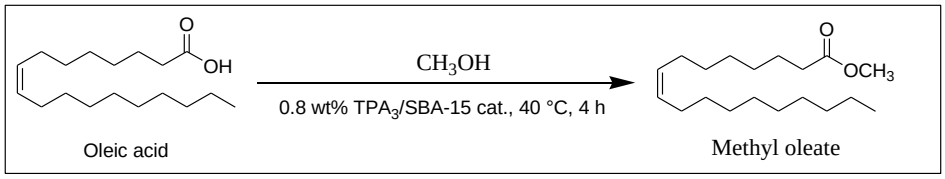

Scheme 1.6

Zhao et al. (2012) developed a Brønsted-Lewis-surfactant-combined HPA catalyst as a water-tolerant heterogeneous catalyst for esterification of free fatty acid with 95%

conversion and excellent 92% yield due to acidic property and catalyst structure. This micellar HPA catalyst was stable during the reaction time and was able to recycle through the simple separation process. Under optimized condition, the conversion of the fatty ester with methanol/acid/catalyst molar ratio about 4856:243:1, reached 95% at 65 °C and 6 h reaction time (**Scheme 1.7**).

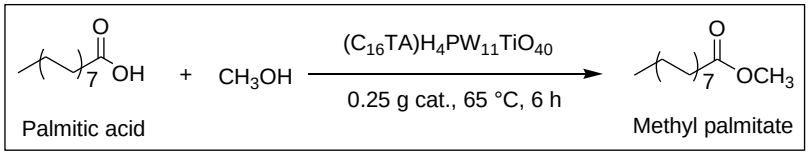

Scheme 1.7

D'Oca et al. (2012) reported the esterification of FFA with ethanol and methanol by insoluble sulfamic acid (SA) catalyst. Under optimized conditions, the FFA conversion was reached up to 95% under mild reaction conditions (10% w/w catalyst, 6:1 alcohol:FFA ratio at 100 °C, 3 h) in the presence of SA catalyst. The catalytic activity reduced significantly after the second cycle of the catalytic reaction (**Scheme 1.8**).

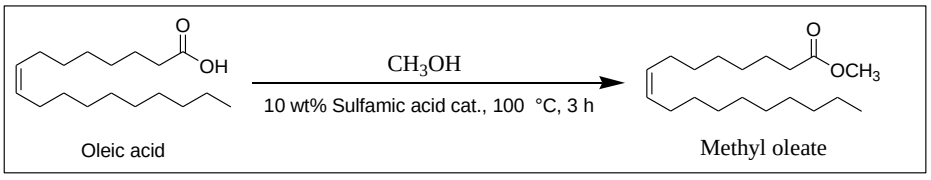

Scheme 1.8

Júnior et al. (2013) prepared tungstophosphoric acid supported flint kaolin catalyst for the synthesis of methyl, ethyl, and butyl oleates form the oleic acid. The reactions were performed at 130 °C, 2 h using excess alcohols and achieved 97% conversion oleate esters. The deactivation of the catalyst was attributed to the mass loss, formation of coke within the pore of catalyst, and leaching of tungstophosphoric acid from the flint kaolin support (**Scheme 1.9**).

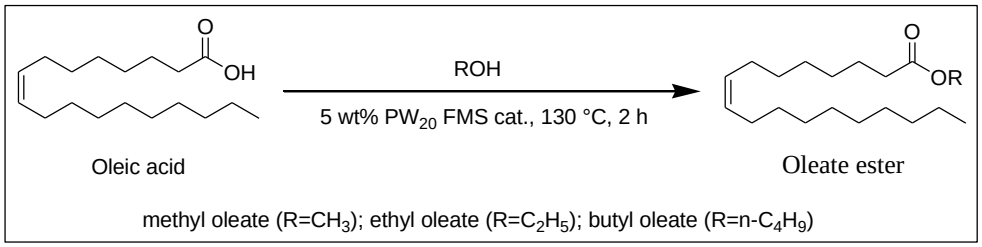

Scheme 1.9

In the same year, Kotwal et al. (2013) developed a three-dimensional mesoporous Ti-SBA-12 and Ti-SBA-16 based catalyst for producing biodiesel and biolubricants from monohydric methyl oleate and polyhydric esters (e.g., glycerol, neopentyl glycol, pentaerythritol) respectively. The conversion of biodiesel was achieved up to 92% at 170 °C (**Scheme 1.10**).

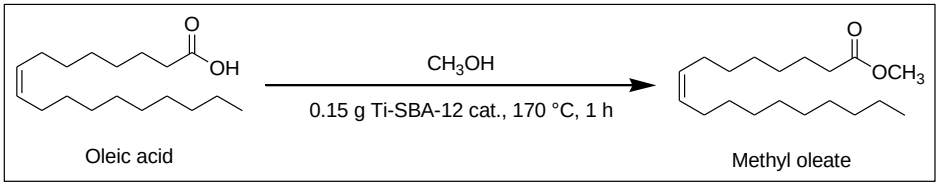

Scheme 1.10

Pires et al. (2014) prepared new catalysts, $H_3PW_{12}O_{40}$ (HPW) supported over the kaolin waste, SBA-15, MCM-41, and MCM-48 zeolites for the esterification of palm oil waste. Those catalysts were characterized and used them in preparation of ethyl ester during palm oil deodorization processes (DDPO). Under optimized condition, using the 25%HPW/MK700 catalyst achieved 83% of ester at 200 °C within 2 h of reaction, and 10 wt% of catalyst (**Scheme 1.11**).

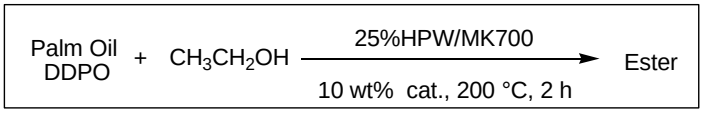

Scheme 1.11

Sun et al. (2015) reported the catalytic efficiency of $H_5BW_{12}O_{40}$ (HBW), $H_3PW_{12}O_{40}$, and Brønsted-surfactant-combined heteropolyacid $(C_{16}TA)H_4BW_{12}O_{40}$, respectively. The catalysts were examined for esterification of free fatty acids (FFAs) using methanol under both homogeneous and heterogeneous medium. It has been observed that HBW showed better conversion than corresponding heterogeneous catalyst $(C_{16}TA)H_4BW_{12}O_{40}$ (**Scheme 1.12**).

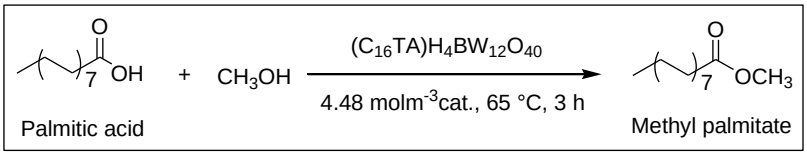

Scheme 1.12

Han et al. (2016) reported different glycine containing phosphotunstate $(PTA)[GlyH]_xH_{3-x}PW_{12}O_{40}$ (x = 1.0-3.0) organic-inorganic hybrid catalysts for the esterification of free fatty acid. All catalysts were characterized by FTIR, TGA, PXRD, ^1H and ^{13}C-NMR, and examined those catalysts for the production of methyl palmitate ester. It has been observed by the ^{31}P-TMPO NMR that $[GlyH]_{1.0}H_{2.0}PW_{12}O_{40}$ gives the highest conversion up to 93.3% and can be reused several times without significant loss of its activity (**Scheme 1.13**).

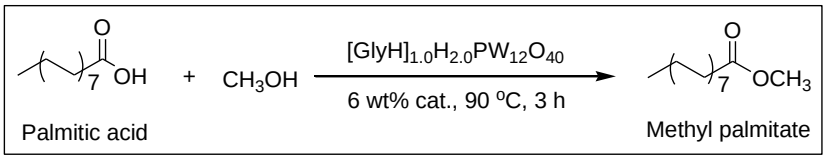

Scheme 1.13

Wang et al. (2017) reported an active catalyst 12-phosphotungstic acid (PTA) modified with 1,2,3-trizaole-4,5-dicarboxylic acid (TDA) for the methyl oleate. TDA-PTA catalyst showed high acidity and efficient catalyst and favored oleic acid esterification with methanol under mild conditions (**Scheme 1.14**).

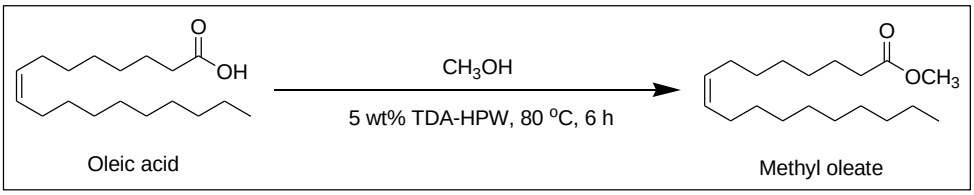

Scheme 1.14

Zhang et al. (2018) reports a series of cerium (Ce^{4+}) containing dodecatungstophosphates catalysts $Ce_xH_{3-3x}PW_{12}O_{40}$ ($Ce_xH_{3-3x}PW$, x=0.4, 0.6, 0.7, 0.8, 0.9, and 1.0). All catalysts were characterized by FTIR, PXRD, pyridine adsorption IR spectra, and examined the catalytic activity biodiesel generation from waste cooking oil (WCO). The $Ce_{0.7}H_{0.9}PW$ showed the best 98% catalytic conversion amongst the $Ce_xH_{3-3x}PW_{12}O_{40}$ series due to the high Bronstead and Lewis acidity (**Scheme 1.15**).

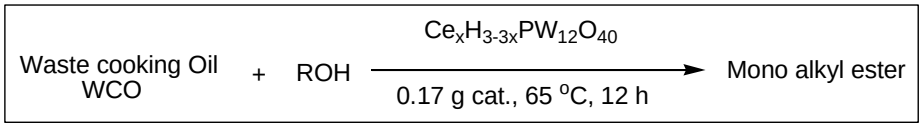

Scheme 1.15

Wang et al. (2018) developed phosphotungstic acid (PTA) combined ionic liquids inorganic-organic hybrid materials, which were further immobilized on SBA-15. The catalyst was used for the esterification of palmitic acid and achieved 88.1% conversion with high catalyst loading (41.2%, 15 wt%) after 8 h reaction at 65 °C. Finally, the catalyst was used up to 5 times without losing its catalytic activity (**Scheme 1.16**).

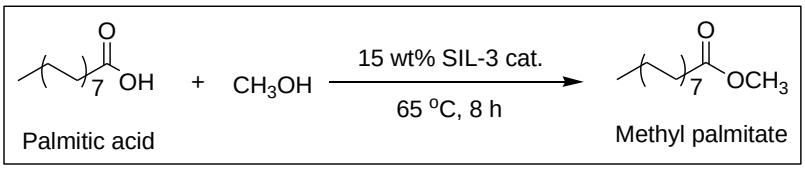

Scheme 1.16

Wang et al. (2019) reported the Poly(ionic liquid) (PIL-3) combined phosphotungstic acid, and its applications in the esterification of palmitic acid and methanol. The best conversion of ester was obtained up to 92% at 65 °C, 8 h of reaction, and 3 wt% of catalyst loading (**Scheme 1.17**).

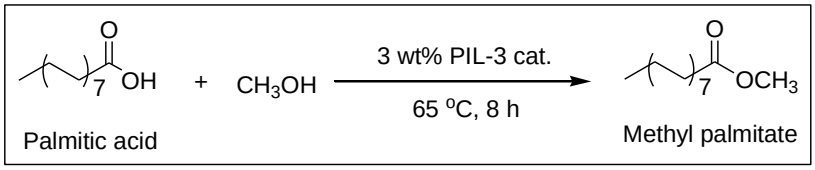

Scheme 1.17

Grunskaya et al. (1998) reported the oxidation of furfural in the presence of sodium molybdate and aqueous hydrogen peroxide. In this process first, the peroxo species of molybdenum was formed, and that oxidized the furfural to produce a mixture of components, e.g., 2(5H)-furanone and tartaric, maleic and succinic acid and obtained 25% of 2(5H)-furanone (**Scheme 1.18**).

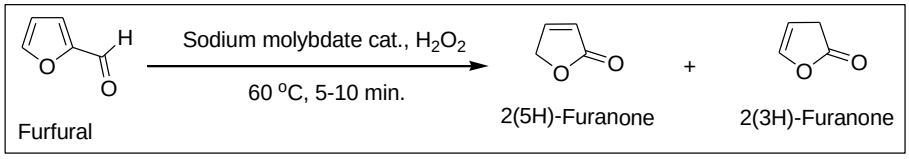

Scheme 1.18

Li et al. (2016) reported the selective oxidation of furfural to 2(5H)-furanone by performic acid, which generated in situ from formic acid and hydrogen peroxide mixture. In the homogeneous system, the yield of 2(5H)-furanone decreased while the yield of Succinic acid increased with an increasing dielectric constant of the solvent (**Scheme 1.19**).

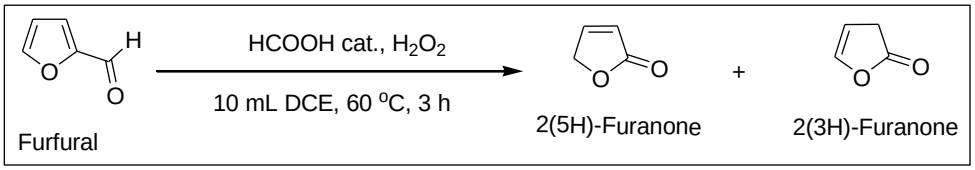

Scheme 1.19

Leng et al. (2009) developed a series of solid organic-inorganic hybrid materials by the combination of propane sulfonate functionalized ILs with Keggin type heteropoly anion. The hybrid catalysts were examined in organic esterification reactions and reused those catalysts atleast seven times without losing their catalytic activities (**Scheme 1.20**).

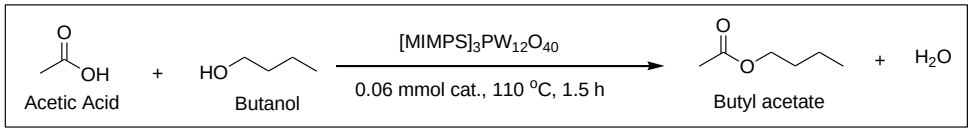

Scheme 1.20

Leng et al. (2012) synthesized SO_3H-functionalized polymeric IL-cations combined Keggin-type heteropoly anions. The catalyst was used for various carboxylic esterification reactions under solvent-free condition. The SO_3H functional groups in the hybrid catalyst account for the excellent catalytic activity, while both the polymeric framework of IL-cation and the large heteropoly anion are responsible for the catalyst's solid nature and in solubility (**Scheme 1.21**).

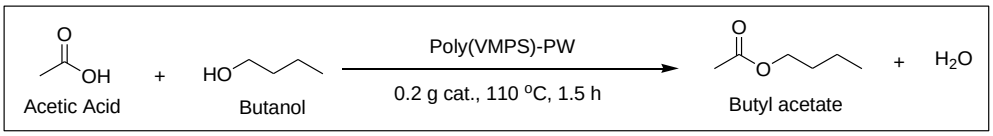

Scheme 1.21

Escobar et al. (2015) reported a series of zirconia-modified PTA catalysts such as $ZrPEGTPA30_{T100}$, $ZrPEGTPA60_{T100}$, $ZrTPA30PEG_{T100}$, and $ZrTPA60PEG_{T100}$ via sol-gel reactions using polyethylene glycol and zirconium isopropoxide as a template. All

those catalysts were characterized by various analytical techniques, e.g., FTIR, BET, ^{31}P-MAS, and potentiometry titration. The ZrPTA30PEG$_{T100}$ catalyst was found to be the most efficient one for the synthesis of n-butyl-2-furoate. Under optimized conditions, e.g., catalyst loading, the mole ratio of 2-furoic acid to n-butanol, and the temperature, the conversion of ester reached to >90% under solvent-free conditions within 24 h at 125 °C using slight excess of the alcohol. The catalysts were reused up to three consecutive cycles without significant loss of activity (**Scheme 1.22**).

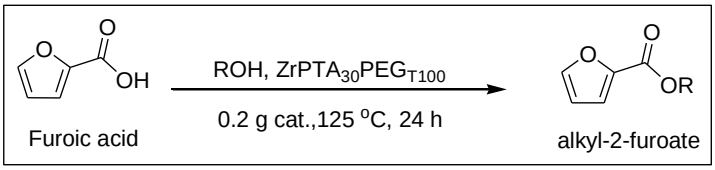

Scheme 1.22

1.10 SCOPE AND OBJECTIVES OF THE PRESENT WORK

Renewable fuels and chemicals produced from biomass are commercially feasible and environmentally friendly alternatives that are made using cheap, abundant, renewable resources. HPA combines the merits of homogeneous and heterogeneous catalysts. It act as an effective homogeneous catalyst during the reaction and is easily separated at the end of the reaction as a heterogeneous catalyst. This work aim is to synthesize HPA supported on novel, inexpensive support, for their use towards different organic transformations reactions (viz. esterification, acetalization, oxidation, and hydrogenation) and synthetic upgrading of furanics and levulinates.

The objectives of the proposed work are as follows:

1. Synthesis and characterization of heteropolyacid-based catalyst.
2. Selective organic transformations such as oxidation, Acetalization, and esterification, by heteropolyacid-based catalyst.

3. Catalytic upgrading of biomass-derived furanic platform chemicals like furfural and Levulinic acid using HPAs as catalysts.
4. Study of recyclability of supported heteropolyacid-based catalyst.

The work was performed to complete the goals set out in the following four chapters.

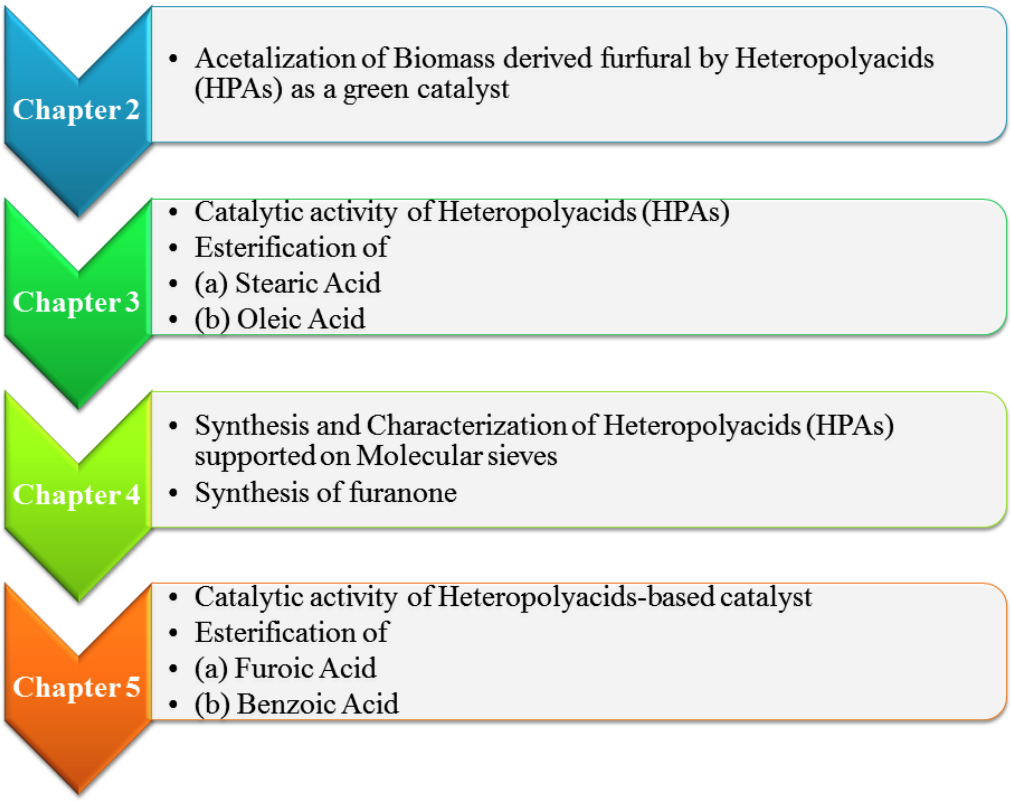

Chapter 2: In this chapter, Keggin-type commercial HPAs have been employed as efficient solid acid catalysts for the acetalization of biomass-derived furfural. A scalable process for the preparation of both open- and cyclic acetals of furfural was developed. The reaction was optimized on parameters such as the type and loading of catalyst, duration of reaction, and ratio of reagents.

Chapter 3: This chapter reports a high-yielding and scalable synthesis of fatty acid esters starting from stearic acid and oleic acid in a closed batch reactor using commercially-available HPA catalysts. The HPAs behaved as a homogeneous catalyst during the

reaction but were made heterogeneous by precipitating at the end of the reaction. The HPA catalyst was recovered and recycled for several cycles without significant loss in mass or activity.

The chapter 3 is divided in to two part, (a) and (b)

Chapter 3 (a): Synthesis of alkyl stearates by esterification of stearic acid.

Chapter 3 (b): Synthesis of alkyl oleates by esterification of oleic acid.

Chapter 4: In this chapter, the catalytic performances of PTA immobilized on ammonium zeolite was evaluated for the selective oxidation of furfural to 2-furanone. The process was scalable, and 2-furanone was isolated in yields up to 40%. The catalyst was prepared by the wet impregnation method and characterized by FTIR, PXRD, and SEM-ICP.

Chapter 5: In this chapter, the synthesis of alkyl benzoates and alkyl-2-furoates from benzoic acid and furoic acid, respectively, is reported. The reactions were performed under solvent-free conditions using HPA catalysts, and the reaction was optimized. The catalysts were successfully recovered and recycled.

The chapter 5 is divided in to two part, (a) and (b)

Chapter 5 (a): Synthesis of alkyl benzoates by esterification of benzoic acid.

Chapter 5 (b): Synthesis of alkyl furoates by esterification of furoic acid.

Chapter 6: The summary and conclusions of the present research work are discussed in this chapter.

CHAPTER 2

A SCALABLE AND HIGH-YIELDING SYNTHESIS OF 2-(2-FURYL)-1,3-DIOXOLANE FROM BIOMASS-DERIVED FURFURAL AND ETHYLENE GLYCOL USING HETEROPOLYACIDS AS GREEN CATALYST

Abstract: *In present work, Keggin-type commercial heteropolyacids (HPAs) have been employed for the first time as efficient solid acid catalysts for the acetalization of biomass-derived furfural with ethylene glycol. The reaction was optimized on parameters such as the type and loading of catalyst, duration of reaction, and the relative ratio of reagents. The reaction was scaled up, and the cyclic acetal 2-(furan-2-yl)-1,3-dioxolane was isolated in 92% yield within 4 h using only 2 wt% of PTA in refluxing benzene.*

2.1 GENERAL INTRODUCTION

Furfural is a well-known renewable chemical building block produced in the hemicellulose fraction of biomass by acid-catalyzed dehydration of pentose sugars (Lange et al. 2012). Furfural and its derivatives are well-documented and have a number of commercial applications as fuel and fuel additives, solvents, chemical feedstock, polymer monomers, agrochemicals, and pharmaceutical products (Serrano-Ruiz et al. 2010). Several high-value commodity chemicals are derived from furfural that includes 2-methylfuran, 2-methyltetrahydrofuran, succinic acid, maleic anhydride, and furfuryl alcohol (Engel et al. 2008; Serrano-Ruiz et al. 2012). The commercial feasibility of these products relies on the scalability of the reaction, process economics, and yield of the product. The processes are often catalytic, and the catalyst plays a crucial role in determining the efficiency of the process. The aldehyde functionality and the furan ring itself are the reaction centers in furfural. The highly reactive aldehyde group may have to be temporarily masked for selective reactions involving the furan ring. Acetalization is a commonly used technique to mask the aldehyde or ketone group during multi-step synthetic transformations.

Cyclic acetals are resistant to nucleophilic attacks, stable in basic and oxidizing reagents, are routinely used in synthetic organic chemistry. Besides, acetals have many unique properties that are suitable for practical industrial applications such as solvents, intermediates, polymers, fragrances, or biofuels (Kochhar et al. 1983; Reddy et al. 2011; Srikrishna and Viswajanani 1995). 2-(2-Furyl)-1,3-dioxolane (**2a**) has been prepared by

reacting furfural and ethylene glycol in the presence of various acid catalysts. Synthesis of **2a** has been attempted using photocatalyst (Yi et al. 2016), acidic ionic liquids (Zhang et al. 2009), metal salts (Aliyan et al. 2010; Yadav et al. 2000), and sulphonic acids (Jin et al. 2014).

Conventionally, the synthesis of acetals (or ketals) invokes homogeneous catalysis using mineral acid catalysts such as H_2SO_4, HCl, and H_3PO_4. However, the acids often lead to poor selectivity, environmental hazards, corrosion of machinery, and issues of catalyst disposal/recycling. The use of excess alcohol reagent and/or continuous removal of the water byproduct ensures a better yield of **2a**. In this regard, HPAs have been used as an efficient and green acid catalyst for a host of organic transformations. HPAs are increasingly being used in the chemistry of renewables (Kozhevnikov 1998; Tsigdinos 1978; Wang and Yang 2015). HPA-based catalysts have desirable properties, including strong acidity, low toxicity, less corrosive nature, well-defined structure, high thermal stability, and tunable solubility (Baker and Glick 1998; Katsoulis 1998; Mizuno and Misono 1998; Srilakshmi et al. 2005). In this work, we report the synthesis of **2a** from furfural and ethylene glycol using commercial HPA catalysts (**Scheme 2.1**). The reaction was optimized on the duration of reaction, type and amount of water removal agent, the ratio of furfural and ethylene glycol, and the loading of HPA catalyst.

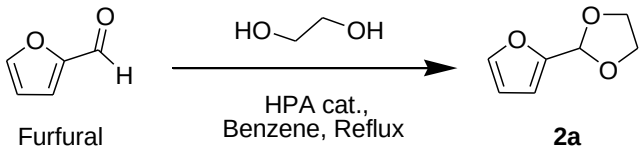

Scheme 2.1 Preparation of **2a** from furfural using HPA catalysts.

Plausible reaction mechanism:

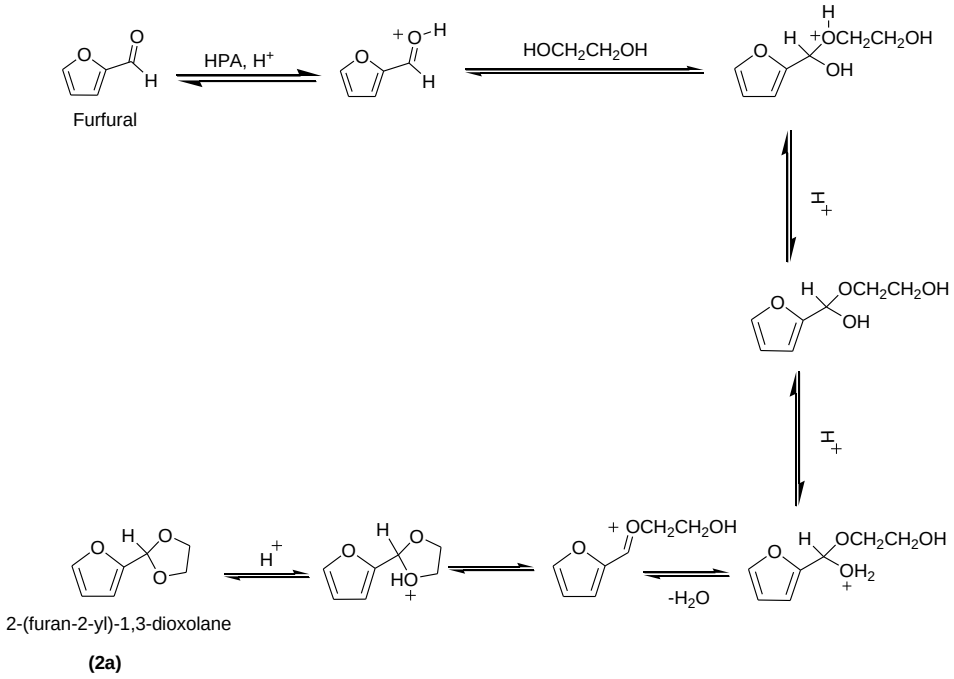

Scheme 2.2 Reaction mechanism for the Acetalization of furfural with ethylene glycol.

2.2 EXPERIMENTAL SECTION

2.2.1 Materials

The catalysts, namely, phosphotungstic acid (PTA), Silicotungstic acid (STA), phosphomolybdic acid (PMA), and silicomolybdic acid (SMA) were purchased from Sigma Aldrich and dried overnight in a hot-air oven at 110 °C before use. Furfural (99%) was purchased from Loba Chemie Pvt. Ltd. and distilled under reduced pressure before use. Benzene (99.5%), ethylene glycol (99%), sodium sulfate (anhydrous), and chloroform (99%) were purchased from Loba Chemie Pvt. Ltd. The solvents were dried over activated molecular sieves (4 Å) prior to use.

2.2.2 Reaction procedure

In a 50 mL round-bottomed flask, furfural (0.500 g, 5.2 mmol), ethylene glycol (0.96 g, 15.4 mmol, 3 eq.), and PTA catalyst (0.010 g, 2 wt%) were added. In the mixture, 20 mL dry benzene and a magnetic stir bar were added. The flask was connected to a Dean-Stark apparatus and placed in a pre-heated oil bath. The reaction mixture was magnetically stirred during the reaction. The progress of the reaction was monitored by TLC and FTIR. After completion of the reaction, the mixture was cooled and filtered. This solid residue on the filter paper containing catalyst was washed with chloroform. The combined solvent was dried over anhydrous Na_2SO_4 and evaporated under reduced pressure in a rotary evaporator. The crude product was chromatographed over silica gel (60-120 mesh, deactivated by triethylamine) using chloroform as eluent. The solvent was evaporated under reduced pressure to provide **2a** (0.670 g, 92%) as a light brown liquid.

2.2.3 Instrument used for the characterization of compounds

FTIR spectra of the samples were collected on a Bruker Alpha FTIR instrument. The FTIR spectrum of samples was collected in the ATR mode and the solid HPA catalysts were collected in the KBr matrix. The ^{1}H-NMR spectra were recorded in a Bruker 400 MHz NMR instrument and the ^{13}C-NMR spectra were recorded in the same instrument in a calculated frequency of 100 MHz.

2.2.3.1 FTIR and NMR (^{1}H and ^{13}C) characterization of 2-(furan-2-yl)-1,3-dioxolane 2a

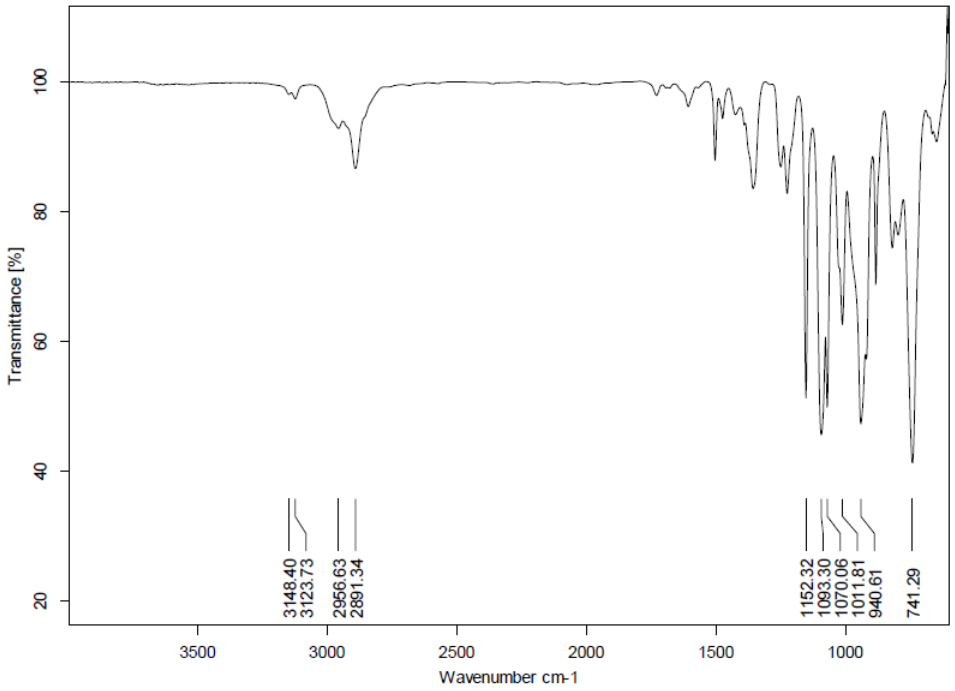

Figure 2.1 FTIR spectrum of 2-(furan-2-yl)-1,3-dioxolane **2a.**

FTIR spectroscopy is a powerful tool that provides conclusive ideas about functional groups present in organic compound. The peaks at 3148 and 3123 cm^{-1} can be attributed to the =C-H stretch in the furan ring of acetal. The peak around 2956 and 2891 cm^{-1} show the stretching vibrations of the sp^3 (-CH) stretching frequency. The characteristic absorption of -C–O stretching frequency is observed in the range of 1000–940 cm^{-1}.

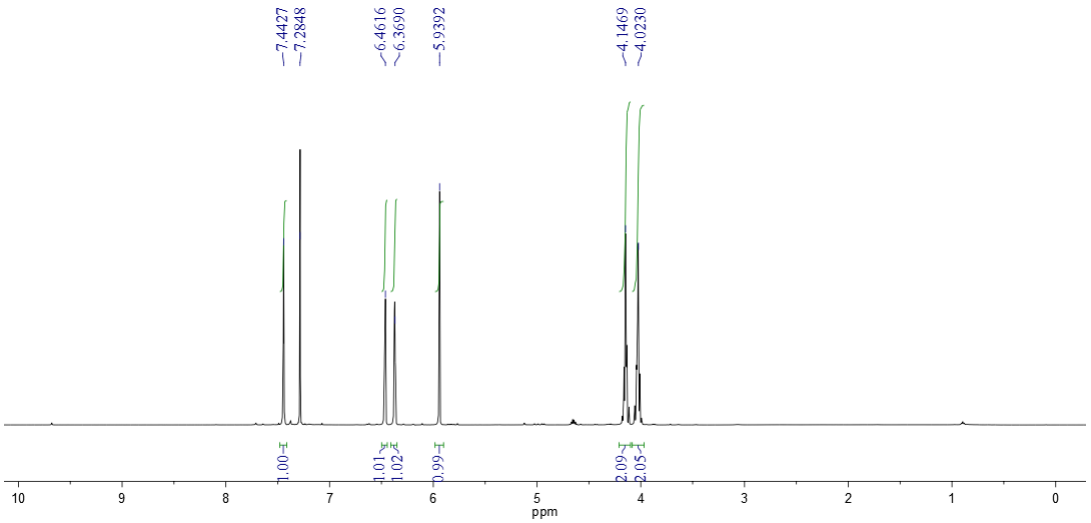

Figure 2.2 ^{1}H-NMR spectrum of 2-(furan-2-yl)-1,3-dioxolane **2a**.

^{1}H-NMR of the isolated acetal shows the 1H singlet peak at 7.4 ppm, the two 1H singlets at 6.44 ppm and 6.3 ppm are due to the furanic proton coupling with each other. The 1H singlet at 5.93 ppm is due to the –C-H proton. The two 2H singlet at 4.15 ppm and 4.02 ppm are due to the protons of CH_2 group.

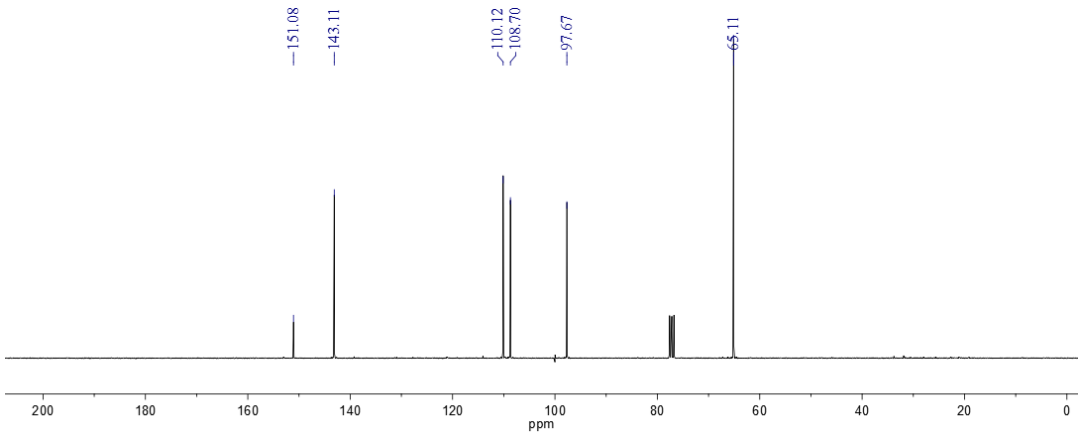

Figure 2.3 ^{13}C-NMR spectrum of 2-(furan-2-yl)-1,3-dioxolane **2a**.

^{13}C-NMR of the isolated cyclic acetal, show the four peaks at 151.1, 143.1, 110.1, and 108.7 ppm are due to the furonic carbon and the peaks at 97.7 ppm is due to acetal carbon attached to the furonic ring. The peak at 65.1 ppm is due to methylene carbon.

2.3 RESULTS AND DISCUSSIONS

The acetalization of furfural with ethylene glycol was performed using HPA catalysts under conventional heating and magnetic stirring. The reaction flask was connected to a Dean-Stark apparatus for azeotropic removal of water byproduct using benzene. Four commercial HPAs, namely, PTA, STA, PMA, and SMA, were examined for their efficiency in producing **2a**. The reaction was monitored by TLC and FTIR spectroscopy, where aliquots were withdrawn at regular intervals and examined for complete conversion of furfural. Conversion of furfural remained low even after overnight reaction using three equivalents of ethylene glycol and 10 wt% of PTA catalyst when the reaction was conducted at room temperature. On the other hand, the reaction completed within 4 h in refluxing benzene using only three equivalents of ethylene glycol and 2 wt% of HPA catalysts. At a shorter reaction time, the conversion of furfural did not reach 100%. The formation of **2a** was not observed in the control reaction without using HPA catalyst. Among the HPAs examined, PTA showed the best catalytic activity providing 92% isolated yield of **2a**, whereas the other three HPA catalysts (i.e., STA, PMA, and SMA) gave only around 70% (**Figure 2.4**). The decomposition of furfural into insoluble humin was observed in all cases but significantly less in the case of PTA, which indirectly supports the observed high yield of **2a**. High yield in PTA may be explained by the relatively stronger acidity of PTA compared to other HPAs examined (Timofeeva 2003). Since the PTA catalyst exhibited the best catalytic performance, it was chosen for further optimizations.

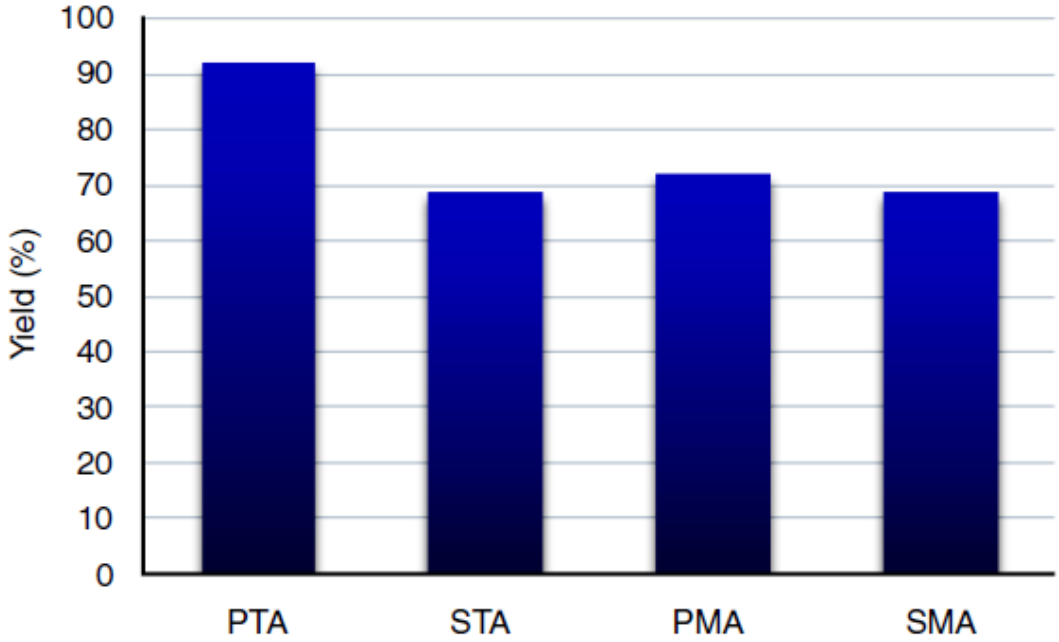

Figure 2.4 Effects of various HPAs catalysts on the yield of 2-(furan-2-yl)-1,3-dioxolane **2a**.

Reaction conditions: Furfural (0.5 g, 5.2 mmol), ethylene glycol (0.96 g, 15.4 mmol, 3 eq.), reflux, 4 h, HPA (0.01 g, 2 wt%), benzene (20 mL).

The loading of PTA catalyst was varied between 1-6 wt% of furfural to study its effect on the yield of **2a** (**Figure 2.5**). Although the reaction completed within 4 h using as little as 1 wt% loading of PTA catalyst, the yield of **2a** was only 85%. Increasing the loading of PTA to 2 wt% increased the yield of **2a** to 92%. However, increasing the loading of PTA further had little effect on the yield of **2a**. The improvement in yield of **2a** between 1-2 wt% loading of PTA catalyst is due to the increase in the number of acidic sites available.

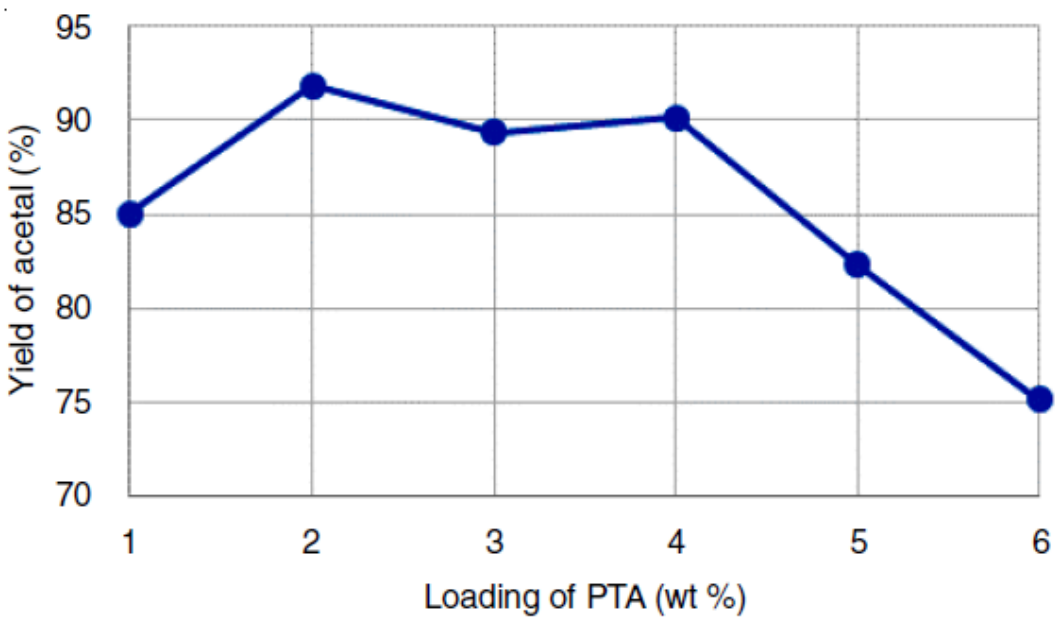

Figure 2.5 Effect of catalyst loading of PTA catalyst on the yield of 2-(furan-2-yl)-1,3-dioxolane **2a**.

Reaction conditions: Furfural (0.5 g, 5.2 mmol), ethylene glycol (0.96 g, 15.4 mmol, 3 eq.), reflux, 4 h, benzene (20 mL).

However, when higher loading of the catalyst was used, the yield of **2a** decreased to 82 and 75% at 5 wt% and 6 wt% of PTA, respectively. This decrease in the yield of **2a** may be due to acid-catalyzed side reactions such as the resinification of furfural. The effect of the molar ratio of furfural and ethylene glycol on the yield of **2a** was also studied. Due to the reversible nature of the acetalization reaction, better yields of acetal are generally obtained in the presence of excess alcohol. However, the use of excess alcohol introduces additional steps of product purification and recovery of unreacted alcohol. Therefore, the effects of the various molar ratios of ethylene glycol over furfural were studied using 2 wt% PTA catalyst in refluxing benzene (**Figure 2.5**). The mole of ethylene glycol was varied between two to five per mole of furfural (**Figure 2.6**). The conversion of furfural was not complete even after 6 h under refluxing benzene when less than two equivalent of ethylene glycol was used. Increasing the ratio from 2:1 to 3:1 increased the yield of **2a** from 79 to 92%. However, a further increase in the equivalent of

ethylene glycol lowered the yield of **2a**. The lowering of the yield of **2a** at more than three equivalent of ethylene glycol may be explained by the dilution of the reactant i.e. there is competitive adsorption on the catalytic sites between furfural and ethylene glycol molecules, and more of ethylene glycol has been adsorbed.

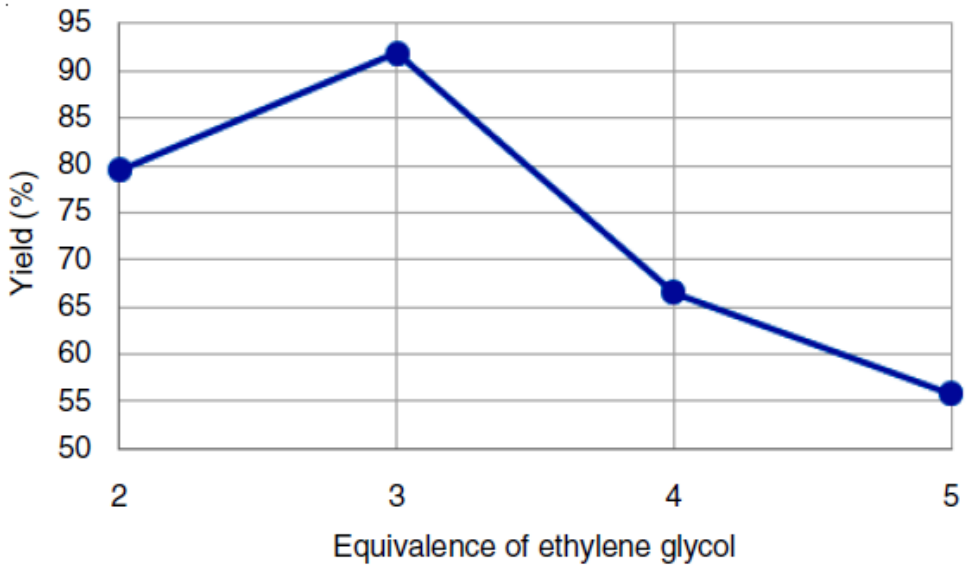

Figure 2.6 Effect of the molar ratio between ethylene glycol and furfural on the isolated yield of 2-(furan-2-yl)-1,3-dioxolane **2a**.

Reaction conditions: Furfural (0.5 g, 5.2 mmol), reflux, 4 h, HPA (0.01 g, 2 wt%), benzene (20 mL).

The efficiency of benzene in removing water from the reaction mixture by azeotropic distillation was compared with other commonly used solvents like cyclohexane and toluene (**Figure 2.7**). Under identical conditions, benzene was found most efficient for the synthesis of **2a**. Whereas toluene behaved better than cyclohexane, it provided a considerably lower yield of **2a** than benzene. Interestingly, without the azeotropic removal of water, the reaction did not complete even after several hours and led to increasing humin formation over time.

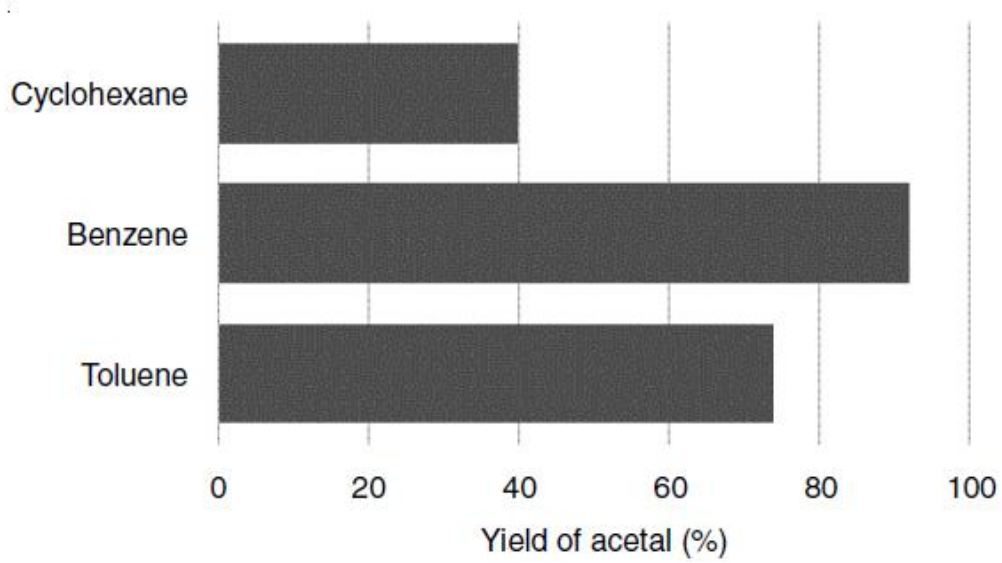

Figure 2.7 Effect of solvent on the yield of 2-(furan-2-yl)-1,3-dioxolane **2a**.

Reaction conditions: Furfural (0.5 g, 5.2 mmol), ethylene glycol (0.96 g, 15.4 mmol, 3 eq.), PTA (0.01 g, 2 wt%), reflux, 4 h, solvent (20 mL)

The amount of benzene was varied to observe its effect on the yield of **2a** (**Figure 2.8**). Whereas less amount of benzene (<15 mL) led to incomplete reaction and poor yields of **2a**, the use of 20 mL benzene provided the best yield. Any higher amounts of benzene dropped the yield of **2a** again due to the dilution effect. The reaction was scaled up to 5 g of furfural. The reaction completed within 4 h in refluxing benzene and provided **2a** in 90% isolated yield.

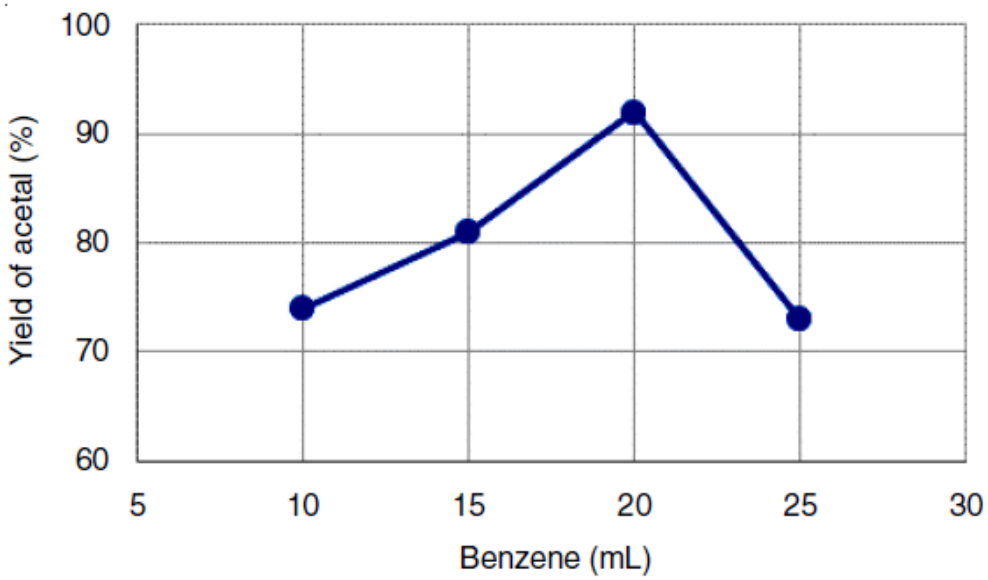

Figure 2.8 Effect of varying quantity of benzene on the yield of 2-(furan-2-yl)-1,3-dioxolane **2a**.

Reaction conditions: Furfural (0.5 g, 5.2 mmol), ethylene glycol (0.96 g, 15.4 mmol, 3 eq.), PTA (0.01 g, 2 wt%), reflux, 4 h.

2.4 CONCLUSION

HPAs have been used as an efficient acid catalyst for the synthesis of 2-(furan-2-yl)-1,3-dioxolane from biomass-derived furfural and ethylene glycol. The cyclic acetal was isolated in 92% yield using a 1:3 molar ratio of furfural and ethylene glycol and only 2 wt% of PTA catalyst. The catalyst was conveniently separated from the reaction mixture by exploiting the differential solubility of HPA catalysts.

CHAPTER 3

SOLVENT-FREE AND SCALABLE PREPARATION OF ALKYL STEARATES AND ALKYL OLEATES FROM FREE FATTY ACIDS USING HETEROPOLYACIDS AS EFFICIENT AND RECYCLABLE CATALYST

Abstract: *This study reports a high-yielding and scalable synthesis of fatty acid esters from stearic acid and oleic acid within a closed batch reactor using commercially-available heteropolyacid catalysts. The reaction was optimized on temperature, molar ratio of fatty acid and alkyl alcohol, and the loading of catalyst. The solvent-free, gram-scale reactions afforded >95% yield of alkyl stearates and >85% yield of alkyl oleates under the optimized conditions (1 mol% phosphotungstic acid (PTA) catalyst, 110* °C*, 4 h for alkyl stearates and 0.2 mol% PTA catalyst, 120* °C*, 4 h for alkyl oleates) by using only slight excess of the alcohol reagent. The PTA catalyst was successfully recovered and reused for five consecutive cycles without significant loss in mass and activity.*

3.1 INTRODUCTION

Acid-catalyzed esterification of carboxylic acids is one of the most versatile chemical transformation in synthetic organic chemistry (Otera and Nishikido 2009). Fatty acid esters are an important class of compound with significant commercial markets as fuels and fuel additives, plasticizers, surfactants, solvents, lubricants, and pharmaceuticals (Aoshima et al. 2005; Baker et al. 2000; Cavalcanti et al. 2018; Greenspan and Gall 1953; Knothe and Steidley 2011; Meffert 1984). Biodiesel, a bio-renewable substitute for petro-diesel, is a cleaner fuel that consists of methyl- or ethyl esters of fatty acids resulting from either the transesterification of triglycerides or the esterification of free fatty acids (FFA) (Leung et al. 2010; Lin and Lin 2012; Meher et al. 2006; Thiruvengadaravi et al. 2012). In recent years, the use of abundant, inexpensive, and preferably waste oils and fats are being preferred as feedstock for biodiesel production (Sadaf et al. 2018; Talebian-Kiakalaieh et al. 2013). However, inexpensive oily feedstock and waste oils such as used cooking oils have a significant proportion of FAA that lead to soap formation during the base-catalyzed trans-esterification reaction (Canakci 2007; Srilatha et al. 2010). Therefore, acid-catalyzed esterification could be a viable alternative for biodiesel production from FFA-rich feedstock (Lotero et al. 2005). Fatty acid esters have also been used as renewable feedstock for the production of diesel-range hydrocarbon fuels by catalytic decarboxylation or hydrodeoxygenation (Mäki-

Arvela et al. 2007; Santillan-Jimenez et al. 2013). The fatty acid esters are also used as crucial chemical intermediates for the synthesis of several high-value products such as amides, sulphonates, fatty alcohols and novel waxes with applications as solvent, softening agents in polymers, textile, cosmetic, and rubber industries (Miyake et al. 2009; Rieke et al. 1997; Xie et al. 2013; Zhang et al. 2014). The acid catalysts examined for the esterification of fatty acids include Brönsted acids, Lewis acids, and various solid acid catalysts (D'Oca et al. 2012b; Hanif et al. 2017; He et al. 2013; Marchetti and Errazu 2008; Park et al. 2010; Rezende and Pinto 2016; Vieira et al. 2013). However, some major issues associated to acid-catalyzed esterification include corrosive nature of the acid catalysts, high volatility and toxicity, and difficulty in recycling. In this regard, heteropolyacids (HPAs) are well-structured metal-oxide clusters with strong Brönsted acidity, low volatility, less corrosiveness, and tunable solubility (Herrmann et al. 2015; Srilatha et al. 2011). HPAs have been used over the past several years as efficient and environment-friendly catalysts for various synthetic organic transformations including esterification, acylation, alkylation, oxidation, etherification, condensation, hydrolysis, and dehydration reactions (Heravi et al. 2013; Kozhevnikov 1998; Ren et al. 2010).

However, homogeneous HPAs have limitations to be used as catalyst including poor thermal stability, high solubility in polar solvents, and low surface area. Therefore, HPAs may be made heterogeneous by anchoring them on various heterogeneous supports such as silica, alumina, clay, and zeolite (Lee et al. 2014). The thermal stability and surface area of the catalysts increase substantially in the supported catalysts. HPAs are increasingly being used in the chemocatalytic valorization of biomass and sustainable chemistry in general (Onkarappa et al. 2019; Ren et al. 2015; Zhang et al. 2016b). Interestingly, the use of HPA catalysts have also been reported for the preparation of fatty acid esters (Caetano et al. 2008; Cardoso et al. 2008; Castanheiro et al. 2017; de Godói Silva et al. 2010). The esterification reactions are routinely carried out using the Fischer esterification protocol where carboxylic acid is refluxed with a large excess of the alcohol reagent in the presence of HPA catalyst. The esterification of oleic acid (OA) with methanol was attempted over a PTA catalyst supported on SBA-15 where 90%

conversion of oleic acid was achieved after 4 h at 40 °C (Brahmkhatri and Patel 2011). Ethyl stearate was prepared in 84% yield by refluxing stearic acid in excess ethanol (50 equivalents) for 10 h in the presence of 11 mol% of PTA catalyst (Cardoso et al. 2008). Excess alcohol favors the reaction equilibrium towards ester formation and compensate for the evaporative loss during refluxing. However, the use of excess alcohol introduces additional steps in the purification of product and recovery of the catalyst. Moreover, long reaction time and higher loading of the acid-catalyst are often required when using large excess of alochol. We envisaged that using a closed pressure vessel for the reaction would stop the evaporative loss of the alcohol reagent and allow achieving temperatures higher the boiling point of alcohol ensuring faster kinetics. The use of near equivalent amount of the alcohol reagent would also help lower the catalyst loading, the product separation, and the catalyst recovery.

This chapter discusses the high-yielding preparation of fatty acid esters from stearic acid (a saturated fatty acid) and oleic acid (an unsaturated fatty acid) over commercially-available HPA catalysts (**Scheme 3.1**). The reactions were carried out in batch-type glass pressure reactor to avoid evaporative loss of alcohol during the course of reaction.

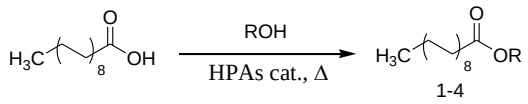

methyl stearate (**3a,** R=CH_3); ethyl stearate (**3b**, R=C_2H_5); propyl stearate (**3c**, R=n-C_3H_7); butyl stearate (**3d**, R=n-C_4H_9)

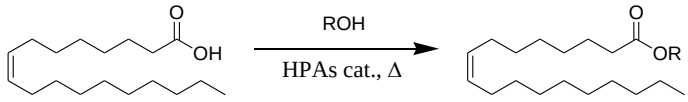

methyl oleate (**3e**, R=CH_3); ethyl oleate (**3f**, R=C_2H_5); propyl oleate (**3g**, R=n-C_3H_7); butyl oleate (**3h**, R=n-C_4H_9), pentyl oleate (**3i**, R=n-C_5H_{11}), hexyl oleate (**3j**, R=n-C_6H_{13})

Scheme 3.1 Preparation of (a) alkyl stearates from stearic acid and b) alkyl oleates from oleic acid using the HPA catalysts.

The esterification reaction of fatty acid was optimized on parameters such as reaction temperature, duration of reaction, type and loading of HPA catalyst, and molar ratio of fatty acid to alcohols for the best yield of fatty acid ester. The recoverability and recyclability of the HPA catalyst were also studied.

3.2 EXPERIMENTAL SECTION

3.2.1 Materials

Stearic acid (98%) and oleic acid (99%) were purchased from Otto Synthesis Private Limited and Spectrochem Private Limited, respectively. Methanol (99.5%), ethanol (99%), 1-propanol (99.5%), 1-butanol (99%), petroleum ether (99%), and chloroform (99%) were purchased from Loba Chemie. Phosphotungstic acid (PTA, $H_3PW_{12}O_{40}$), Silicotungstic acid (STA, $H_4SiW_{12}O_{40}$) and Phosphomolybdic acid (PMA, $H_3PMo_{12}O_{40}$) were purchased from Sigma. Stearic acid and oleic acid were used as received without further purifications. The alcohols were used after overnight drying over pre-activated molecular sieves (4 Å). The catalysts were dried at 110 °C for 12 h in a hot-air oven prior use.

3.2.2 Catalytic reactions (A): Esterification of stearic acids over HPA catalysts

A typical procedure for the esterification of stearic acid is as follows: Stearic acid (1.00 g, 3.51 mmol) and 1-propanol (0.316 g, 5.27 mmol, 1.5 eq.) were charged into a round-bottomed glass pressure reactor (100 mL) fitted with a magnetic stir bar and a Teflon screw-top. Anhydrous PTA (101 mg, 1 mol%) was weighed in air and added to the solution. The reactor was sealed, placed in a pre-heated oil bath, and stirred magnetically for 4 h. After reaction, the reactor was cooled down to room temperature and opened. Petroleum ether (10 mL) was added into the mixture and the product was solubilized. The catalyst was precipitated and centrifuged the reaction mixture to get colourless supernatant. The colourless supernatant was carefully decanted into a beaker. The precipitated catalyst was

washed with petroleum ether (3×10mL). The petroleum ether layers were combined, dried over anhydrous Na_2SO_4, and evaporated under reduced pressure in a rotary evaporator to obtain crude propyl stearate **3c**. The crude mixture was chromatographed (silica gel, petroleum ether) to get purified **3c** (1.120 g, 98%) as a clear liquid. The reaction flask with wet catalyst was placed in a hot-air oven and heated at 110 °C for 12 h. Mass of the dried PTA catalyst was measured before using it in the next catalytic cycle.

3.2.3 Instrument used for the characterization of compounds

FTIR spectra of the samples were collected on a Bruker Alpha FTIR instrument. The FTIR spectrum of samples was collected in the ATR mode and the solid HPA catalysts were collected in the KBr matrix. The ^{1}H-NMR spectra were recorded in a Bruker 400 MHz NMR instrument and the ^{13}C-NMR spectra were recorded in the same instrument in a calculated frequency of 100 MHz.

3.2.3.1 FTIR and NMR (^{1}H and ^{13}C) characterization of methyl stearate 3a

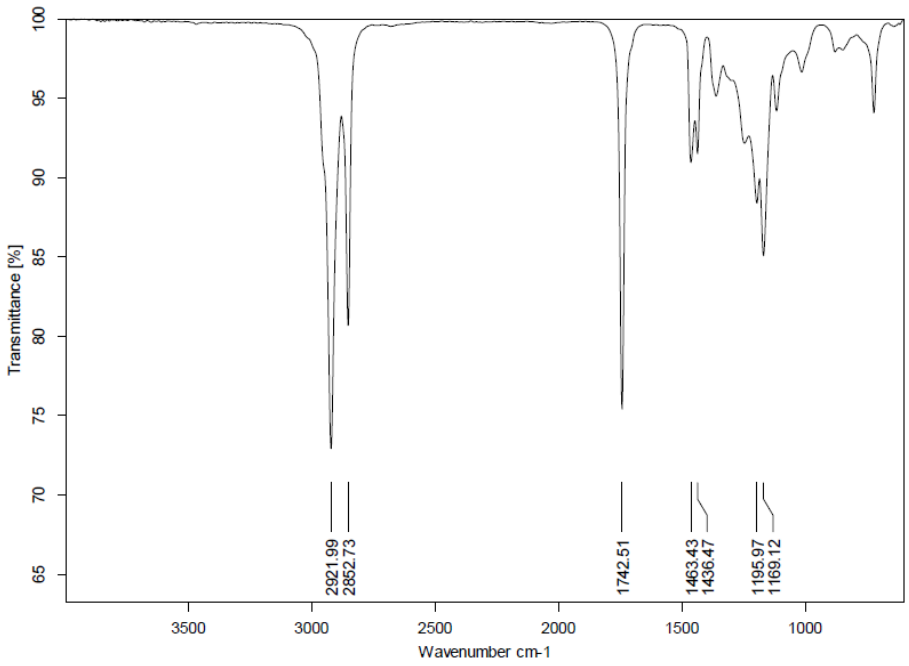

Figure 3.1 FTIR spectrum of methyl stearate **3a**.

The peak at 2921 and 2852 cm^{-1} is responsible for the sp^3 -C-H stretching frequency. The peak at 1742.51 cm^{-1}corresponds to the ester C=O stretching frequency and 1169 cm^{-1} is due to C-O strecting frequency of ester group.

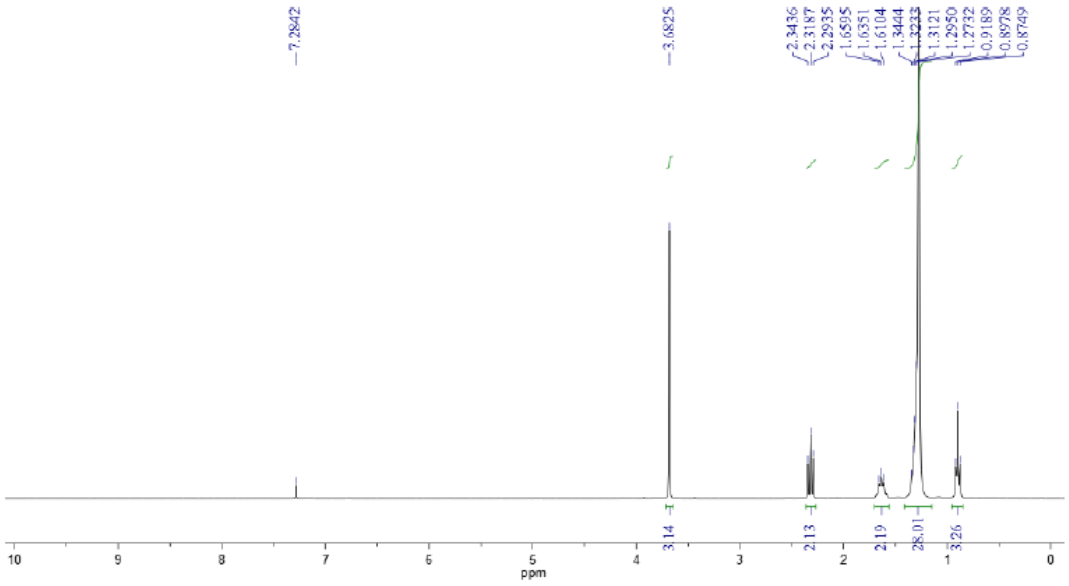

Figure 3.2 ^{1}H-NMR spectrum of methyl stearate **3a**.

^{1}H-NMR of the isolated methyl stearate shows the 3H singlet peak at 3.14 ppm is due to -OCH_2 protons. The 2H triplet at 2.31 ppm is due to the -CH_2 proton directly attached to ester carbon. The 2H triplet, 28H multiplet and 3H triplet at 1.63 ppm, 1.31 ppm and 0.89 ppm respectively are due to the -CH_2-$(CH_2)_{14}$-CH_3 protons.

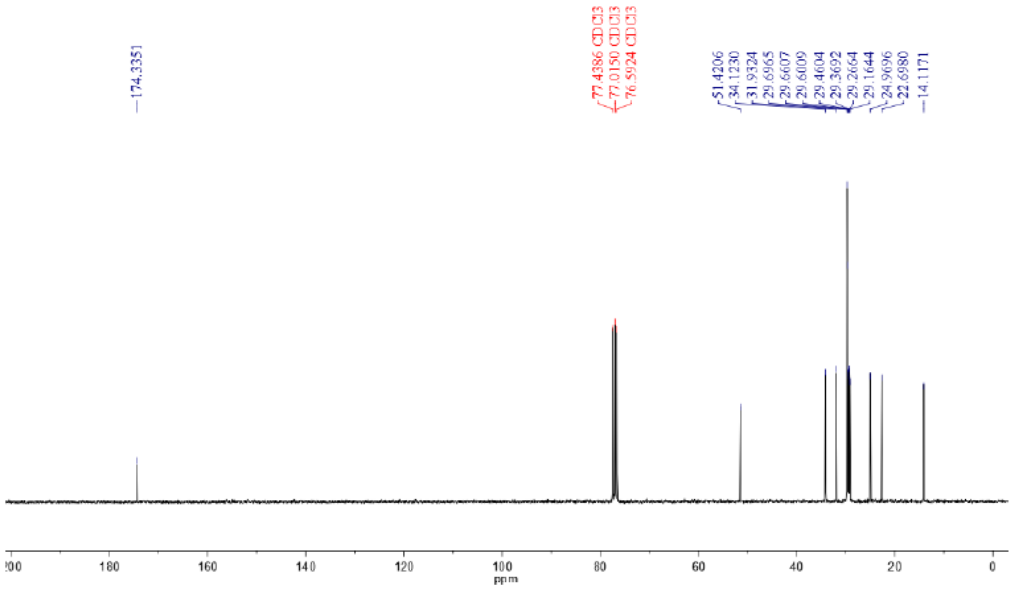

Figure 3.3 ^{13}C-NMR spectrum of methyl stearate **3a**.

^{13}C-NMR of the isolated methyl stearate, show the peaks at 174.2 ppm are due to the C=O of ester carbon, the peaks at 51.4 is due to O-CH_3 carbon attached to the ester group. The peaks at 34.1-22.7 are due to methylene carbon and 14.1 of is due to CH_3 carbon.

3.2.3.2 FTIR and NMR (^{1}H and ^{13}C) characterization of ethyl stearate 3b

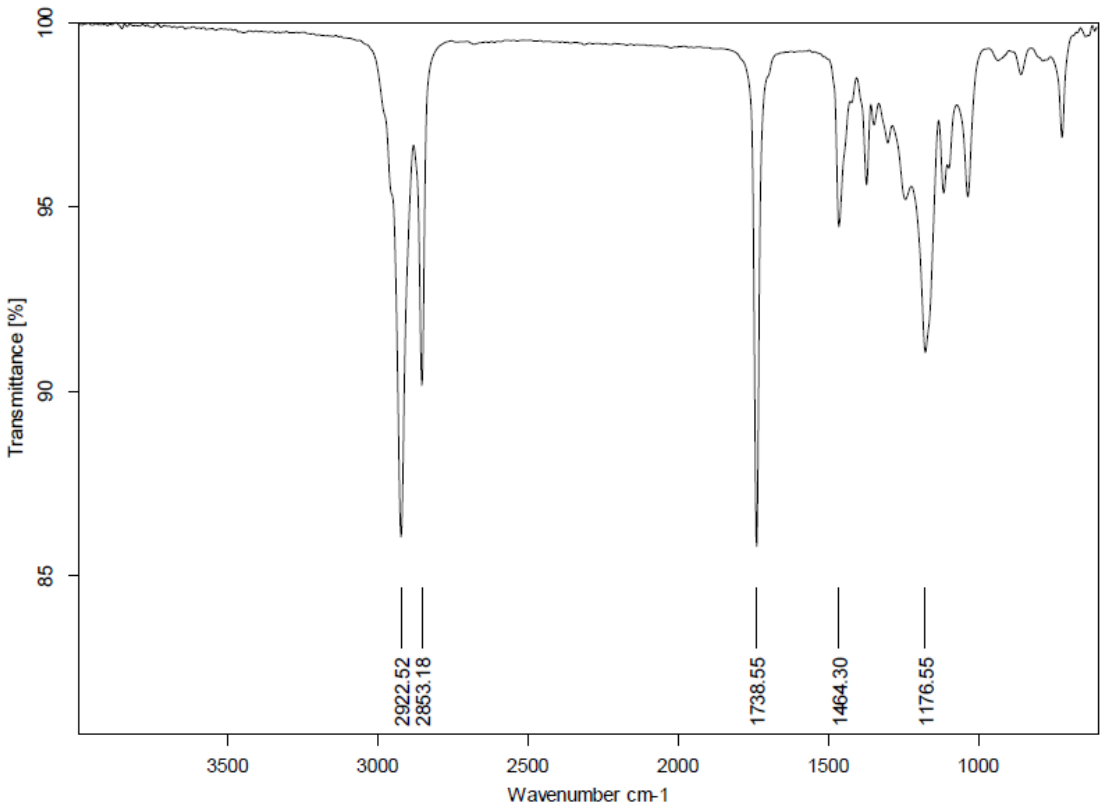

Figure 3.4 FTIR spectrum of ethyl stearate **3b**.

The peak at 2922 and 2853 cm^{-1} is responsible for the sp^3 -C-H stretching frequency. The peak at 1738 cm^{-1}corresponds to the ester C=O stretching frequency and 1176 cm^{-1} is due to C-O stretching frequency of ester group.

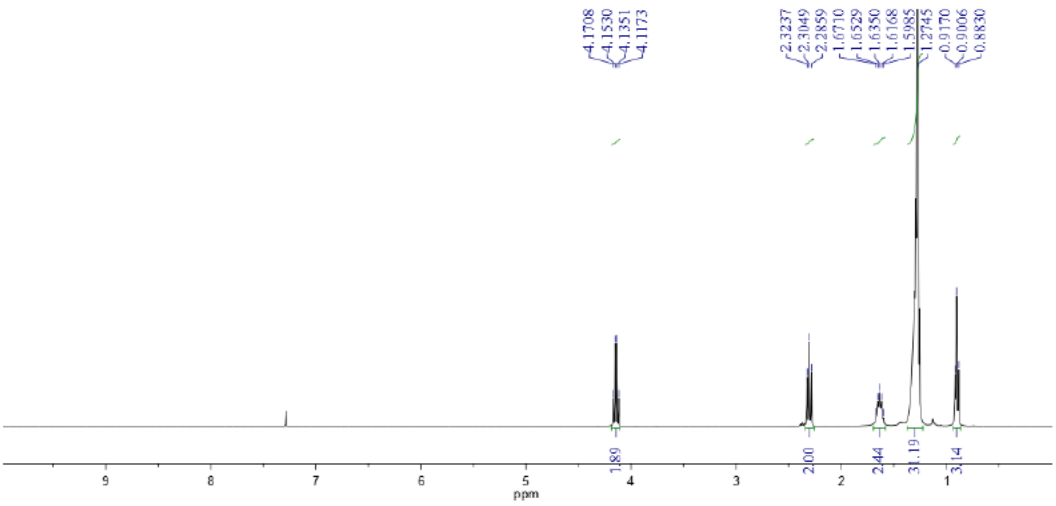

Figure 3.5 ^{1}H-NMR spectrum of ethyl stearate **3b**.

^{1}H-NMR of the isolated ethyl stearate shows the 2H quartet peak at 4.15 ppm and 3H triplet peak at 0.90 ppm are due to -OCH_2CH_3 protons, respectively. The 2H triplet at 2.32 ppm is due to the -CH_2 proton directly attached to ester carbon. The 2H multiplet and 31H multiplet at 1.63 ppm and 1.27 ppm, respectively are due to the -CH_2-$(CH_2)_{31}$ protons.

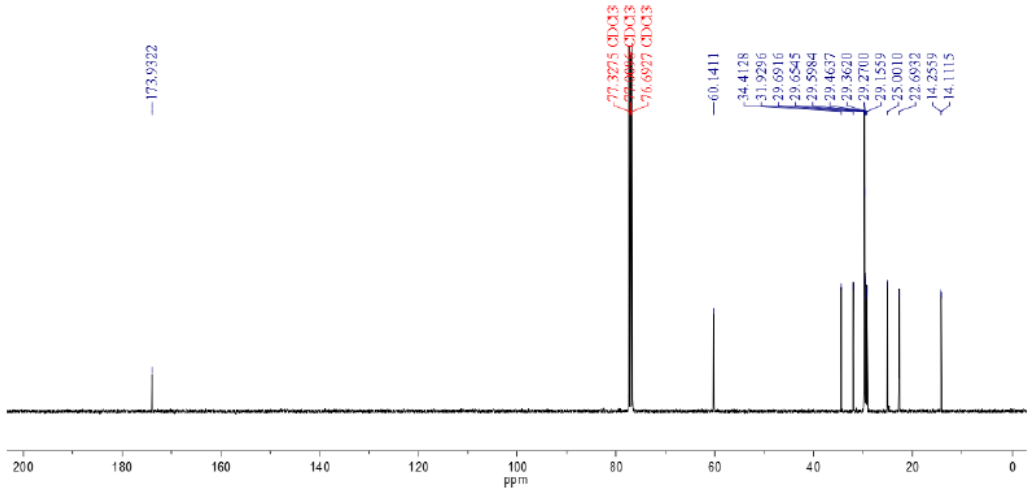

Figure 3.6 ^{13}C-NMR spectrum of ethyl stearate **3b**.

^{13}C-NMR of the isolated ethyl stearate, show the peaks at 173.9 ppm are due to the C=O of ester carbon, the peaks at 60.1 ppm and 14.2 ppm are due to O-CH_2CH_3 carbon attached to the ester group. The peaks at 34.4-22.7 ppm are due to methylene carbon and 14.1 ppm of is due to CH_3 carbon.

3.2.3.3 FTIR and NMR (^{1}H and ^{13}C) characterization of propyl stearate 3c

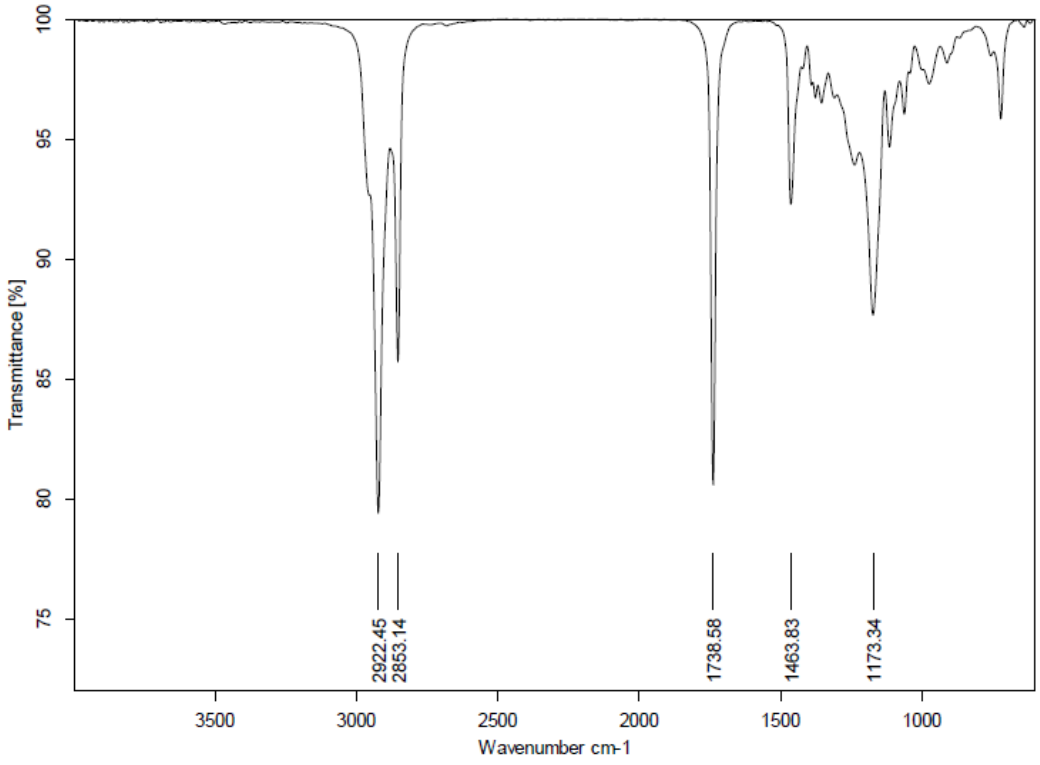

Figure 3.7 FTIR spectrum of propyl stearate **3c**.

The peak at 2922 and 2853 cm^{-1} is responsible for the sp^3 -C-H stretching frequency. The peak at 1738 cm^{-1}corresponds to the ester C=O stretching frequency and 1173 cm^{-1} is due to C-O stretching frequency of ester group.

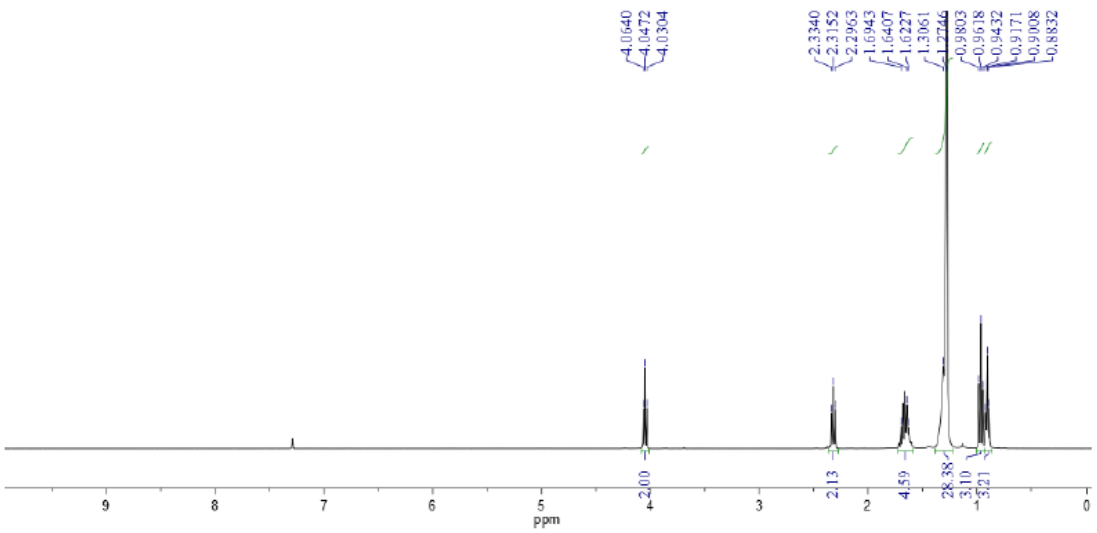

Figure 3.8 ^{1}H-NMR spectrum of propyl stearate **3c**.

^{1}H-NMR of the isolated propyl stearate shows the 2H triplet peak at 4.05 ppm is due to -OCH_2 protons. The 2H triplet at 2.31 ppm, 4H at 1.64 ppm is due to the -CH_2 protons and 3H protons at 0.96 ppm due to -CH_3 protons. The 28H multiplet and 3H triplet at 1.27 ppm and 0.90 ppm respectively are due to the -$(CH_2)_{14}$-CH_3 protons.

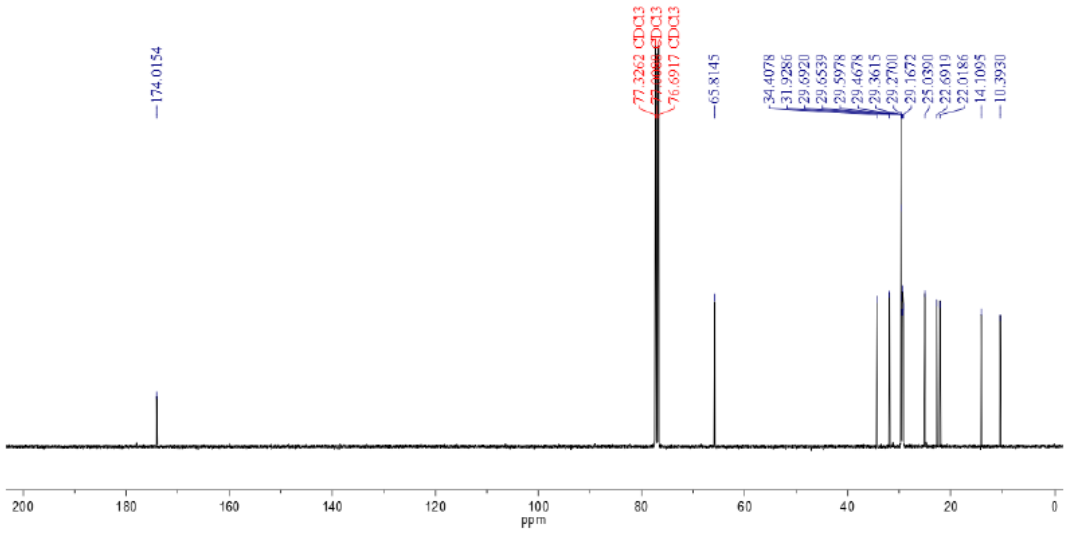

Figure 3.9 ^{13}C-NMR spectrum of propyl stearate **3c**.

^{13}C-NMR of the isolated methyl stearate, show the peaks at 174.0 ppm are due to the C=O of ester carbon, the peaks at 65.8 ppm is due to O-CH_2- carbon attached to the ester group. The peaks at 34.4-22.0 ppm are due to methylene carbon and 14.1 ppm and 10.4 ppm of is due to CH_3 carbon.

3.2.3.4 FTIR and NMR (^{1}H and ^{13}C) characterization of butyl stearate 3d

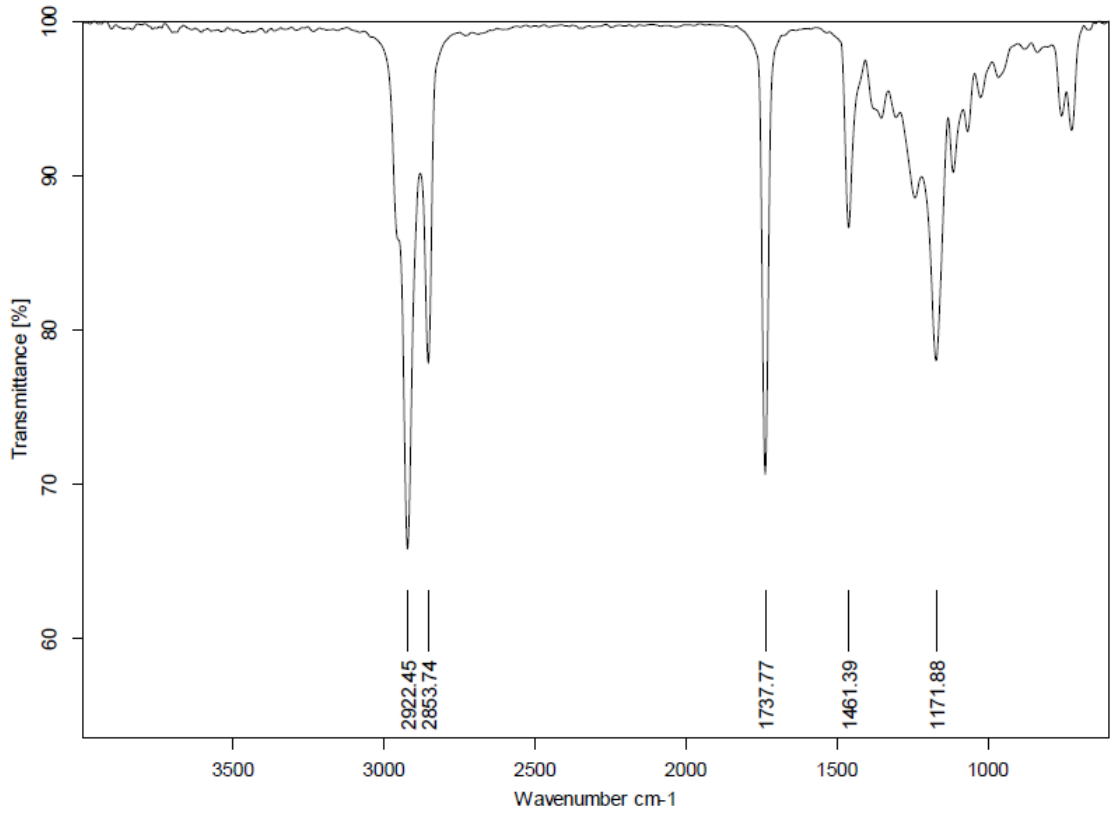

Figure 3.10 FTIR spectrum of butyl stearate **3d**.

The peak at 2922 and 2854 cm^{-1} is responsible for the sp^3 -C-H stretching frequency. The peak at 1737 cm^{-1}corresponds to the ester C=O stretching frequency and 1172 cm^{-1} is due to C-O stretching frequency of ester group.

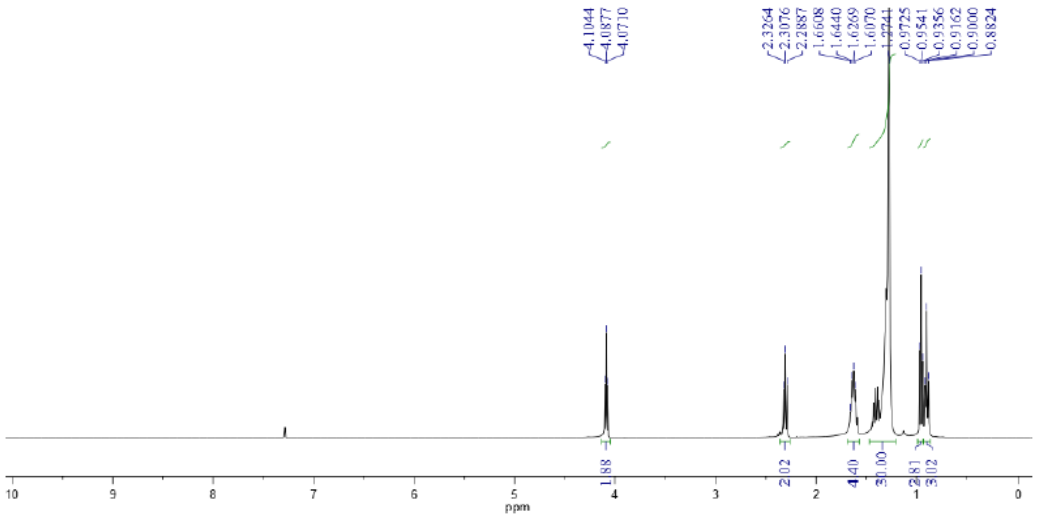

Figure 3.11 ^{1}H-NMR spectrum of butyl stearate **3d**.

^{1}H-NMR of the isolated butyl stearate shows the 2H triplet peak at 4.09 ppm is due to -OCH_2 protons. The 2H triplet at 2.31 ppm, 4H at 1.63 ppm is due to the -CH_2 protons and 3H protons at 0.95 ppm due to -CH_3 protons. The 30H multiplet at 1.27 ppm and 3H triplet at 0.90 ppm are due to the -$(CH_2)_{15}$-CH_3 protons.

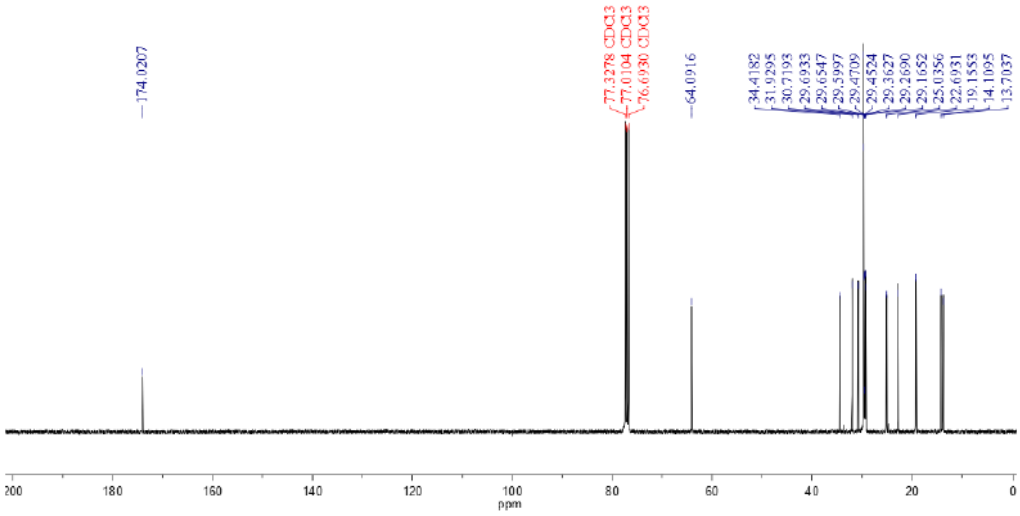

Figure 3.12 ^{13}C-NMR spectrum of butyl stearate **3d**.

^{13}C-NMR of the isolated methyl stearate, show the peaks at 174.0 ppm are due to the C=O of ester carbon, the peaks at 64.1 ppm is due to O-CH_2- carbon attached to the ester group. The peaks at 34.4-19.1 ppm are due to methylene carbon and 14.1 ppm and 103.7 ppm of are due to CH_3 carbon.

3.2.4 Catalytic reactions (B): Esterification of oleic acid over HPAs catalysts

Typical procedure for the esterification of Oleic acid: Oleic acid (1.00 g, 3.54 mmol) and a 1-butanol (0.39 g, 5.26 mmol, 1.5 eq.) were charged into a round-bottomed glass pressure reactor (100 mL) fitted with a magnetic stir rod and Teflon screw top. Oven-dried PTA (20 mg, 0.2 mol%) was weighed in air and added to the solution. The reactor was sealed and placed in a pre-heated oil bath and stirred magnetically for 4 h. After reaction, the reactor was cooled to room temperature and opened. Then petroleum ether (10 mL) was added into mixture and carefully decanted into a beaker and again two times washed with petroleum ether (10 mL), dried over anhydrous Na_2SO_4. The precipitate was washed with petroleum ether (2×10 mL). The petroleum ether layers were combined, dried over anhydrous Na_2SO_4, and evaporated under reduced pressure in a rotary evaporator to obtain colourless oil. The crude mixture was chromatographed (silica gel, petroleum ether) and the solvent was evaporated to get butyl oleate **3h** (2.108 g, 85%) as a clear liquid.

3.2.5 Instrument used for the characterization of compounds

FTIR spectra of the samples were collected on a Bruker Alpha FTIR instrument. The FTIR spectrum of samples was collected in the ATR mode and the solid HPA catalysts were collected in the KBr matrix. The ^{1}H-NMR spectra were recorded in a Bruker 300 MHz NMR instrument and the ^{13}C-NMR spectra were recorded in the same instrument in a calculated frequency of 75 MHz.

3.2.5.1 FTIR and NMR (^{1}H and ^{13}C) characterization of methyl oleate 3e

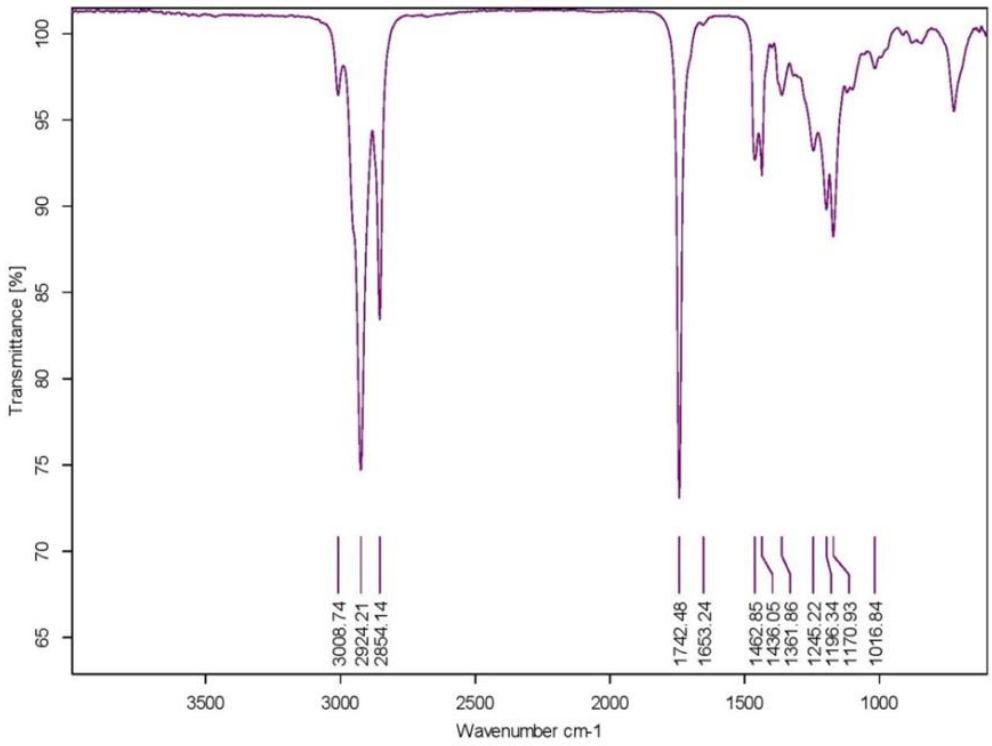

Figure 3.13 FTIR spectrum of methyl oleate **3e**.

The peak at 3008 cm^{-1} is due to sp^2 –C-H stretching frequency and the peak at 2924 and 2854 cm^{-1} is responsible for the sp^3 -C-H stretching frequency. The peak at 1742.48 cm^{-1}corresponds to the ester C=O stretching frequency, 1653 cm^{-1} is due to C=C stretching frequency and 1170 cm^{-1} is due to C-O strecting frequency of ester group.

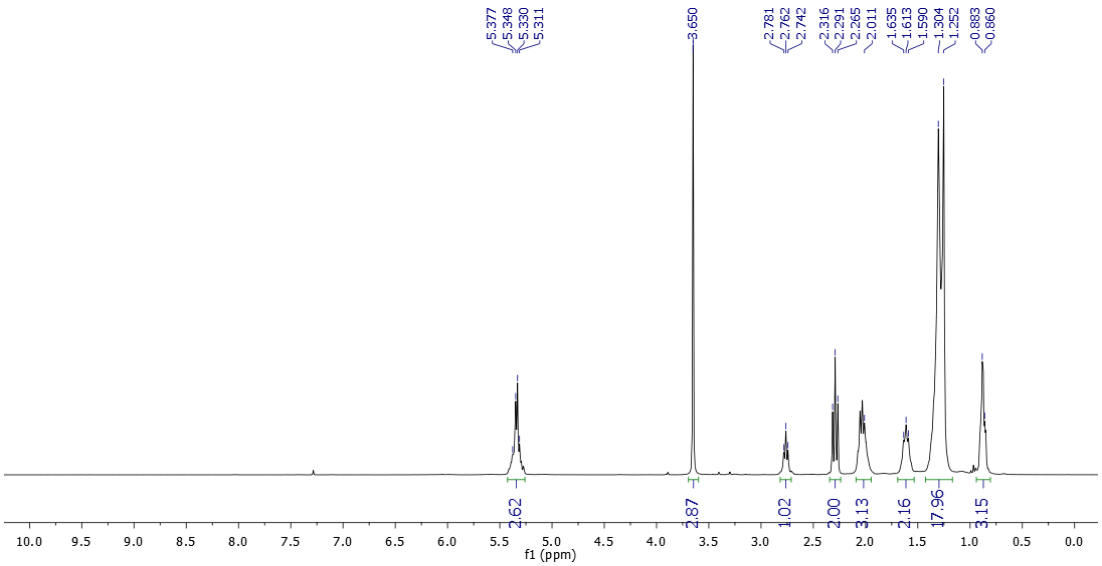

Figure 3.14 ^{1}H-NMR spectrum of methyl oleate **3e**.

^{1}H-NMR of the isolated methyl oleate show the 2H quartet is due to olefinic protons of oleate. The 3H singlet at 3.65 is due to to protons of methoxy (-OCH_3) group. The 29H resonating peaks in the range of 2.78-0.86 ppm are due to the aliphatic oleate protons.

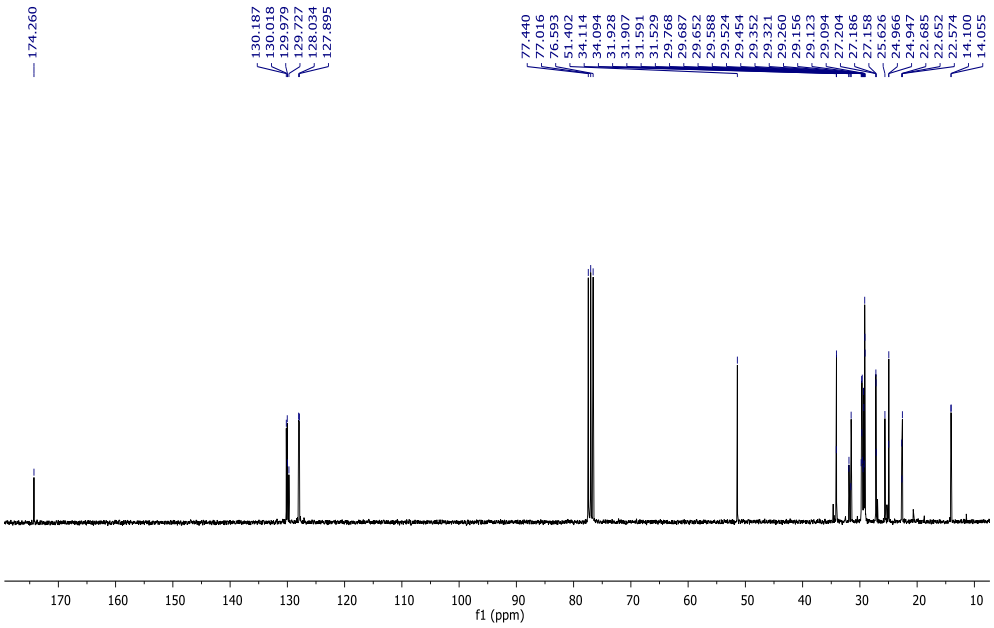

Figure 3.15 ^{13}C-NMR spectrum of methyl oleate **3e**.

^{13}C-NMR of the isolated methyl oleate, show the peaks at 174.2 ppm are due to the C=O of ester carbon, the peaks at 130.0 ppm and 128.0 ppm are due to oleifinic carbon and the peaks at 51.4 ppm is due to O-CH_3 carbon attached to the ester group. The peaks at 34.1-22.5 ppm are due to methylene carbon and 14.1 ppm of is due to CH_3 carbon.

3.2.5.2 FTIR and NMR (^{1}H and ^{13}C) characterization of ethyl oleate 3f

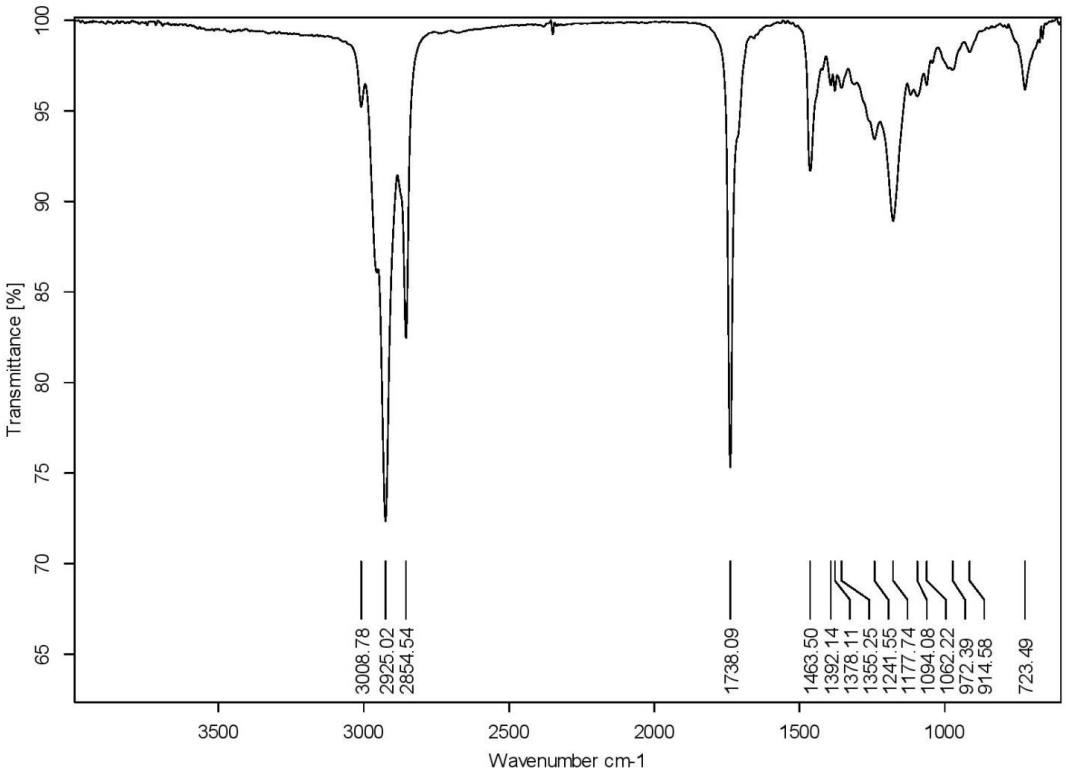

Figure 3.16 FTIR spectrum of ethyl oleate **3f**.

The peak at 3008 cm^{-1} is due to sp^2 –C-H stretching frequency and the peak at 2925 and 2854 cm^{-1} is responsible for the sp^3 -C-H stretching frequency. The peak at 1738 cm^{-1}corresponds to the ester C=O stretching frequency and 1177 cm^{-1} is due to C-O stretching frequency of ester group.

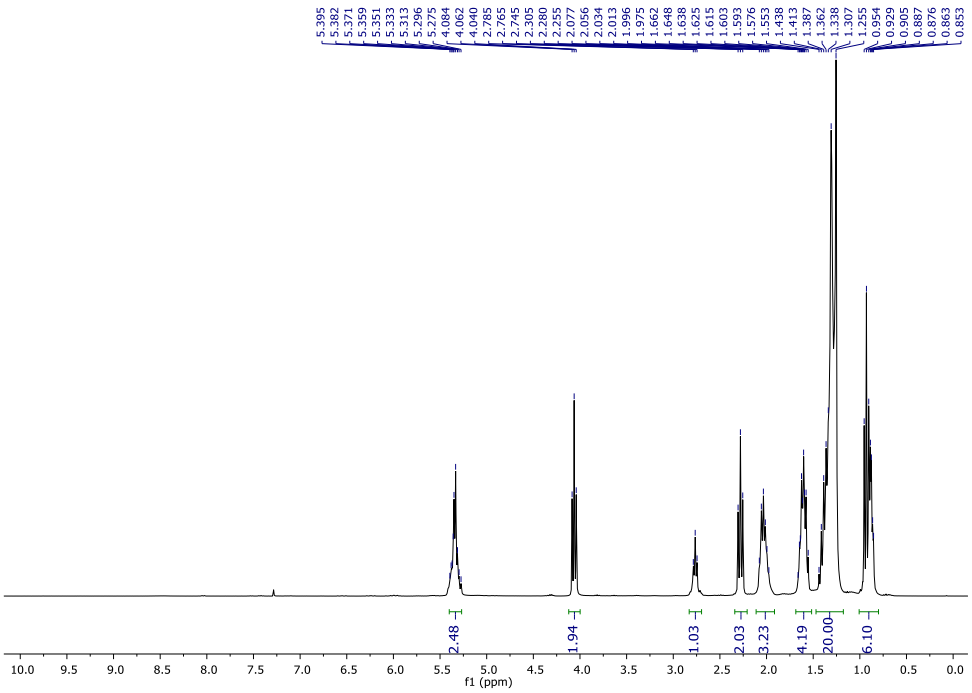

Figure 3.17 ^{1}H-NMR spectrum of ethyl oleate **3f**.

^{1}H-NMR of the isolated ethyl oleate show the 2H multiplet is due to olefinic protons of oleate. The 2H quartet at 4.11 ppm and 3H triplet at 0.88 ppm are due to protons of methoxy (-OCH_2) and -CH_3 group. The 30H resonating peaks in the range of 2.76-1.26 ppm are due to the aliphatic oleate protons.

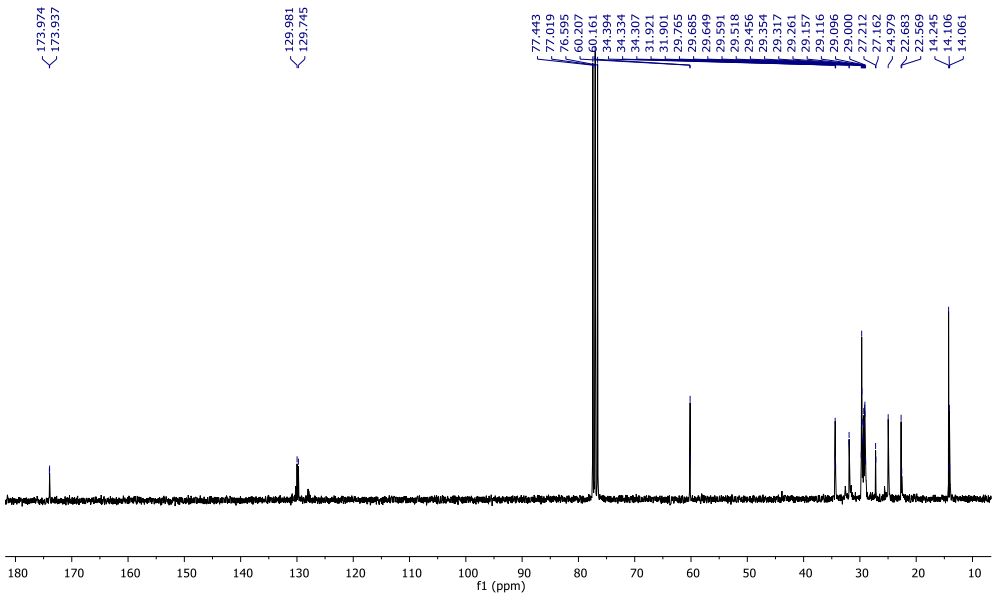

Figure 3.18 ^{13}C-NMR spectrum of ethyl oleate **3f**.

^{13}C-NMR of the isolated ethyl oleate, show the peaks at 173.9 ppm are due to the C=O of ester carbon, the peaks at 129.9 ppm and 129.7 ppm are due to olefinic carbon and the peaks at 60.2 ppm is due to O-CH_2 carbon attached to the ester group. The peaks at 34.3-22.5 ppm are due to methylene carbons and 14.1 ppm of is due to CH_3 carbon.

3.2.5.3 FTIR and NMR (^{1}H and ^{13}C) characterization of propyl oleate 3g

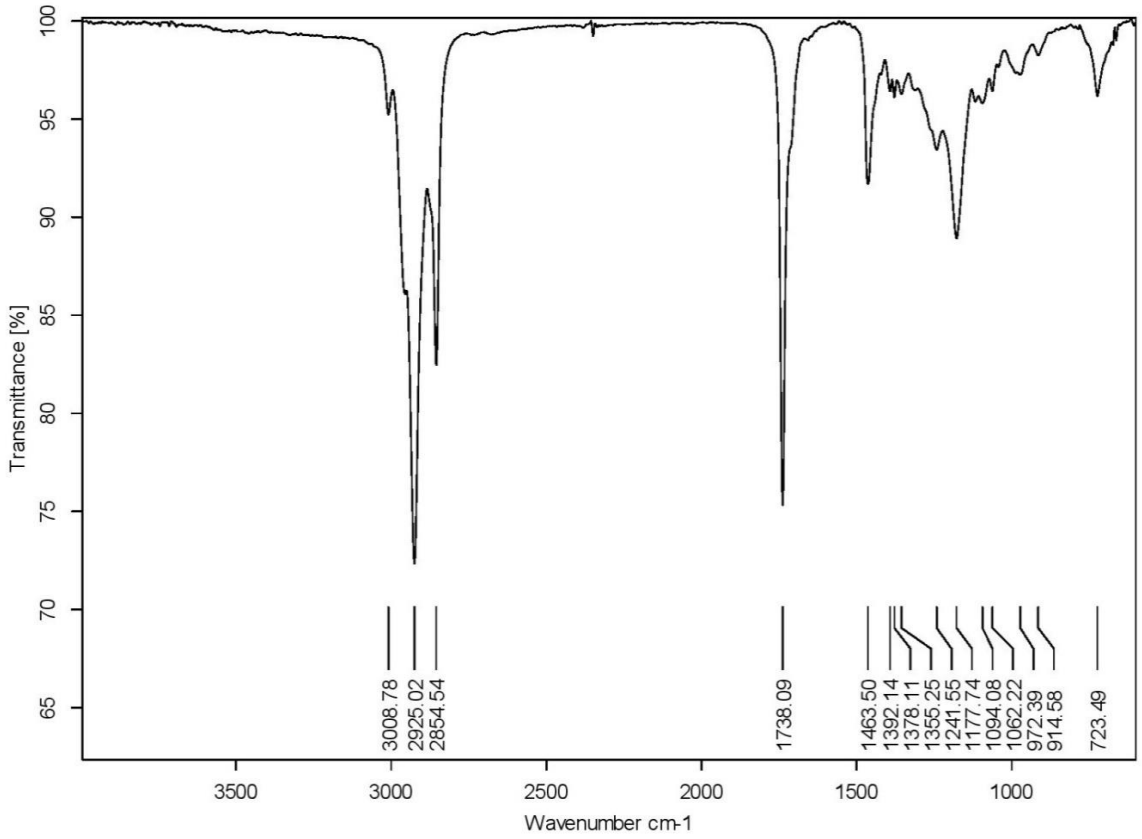

Figure 3.19 FTIR spectrum of propyl oleate **3g**.

The peak at 3008 cm^{-1} is due to sp^2 –C-H stretching frequency and the peak at 2925 and 2854 cm^{-1} is responsible for the sp^3 -C-H stretching frequency. The peak at 1738 cm^{-1}corresponds to the ester C=O stretching frequency and 1177 cm^{-1} is due to C-O stretching frequency of ester group.

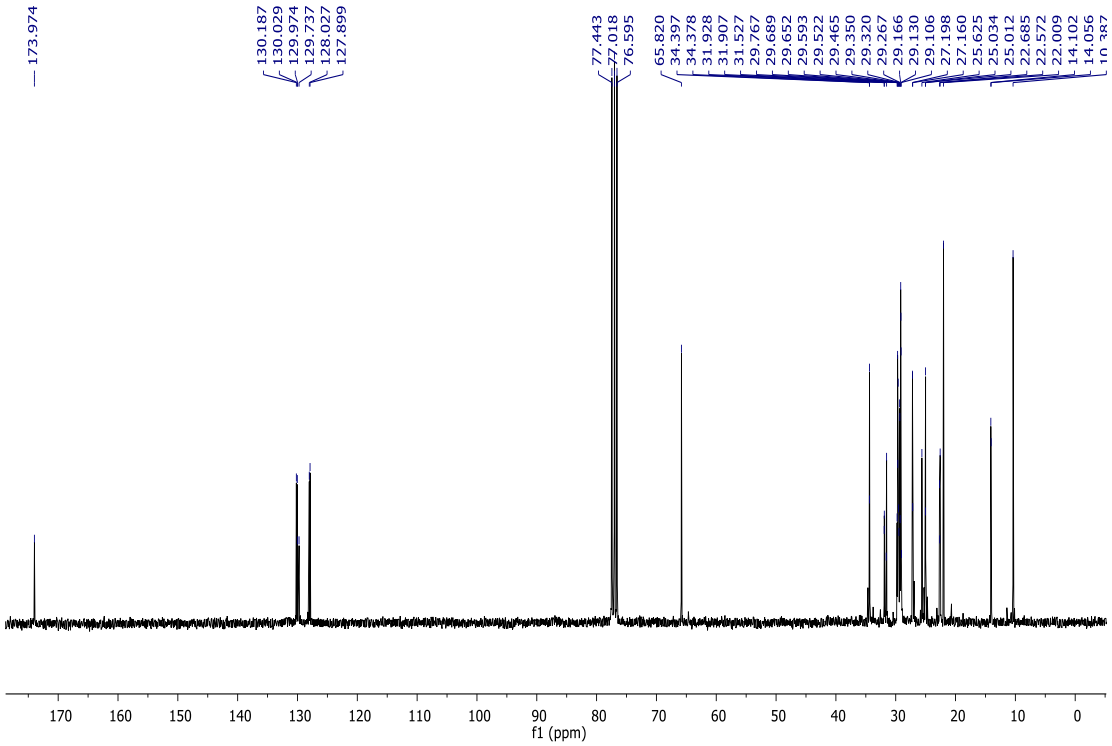

Figure 3.20 ^{13}C-NMR spectrum of propyl oleate **3g**.

^{13}C-NMR of the isolated propyl oleate, show the peaks at 173.9 ppm are due to the C=O of ester carbon, the peaks at 130.0 ppm and 127.9 ppm are due to olefinic carbon and the peaks at 65.8 ppm is due to O-CH_2 carbon attached to the ester group. The peaks at 34.3-22.0 ppm are due to methylene carbons, and 14.1 ppm and 10.3 ppm is due to CH_3 carbons.

3.2.5.4 FTIR and NMR (^{1}H and ^{13}C) characterization of butyl oleate 3h

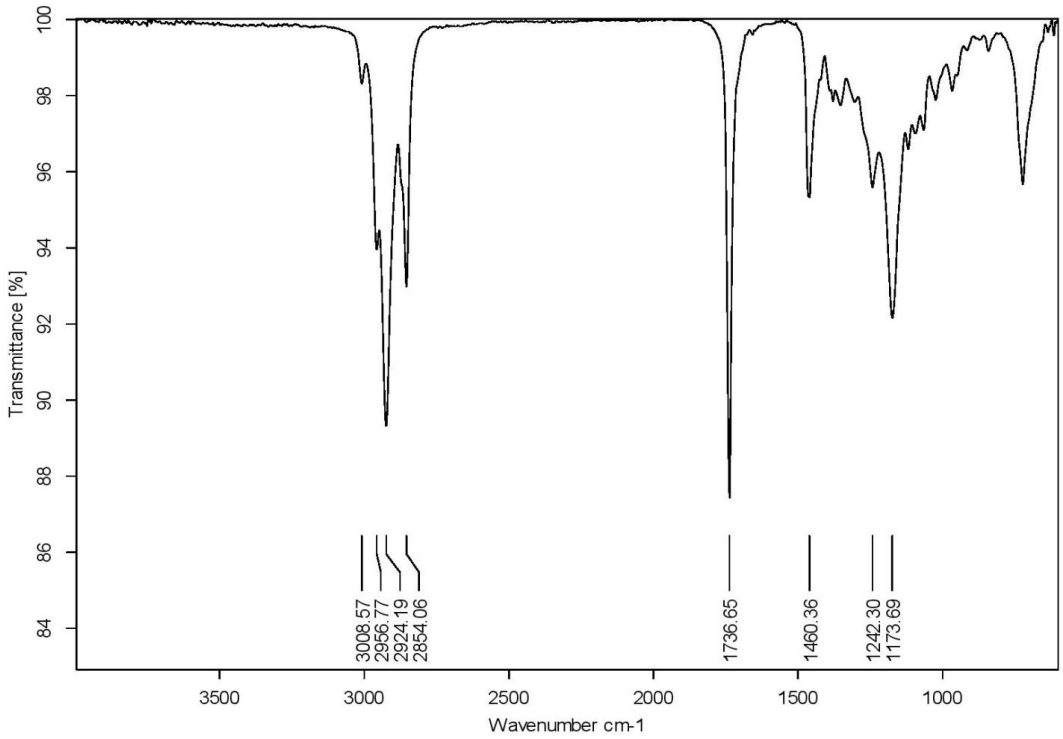

Figure 3.21 FTIR spectrum of butyl oleate **3h**.

The peak at 3008 cm^{-1} is due to sp^2 –C-H stretching frequency and the peak at 2956 and 2854 cm^{-1} is responsible for the sp^3 -C-H stretching frequency. The peak at 1736 cm^{-1}corresponds to the ester C=O stretching frequency and 1173 cm^{-1} is due to C-O stretching frequency of ester group.

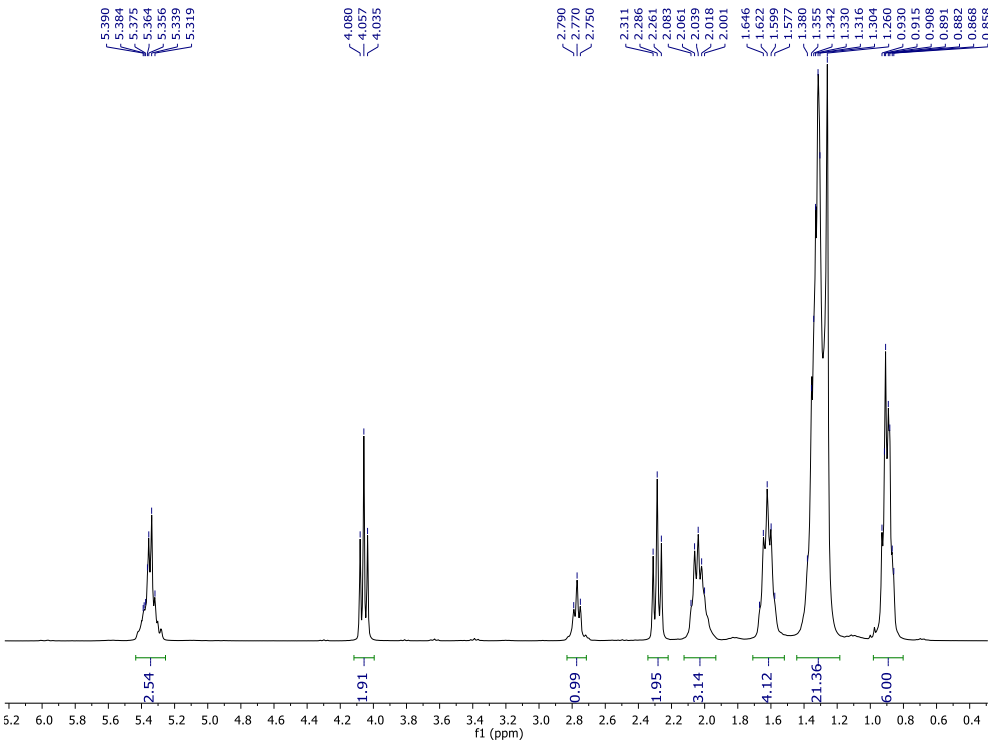

Figure 3.22 ^{1}H-NMR spectrum of butyl oleate **3h**.

^{1}H-NMR of the isolated butyl oleate show the 2H multiplet at 5.36 ppm is due to olefinic protons of oleate. The 2H quartet at 4.05 ppm is due to protons of methoxy (-OCH_2) proton. The 37H resonating peaks in the range of 2.77-0.85 ppm are due to the aliphatic oleate protons.

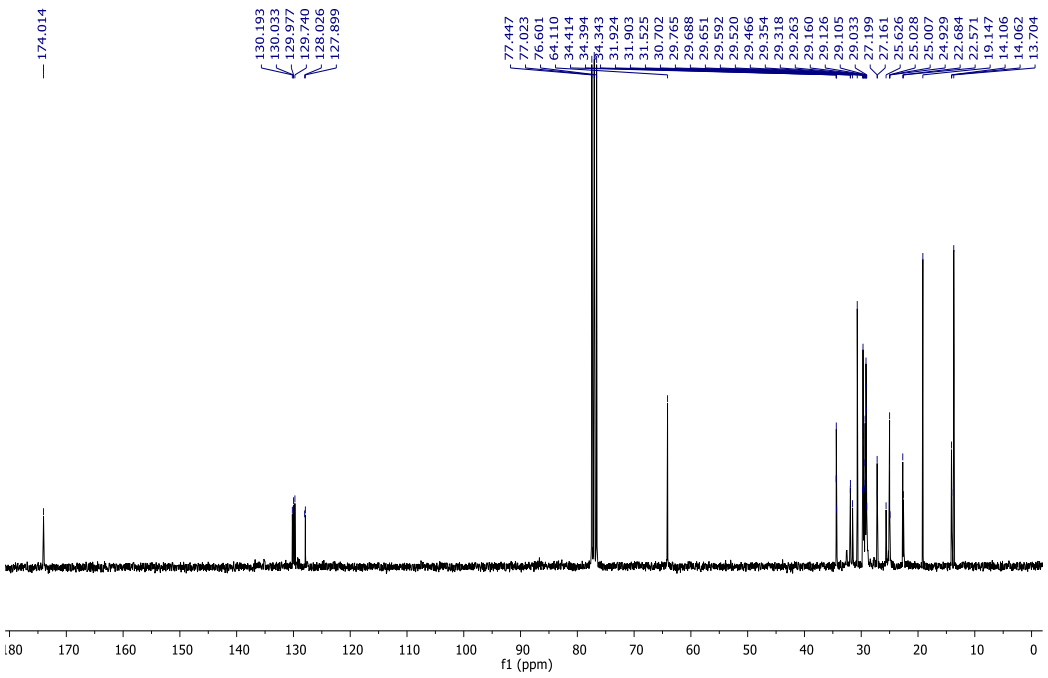

Figure 3.23 ^{13}C-NMR spectrum of butyl oleate **3h**.

^{13}C-NMR of the isolated butyl oleate, show the peaks at 174.0 ppm are due to the C=O of ester carbon, the peaks at 130.1 ppm and 128.0 ppm are due to olefinic carbon and the peaks at 64.1 ppm is due to O-CH_2 carbon attached to the ester group. The peaks at 34.3-19.1 ppm are due to methylene carbons, and 14.1 ppm and 13.7 ppm is due to CH_3 carbons.

3.2.5.5 FTIR and NMR (^{1}H and ^{13}C) characterization of pentyl oleate 3i

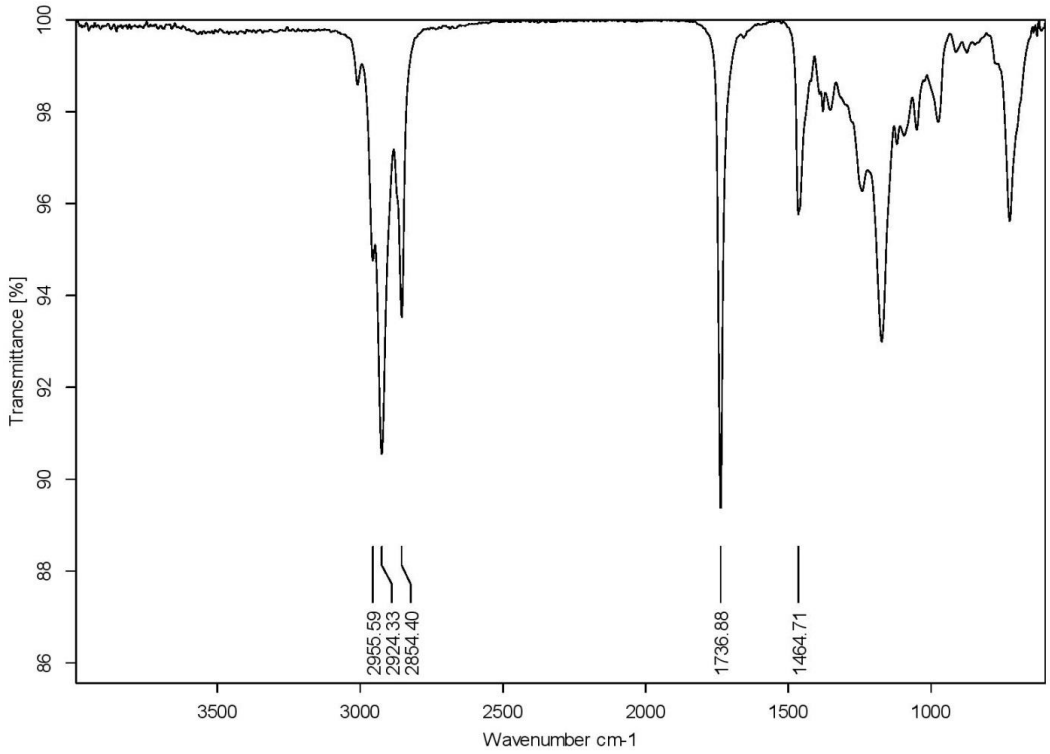

Figure 3.24 FTIR spectrum of pentyl oleate **3i**.

The peak at 2955 and 2854 cm^{-1} is responsible for the sp^3 -C-H stretching frequency. The peak at 1736 cm^{-1}corresponds to the ester C=O stretching frequency of ester group.

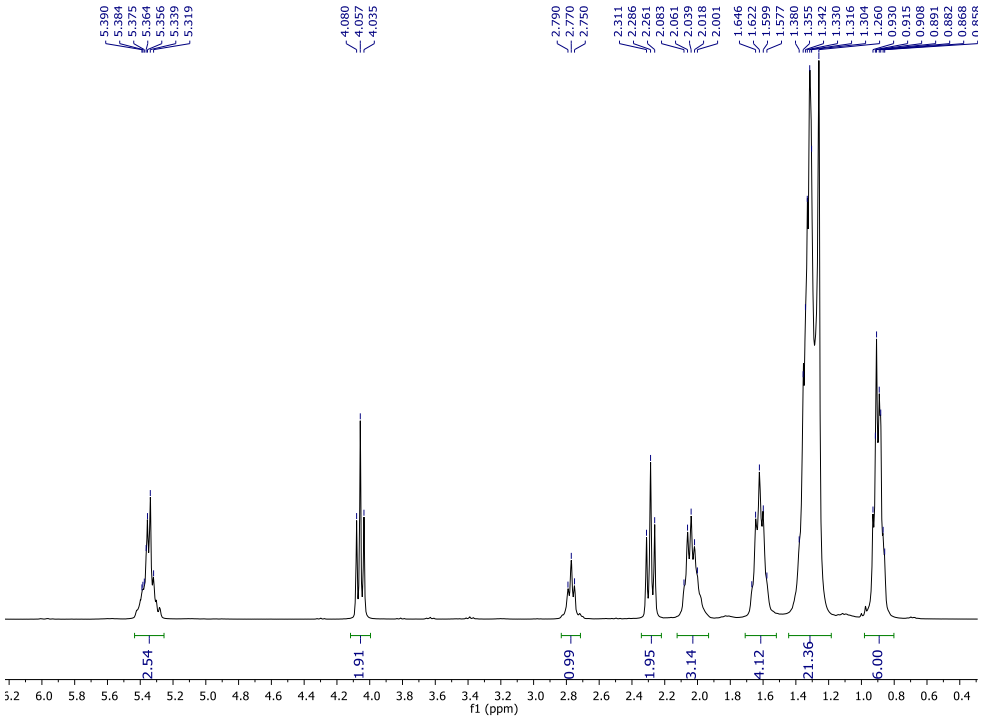

Figure 3.25 ^{1}H-NMR spectrum of pentyl oleate **3i**.

^{1}H-NMR of the isolated pentyl oleate show the 2H multiplet at 5.36 ppm is due to olefinic protons of oleate. The 2H triplet at 4.05 ppm is due to protons of methoxy (-OCH_2) proton. The 37H resonating peaks in the range of 2.77-0.85 ppm was due to the aliphatic oleate protons.

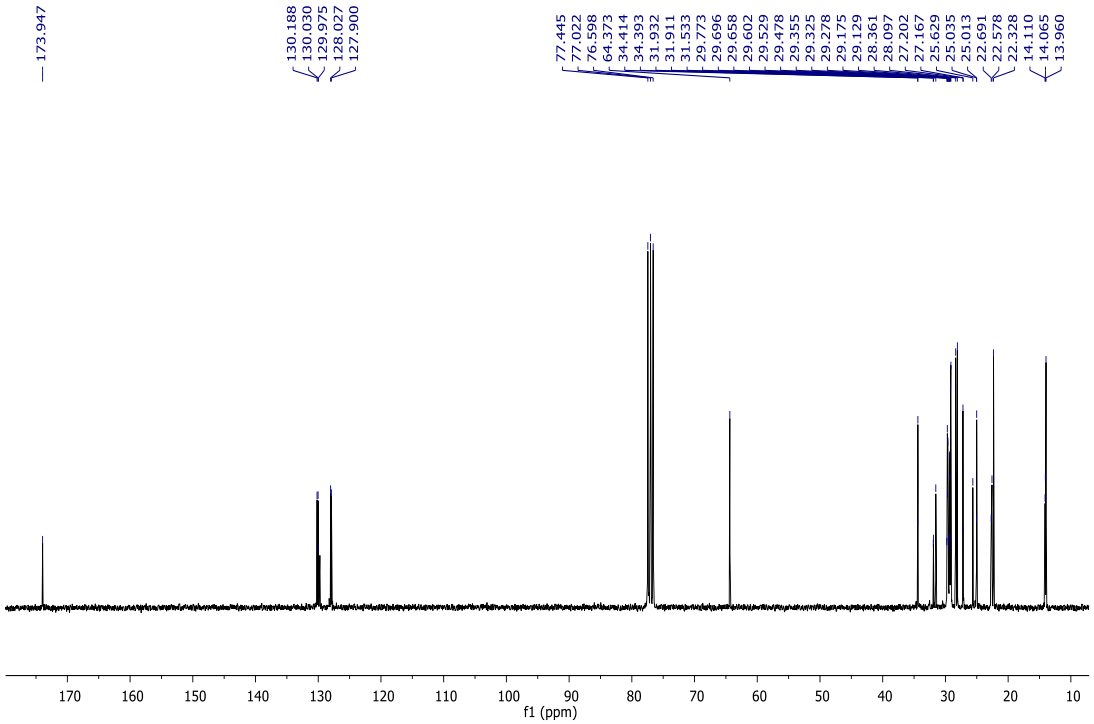

Figure 3.26 ^{13}C-NMR spectrum of pentyl oleate **3i**.

^{13}C-NMR of the isolated pentyl oleate, show the peaks at 173.9 ppm are due to the C=O of ester carbon, the peaks at 130.0 ppm and 128.1 ppm are due to olefinic carbon and the peaks at 64.3 ppm is due to O-CH_2 carbon attached to the ester group. The peaks at 34.3-22.3 ppm are due to methylene carbons, and 14.1 ppm and 13.7 ppm is due to CH_3 carbons.

3.2.5.6 FTIR and NMR (^{1}H and ^{13}C) characterization of hexyl oleate 3j

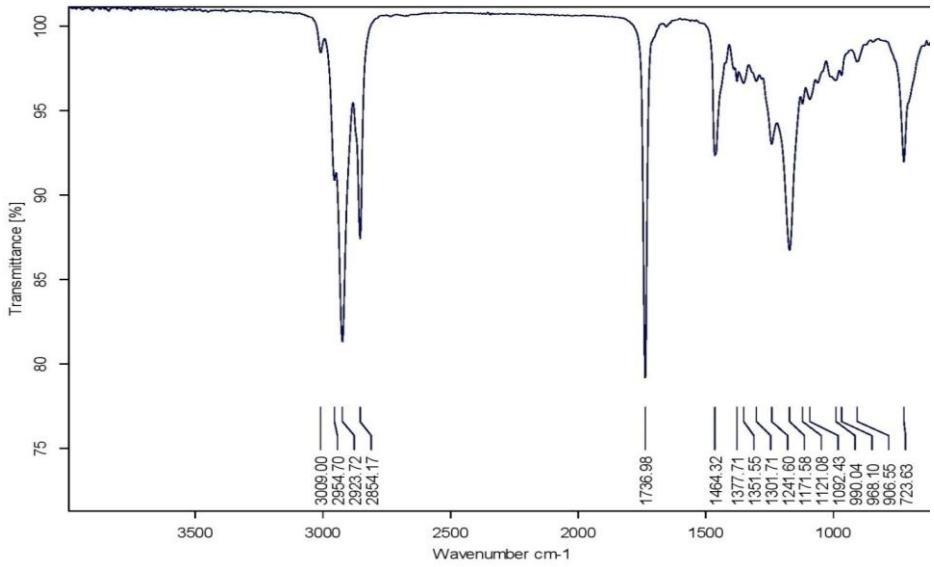

Figure 3.27 FTIR spectrum of Hexyl oleate **3j**.

The peak at 3009 cm^{-1} is due to sp^2 –C-H stretching frequency and the peak at 2854 cm^{-1} is responsible for the sp^3 -C-H stretching frequency. The peak at 1736 cm^{-1}corresponds to the ester C=O stretching frequency and 1171 cm^{-1} is due to C-O stretching frequency of ester group.

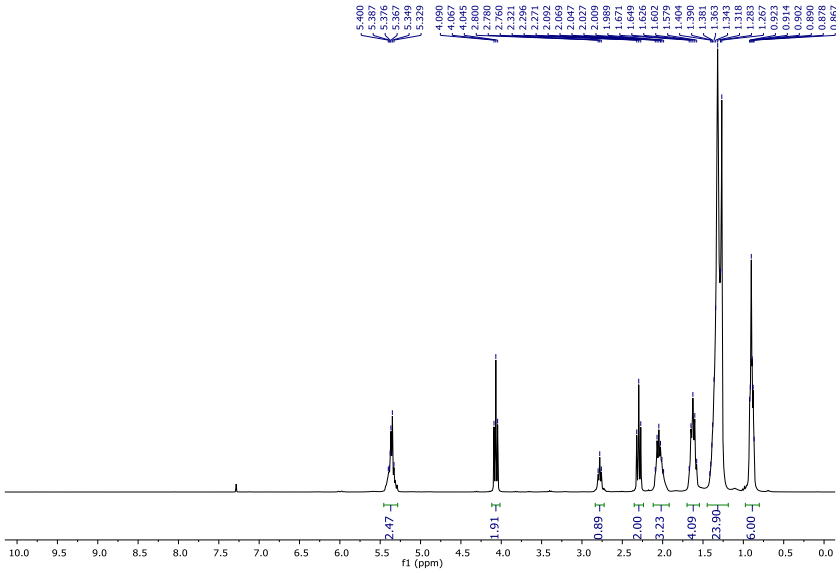

Figure 3.28 ^{1}H-NMR spectrum of Hexyl oleate **3j**.

^{1}H-NMR of the isolated hexyl oleate show the 2H multiplet at 5.37 ppm is due to olefinic protons of oleate. The 2H triplet at 4.06 ppm is due to protons of methoxy (-OCH_2) proton. The 40H resonating peaks in the range of 2.8-0.85 ppm are due to the aliphatic oleate protons.

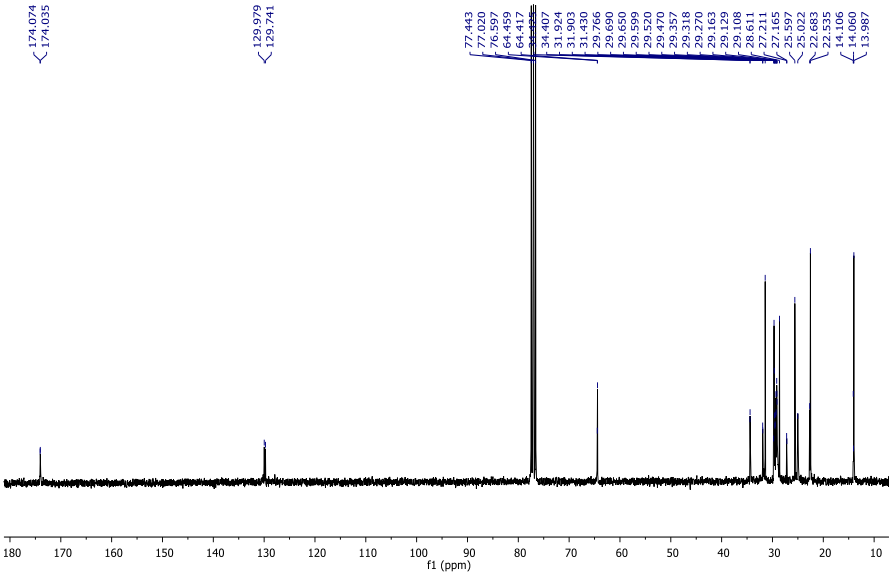

Figure 3.29 ^{13}C-NMR spectrum of Hexyl oleate **3j**.

^{13}C-NMR of the isolated hexyl oleate, show the peaks at 174.0 ppm are due to the C=O of ester carbon, the peaks at 129.9 ppm and 129.7 ppm are due to olefinic carbon and the peaks at 64.4 ppm is due to O-CH_2 carbon attached to the ester group. The peak at 34.3-22.5 ppm are due to methylene carbons, and 14.1 ppm and 13.9 ppm is due to CH_3 carbons.

3.3 RESULTS AND DISCUSSIONS

3.3.1 Esterification of stearic acid over Heteropolyacids (HPAs)

Propyl stearate **3c** was chosen as the model substrate for reaction optimization. In a typical reaction, stearic acid, 1-propanol (1.5 eq.), and PTA (1 mol%, with respect to

mole of stearic acid used) were taken in a 100 mL glass pressure vessel, sealed, and stirred magnetically during the course of the reaction. The PTA catalyst remained suspended in the reaction mixture and phase separated from the product after reaction. Propyl stearate was isolated from the reaction mixture by solubilizing in petroleum ether. The crude product was analysed by FTIR and ^{1}H-NMR spectroscopy for complete conversion and purified by column chromatography (silica gel).

3.3.2 Effect of reaction temperature

The effect of reaction temperature on the conversion of stearic acid and yield of alkyl stearates was studied using PTA as the acid catalyst. The reaction produced <10% yield of propyl stearate even after stirring for 12 h at room temperature. Increasing the temperature to 80 °C afforded 3 in 76% isolated yield within 4 h (**Figure 3.30**). Upon increasing the temperature to 90 °C and 100 °C, the yield of **3c** increased to 89% and 96%, respectively. The mass balance was essentially unreacted SA. The yield of **3c** reached 98% after 4 h reaction when the reaction was conducted at 110 °C. The ^{1}H-NMR spectrum of the crude product did not show any unreacted SA certifying its quantitative conversion.

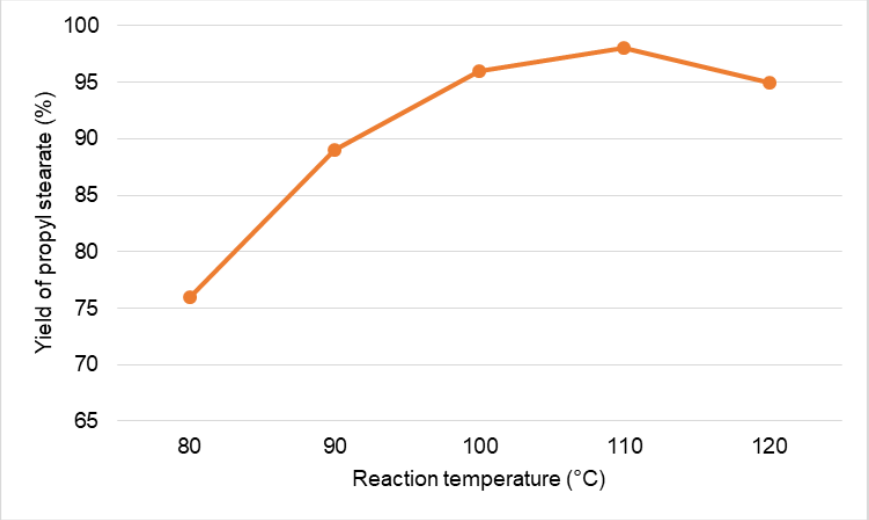

Figure 3.30 Effect of reaction temperature on the yield of propyl stearates **3c**.

Reaction conditions: SA (3.51 mmol), propanol (5.25 mmol), 4 h, HPA (1 mol%).

3.3.3 Effect of mole ratio of SA to propanol

In order to investigate the effect of molar ratio of SA and 1-propanol on the yield of propyl stearate **3c**, the reaction was carried out at 110 °C for 4 h using 1 mol% of PTA as catalyst. The molar ratio of SA to 1-propanol was varied between 1:1 and 1:4. The results show that the yield of **3c** at ratios above 1:1.5 is nearly constant (**Figure 3.31**). However, using ratios lower than 1:1.5 lowered the yield of **3c** due to incomplete reaction. Using equivalent amount of 1-propanol, **3c** was isolated in 90% yield. Increasing the equivalence of 1-propanol from 1 to 1.5 increased the yield of **3c** incrementally and reached maximum at 98% at 1.5 equivalent of 1-propanol.

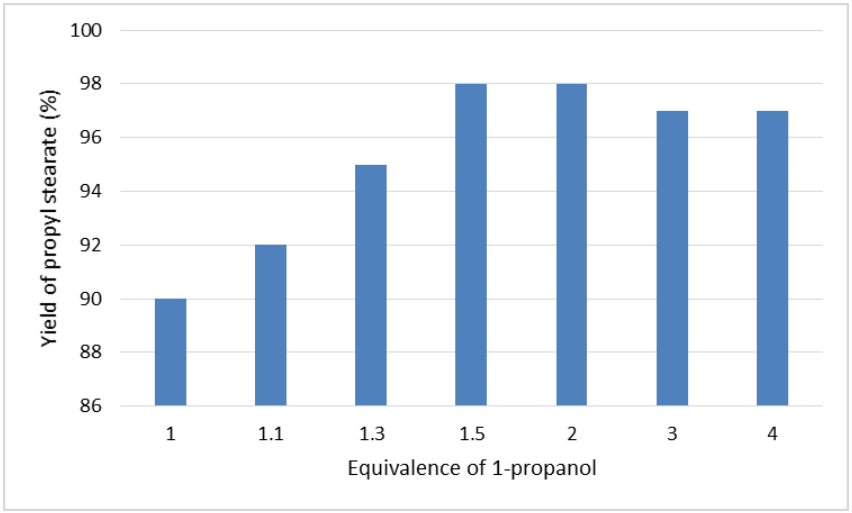

Figure 3.31 Effect of equivalence of 1-propanol with respect to SA on the isolated yield of propyl stearate **3c**.

Reaction conditions: SA (3.51 mmol), propanol, 110 °C, 4 h, HPA (1 mol%).

3.3.4 Efficiency of various HPA catalysts

To investigate the efficiency of different HPA, the esterification reaction was independently carried out using four commercially-available HPAs, namely,

phosphotungstic acid (PTA), phosphomolybdic acid (PMA), silicotungstic acid (STA), and silicomolybdic acid (SMA). The esterification of stearic acid with 1-propanol was carried out at 110 °C for 4 h using 1 mol% of HPA catalysts. Among the four HPAs examined, PTA was found to be most effective catalyst. Use of PTA as catalyst afforded propyl stearate **3c** in 96% yield whereas PMA, STA, and SMA afforded the same in 86%, 87%, and 90% yields, respectively (**Figure 3.32**). The results may be explained by the highest acidity of PTA among all the HPA catalysts examined.

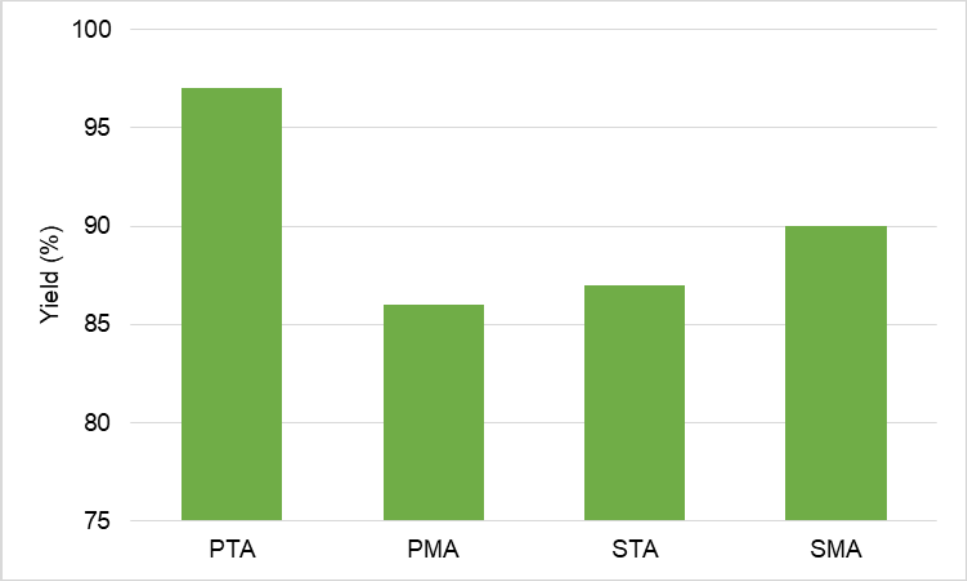

Figure 3.32 Efficiency of various HPAs on the yield of propyl stearate **3c**.

Reaction conditions: SA (3.51 mmol), propanol (5.25 mmol), 110 °C, 4 h, HPA (1 mol%).

3.3.5 Effect of catalyst loading

PTA being found to be the most active catalyst, the effect of loading of PTA on the isolated yield of **3c** was investigated keeping the other reaction parameters unaltered. When the loading of PTA catalyst was lowered to 0.4 mol%, the yield was 90% after 4 h at 110 °C. The yield increased up to 93% after 6 h (**Figure 3.33**). The yield increased incrementally up to 1 mol% and reached maximum of 98% and then decreased to 91% at

1.2 mol%. Lower yield of **3c** at higher loading of PTA catalyst is due to acid-promoted decompositions reactions and ether formation from alcohols and thereby lowering the amount of alcohol available to react with stearic acid.

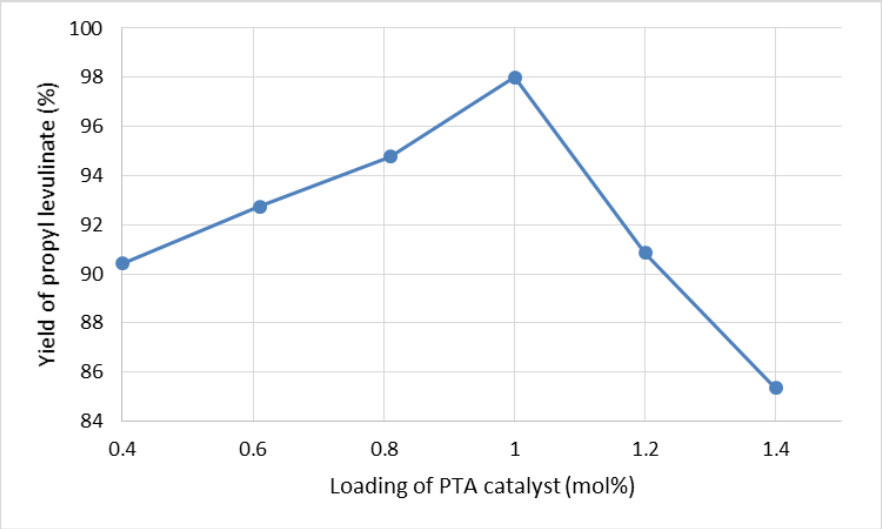

Figure 3.33 Effect of loading of PTA catalyst on the isolated yield of propyl stearate **3c**.

Reaction conditions: SA (3.51 mmol), propanol (5.25 mmol), 110 °C, 4 h.

3.3.6 Effect of different alcohol

The optimized reaction for **3c** was applied for the production of **3a-3d** from SA using 1 mol% PTA catalyst. The reactions were performed in a glass pressure tube fitted with a teflon screw top. The set up allows to reach temperature without evaporative loss of the alcohols during reaction. Where methyl stearate **3a** was isolated in 96% yield, 97% yield ethyl stearate **3b**, 98% yield propyl stearate **3c,** and the butyl stearate **3d** was obtained in 98% isolated yield (**Figure 3.34**).

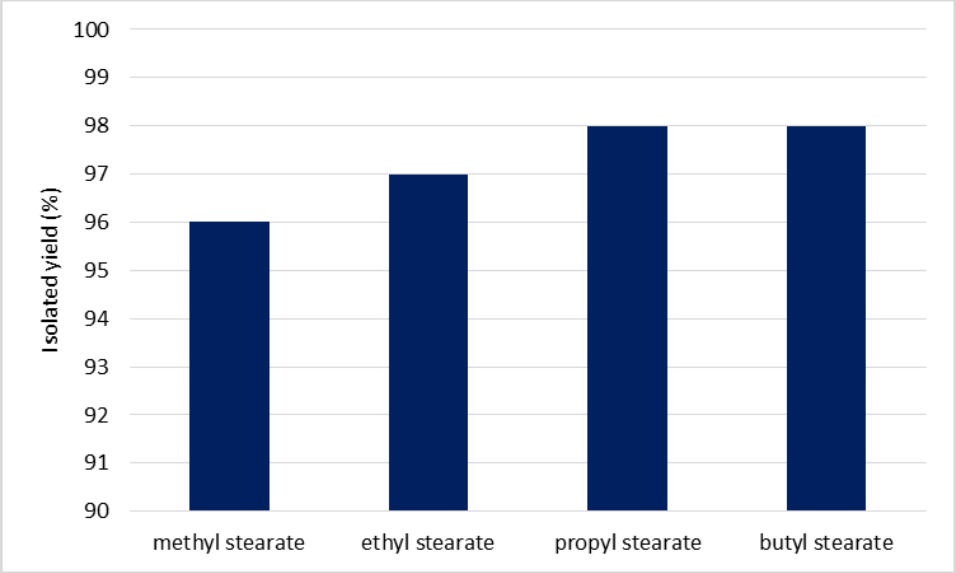

Figure 3.34 Preparation of alkyl stearates (**3a-3d**) from stearic acid.

Reaction Conditions: SA: alcohol (1:1.5) (molar ratio), 110 °C, 4 h, PTA (1 mol%).

Optimized conditions: Mole ratio of SA to alcohol=1:1.5, catalyst loading=1mol%, temperature=110 °C, time=4 h.

3.3.7 Recycling and recovery of catalysts

Recyclability of the catalyst is one of the most important parameters for the green indices and process economics. The PTA catalyst used in the preparation of propyl stearate **3c** was recycled and reused for five consecutive runs. After reaction, the catalyst was precipitated by petroleum ether and separated from the PTA catalyst by decantation or centrifugation. The catalyst was then dried in oven at 110 °C for 12 h before submitting for consecutive runs. The mass loss of PTA catalyst can be minimized by drying the catalyst in the reaction vessel itself. A typical mass loss of 1-2% was observed between consecutive runs. The yield of propyl stearate **3c** decreased minimally till the 3rd run and provided 95% isolated yield. Marginal decrease in yield of **3c** was observed at the 4^{th} and 5^{th} cycles where it was isolated in 92% and 88% yield, respectively (**Figure 3.35**). The amounts of SA and 1-propanol were adjusted in each trial based on the mass

of PTA recovered. The marginally lower yield of **3c** in the 4th and 5th cycle may be attributed to the smaller scale of reaction with the yield being more sensitive to the physical mass loss during product isolation and purification.

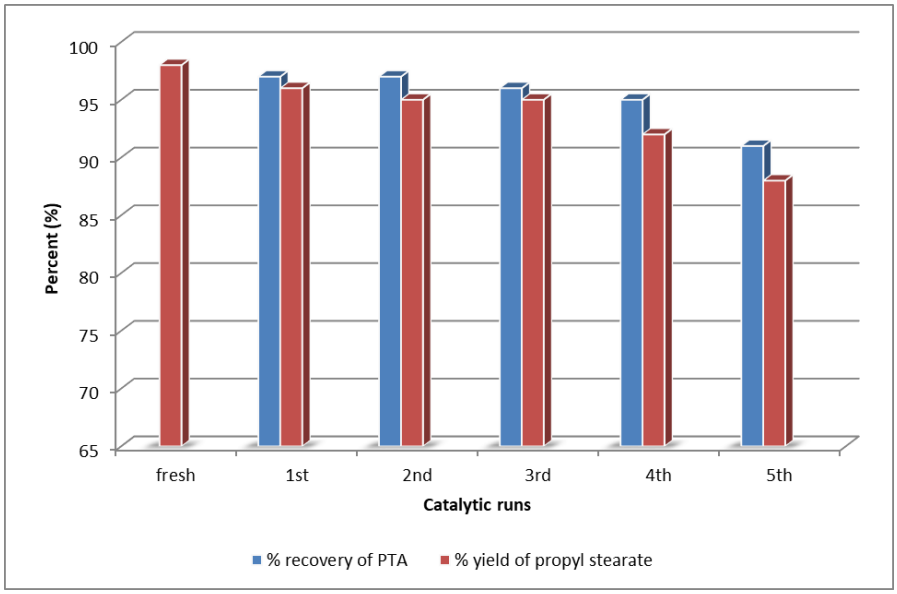

Figure 3.35 Recovery and reuse of PTA catalyst in the preparation of propyl stearate **3c**.

Reaction conditions: SA (3.51 mmol), propanol (5.25 mmol), 110 °C, 4 h, HPA (1 mol%).

3.3.8 Characterization of recycled catalysts

The regenerated catalysts were characterized by FTIR, ^{31}P-NMR and TGA in order to confirm the retention of the catalyst structure, after the completion of the reaction. After each cycle, the dried PTA catalyst was characterized by FTIR to ensure no change in its structural integrity (**Figure 3.36**). The peak at 1080 cm^{-1} is the characteristic peak for the P-O stretching frequency. The peaks at 982 cm^{-1} and 889 cm^{-1} correspond to W=O and W-O stretching frequencies, respectively.

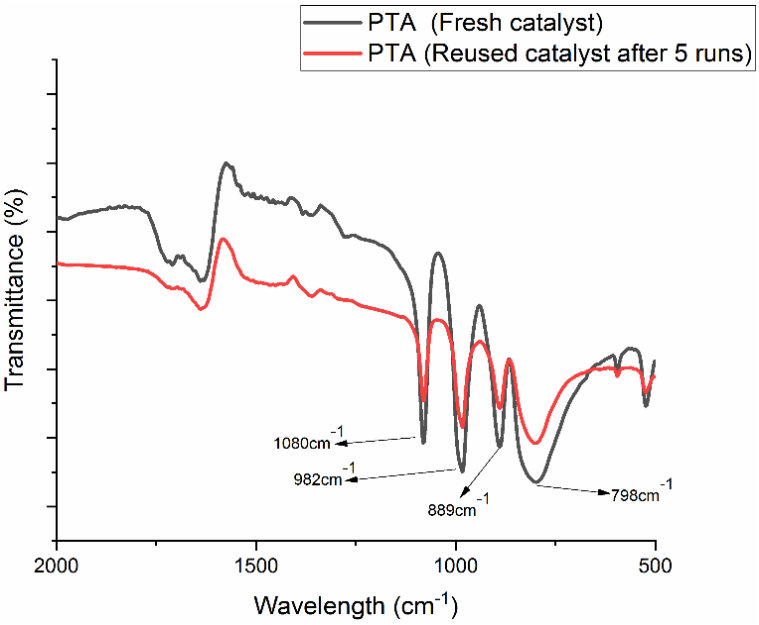

Figure 3.36 FTIR spectra of the fresh PTA (dried) and recycled (5th cycle) PTA.

In addition, the catalyst was after the fifth cycle was characterized by ^{31}P-NMR spectroscopy and thermogravimetric (TGA) analysis.

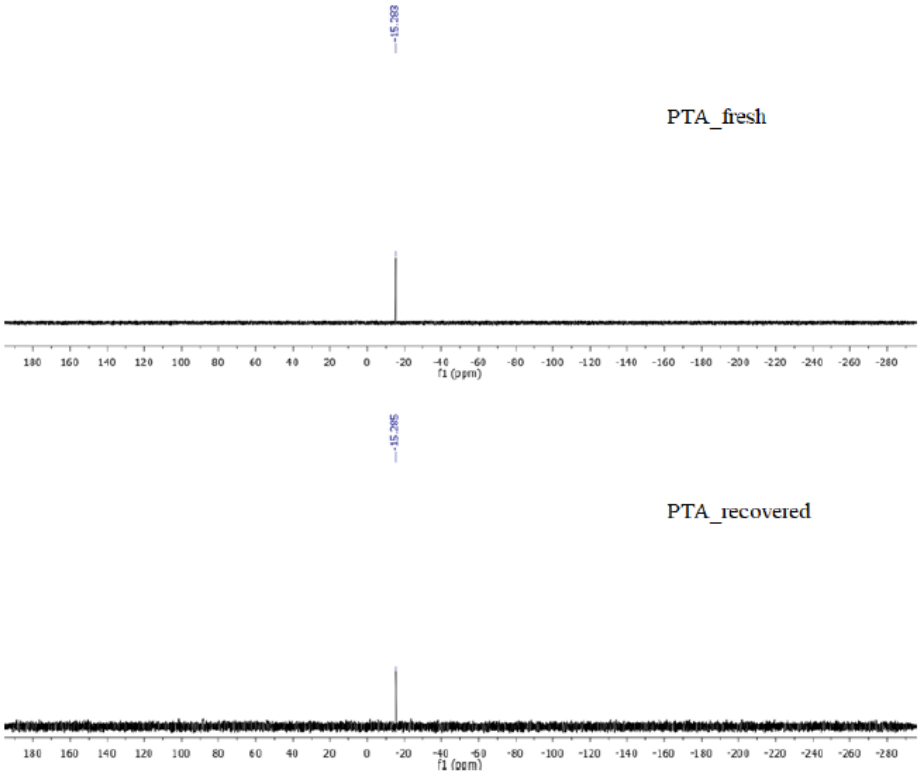

Figure 3.37 ^{31}P-NMR spectra of fresh and recovered PTA catalyst.

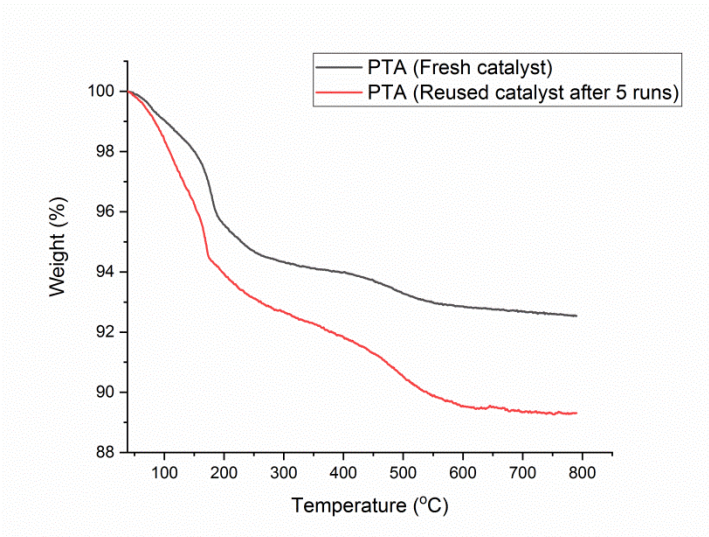

Figure 3.38 TGA graph of the fresh and recycled PTA catalyst.

Table 3.1 Esterification of stearic acid using PTA catalyst

Tabular Data for esterification of Stearic Acid

Effect of temperature

Entry	Temperature (°C)	Yield (%)
1	80	76
2	90	89
3	100	96
4	110	98
5	120	95

Effect of reaction temperature on the yield of propyl stearate **3c**.

Reaction conditions: SA (3.51 mmol), propanol (5.25 mmol), 4 h, HPA (1 mol%).

Effect of molar ratio

Entry	Equivalence of 1-propanol	Yield (%)
1	1	90
2	1.1	92
3	1.3	95
4	1.5	98
5	2	98
6	3	97
7	4	97

Effect of equivalence of 1-propanol with respect to SA on the isolated yield of propyl stearate **3c**.

Reaction conditions: SA (3.51 mmol), propanol, 110 °C, 4 h, HPA (1 mol%).

Efficiency of various HPA catalysts

Entry	HPAs Catalyst	Yield (%)
1	PTA	98
2	PMA	86
3	STA	87
4	SMA	90

Efficiency of various HPAs on the yield of propyl stearate **3c**.

Effect of loading of PTA catalyst

Entry	Loading of PTA Catalyst (mol%)	Yield (%)
1	0.4	90
2	0.6	93
3	0.8	95
4	1	98
5	1.2	91
6	1.4	85

Reaction conditions: SA (3.51 mmol), propanol (5.25 mmol), 110 °C, 4 h, HPA (1 mol%).		Effect of loading of PTA catalyst on the isolated yield of propyl stearate **3c**. **Reaction conditions**: SA (3.51 mmol), propanol (5.25 mmol), 110 °C, 4 h.

Efficiency of different alcohol			
Entry	**Alcohol**	**Product**	**Yield (%)**
1.	Methanol	Methyl stearate	96
2.	Ethanol	Ethyl stearate	97
3.	Propanol	Propyl stearate	98
4.	Butanol	Butyl stearate	98
Reaction Condition: SA: alcohol (1:1.5) (molar ratio), 110 °C, 4 h, PTA (1 mol%).			

Recycling and reuse of catalysts		
Entry	**Recovery rate**	**Yield (%)**
Fresh	100	98
First	97	97
Second	97	95
Third	96	95
Fourth	96	91
Fifth	91	86
Recovery and reuse of PTA catalyst in the preparation of propyl stearate **3c**. **Reaction conditions**: SA (3.51 mmol), propanol (5.25 mmol), 110 °C, 4 h, HPA (1 mol%).		

3.3.9 Esterification of oleic acid (OA) over HPA catalysts

Similar to the previous section 3(A), optimization studies were carried out for maximum conversion.

The conversion of oleic acid into alkyl oleates was studied using different HPAs, oleic acid to alcohol ratios, temperatures of reaction, and catalyst loading in order to find the best reaction conditions. Butyl oleate **3h** has been selected as the model substrate for optimizing the reaction. In a typical reaction, oleic acid, 1-butanol (1.5 eq.), and PTA (0.2 mol%, with respect to mole of oleic acid used) were taken in a 100 mL glass pressure vessel, sealed, and stirred magnetically during the course of the reaction. In the reaction mixture, the PTA catalyst remained suspended and after reaction separated from the product. Butyl oleate **3h** was extracted in petroleum ether and separated from the PTA catalyst. The progress of the reaction and the purity of the product was analyzed by FTIR and ^{1}H-NMR spectroscopy.

3.3.10 Effect of reaction temperature

The effect of reaction temperature on oleic acid conversion and alkyl oleate yield was investigated using PTA as the acid catalyst. Even after stirring for 12 h at room temperature, the reaction produced <13% yield of butyl oleate. Increasing the temperature to 90 °C afforded **3h** in 43 % isolated yield within 4 h (**Figure 3.39**). When the temperature increased to 100 °C and 110 °C, the yield of **3h** increased to 64% and 79%, respectively. The mass balance was essentially unreacted OA. After 4 h, the yield of **3h** reached 85 % when the reaction was carried out at 120 °C. On increasing the temperature further, the yield of **3h** decreased possibly due to the decomposition of PTA and oleates.

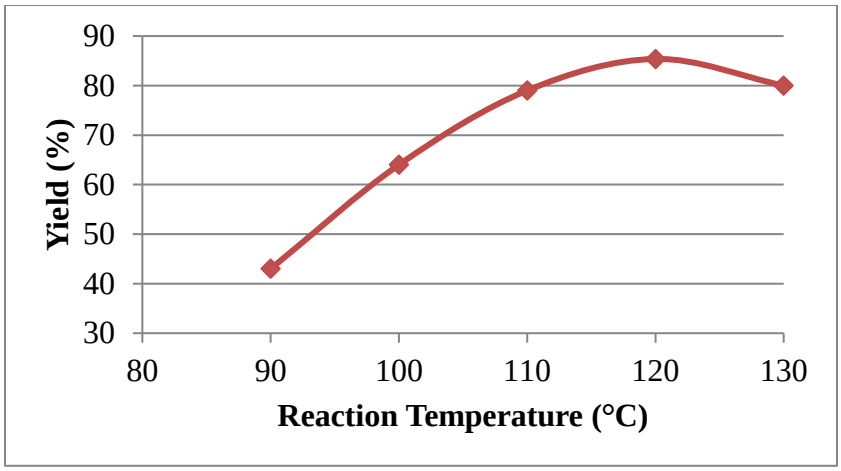

Figure 3.39 Effect of reaction temperature on the yield of butyl oleates **3h**.

Reaction conditions: OA (3.54 mmol), Butanol (5.26 mmol), 4 h, PTA (0.2 mol%).

3.3.11 Effect of mole ratio of OA to 1-butanol

In order to investigate the effect of molar ratio of OA and 1-butanol on the yield of butyl oleate **3h**, the reaction was carried out at 120 °C for 4 h using 0.2 mol% of PTA as catalyst. The molar ratio of OA to 1-butanol was varied between 1:1 and 1:3. The results show that the yield of **3h** is highest at ratios 1:1.5 (**Figure 3.40**). However, the use of any lesser quantities of 1-butanol led to incomplete reaction. Using equivalent amount of 1-butanol, **3h** was isolated in 76% yield. Increasing the equivalence of 1-butanol from 1 to 1.5 increased the yield of **3h** incrementally and reached maximum at 85% at 1.5 equivalent of 1-butanol. Not much difference was observed with a further increase in the equivalance of 1-butanol. Further reactions were therefore performed in the acid to alcohol molar ratio of 1:1.5.

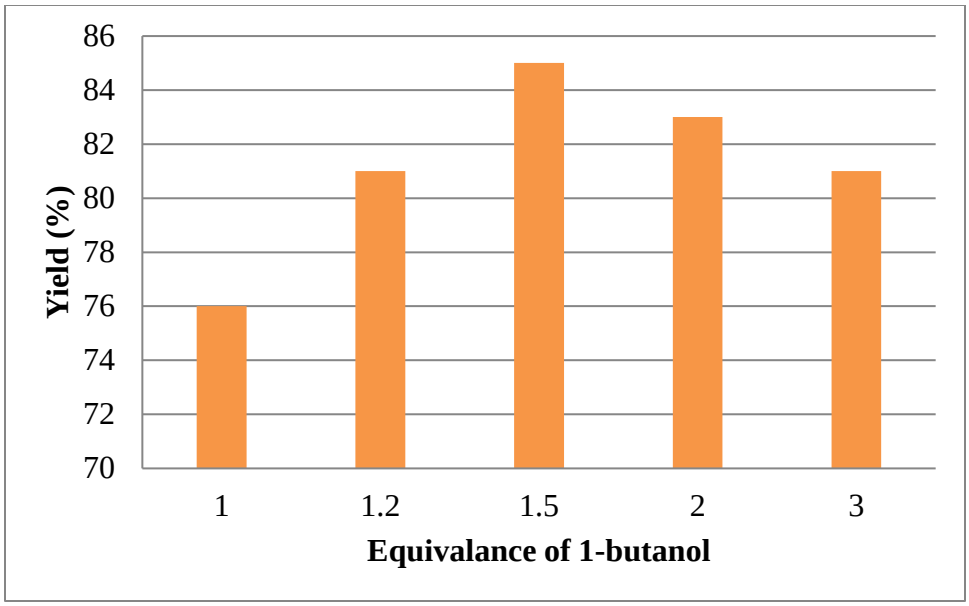

Figure 3.40 Effect of equivalence of 1-butanol with respect to OA on the isolated yield of butyl oleate **3h**.

Reaction conditions: OA (3.54 mmol), Butanol, 120 °C, 4 h, PTA (0.2 mol%).

3.3.12 Efficiency of different HPA in preparing alkyl oleates

Similar to stearic acid, the esterification of oleic acid was carried out in the presence of PTA, PMA, STA, and SMA. The esterification of oleic acid with 1-butanol was carried out at 120 °C for 4 h using 0.2 mol% of the HPA catalysts. PTA was found to be the most effective catalyst among the four HPAs examined. The use of PTA as catalyst afforded butyl oleate **3h** in 85% yield whereas PMA, STA, and SMA afforded the same in 71%, 80%, and 63% yields, respectively, under identical conditions (**Figure 3.41**). The findings can be explained by the highest acidity of PTA among the examined HPA catalysts.

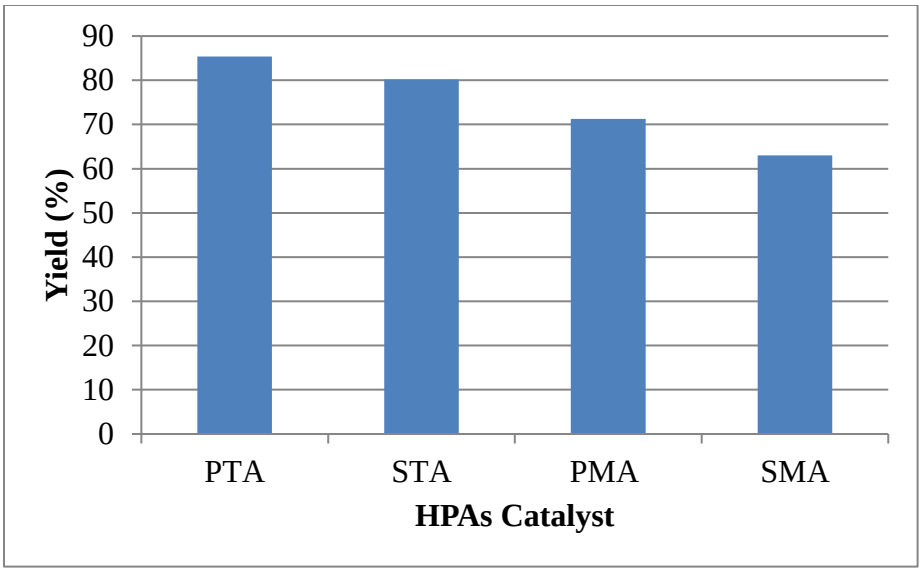

Figure 3.41 The efficiency of various HPAs on the yield of butyl oleate **3h**.

Reaction conditions: OA (3.54 mmol), Butanol (5.26 mmol), 120 °C, 4 h, PTA (0.2 mol%).

3.3.13 Effect of catalyst loading

PTA being found to be the most active catalyst, the effect of PTA loading on the isolated yield of **3h** was investigated keeping the other reaction parameters unchanged. When the loading of PTA catalyst was lowered to 0.05 mol%, the yield was 25% after 4 h at 120 °C. The yield increased up to 43% after 6 h (**Figure 3.42**). The yield increased incrementally up to 0.2 mol% and reached maximum of 85% and then decreased to 78% at 0.3 mol%. Lower yield of **3h** at higher loading of PTA catalyst is due to acid-promoted decompositions reactions and ether formation from alcohols and thereby lowering the amount of alcohol available to react with oleic acid.

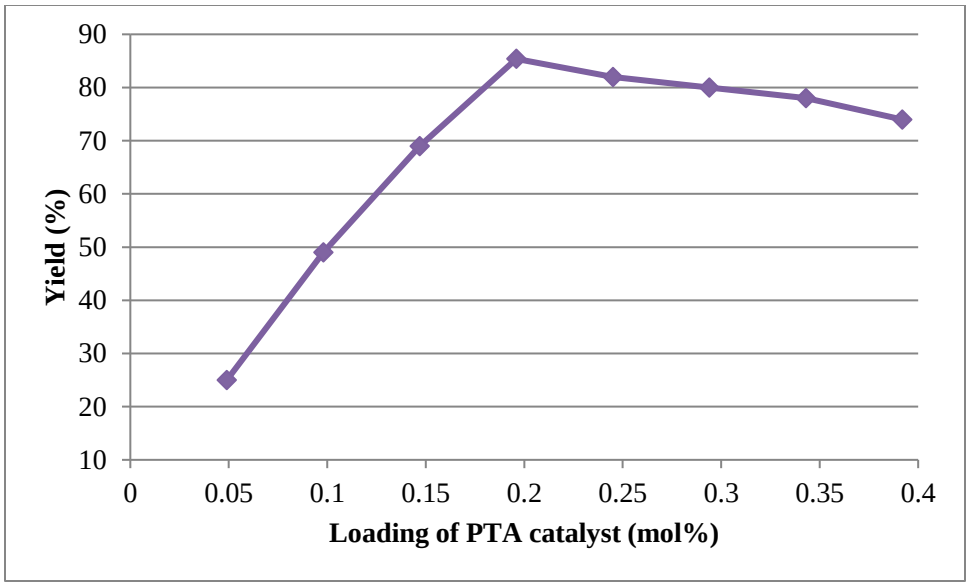

Figure 3.42 Effect of loading of PTA catalyst on the isolated yield of butyl oleate **3h**.

Reaction conditions: OA (3.54 mmol), alcohol (5.26 mmol), 120 °C, 4 h.

3.3.14 Effect of different alcohol

The optimized reaction for **3h** was applied for the production of **3e-3j** from OA using 1 mol% PTA catalyst. The reactions were performed in a glass pressure tube fitted with a teflon screw top. The set up allows to reach temperature without evaporative loss of the alcohols during reaction. Where methyl oleate **3e** was isolated in 71% yield, 75% yield ethyl oleate **3f**, 70% yield propyl oleate **3g**, 85% yield butyl oleate **3h**, 87% yield pentyl oleate **3i** and the hexyl oleate **3j** was obtained in 87% isolated yield (**Figure 3.43**).

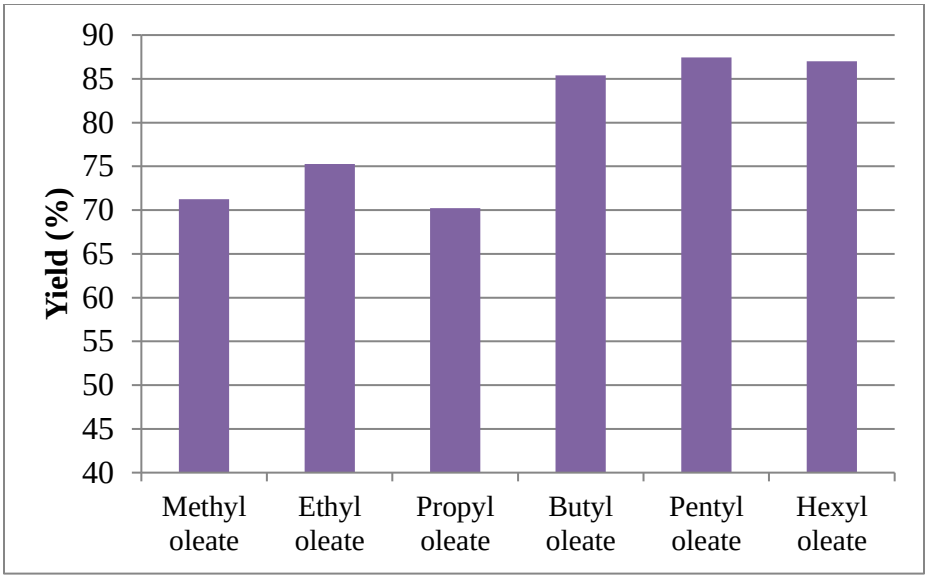

Figure 3.43 Preparation of alkyl oleates (**3e-3j**) from oleic acid.

Reaction Conditions:

Methyl oleate and Ethyl oleate: OA: alcohol (1:1.9) (molar ratio), 120 °C, 8 h, PTA (0.4 mol%).

Propyl oleate: OA: alcohol (1:1.9) (molar ratio), 120 °C, 6 h, PTA (0.4 mol%).

Butyl oleate: OA: alcohol (1:1.5) (molar ratio), 120 °C, 4 h, PTA (0.2 mol%).

Pentyl oleate: OA: alcohol (1:1.8) (molar ratio), 120 °C, 4 h, PTA (0.2 mol%).

Hexyl oleate: OA: alcohol (1:2) (molar ratio), 130 °C, 6 h, PTA (0.2 mol%).

Optimized conditions: 85% yield, mole ratio OA to alcohol=1:1.5; amount of catalyst=0.2 mol%, temperature=120 °C and time=4 h.

Table 3.2 Esterification of oleic acid using PTA catalyst.

Tabular Data for esterification of Oleic Acid

Effect of temperature

Entry	Temperature (°C)	Yield (%)
1	90	43
2	100	64
3	110	79
4	120	85
5	130	80

Effect of reaction temperature on the yield of butyl oleates **3h**.
Reaction conditions: OA (3.54 mmol), Butanol (5.26 mmol), 4 h, PTA (0.2 mol%).

Effect of molar ratio

Entry	Equivalence of 1-butanol	Yield (%)
1	1	76
2	1.2	81
3	1.5	85
4	2	83
5	3	81

Effect of equivalence of 1-butanol with respect to OA on the isolated yield of butyl oleate **3h**.
Reaction conditions: OA (3.54 mmol), Butanol, 120 °C, 4 h, PTA (0.2 mol%).

Efficiency of various HPA catalysts

Entry	HPAs Catalyst	Yield (%)
1	PTA	85
2	STA	80
3	PMA	71
4	SMA	63

The efficiency of various HPAs on the yield of butyl oleate **3h**.
Reaction conditions: OA (3.54 mmol), Butanol (5.26 mmol), 120 °C,

Effect of loading of PTA catalyst

Entry	Loading of PTA Catalyst (mol%)	Yield (%)
1	0.05	25
2	0.1	49
3	0.15	69
4	0.2	85
5	0.25	82
6	0.3	80
7	0.35	78
8	0.4	74

4 h, PTA (0.2 mol%).		Effect of loading of PTA catalyst on the isolated yield of butyl oleate **3h**. **Reaction conditions**: OA (3.54 mmol), alcohol (5.26 mmol), 120 °C, 4 h.

Efficiency of different alcohol			
Entry	Alcohol	Product	Yield (%)
1.	Methanol	Methyl oleate **3e**	71
2.	Ethanol	Ethyl oleate **3f**	75
3.	Propanol	Propyl oleate **3g**	70
4.	1-butanol	Butyl oleate **3h**	85
5.	1-pentanol	Pentyl oleate **3i**	87
6.	1-hexanol	Hexyl oleate **3j**	87
Preparation of alkyl oleates (**3e-3j**) from oleic acid.			

The Fischer esterification reactions are traditionally carried out using large excess of the alcohol reagent with carboxylic acid in presence of HPA catalyst. Excess alcohol favors the reaction equilibrium towards ester formation and compensate for the evaporative loss during refluxing. However, use of excess reagent introduces additional steps in product purification and catalyst recovery increasing the overall process cost. Moreover, long reaction time and higher loading of the acid-catalyst are often required for the esterification reactions. In comparison with traditional process, we envisaged that using a closed pressure vessel for the reaction would stop evaporative loss of the alcohol reagent and allow achieving temperatures higher the boiling point of alcohol ensuring faster reaction. Use of equivalent amount of the alcohol reagent would also help lower the catalyst loading, ease product separation and catalyst recovery.

3.4 CONCLUSION

PTA was found to be the most effective catalyst among four HPA catalysts examined for the preparation of fatty acid esters from fatty acid within a glass pressure reactor. The solvent-free, gram-scale reactions afforded >95% yield of alkyl stearates and >85% yield of alkyl oleates under the optimized conditions. The PTA catalyst was successfully recycled and reused up to five consecutive cycles without significant loss in mass or decrease in catalytic activity.

CHAPTER 4

OXIDATION OF BIOMASS DERIVED FURFURAL TO FURANONE BY USING HETEROPOLYACIDS SUPPORTED MOLECULAR SIEVES

Abstract: *A series of phosphotungstic acid supported on ammonium zeolite (PTA-NH_4YZ) catalysts were prepared and used for the catalytic oxidation of furfural to 2-furanone in aqueous hydrogen peroxide. The catalysts were characterized by PXRD, FTIR, TGA, and SEM analyses. The solvent-free, gram-scale reaction was optimized on temperature, duration, loading of catalyst, and furfural to H_2O_2 molar ratio. The 20%PTA-NH_4YZ catalyst showed the best catalytic activity giving 2-furanone in 40% isolated yield. Around 20% of succinic acid was recovered from the aqueous fraction.*

4.1 INTRODUCTION

Furfural has been at the center of the biorefinery research having established markets for several of its derivatives. Some of the notable derivatives of furfural include furfuryl alcohol, 2-furoic acid, 2-methyltetrahydrofuran, succinic acid, maleic acid, and 2-furanone (Alonso-Fagúndez et al. 2014; Alonso Fagúndez et al. 2012; Cao et al. 1996; Choudhary et al. 2013; Gallezot 2012; Krystof et al. 2013; Lan et al. 2014). 2-Furanone can be looked upon as a renewable chemical intermediate for the synthesis of several important classes of compounds like butyrolactone, 2-pyrrolidone, and various biologically-active molecules (Hashem and Kleinpeter 2001). There are only limited reports on the preparation of 2-furanone from furfural using HPA-based catalysts.

Furanone can be obtained from hydroxybutyrolactones, deoxygenation of substituted butanoic acids, hydrolysis of 2-methoxyfuran and catalytic cyclocarbonylation of terminal alkynols (Garst and Schmir 1974; Glattfeld et al. 1931; Yu and Alper 1997). However, the above processes suffer from one or the other issues, such as costly reagent(s), demanding reaction conditions, and poor yield. Grunskaya et al. (1998) reported the oxidation of furfural to 2(5H)-furanone in 25% yield. Cao et al. (1996) improved the yield to 37% yield by performing the oxidation reaction in a bi-phasic system using 1,2-dichloroethane (DCE) as a solvent. Hashem and Kleinpeter (2001); Poskonin (2009) reported a niobium(V)-catalyzed synthesis of 2-furanone using H_2O_2 as the oxidant. Although decent yield (ca. 60%) was obtained, the reaction duration was long (ca. 80 h).

HPA was used as a homogeneous catalyst for the oxidation of furfural in an aqueous-organic biphasic system (Marino et al. 2008). Keggin-type heteropolytungstic acid, $PW_{12}O_{40}^{3-}$ forms phosphoperoxotungstate $[PW_4O_8(O_2)_8]^{3-}$ by reacting with aqueous H_2O_2 (Agirrezabal-Telleria et al. 2014; Mamman et al. 2008). Peroxocomplexes with molybdenum or tungsten were suggested as stoichiometric or catalytic oxidants (Kato et al. 2007; Zhou et al. 2007). Although many efficient H_2O_2-based oxidation systems have been developed, most of them are homogeneous and have common disadvantages, such as difficult separation and poor reusability of the catalyst.

In this study, a series of PTA-NH_4YZ catalysts were prepared and characterized by PXRD, FTIR, SEM, and TGA. The catalysts were examined for the selective oxidation of furfural to 2-furanone **4a** using H_2O_2 (30% aq.) as the oxidant (**Scheme 4.1**). The influence of various reaction parameters such as temperature, duration, loading of catalyst, and furfural to H_2O_2 molar ratio was studied on the conversion of furfural and yield of 2-furanone **4a**. 20%PTA-NH_4YZ showed the best activity for the solvent-free oxidation of furfural in aqueous H_2O_2. Under optimized conditions, the reaction could be scaled up to several grams scale, and 2-furanone **4a** was obtained in 40% isolated yield. Around 20% succinic acid was isolated from the aqueous fraction.

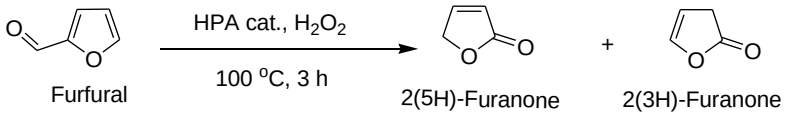

Scheme 4.1 Selective oxidation of furfural to 2-furanone **4a** using HPA catalysts.

Reaction mechanism:

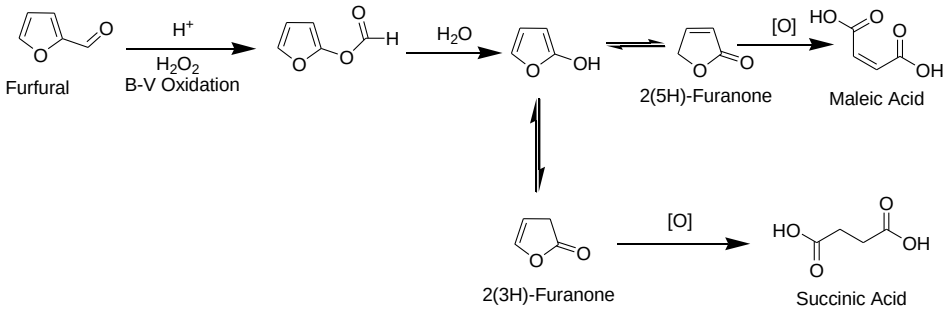

Scheme 4.2 The reaction mechanism for furfural oxidation.

4.2 EXPERIMENTAL SECTION

4.2.1 Materials

Silicotungustic acid ($H_4SiW_{12}O_{40}$), Phosphotungustic acid ($H_3PW_{12}O_{40}$), Phosphomolybdic acid ($H_3PMo_{12}O_{40}$), Furfural (99%), Hydrogen peroxide (30 wt%, aqueous), and Methanol (99%) were received from Loba Chemie Pvt. Ltd. Ammonium zeolite was purchased from Sigma. The HPA catalysts were dried at 110 °C for 24 h before use.

4.2.2 Synthesis of HPA supported NH_4YZ catalysts

The PTA-NH_4YZ catalyst was prepared by following a literature procedure. PTA was dissolved in methanol and added slowly to the methanolic suspension of NH_4YZ. The suspension was stirred for 20 h at room temperature and subsequently dried by solvent evaporation under reduced pressure. The resultant free-flowing powder was then dried overnight at 80 °C in a hot-air oven. The dried catalyst was then calcined at 120 °C for 3 h in a programmable furnace. The amount of PTA was varied between 10-30%.

4.2.3 Characterization techniques

The FTIR spectra of the solids were obtained using a Bruker Alpha FTIR spectrometer, equipped with silicon carbide as the IR source. The samples were ground with KBr and made into pellets. The spectrum was chosen in between 400 to 4000 cm^{-1}. The samples under study were recorded with 16 scans with a resolution of 4 cm^{-1}.

The X-ray diffraction (XRD) patterns were recorded in a RIGAKU Miniflex 600 instrument equipped with a built-in recorder, CuKα radiation (λ = 1.5406 Å), nickel filter, 20 mA and 40 kV in the high voltage source, and scanning angle (2θ) between 10-60° at a scanning rate of two degrees per min.

Scanning electron micrographs were recorded in a JEOL JSM 6380 system to study the morphology of the solids.

Thermal stability of the catalysts was studied by Thermogravimetric analysis (TGA; PerkinElmer, TGA 4000) at a heating rate of 10 °C/min in flowing N_2 (20 mL/min).

4.2.4 Catalyst reactions

The liquid-phase oxidation of furfural was carried out in a round-bottomed flask under conventional heating and magnetic stirring. The solid acid catalyst was suspended in 30% aqueous H_2O_2, and furfural was carefully added to the suspension. The reaction mixture was refluxed for the stipulated time. The progress of the reaction was monitored by TLC and FTIR spectroscopy. After the reaction, the mixture was cooled down to room temperature, and the suspension was extracted with chloroform (3x10 mL). The chloroform layers were combined, dried over anhydrous Na_2SO_4, and evaporated under reduced pressure to get crude 2-furanone **4a** as a light yellow liquid. The product was purified by column chromatography (Silica gel, chloroform) and isolated in 40% yield. A typical

reaction mixture contained 0.1 g of 20%PTA-NH_4YZ, 0.5 g (5.20 mmol) of furfural, and 4 mL (6.27 eq.) of aqueous H_2O_2 (30%).

4.2.5 Instrument used for the characterization of compounds

FTIR spectra of the samples were collected on a Bruker Alpha FTIR instrument. The FTIR spectrum of samples was collected in the ATR mode and the solid HPA catalysts were collected in the KBr matrix. The ^{1}H-NMR spectra were recorded in a Bruker 400 MHz NMR instrument and the ^{13}C-NMR spectra were recorded in the same instrument in a calculated frequency of 100 MHz.

4.2.5.1 FTIR and NMR (^{1}H and ^{13}C) characterization of furanone 4a

FTIR spectroscopy is a powerful technique that provides a clear idea about the stretching and bending frequencies of the functional groups present in the compound of interest.

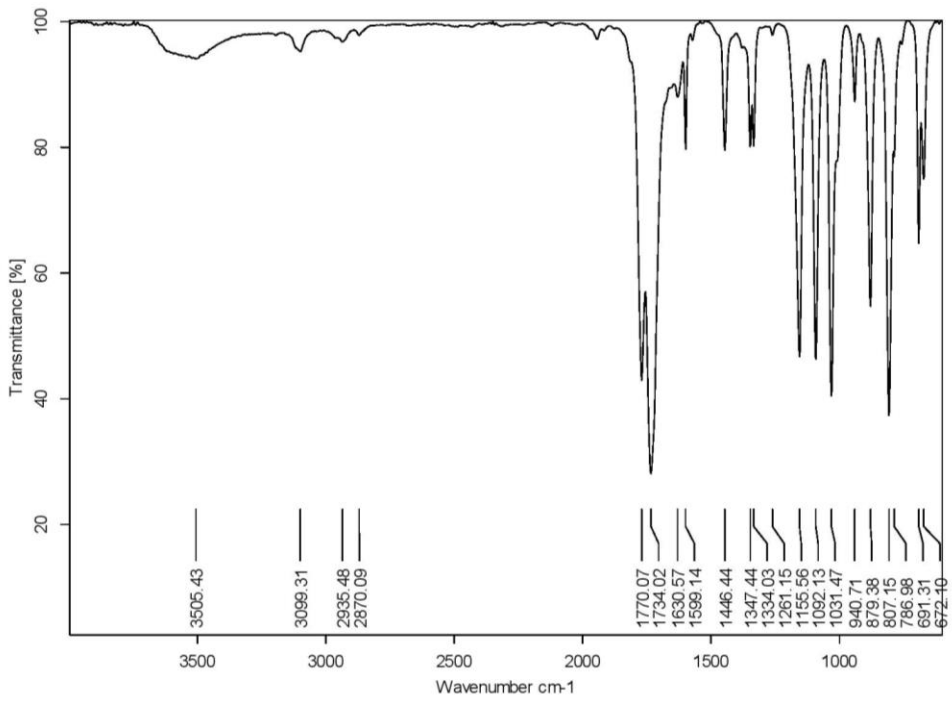

Figure 4.1 FTIR spectrum of 2-furanone **4a**.

The peak at 3099 cm^{-1} is responsible for the sp^2 =C-H stretch in the furan ring of 2-furanone. The peaks at 2928 cm^{-1} and 2866 cm^{-1} are attributed to the stretching vibrations of the -CH_2 group (symmetric and asymmetric). The strong peak at 1770 cm^{-1} corresponds to the –C=O stretching in 2(3H)furanone, and the peak at 1734 cm^{-1} corresponds to the same in 2(5H)furanone.

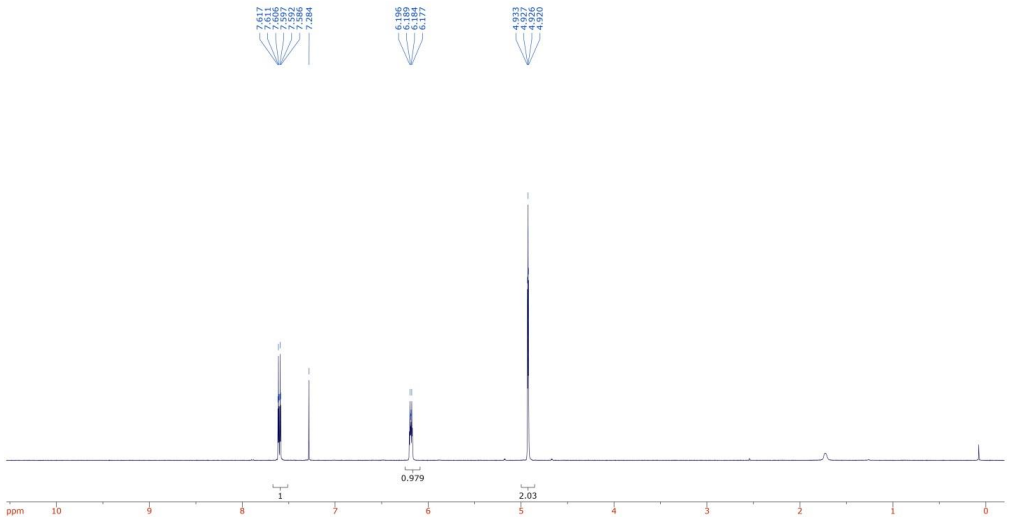

Figure 4.2 ^{1}H-NMR spectrum of 2-furanone **4a**.

^{1}H-NMR of the isolated furanone shows the peak at 6.19 ppm and 7.61 ppm is due to the lactone proton. The 2H doublet at 4.9 ppm is due to the CH_2 group.

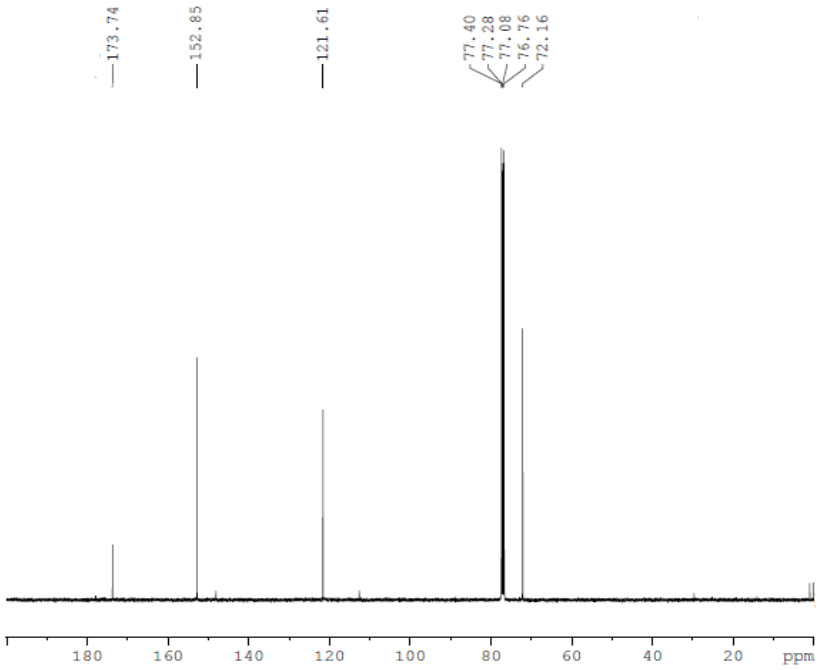

Figure 4.3 ^{13}C-NMR spectrum of 2-furanone **4a**.

^{13}C-NMR of the isolated furanone, show the peak at 173.7 ppm is due to the cyclic ester carbon, the peaks at 152.8 ppm and 121.6 ppm is due to alkenyl carbon (C=C). The peak at 72.1 ppm is due to methylene carbon.

4.3 RESULTS AND DISCUSSIONS

4.3.1 Characterization of heteropolyacids supported NH_4YZ catalysts

The PXRD pattern of NH_4YZ, fresh 20%PTA/NH_4YZ, and recovered 20%PTA/NH_4YZ catalyst are shown in **Figure 4.4**. The crystalline nature of the catalyst is apparent in the PXRD spectrum. The PXRD diffraction pattern showed an additional set of peaks that represents the cubic structure of $(NH_4)_3PW_{12}O_{40}$ (Mioč et al. 1994). It can be assumed that the interaction between $H_3PW_{12}O_{40}$ and supports such as SiO_2, TiO_2, or ZrO_2 is by direct proton transfer (Lefebvre 1992).

$$\text{M-OH} + H_3PW_{12}O_{40} \longrightarrow [\text{M-OH}_2^+] + [H_2PW_{12}O_{40}^-]$$

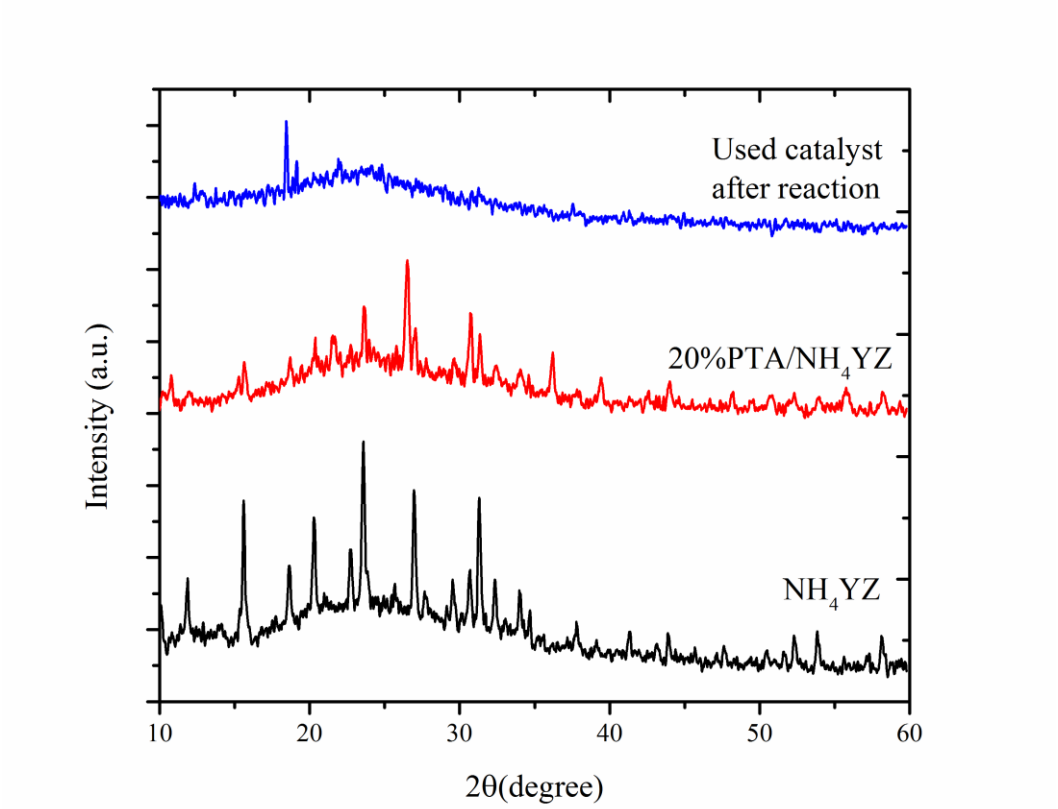

Figure 4.4 XRD spectra of (a) NH_4YZ and (b) 20%PTA/NH_4YZ (c) Used catalyst after reaction.

The FTIR spectrum of PTA (**Figure 4.5**) shows bands at 1081, 982, 888, 793, 595, and 524 cm^{-1} (Massart et al. 1977). The first five bands were assigned to the P-O_a, W-O_d, W-O_b-W, W-O_c-W stretching vibrations, and O_a-P-O_a, bending vibrations, respectively. In the 20%PTA-NH_4YZ, NH_4YZ, and PTA samples, a band at 890 cm^{-1} were assigned to the W-O_b-W stretching, the relative intensity of which increases with the increase in loading of PTA. In the spectra of the 20%PTA/NH_4Y, NH_4YZ, and PTA samples (**Figure 4.5**). A broad peak at 790 cm^{-1} is assigned to the Si-O stretching vibration (Othman et al. 2006).

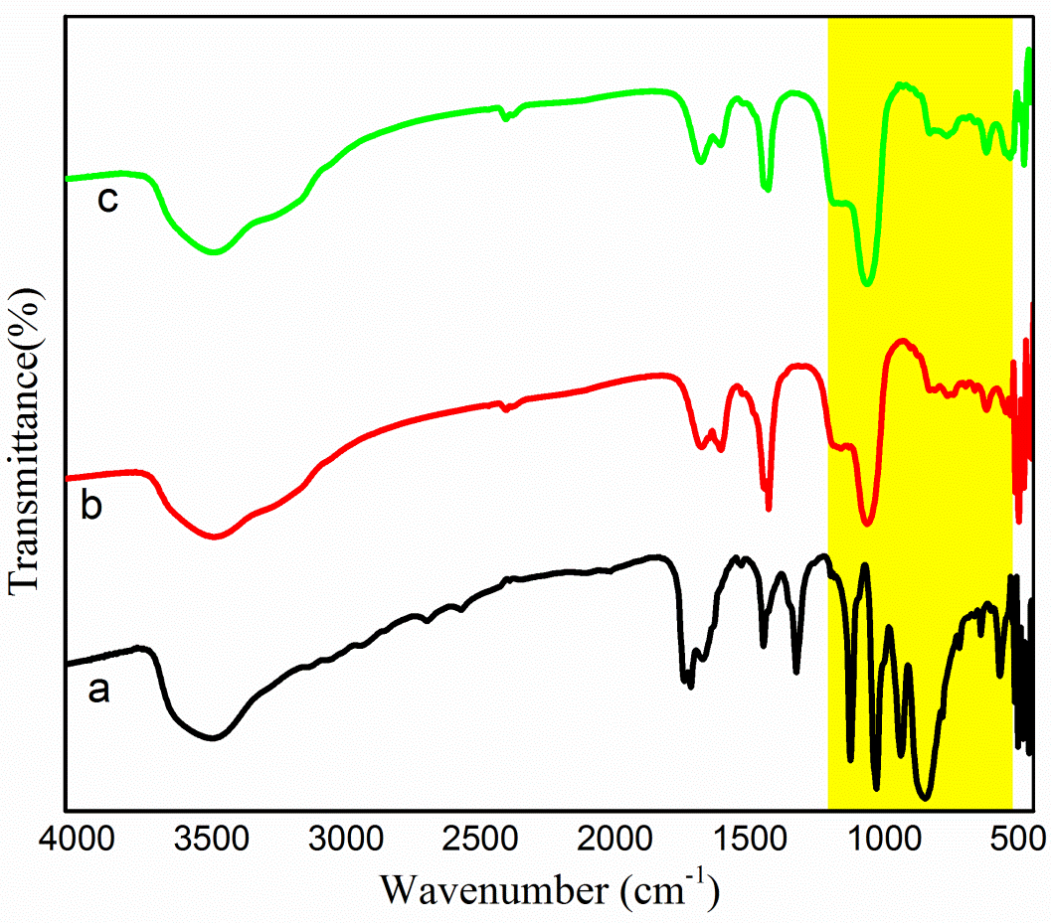

Figure 4.5 FTIR spectra of (a) PTA (b) NH_4YZ and (c) 20%PTA/NH_4YZ.

SEM images of the NH_4YZ and 20%PTA-NH_4YZ catalysts (before and after reaction) are illustrated in **Figure 4.6**. When PTA is supported onto NH_4YZ, the edge of the carrier particle becomes obscure, and a few of PTA particles are observed on the surface of the NH_4YZ particles. Thereby, the PTA particles dispersed uniformly on the NH_4YZ surface, and their numbers in the SEM images increased gradually as the loading of PTA was increased. The PTA clusters were found to be located within the pores of NH_4YZ. The PTA was found to be leached out of the NH_4YZ support after the reaction

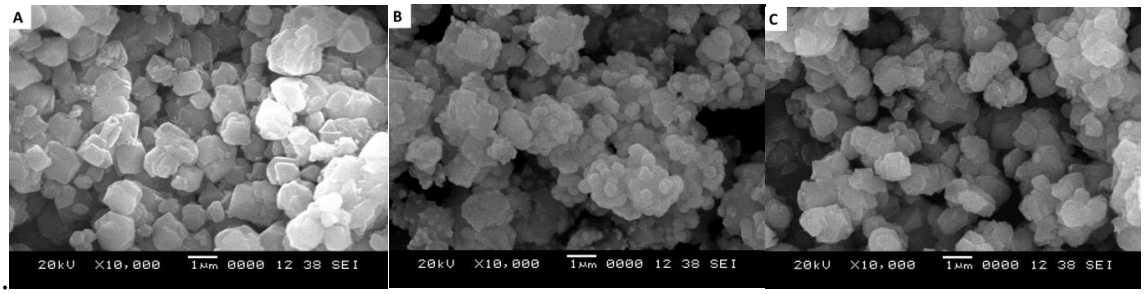

Figure 4.6 SEM image of the catalysts for (a) NH_4YZ (b) 20%PTA/NH_4YZ (Fresh) (c) After reaction (Recovered).

The initial weight loss below 250 °C (8% of the initial mass) can be attributed to the loss of water and ammonia (**Figure 4.7**). The exothermic peak can be due to the decomposition of the Keggin anion, which happens without significant weight loss.

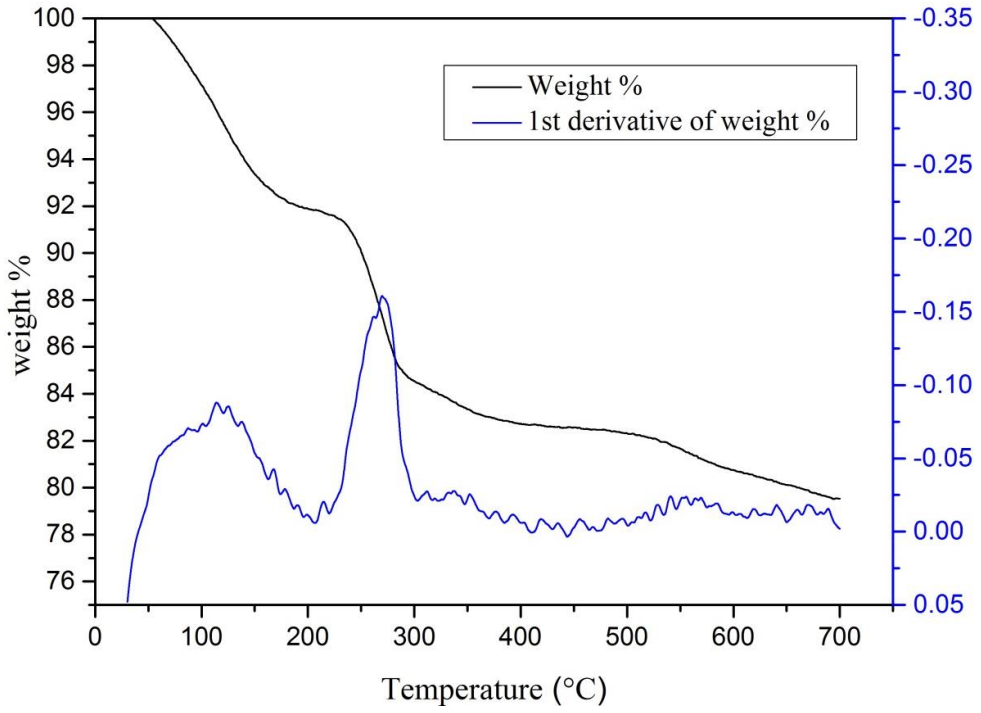

Figure 4.7 Thermal analysis diagrams of 20%PTA/NH_4YZ catalyst.

4.3.2 Catalytic study for selective oxidation of furfural

2-Furanone **4a** did not form in the absence of either the catalyst or H_2O_2 (entry 1). The reaction of furfural with H_2O_2 alone produced 2-furoic acid in combination with other acids like maleic acid or succinic acid. When the reaction was carried out in the presence of the catalyst but without H_2O_2, the furanic resins formed. The product mixture was analyzed and estimated using FTIR and NMR spectra. 20%PTA-NH_4YZ showed the best selectivity towards 2-furanone **4a** (entry 5) among the catalysts examined (**Table 4.1**). Around 20% succinic acid was isolated from the aqueous fraction. An active peroxo species is formed when PTA interacts with H_2O_2, which then reacts with furfural.

Table 4.1 Comparison of catalytic activities for H_2O_2, oxidation of furfural among the various supported polyoxometalates over NH_4YZ

Entry	Catalysts	Yields (%)
1	Without catalyst	-
2	PTA	30
3	NH_4YZ	16
4	20%STA-NH_4YZ	23
5	20%PMA-NH_4YZ	19
6	20%PTA-NH_4YZ	40
7	20%SMA-NH_4YZ	26
8[a]	20%PTA-NH_4YZ	32
9	20%PTA-NaYZ	33
10	20%STA-V_2O_5	9
11	20%STA-Nb_2O_5	18
12	20%STA-SiO_2	20
13	20%PTA-BN	17

Reaction conditions: Furfural (0.5 g), 30% Hydrogen peroxide (4 mL), Catalyst (0.10 g), 100 °C, 3 h; (a) Reused catalyst

4.3.3 Effect of the catalyst type

The selective oxidation reaction was carried out independently using PTA, STA, and PMA over NH_4YZ catalyst. The oxidation of furfural with H_2O_2 as an oxidant and using 100 mg (compared to furfural used) supported catalyst was carried out at 100 °C for 3 h. Among the three HPAs supported catalysts examined, PTA was found to be the most effective catalyst for the oxidation of furfural. Use of PTA as a supported catalyst afforded **4a** in 40% yield. Under identical conditions, the PMA-NH_4YZ and STA-NH_4YZ catalysts afforded the same in 19% and 23%, respectively (**Figure 4.8**).

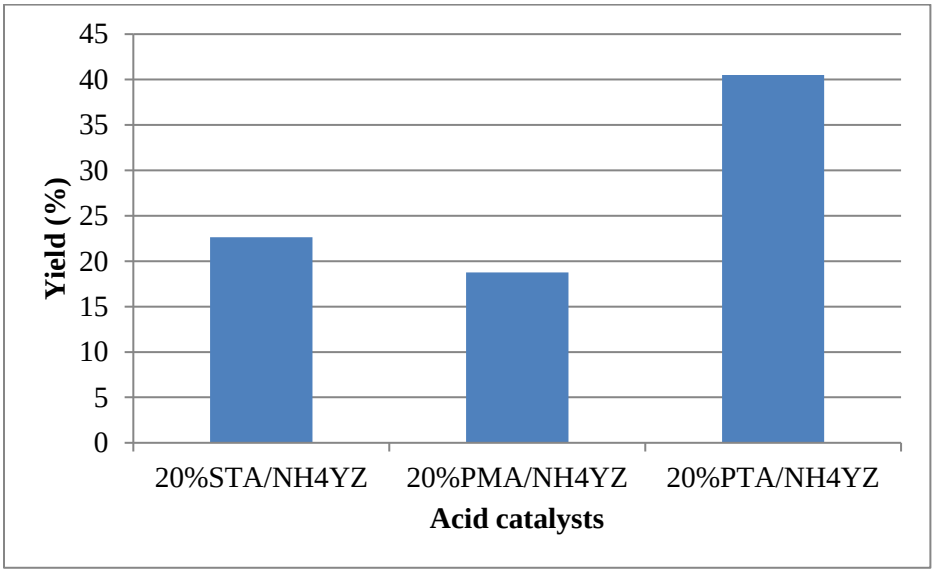

Figure 4.8 The efficiency of different HPAs on the yield of 2-furanone **4a**.

Reaction conditions: furfural (0.5 g), H_2O_2 (4 mL, 30%), 100 °C, 3 h, Catalyst (100 mg).

4.3.4 The effect of PTA loading on NH_4YZ zeolites

The loading of PTA was varied between 10-30 wt% over NH_4YZ zeolite. Out of these catalysts, the 20 wt% PTA-NH_4YZ provided 40% yield of **4a**, whereas the 10 wt% PTA-NH_4YZ and 30 wt% PTA-NH_4YZ gave **4a** is 29% and 27% yield, respectively (**Figure 4.9**).

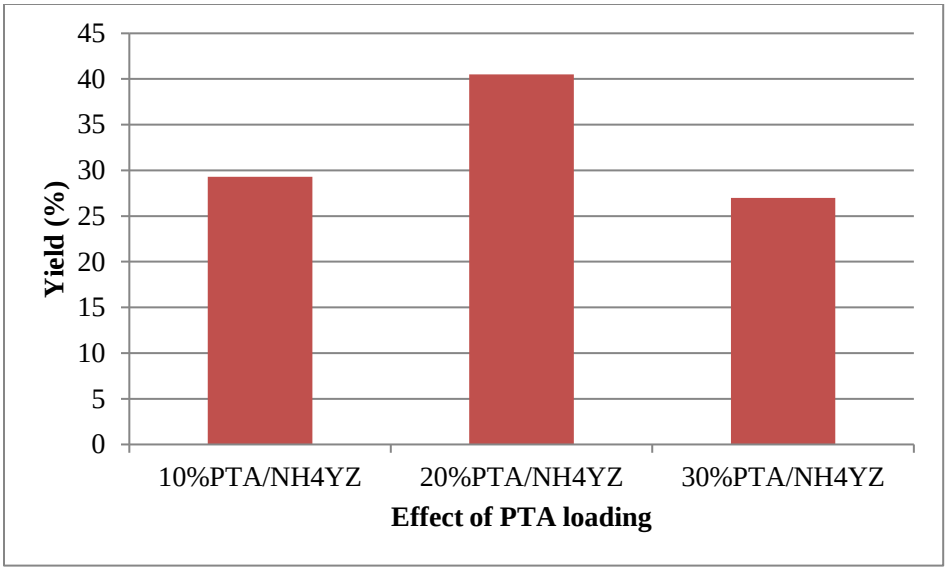

Figure 4.9 Effect of PTA loading over NH_4YZ zeolites.

Reaction conditions: furfural (0.5 g), 4 mL H_2O_2 (30%, aq.); 100 °C, 3 h, 20%PTA/NH_4YZ (100 mg).

4.3.5 Effect of catalyst loading

20%PTA-NH_4YZ was found to be the most effective catalyst for the oxidation of furfural to 2-furanone **4a**. The effect of catalyst loading on the isolated yield of 2-furanone **4a** was investigated, keeping the other parameters of the reaction unchanged. The experimental results are shown in **Figure 4.10**.

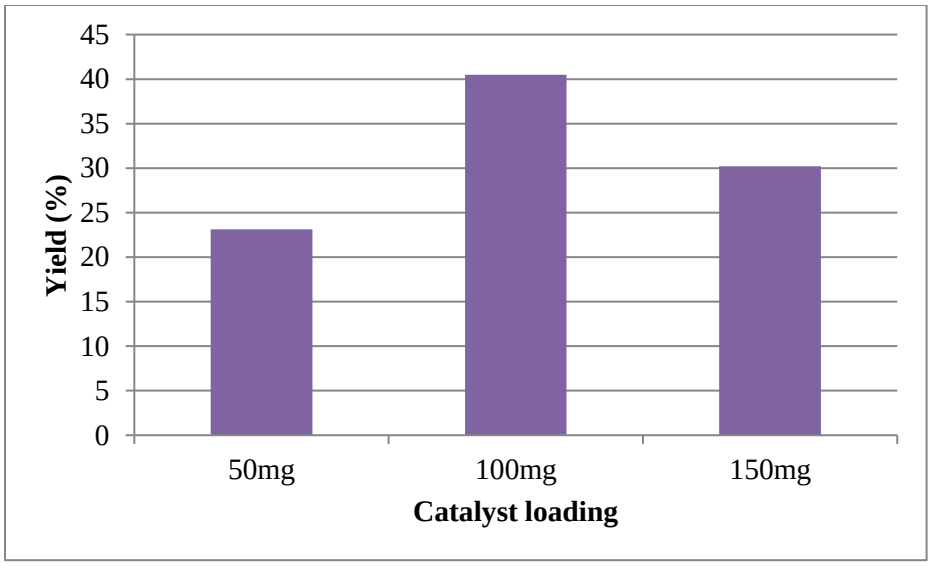

Figure 4.10 Effect of the catalyst loading on yield of 2-furanone **4a**.

Reaction conditions: furfural (0.5 g), 4 mL H_2O_2 (30% aq.), 100 °C, 3 h, 20%PTA/NH_4YZ Catalyst (100 mg).

As the amount of catalysts increased, the percentage conversion of furfural increased as well. It is very interesting to observe the difference in product selectivity with increased catalyst concentration. Lower conversion of furfural with 50 mg catalyst resulted in 23% yield of 2(5H)-furanone. The maximum conversion was obtained with 100 mg of the catalyst. The yield of 2(5H)-furanone decreased to 30% with increasing amounts of catalysts (more than 100 mg). This may be due to the fact that the faster kinetics coverts the 2(5H)-furanone into succinic acid.

4.3.6 Effect of the amount of H_2O_2

The effect of the amount of H_2O_2 on the yield of furanone is shown in **Figure 4.11**. It can be seen that the yield of furanone **4a** increased with respect to hydrogen peroxide equivalent. The reaction did not complete using 1-2 mL of H_2O_2. As the H_2O_2 amount increased to 3 mL, **4a** formed in a noticeable amount (ca. 18%). Increasing the amount of H_2O_2 to 4 mL increased the yield of **4a** incrementally and reached a maximum

of 40%. A drastic drop in the yield of **4a** to 29% was observed with an increase in H_2O_2 to 5 mL due to the over oxidation of **4a**.

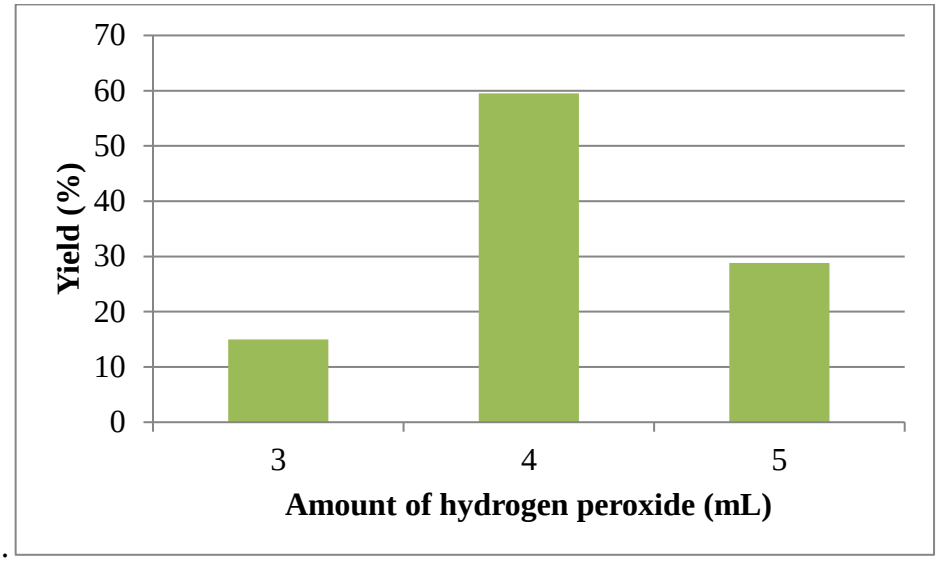

Figure 4.11 Effect of the H_2O_2 on the yield of 2-furanone **4a**.

Reaction conditions: furfural (0.5 g), 100 °C, 3 h, 20%PTA/NH_4YZ Catalyst (100 mg).

4.3.7 Effect of the temperature

The reaction temperature was varied from 80-100 °C, keeping the other reaction parameters unaltered. There is an increase in the yield of 2-furanone **4a** by increasing the temperature of the reaction from 80 °C to 100 °C. The yield of **4a** reached 40% after 3 h reaction when the reaction was carried out at 100 °C.

4.3.8 Catalyst recycling

The recoverability and reusability of the supported catalysts have been studied (entry 8). The catalyst was recovered from the reaction by filtration, dried in the oven, and resubmitted for the subsequent runs. The recycling experiment (**Table 4.1**) showed that the catalyst lost its activity significantly. A decrease in the catalytic activity of 20%PW/NH4YZ was mainly attributed to the leaching of PTA from NH_4YZ support. It

has been reported that H_2O_2 leads to a dramatic decrease in activity and selectivity of some metal-catalysts (Hasik et al. 1994).

Table 4.2 Comparison with other identified catalysts of furfural oxidation

Entry	Catalyst (amount)	Oxidant	Solvent	Tem. (ºC)	Time (h)	Yield	Year
1	Mo (VI) or Cr (VI)	Autocatalysis		60	-	25%	1998
2	Bi-phasic system	-	DCE	60-70	>10	37%	1996
3	Nb(V) acetate tetrahydrate	H_2O_2	Water	60	-	60%	2009
4	Formic acid	H_2O_2	DCE/EtOAc	100	80	62%	2016
5	20%PTA-NH_4YZ	H_2O_2	-	100	3	40%	Present work

4.4. CONCLUSIONS

PTA supported on NH_4YZ zeolite was used as the catalyst for the selective oxidation of biomass-derived furfural to 2-furanone using H_2O_2 as a green oxidant. The 20wt%PTA-NH_4YZ provided 2-furanone in 40% yield within 3 h at 100 °C using an excess of oxidant. Around 20% succinic acid was isolated from the aqueous fraction. The solvent-free synthesis is scalable, and product separation is straightforward.

CHAPTER 5

EFFICIENT PREPARATION OF ALKYL BENZOATES AND ALKYL 2-FUROATES BY HETEROPOLYACID-CATALYZED ESTERIFICATION OF BENZOIC ACID AND 2-FUROIC ACID

Abstract: *This study reports a high-yielding and scalable preparation of alkyl benzoates and alkyl furoates from benzoic acid and furoic acid, respectively using heteropolyacid as an efficient and recyclable acid catalyst. A gram-scale synthetic protocol was developed that afforded alkyl benzoates and alkyl furoates in excellent isolated yields (>85%) within 4 h at 120 °C using slight excess of the alcohol reagent and <1 mol% of the phosphotungstic acid catalyst under solvent-free conditions. The PTA catalyst was conveniently recovered and reused for three consecutive cycles without significant loss in mass or activity.*

5.1 INTRODUCTION

Esters of aromatic acids such as benzoic acid and 2-furoic acid have significant industrial applications as solvents (Feng and Zhang 2017), surfactant (Gradzielski et al. 2019), food additive (del Olmo et al. 2017), plasticizers (Erythropel et al. 2018; Hosney et al. 2018), monomer for polymers (Bart and Cavallaro 2014), agrochemicals (Chang et al. 2014), and pharmaceuticals (Bamoharram et al. 2007). Alkyl 2-furoates can be used for marine protective coatings as antifouling agents (Escobar et al. 2019). Esters of terephthalic acid are used as a monomer for terephthalates (Flores et al. 2018), whereas the diesters of phthalic acid are commercial plasticizers (Li et al. 2007). In the absence of a catalyst, the esterification reaction with alcohol is very slow. Therefore, the reaction is routinely performed in the presence of an acid catalyst (Xue et al. 2018). Alternatively, benzoate esters can be synthesized by transesterification of a readily available ester like methyl benzoate (Blümel et al. 2016). In selecting acid catalysts for the esterification reaction, catalytic activity, stability, and reusability are some of the important parameters. Acid catalysts such as mineral acids, Lewis acids, and ion-exchange resins have been used (Barbosa et al. 2006; Chakraborti et al. 2009; Li et al. 2008; Polucci et al. 2013; Rajabi et al. 2016; Sun et al. 2006; Won et al. 2007). The alcohol reagent is generally used in excess to favor the equilibrium towards the ester formation and also to compensate for the evaporative loss during the reaction. However, the use of excess alcohol introduces additional steps in product purification and catalyst

recycling. Some of the crucial parameters that decide the efficiency of the acid catalyst include acid strength, selectivity, stability, handling, and toxicity. In this regard, HPAs are well-defined solid acids with high Brönsted acidity, low volatility, low toxicity, and less corrosiveness (Katsoulis 1998; Onkarappa et al. 2019). Over the past decade, the HPA-based homogeneous and heterogeneous catalysts have increasingly being used as environment-friendly catalysts for various synthetic organic transformations (Heravi et al. 2013). Interestingly, the use of HPA catalysts supported on heterogeneous support has already been reported for the preparation of alkyl benzoates and alkyl 2-furoates (Bamoharram et al. 2007; Escobar et al. 2015; Keshavarz et al. 2019). Heterogeneous catalysts are often preferred over their homogeneous counterpart because of advantages such as safer catalyst handling, relatively straightforward product purification and convenient catalyst recovery (Fadhel et al. 2010). However, the heterogeneous catalysts generally require harsher reaction conditions and the leaching of active catalyst from the supporting material is frequently encountered. On the other hand, homogeneous catalysts work under relatively milder conditions and the problem of leaching from supporting material does not apply. However, for homogeneous catalysis, the separation and recycling of catalyst from the reaction mixture is challenging.

Hereby, we report the use of commercially-available HPA catalysts to esterify furoic acid, benzoic acid, and its derivatives under homogeneous conditions within a glass pressure reactor of batch type. We envisaged that using a sealed vessel for the reaction would enable the boiling point of alcohol to reach the equilibrium faster by achieving reaction temperatures higher. The setup also helps stop the volatile reagent's evaporative loss and allows less alcohol reagent equivalent to be used. Using only a slight excess of the alcohol reagent helps lower the loading of the catalyst, making the separation of the product straightforward, and ease the recyclability of the catalyst. In this work, a solvent-free, scalable, and high-yielding preparation of alkyl benzoates and alkyl-2-furoates from benzoic acid and furoic acid, respectively is reported using commercially-available Keggin-type HPA catalysts (**Scheme 5.1**).

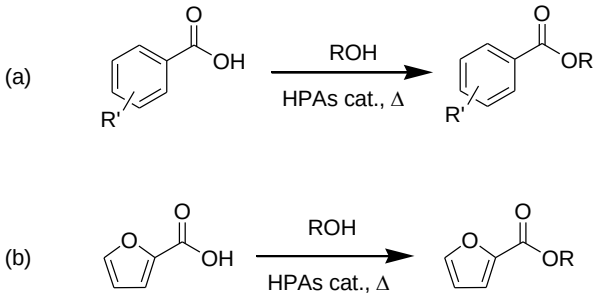

Scheme 5.1 Esterification of (a) benzoic acid, and (b) 2-furoic acid using HPA catalysts.

Reaction mechanism:

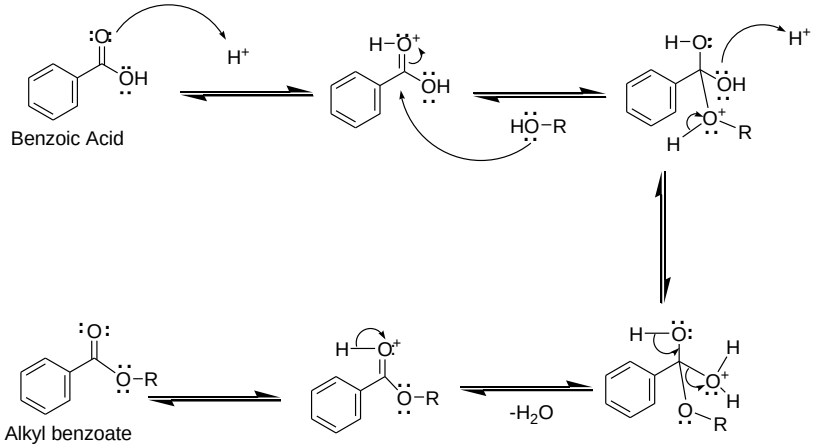

Scheme 5.2 Probable reaction mechanism of the esterification of Benzoic acid.

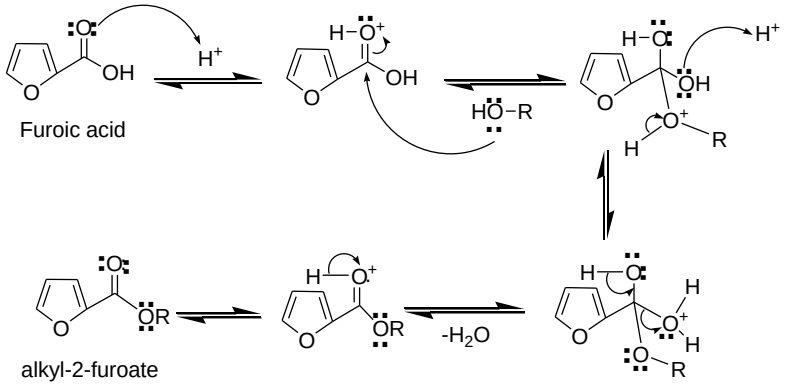

Scheme 5.3 Probable reaction mechanism of the esterification of furoic acid.

The reaction was optimized on the type and loading of HPA catalyst, the temperature of the reaction, and the molar ratio of the reagents used. The catalyst was precipitated from the reaction mixture by adding a non-polar solvent and centrifuged. The catalyst was successfully recycled for three consecutive cycles without significant loss in mass or catalytic activity.

5.2 EXPERIMENTAL SECTION

5.2.1 Materials

Benzoic acid (99%), phthalic acid (99%), terephthalic acid (99%), 4-methylbenzoic acid (99%), 4-chlorobenzoic acid (99%), 4-methoxybenzoic acid (99%), 2-methylbenzoic acid, 4-nitrobenzoic acid (99%), salicylic acid (99%), 2-bromobenzoic acid (99%), and *trans*-cinnamic acid (99%) were purchased from Loba Chemie. Furoic acid (98%) was prepared from biomass derived furfural using reported method (Wilson 1926). Methanol (99.5%), ethanol (100%), 1-propanol (99.5%), 1-butanol (99%), 1-pentanol (99%), 1-hexanol (99%), propane-1,3-diol (99%), petroleum ether (98%), and chloroform (99%) were purchased from Loba Chemie. Phosphotungstic acid (PTA), Silicotungstic acid (STA), Silicomolybdic acid (SMA), and Phosphomolybdic acid (PMA) were purchased from Sigma. The HPA catalysts were dried in a hot-air oven at 110 °C for 12 h prior use. The alcohols were dried over pre-activated molecular sieves (4 Å) for 24 h prior use. The FTIR spectra of the samples were collected on a Bruker Alpha FTIR instrument. The FTIR spectra of esters were collected in the ATR mode and FTIR spectra of the PTA catalysts were collected in the KBr matrix. The ^{1}H-NMR spectra were recorded in a Bruker Nanobay 300 MHz NMR instrument, and the ^{13}C-NMR spectra were recorded in the same instrument in a calculated frequency of 75 MHz. Deuterated chloroform (99.8 atom% D) was used as the NMR solvent for all esters. Deuterium oxide (99.9 atom% D) was used as the solvent to record the ^{31}P NMR spectrum of PTA catalyst.

5.2.2 Catalytic reactions (A): Esterification of benzoic acid over HPA catalysts

Benzoic acid (1.00 g, 8.19 mmol) and a 1-butanol (0.910 g, 12.30 mmol, 1.5 eq.) were charged into a round-bottomed glass pressure reactor (50 mL) fitted with a magnetic stir rod and Teflon screw top. Oven-dried PTA (100 mg, 0.4 mol%) was weighed in air and added to the solution. The reactor was sealed and placed in a pre-heated oil bath (120 °C) and stirred magnetically for 4 h. After the reaction, the reactor was cooled to room temperature and opened. Petroleum ether (10 mL) was added into the mixture, and the product was solubilized. The colorless supernatant was carefully decanted into a beaker. The precipitated catalyst was washed with petroleum ether (3×10 mL). The petroleum ether layers were combined, dried over anhydrous Na_2SO_4, and evaporated under reduced pressure in a rotary evaporator to obtain colorless oil. The crude mixture was chromatographed (silica gel, chloroform) and the solvent evaporated to get butyl benzoate **5d** (1.120 g, 98%) as a clear liquid. The recovered catalyst was dried in a hot-air oven at 110 °C for 12 h.

5.2.3 Instrument used for the characterization of compounds

FTIR spectra of the samples were collected on a Bruker Alpha FTIR instrument. The FTIR spectrum of samples was collected in the ATR mode and the solid HPA catalysts were collected in the KBr matrix. The ^{1}H-NMR spectra were recorded in a Bruker 300 MHz NMR instrument and the ^{13}C-NMR spectra were recorded in the same instrument in a calculated frequency of 75 MHz.

5.2.3.1 FTIR and NMR (^{1}H and ^{13}C) characterization of methyl benzoate 5a

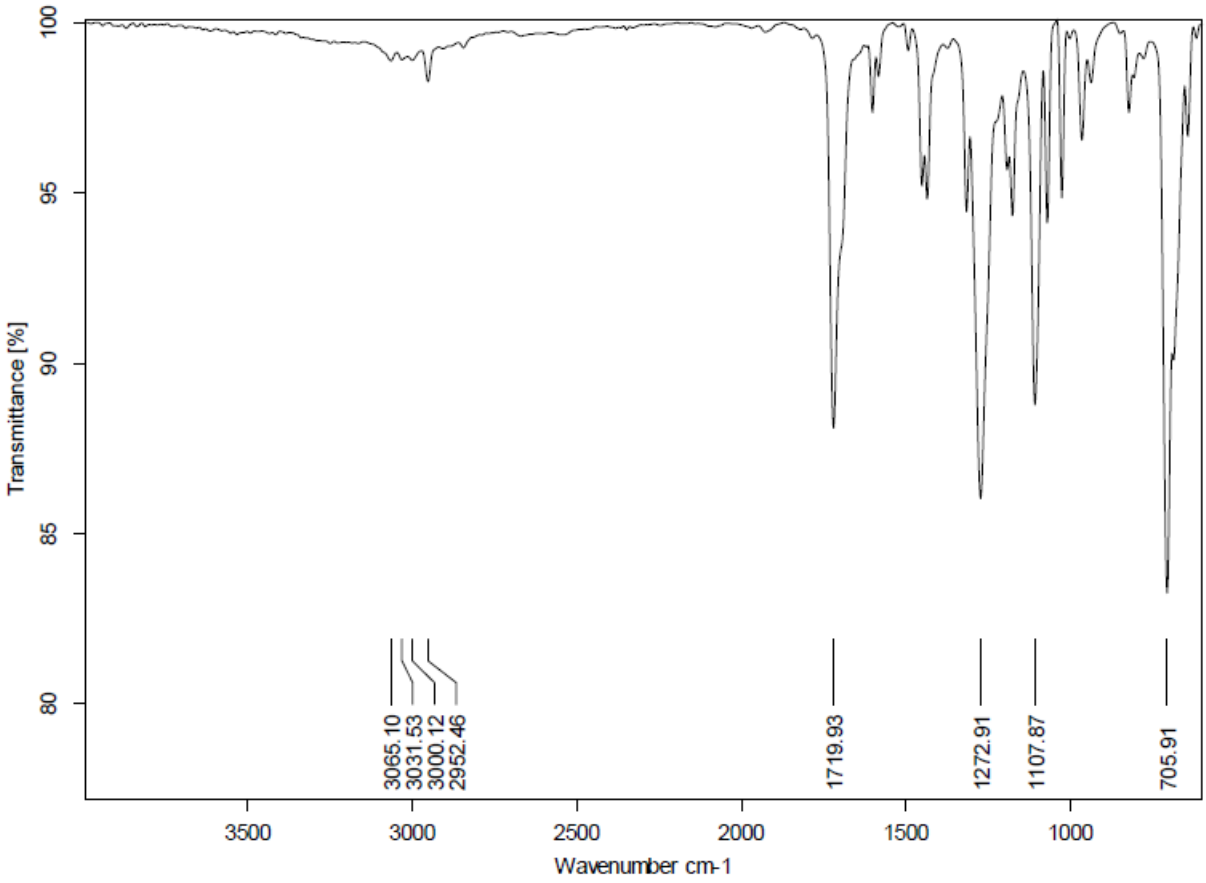

Figure 5.1 FTIR spectrum of methyl benzoate **5a**.

The peak at 3066 cm^{-1} is due to sp^2 –C-H stretching frequency and the peak at 2952 cm^{-1} is responsible for the sp^3 -C-H stretching frequency. The peak at 1720 cm^{-1} corresponds to the ester C=O stretching frequency, 1683 cm^{-1} is due to C=C stretching frequency and 1107 cm^{-1} is due to C-O stretching frequency of ester group.

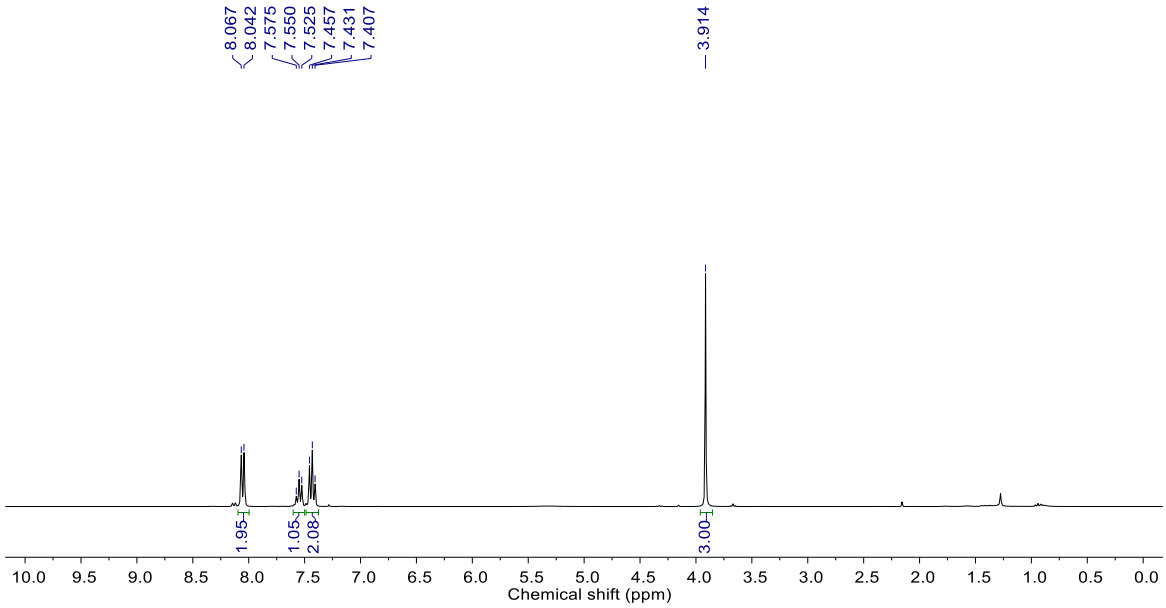

Figure 5.2 ^{1}H-NMR spectrum of methyl benzoate **5a**.

^{1}H-NMR of the isolated methyl benzoate show the 2H doublet, 2H triplet, and 1H triplet at 8.05 ppm, 7.43 ppm, and 7.55 ppm are due to the aromatic ortho, meta, and para protons respectively. The 3H singlet at 3.91 ppm is due to protons of methoxy (-OCH_3) group.

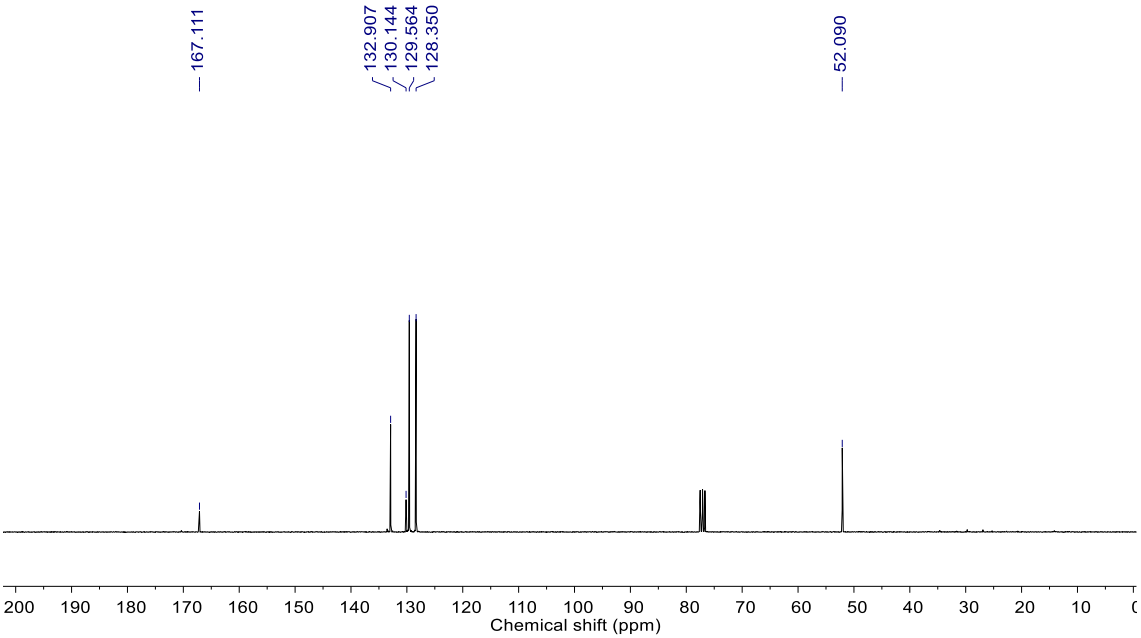

Figure 5.3 ^{13}C-NMR spectrum of methyl benzoate **5a**.

^{13}C-NMR of the isolated methyl benzoate show the peak at 167.1 ppm is due to the ester carbon (C=O), the four peaks at 132.9 ppm, 130.1 ppm, 129.5 ppm, and 128.35 ppm are due to the carbon atoms in the benzene ring. The peak at 52.0 ppm is corresponding to –OCH_3 carbon.

5.2.3.2 FTIR and NMR (^{1}H and ^{13}C) characterization of ethyl benzoate 5b

^{1}H-NMR ($CDCl_3$, 300 MHz) δ (ppm): 8.08 (d, 2H, d, *J* = 7.5 Hz), 7.56 (t, 1H, *J* = 7.5 Hz), 7.44 (t, 2H, *J* = 7.5 Hz), 4.41 (q, 2H, *J* = 6.9 Hz), 1.41 (t, 3H, *J* = 6.9 Hz); ^{13}C-NMR ($CDCl_3$, 75 MHz) δ (ppm):166.6, 132.8, 130.5, 129.5, 128.3, 60.9, 14.3; FTIR (ATR, cm^{-1}): 3063, 2982, 1715, 1270, 1106.

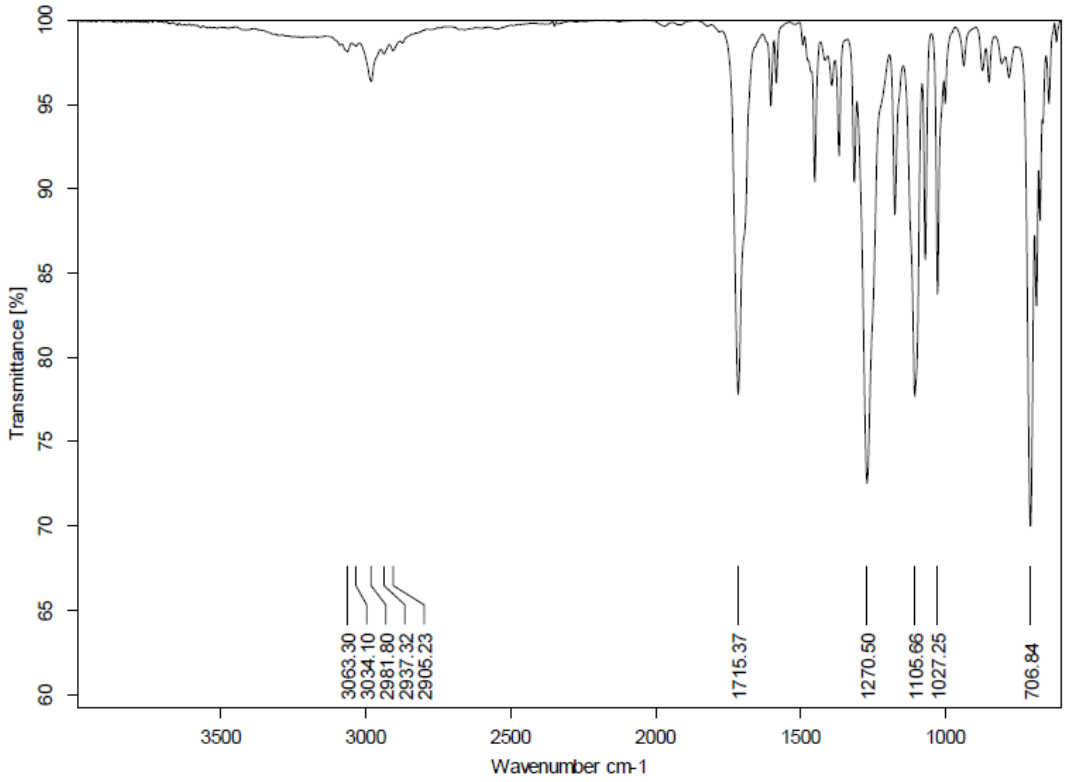

Figure 5.4 FTIR spectrum of ethyl benzoate **5b**.

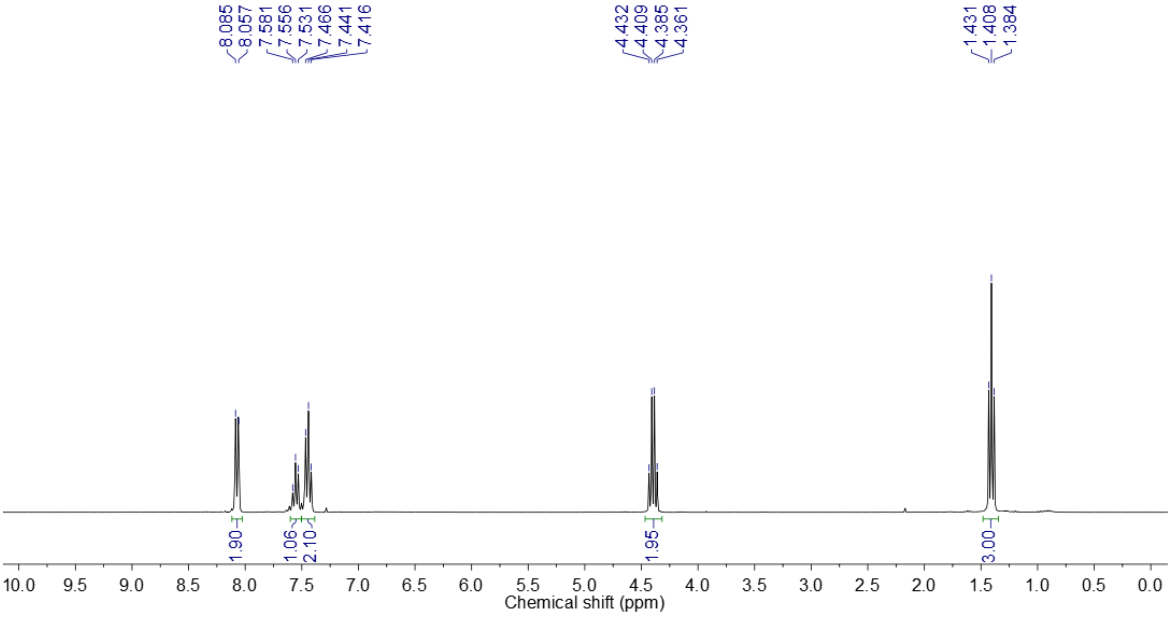

Figure 5.5 ^{1}H-NMR spectrum of ethyl benzoate **5b**.

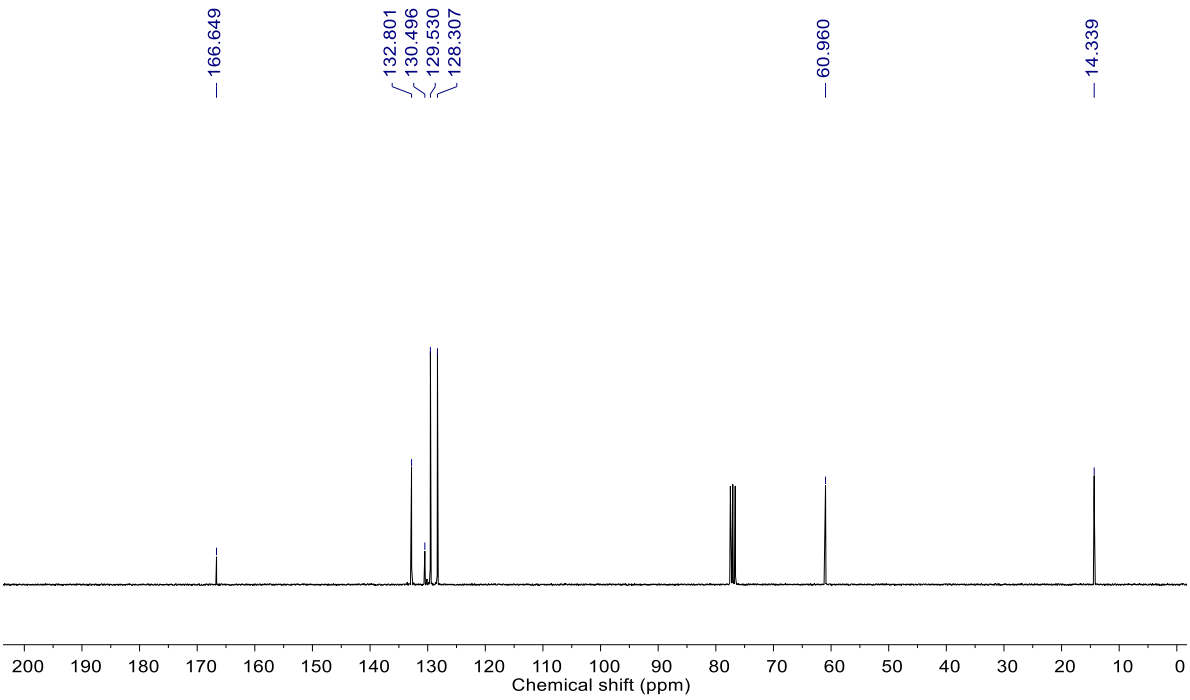

Figure 5.6 ^{13}C-NMR spectrum of ethyl benzoate **5b**.

5.2.3.3 FTIR and NMR (^{1}H and ^{13}C) characterization of propyl benzoate 5c

^{1}H-NMR ($CDCl_3$, 300 MHz) δ (ppm): 8.06 (d, 2H, *J* = 7.5 Hz), 7.54 (t, 1H, *J* = 7.5 Hz), 7.43 (t, 2H, *J* = 7.5 Hz), 4.31 (t, 2H, *J* = 6.6 Hz), 1.83 (m, 2H), 1.05 (t, 3H, *J* = 7.5 Hz); ^{13}C-NMR (($CDCl_3$, 75 MHz) δ (ppm): 166.7, 132.8, 130.5, 129.5, 128.3, 66.5, 22.1, 10.5; FTIR (ATR, cm^{-1}): 3066, 2968, 1716, 1269, 1107.

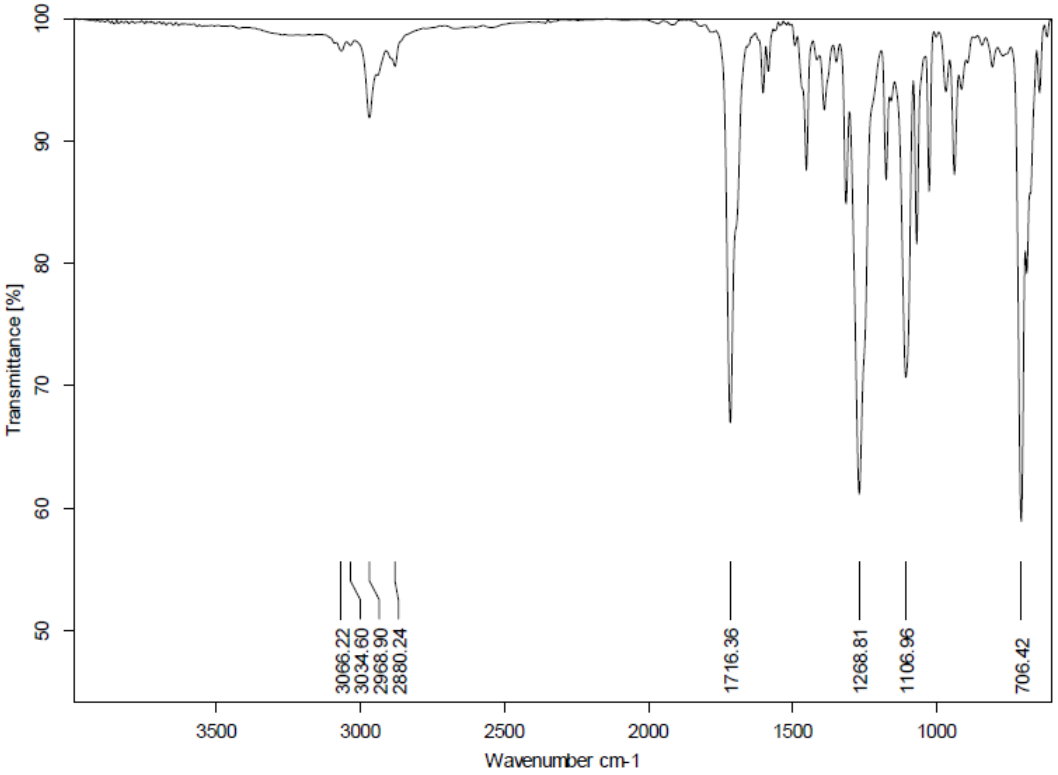

Figure 5.7 FTIR spectrum of propyl benzoate **5c**.

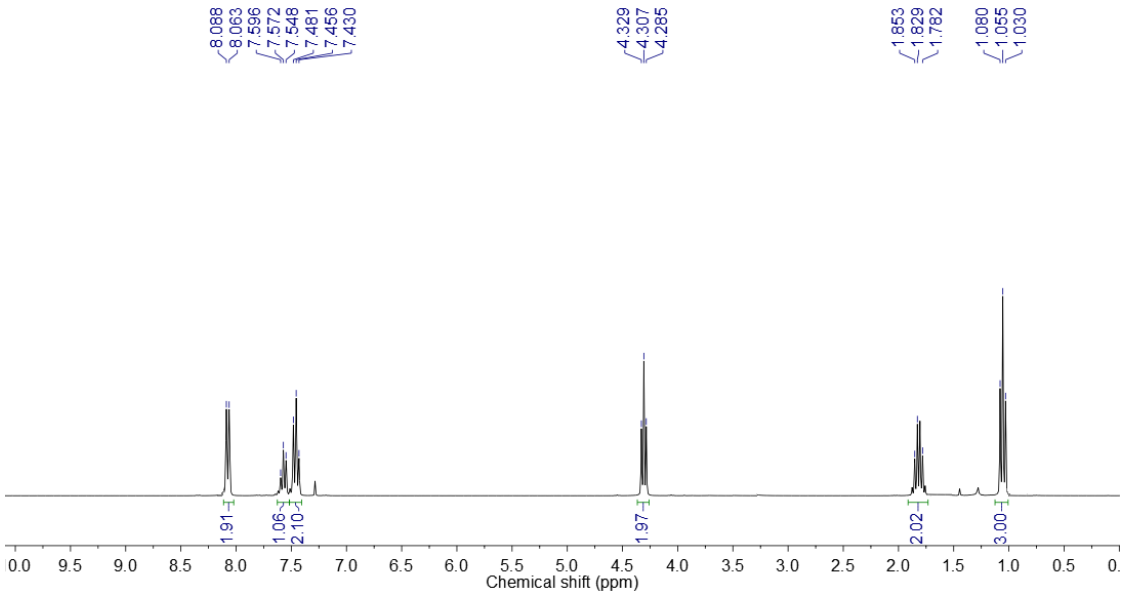

Figure 5.8 ^{1}H-NMR spectrum of propyl benzoate **5c**.

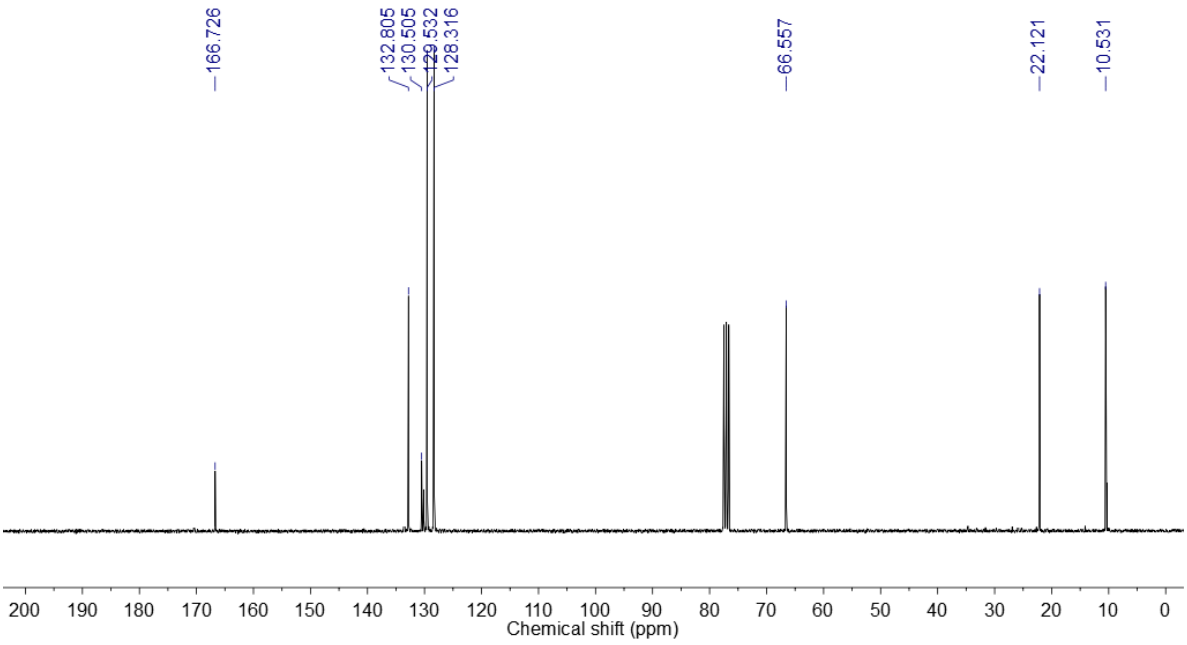

Figure 5.9 ^{13}C-NMR spectrum of propyl benzoate **5c**.

5.2.3.4 FTIR and NMR (^{1}H and ^{13}C) characterization of butyl benzoate 5d

^{1}H-NMR ($CDCl_3$, 300 MHz) δ (ppm): 8.06 (d, 2H, *J* = 7.5 Hz), 7.57 (t, 1H, *J* =7.5 Hz), 7.46 (t, 2H, *J* = 7.5 Hz), 4.34 (t, 2H, *J* = 6.6 Hz), 1.76 (2H, m), 1.48 (2H, m), 0.99 (t, 3H, *J* = 7.5 Hz); ^{13}C-NMR ($CDCl_3$, 75 MHz) δ (ppm):166.7, 132.8, 130.5, 129.5, 128.3, 64.8, 30.8, 19.3, 13.8; FTIR (ATR, cm^{-1}): 3064, 2959, 1717, 1269, 1108.

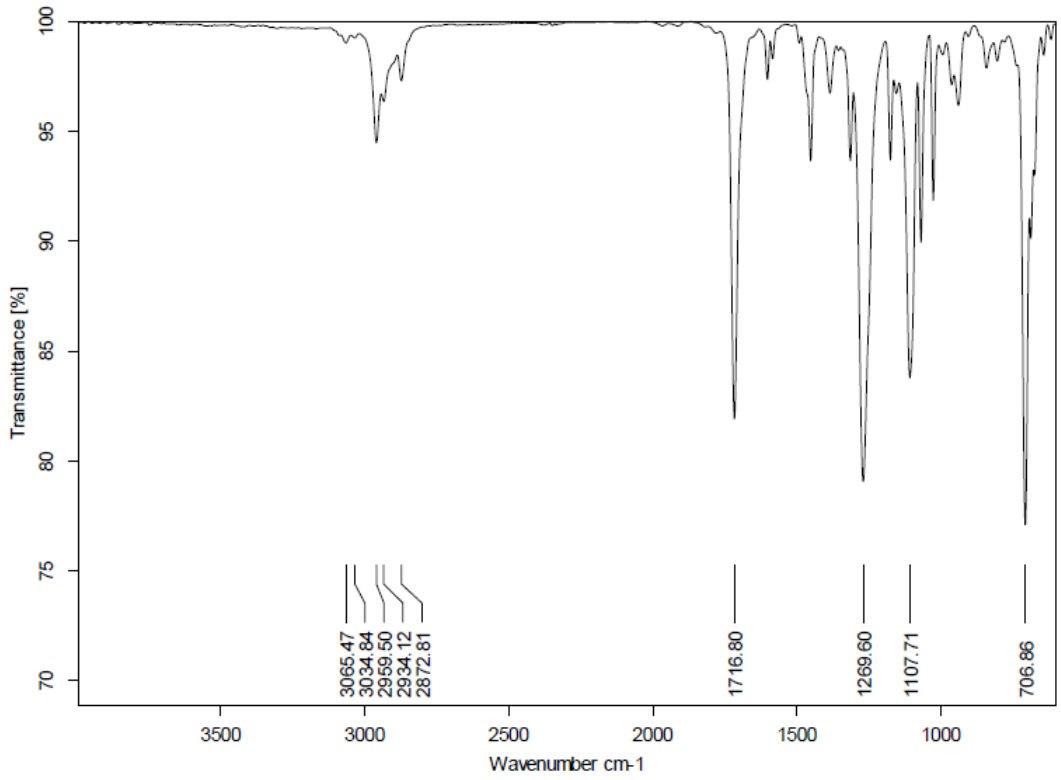

Figure 5.10 FTIR spectrum of butyl benzoate **5d**.

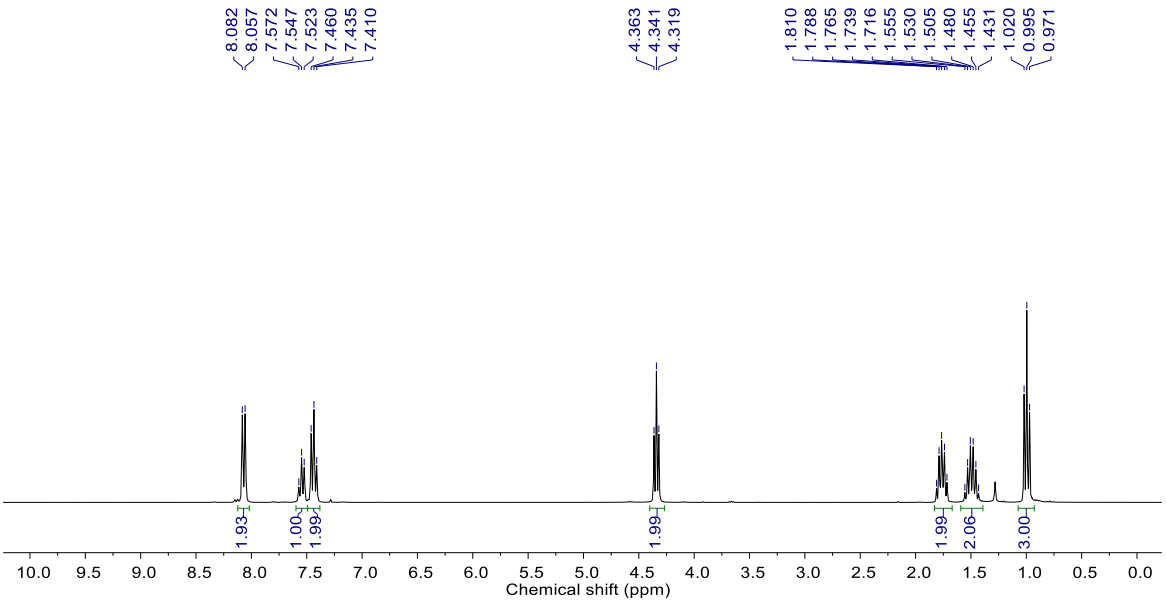

Figure 5.11 ^{1}H-NMR spectrum of butyl benzoate **5d**.

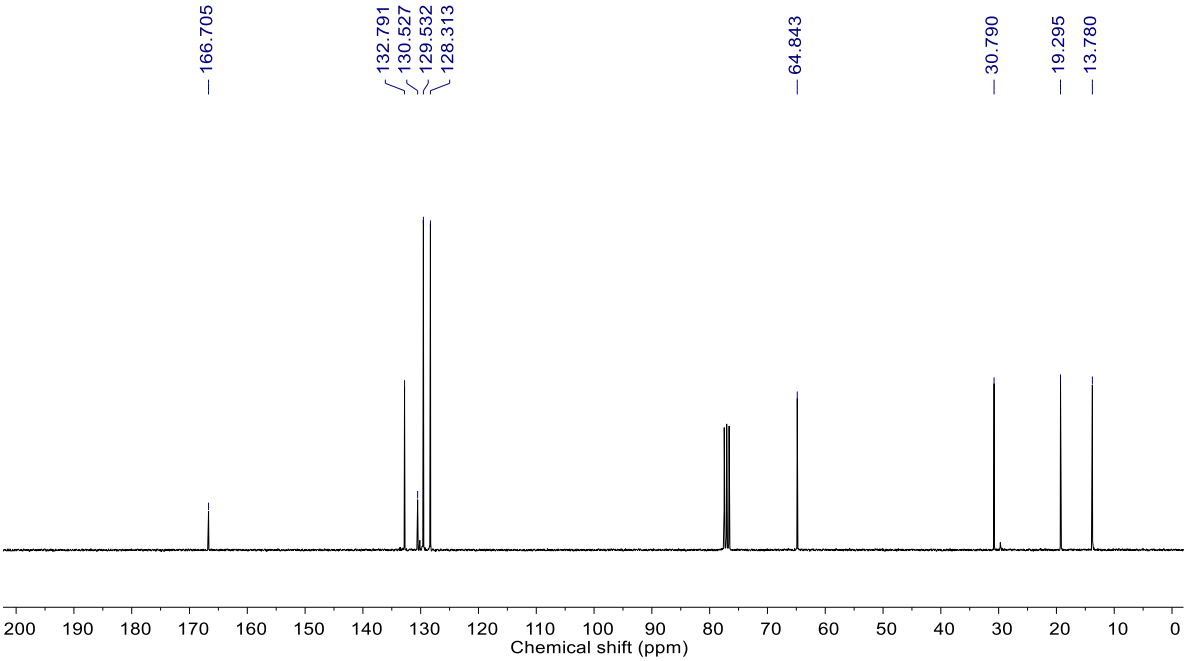

Figure 5.12 ^{13}C-NMR spectrum of butyl benzoate **5d**.

5.2.3.5 FTIR and NMR (^{1}H and ^{13}C) characterization of pentyl benzoate 5e

^{1}H-NMR ($CDCl_3$, 300 MHz) δ (ppm): 8.06 (d, 2H, *J* = 8.1 Hz), 7.57 (t, 1H, *J* = 8.1 Hz), 7.46 (t, 2H, *J* = 8.1 Hz), 4.34 (t, 2H, *J* = 6.6 Hz), 1.79 (m, 2H), 1.43 (m, 4H), 0.96 (t, 3H, *J* = 6.9 Hz); ^{13}C-NMR ($CDCl_3$, 75 MHz) δ (ppm):166.7, 132.8, 130.5, 129.5, 128.3, 65.1, 28.4, 28.2, 22.4, 14.0; FTIR (ATR, cm^{-1}): 3066, 2957, 1717, 1269, 1108.

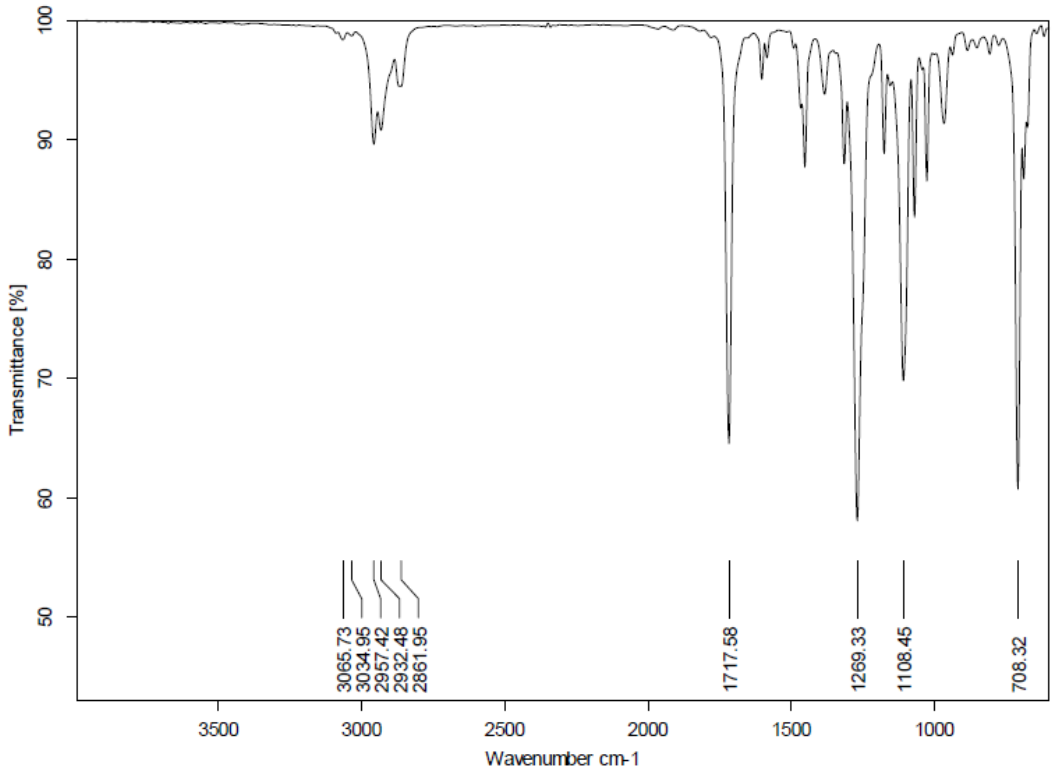

Figure 5.13 FTIR spectrum of pentyl benzoate **5e**.

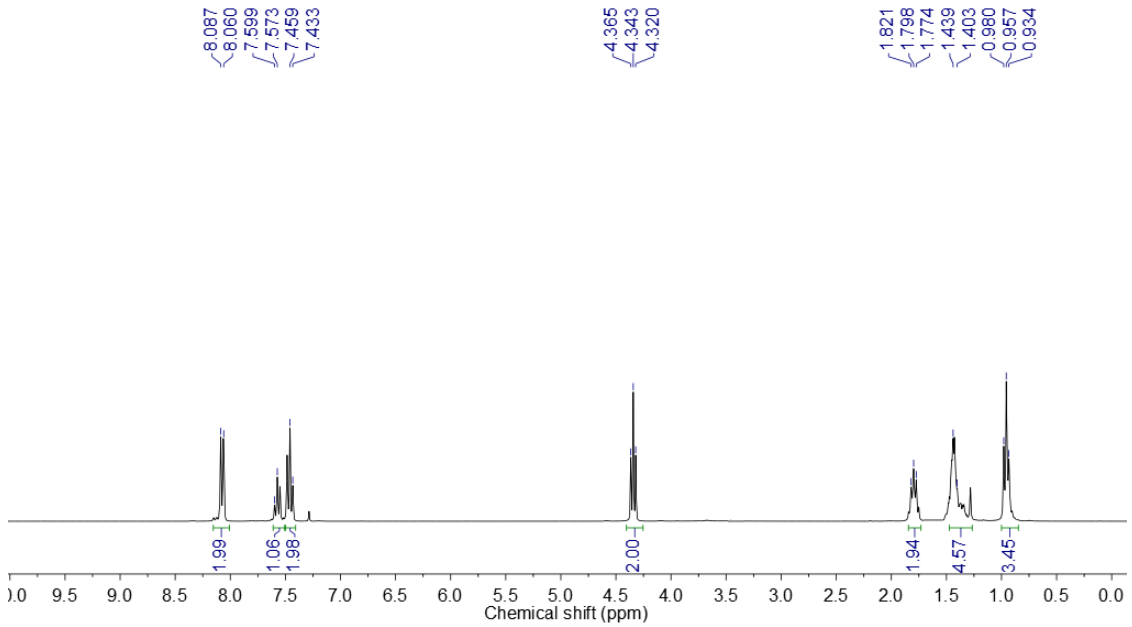

Figure 5.14 ^{1}H-NMR spectrum of pentyl benzoate **5e**.

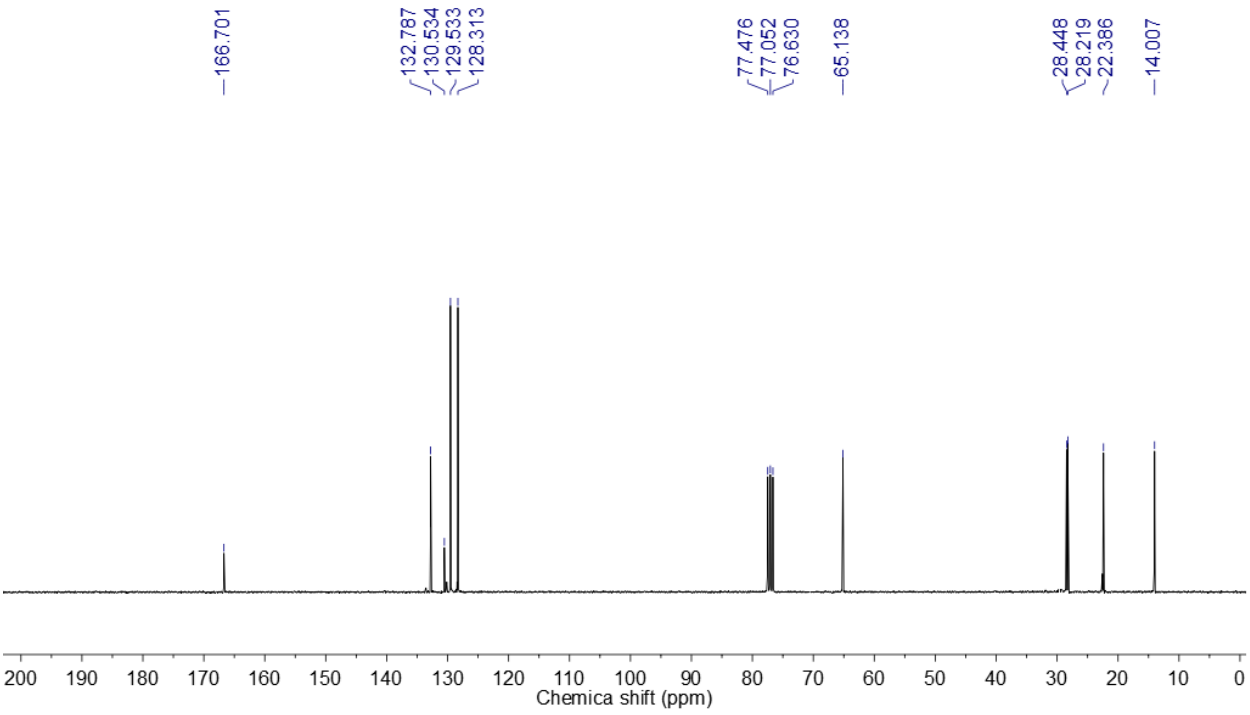

Figure 5.15 ^{13}C-NMR spectrum of pentyl benzoate **5e**.

5.2.3.6 FTIR and NMR (^{1}H and ^{13}C) characterization of hexyl benzoate 5f

^{1}H-NMR ($CDCl_3$, 300 MHz) δ (ppm): 7.96 (d, 2H, *J* = 7.2 Hz), 7.44 (t, 1H, *J* = 7.2 Hz), 7.33 (t, 2H, *J* = 7.2 Hz), 4.22 (t, 2H, *J* = 6.6 Hz), 1.64 (m, 2H), 1.26 (m, 6H), 0.81 (t, 3H, *J* = 4.8 Hz); ^{13}C-NMR ($CDCl_3$, 75 MHz) δ (ppm): 166.7, 132.8, 130.5, 129.5, 128.3, 65.1, 31.5, 28.7, 25.7, 22.6, 14.0; FTIR (ATR, cm^{-1}): 3064, 2955, 1717, 1268, 1109.

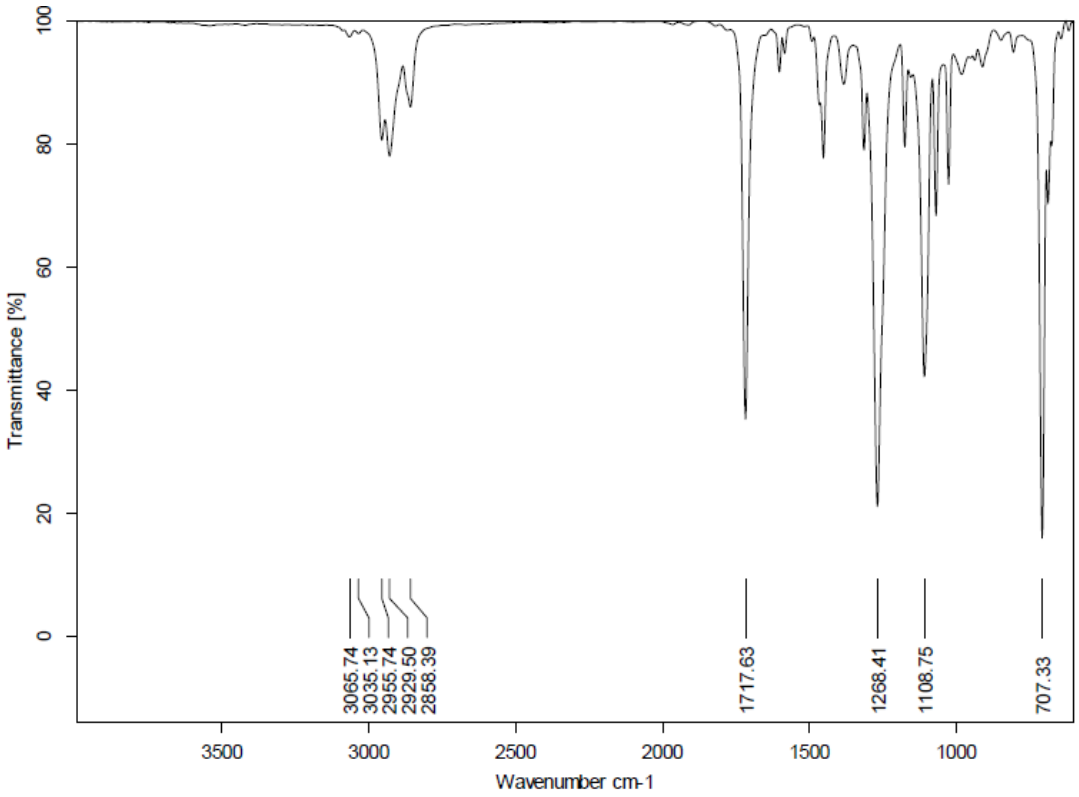

Figure 5.16 FTIR spectrum of hexyl benzoate **5f**.

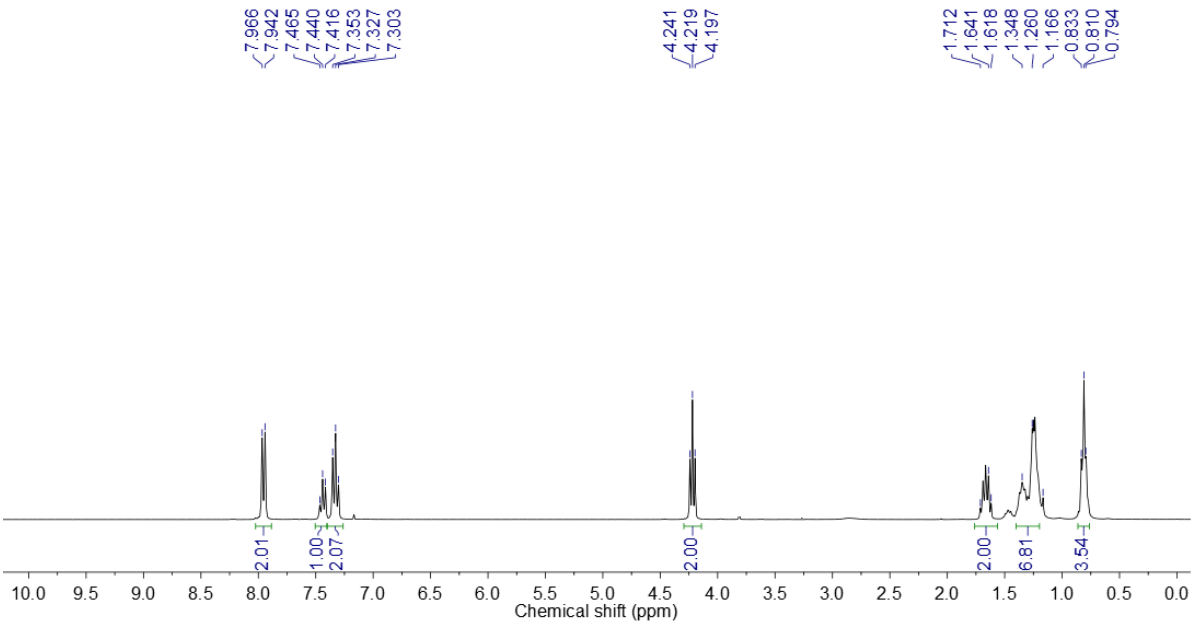

Figure 5.17 ^{1}H-NMR spectrum of hexyl benzoate **5f**.

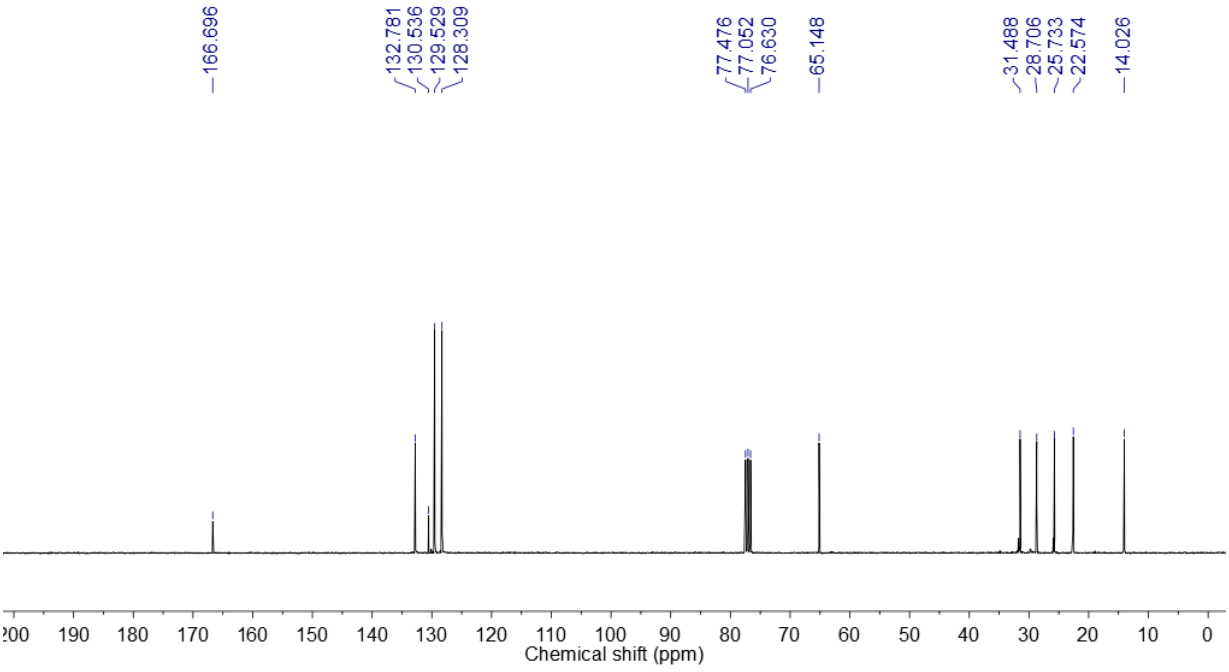

Figure 5.18 ^{13}C-NMR spectrum of hexyl benzoate **5f**.

5.2.3.7 FTIR and NMR (^{1}H and ^{13}C) characterization of propane-1,3-diyl dibenzoate 5g

^{1}H-NMR ($CDCl_3$, 300 MHz) δ (ppm): 8.06 (d, 4H, *J* = 8.4 Hz), 7.60 (t, 2H, *J* = 8.4 Hz), 7.46 (t, 4H, *J* = 8.4 Hz), 4.54 (t, 4H, *J* = 6.3 Hz), 2.29 (pentate, 2H, *J* = 6.3 Hz); ^{13}C-NMR ($CDCl_3$, 75 MHz) δ (ppm): 166.5, 133.0, 130.1, 129.6, 128.4, 61.8, 28.3; FTIR (ATR, cm^{-1}): 3062, 2963, 1712, 1263, 1062.

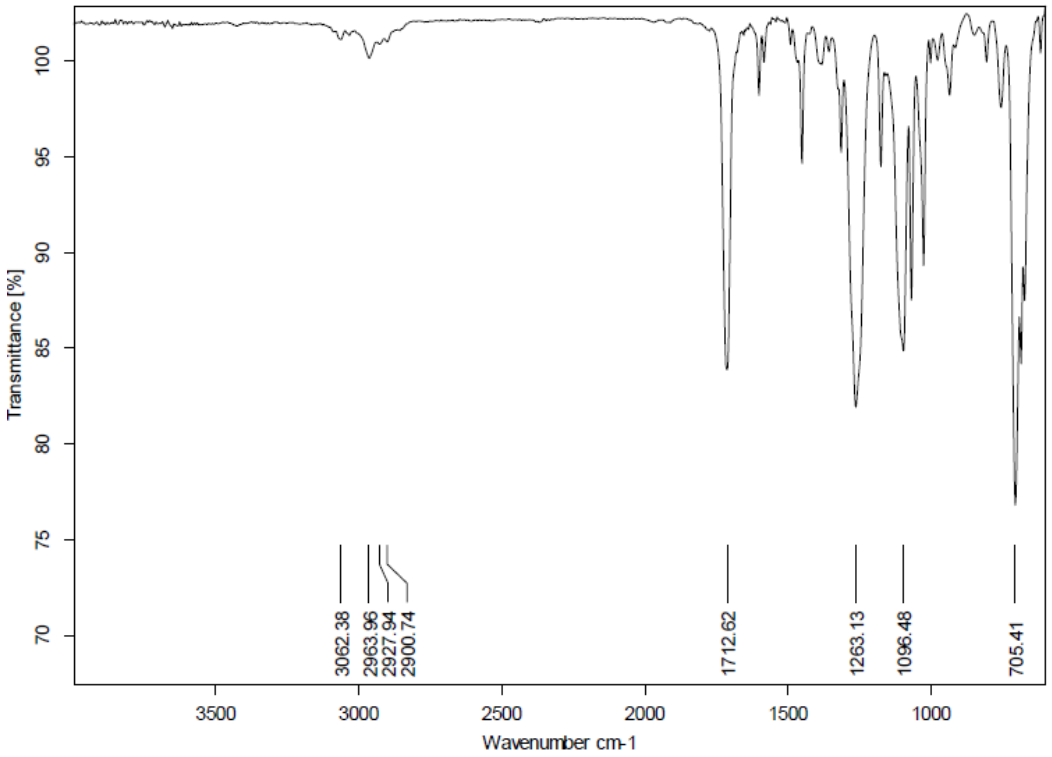

Figure 5. 19 FTIR spectrum of propane-1,3-diyl dibenzoate **5g**.

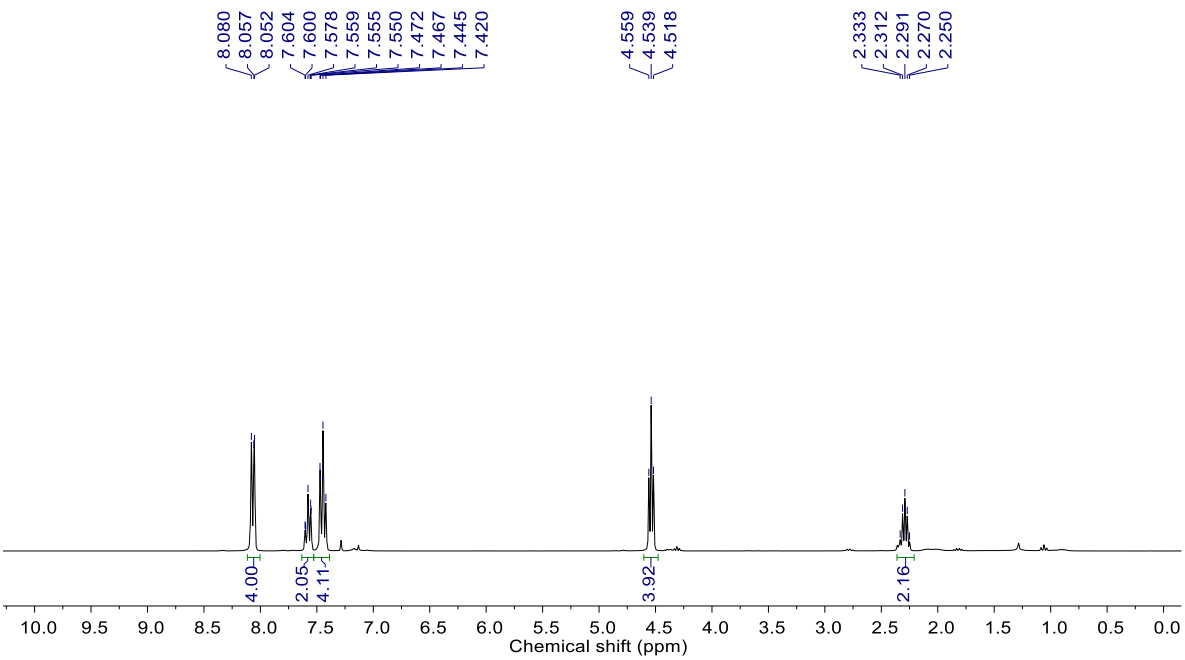

Figure 5.20 ^{1}H-NMR spectrum of propane-1,3-diyl dibenzoate **5g**.

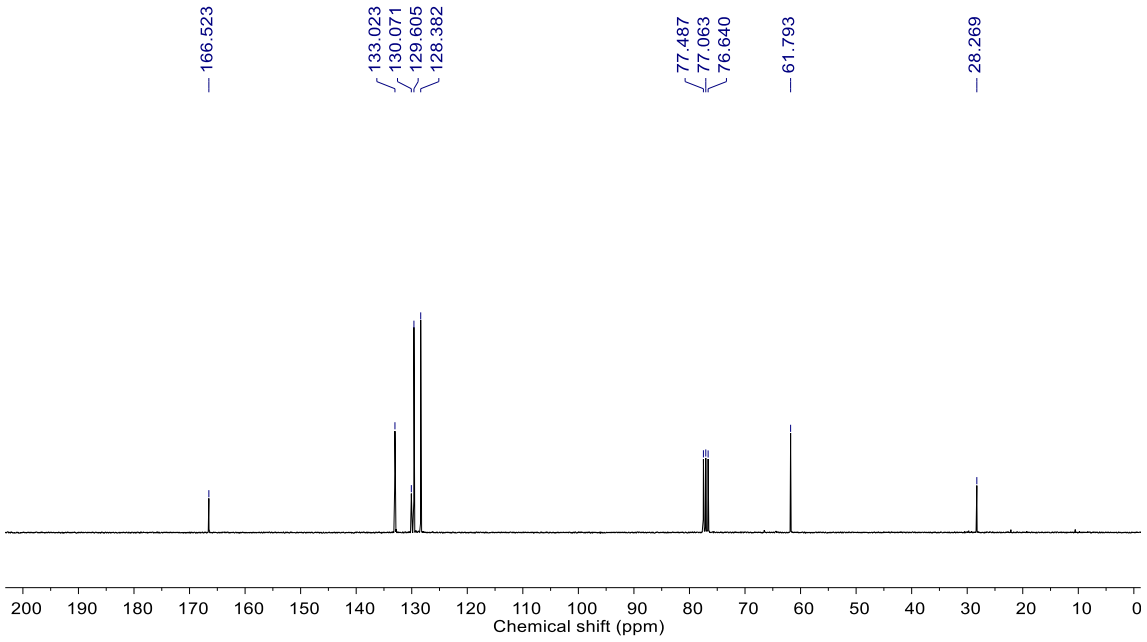

Figure 5.21 ^{13}C-NMR spectrum of propane-1,3-diyl dibenzoate **5g**.

5.2.3.8 FTIR and NMR (^{1}H and ^{13}C) characterization of butyl 4-chlorobenzoate 5h

^{1}H-NMR ($CDCl_3$, 300 MHz) δ (ppm): 8.00 (d, 2H, *J* = 8.4 Hz), 7.40 (d, 2H, *J* = 8.4 Hz), 4.33 (t, 2H, *J* = 6.3 Hz), 1.78 (m, 2H), 1.47 (m, 2H), 0.99 (t, 3H, *J* = 7.2 Hz); ^{13}C-NMR ($CDCl_3$, 75 MHz) δ (ppm): 165.8, 139.2, 130.9, 128.9, 128.6, 65.1, 30.7, 19.3, 13.7; FTIR (ATR, cm^{-1}): 2959, 1717, 1268, 1090.

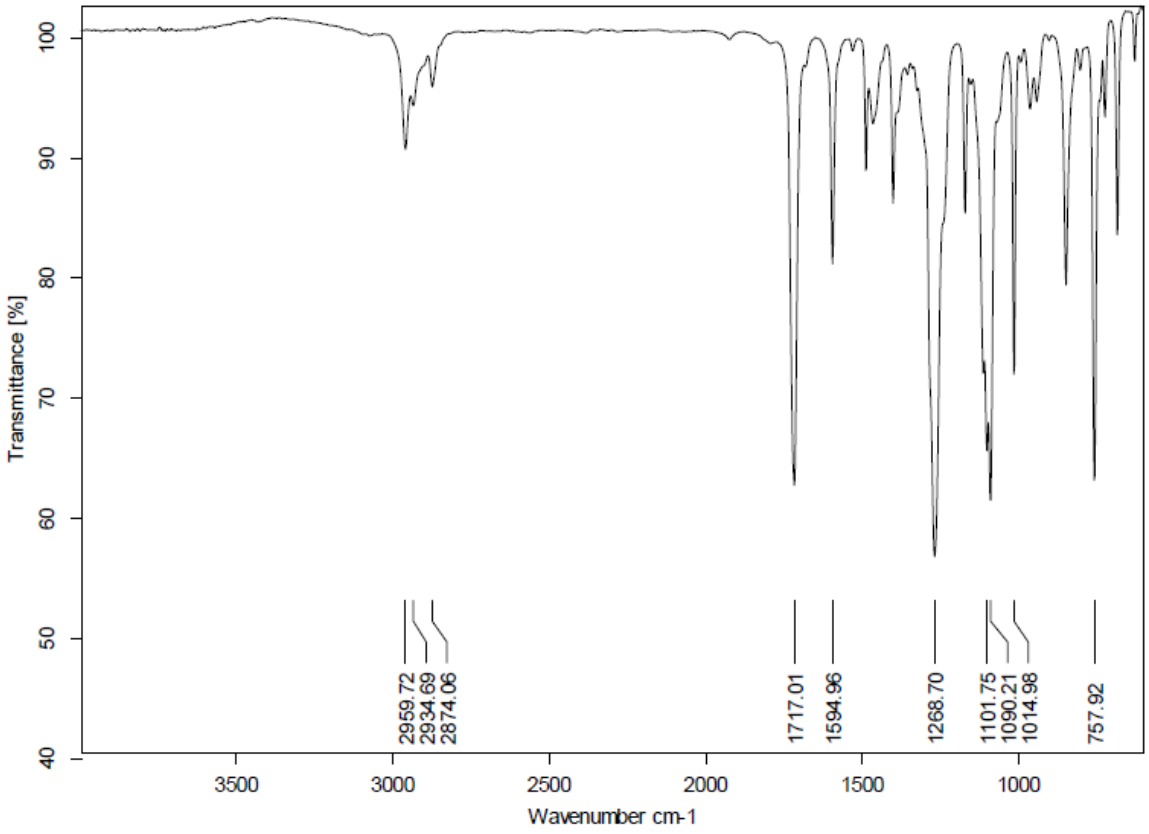

Figure 5.22 FTIR spectrum of butyl 4-chlorobenzoate **5h**.

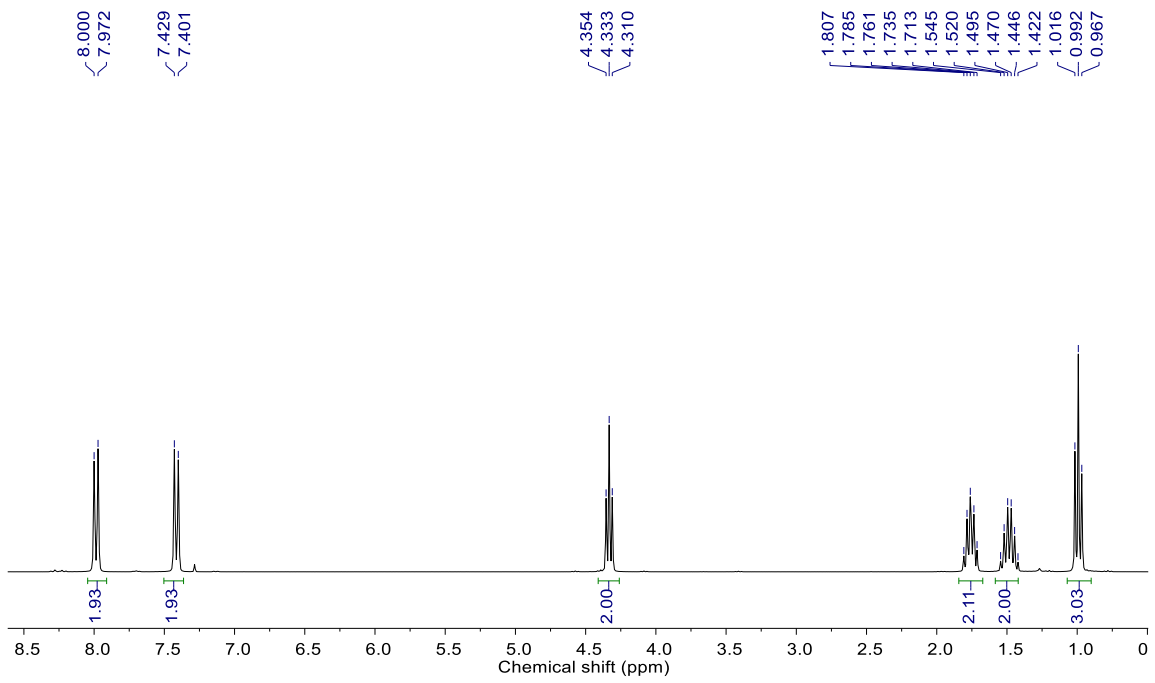

Figure 5.23 ^{1}H-NMR spectrum of butyl 4-chlorobenzoate **5h**.

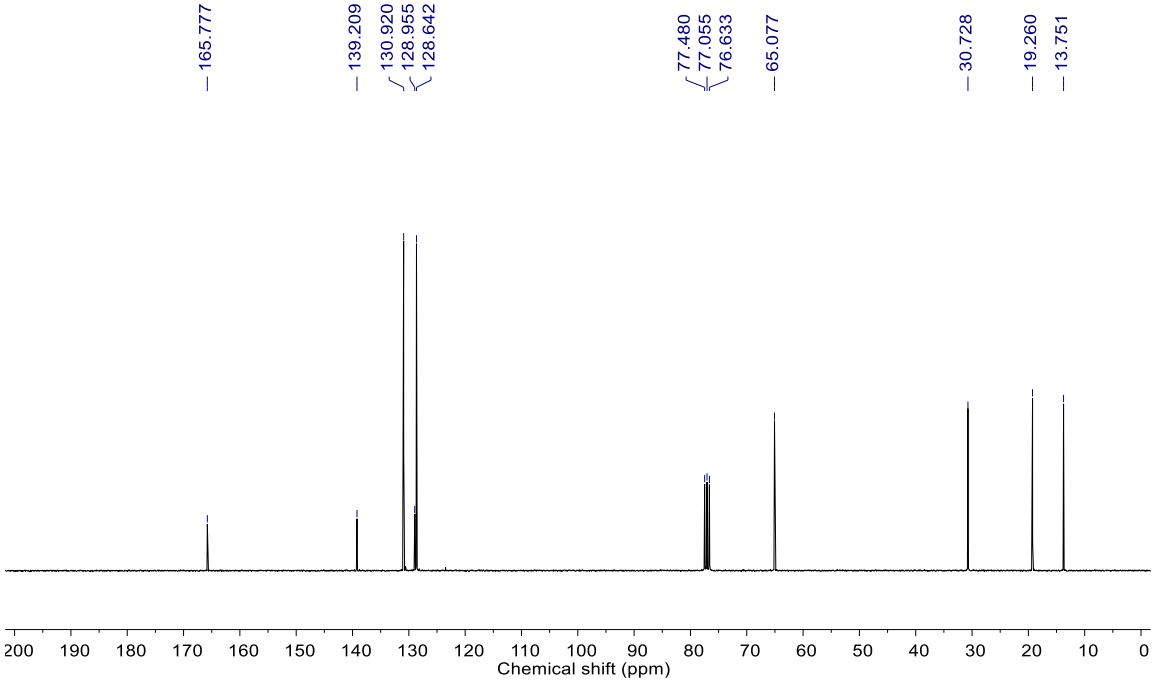

Figure 5.24 ^{13}C-NMR spectrum of butyl 4-chlorobenzoate **5h**.

5.2.3.9 FTIR and NMR (^{1}H and ^{13}C) characterization of butyl 4-methoxybenzoate 5i

^{1}H-NMR ($CDCl_3$, 300 MHz) δ (ppm): 7.83 (d, 2H, *J* = 8.1 Hz), 7.12 (d, 2H, *J* = 8.1 Hz), 4.22 (t, 2H, *J* = 6.6 Hz), 2.30 (s, 3H), 1.67 (m, 2H), 1.37 (m, 2H), 0.88 (t, 3H, *J* = 7.5 Hz); ^{13}C-NMR ($CDCl_3$, 75 MHz) δ (ppm):166.7, 143.4, 129.5, 129.0, 127.8, 64.6, 30.8, 21.6, 19.3, 13.8; FTIR (ATR, cm^{-1}): 3034, 2959, 1714, 1270, 1102.

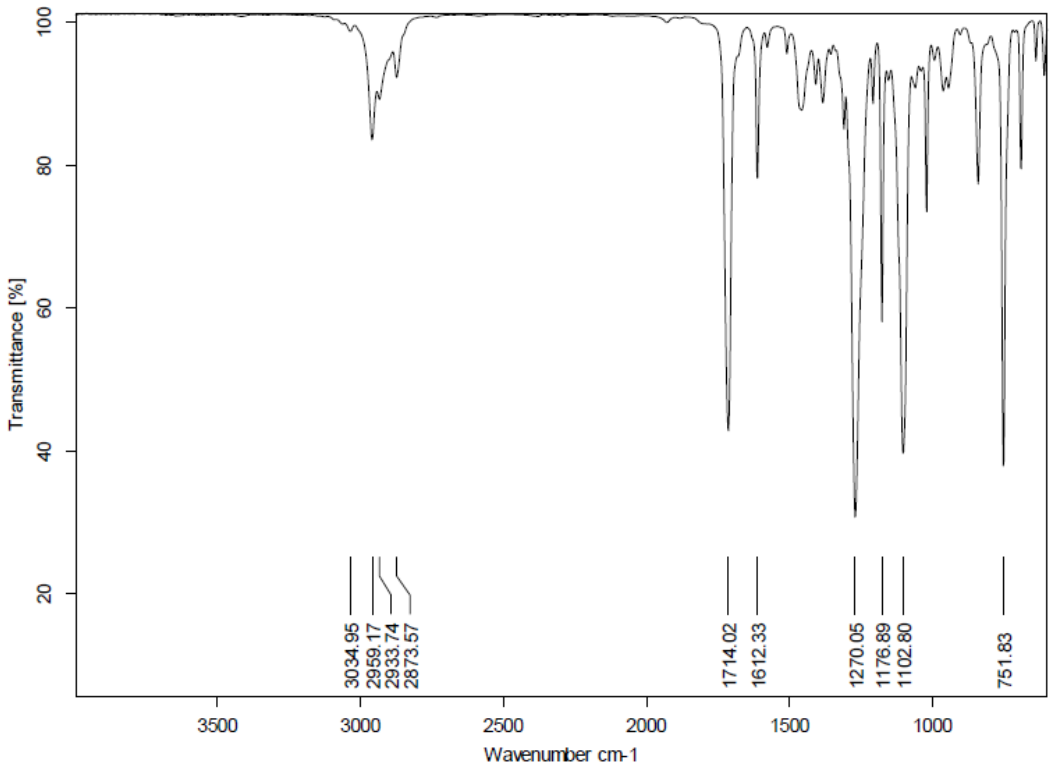

Figure 5.25 FTIR spectrum of butyl 4-methoxybenzoate **5i**.

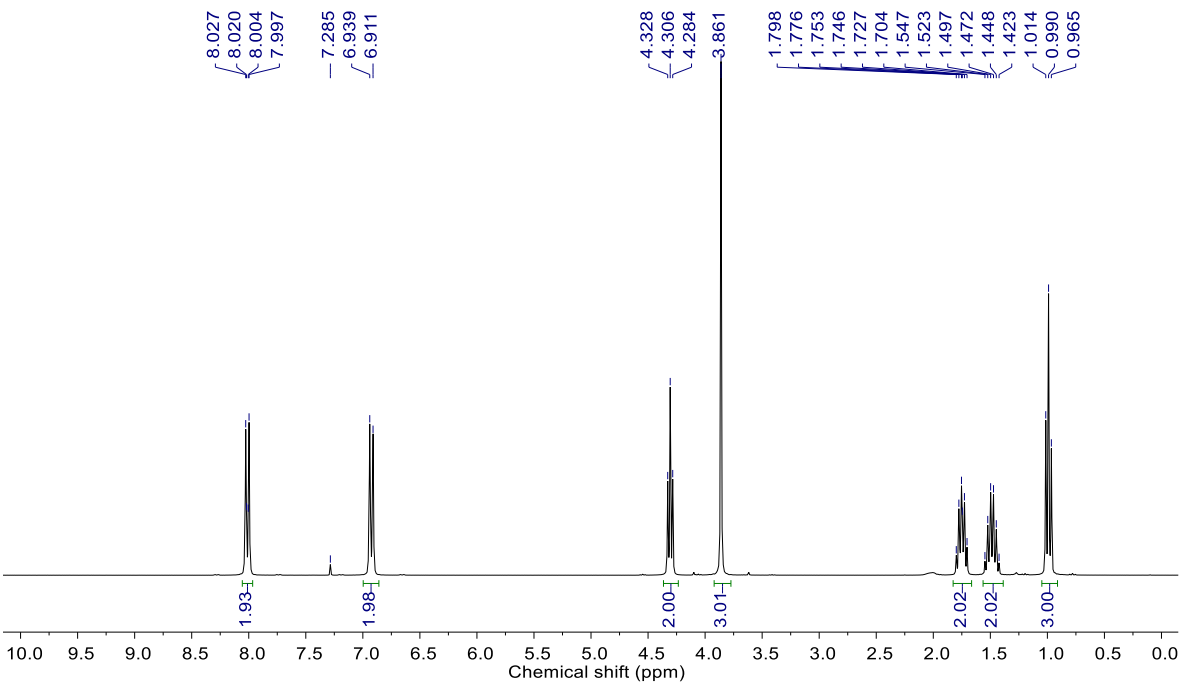

Figure 5.26 ^{1}H-NMR spectrum of butyl 4-methoxybenzoate **5i**.

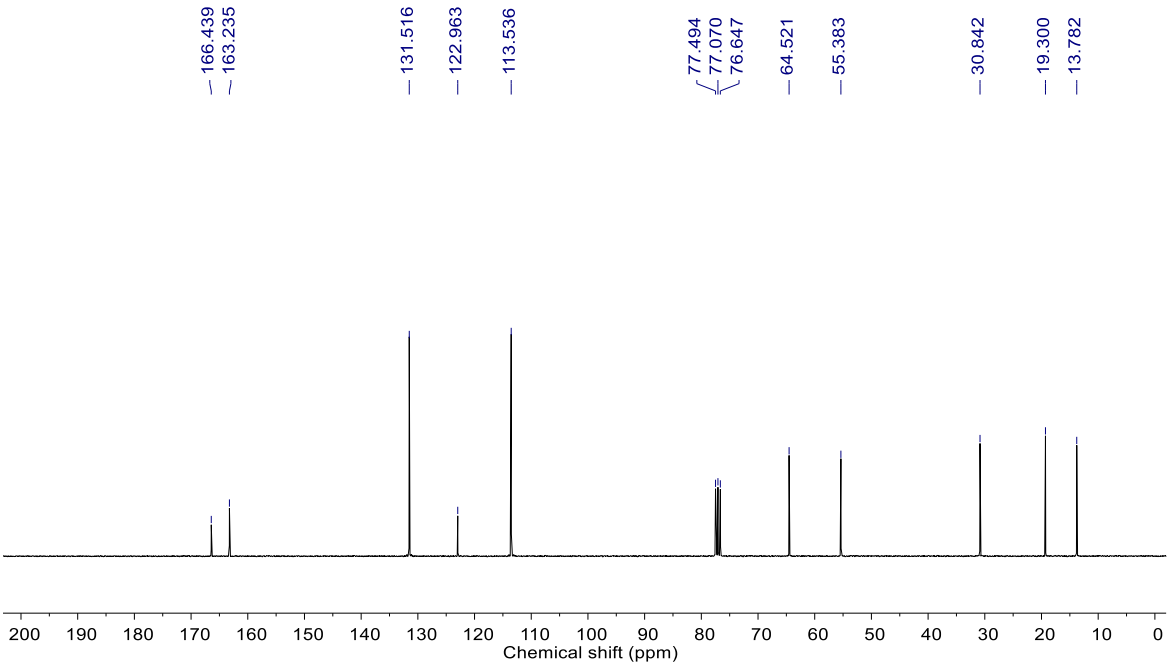

Figure 5.27 ^{13}C-NMR spectrum of butyl 4-methoxybenzoate **5i**.

5.2.10 FTIR and NMR (^{1}H and ^{13}C) characterization of butyl 4-nitrobenzoate 5j

^{1}H-NMR ($CDCl_3$, 300 MHz) δ (ppm): 8.28 (d, 2H, *J* = 8.7 Hz), 8.21 (d, 2H, *J* = 8.7 Hz), 4.39 (t, 2H, *J* = 6.6 Hz), 1.79 (m, 2H), 1.48 (m, 2H), 1.00 (t, 3H, *J* = 7.5 Hz); ^{13}C-NMR (, $CDCl_3$, 75 MHz) δ ppm 164.7, 150.5, 135.9, 130.6, 123.5, 65.8, 30.6, 19.2, 13.7; FTIR (ATR, cm^{-1}): 3112, 2960, 1720, 1270, 1100.

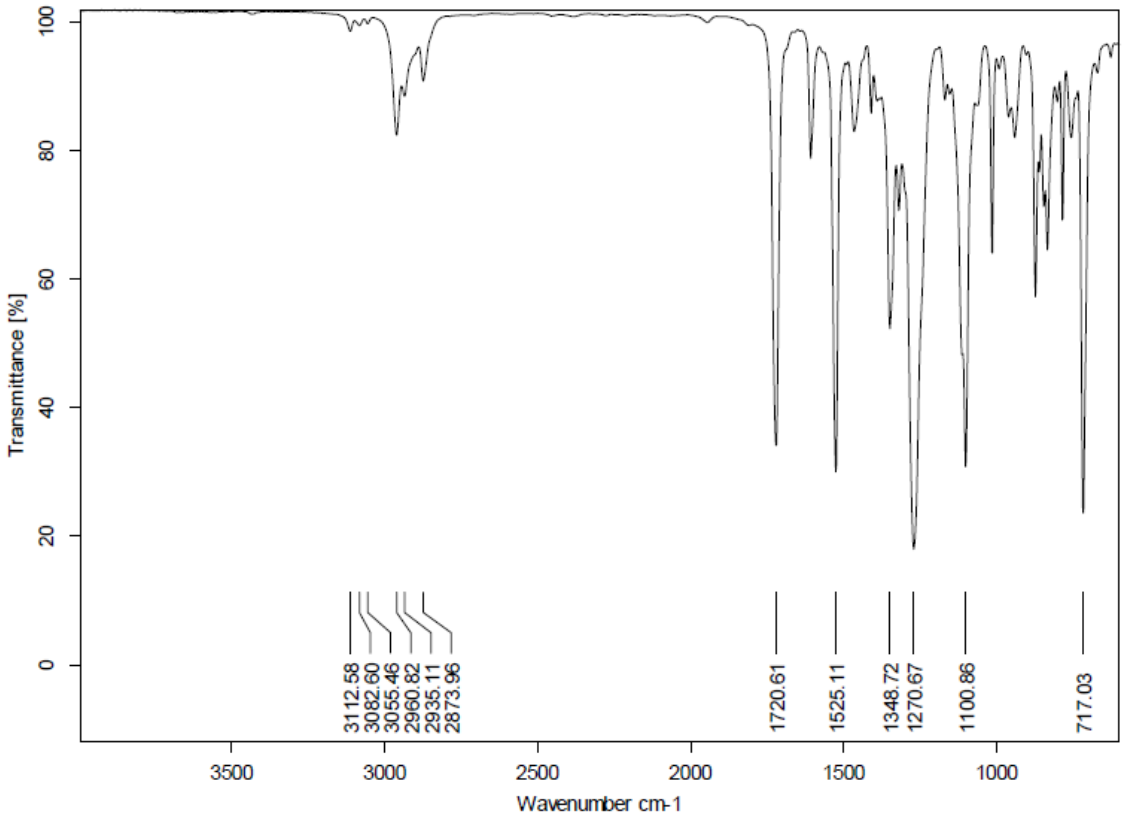

Figure 5.28 FTIR spectrum of butyl 4-nitrobenzoate **5j**.

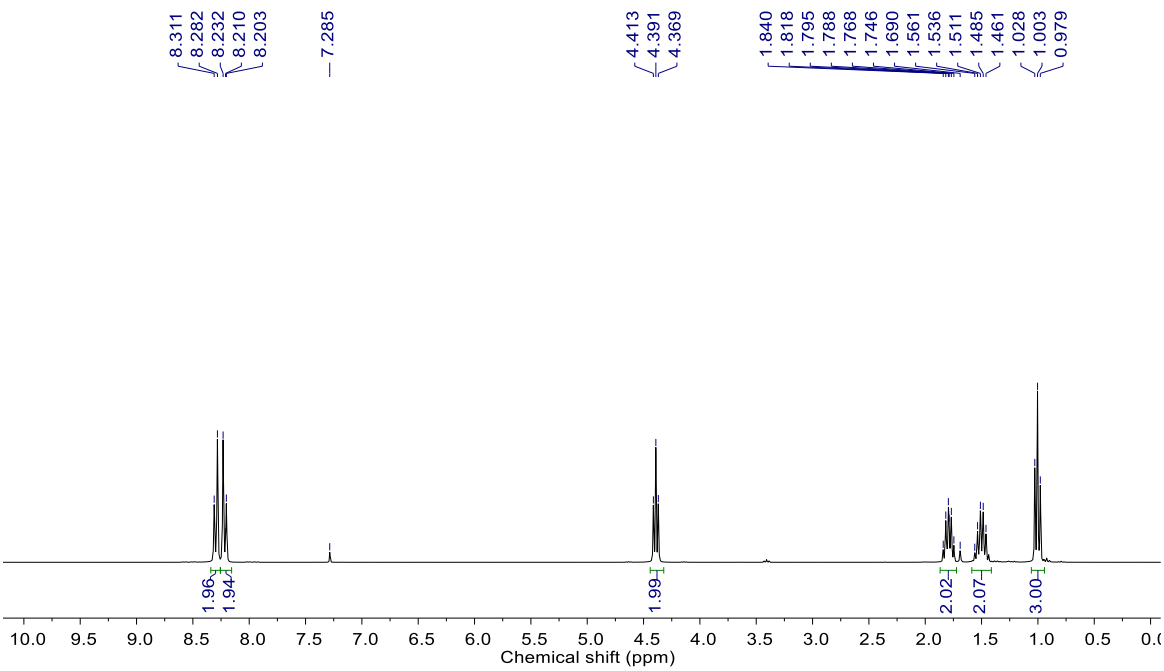

Figure 5.29 ^{1}H-NMR spectrum of butyl 4-nitrobenzoate **5j**.

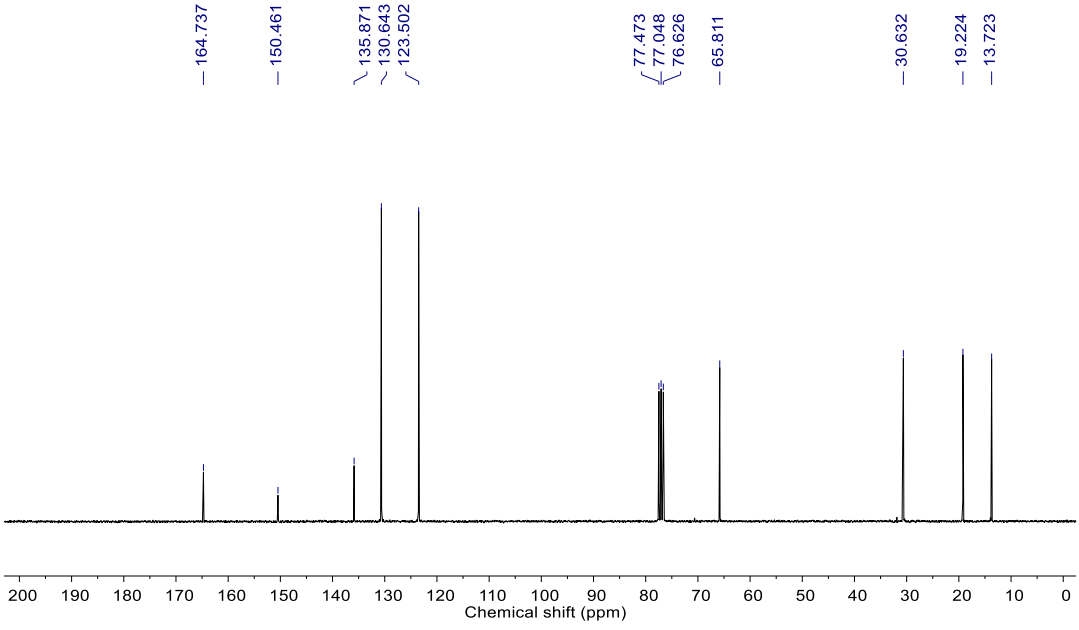

Figure 5.30 ^{13}C-NMR spectrum of butyl 4-nitrobenzoate **5j**.

5.2.11 FTIR and NMR (^{1}H and ^{13}C) characterization of butyl 4-methylbenzoate 5k

^{1}H-NMR ($CDCl_3$, 300 MHz) δ (ppm): 7.83 (d, 2H, *J* = 8.1 Hz), 7.12 (d, 2H, *J* = 8.1 Hz), 4.22 (t, 2H, *J* = 6.6 Hz), 2.30 (s, 3H), 1.67 (m, 2H), 1.37 (m, 2H), 0.88 (t, 3H, *J* = 7.5 Hz); ^{13}C-NMR ($CDCl_3$, 75 MHz) δ (ppm):166.7, 143.4, 129.5, 129.0, 127.8, 64.6, 30.8, 21.6, 19.3, 13.8; FTIR (ATR, cm^{-1}): 3034, 2959, 1714, 1270, 1102.

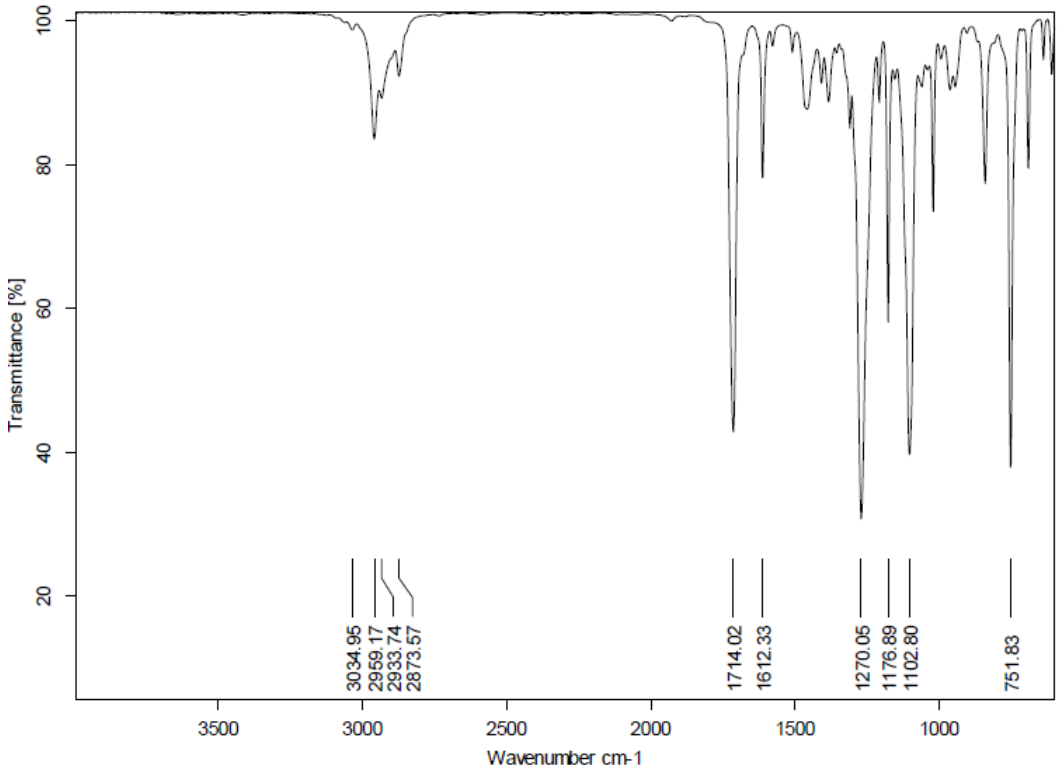

Figure 5.31 FTIR spectrum of butyl 4-methylbenzoate **5k**.

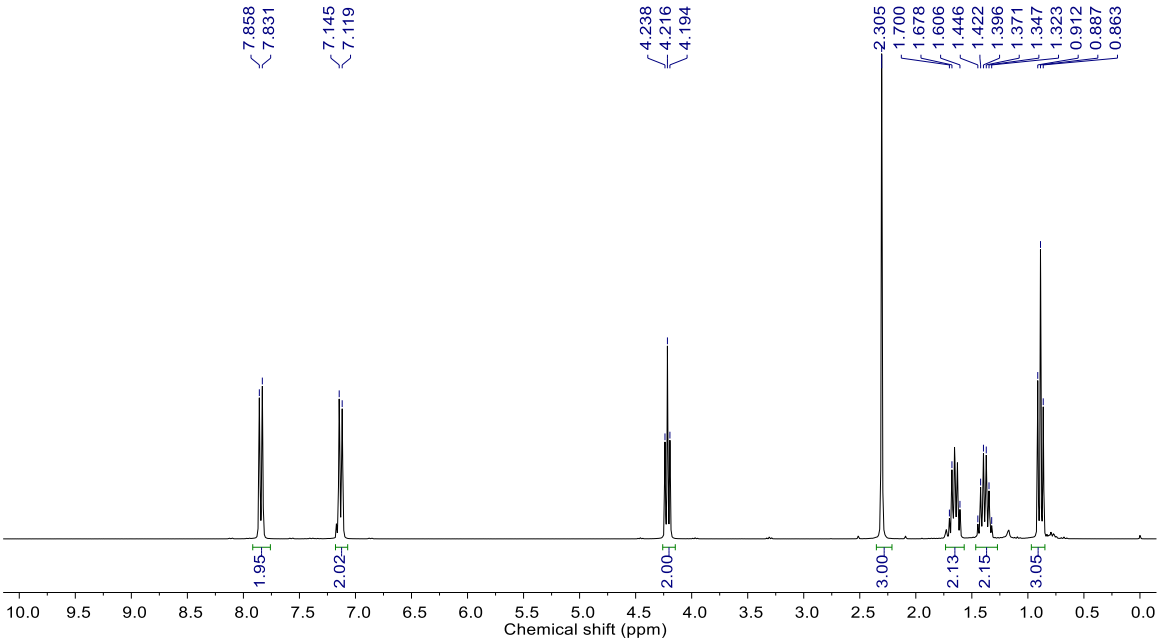

Figure 5.32 ^{1}H-NMR spectrum of butyl 4-methylbenzoate **5k**.

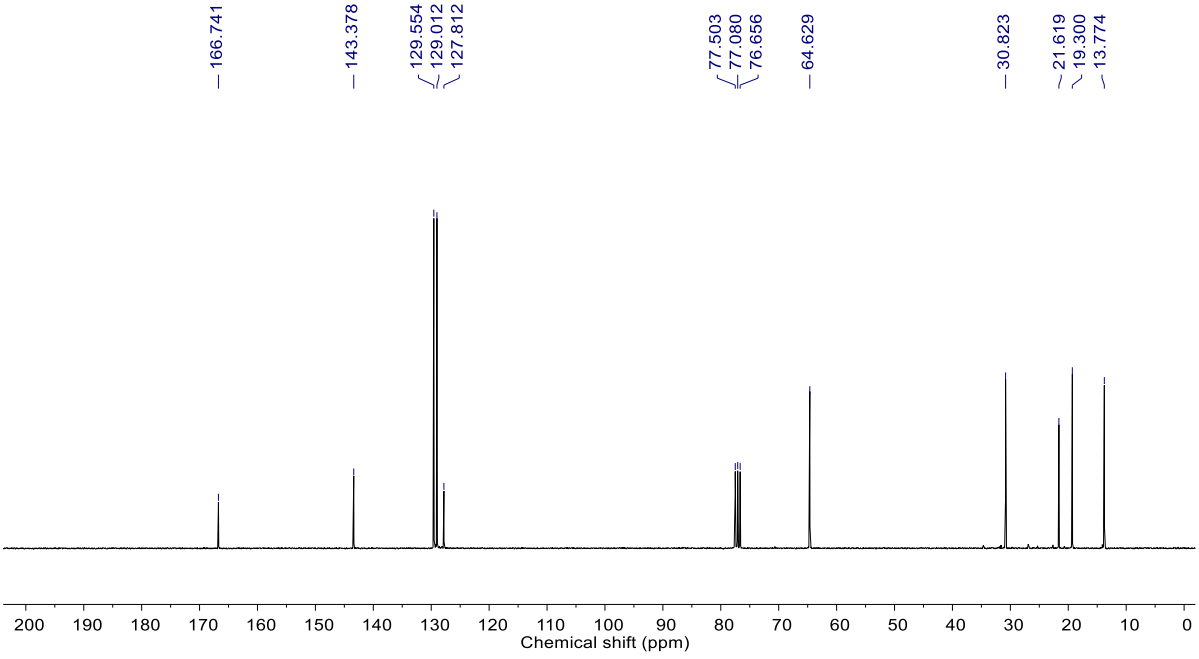

Figure 5.33 ^{13}C-NMR spectrum of butyl 4-methylbenzoate **5k**.

5.2.12 FTIR and NMR (^{1}H and ^{13}C) characterization of dibutyl phthalate 5l

^{1}H-NMR ($CDCl_3$, 300 MHz) δ (ppm): 7.73 (dd, 2H, *J* = 5.7 Hz, 3.6 Hz), 7.54 (dd, 2H, *J* = 5.7 Hz, 3.6 Hz), 4.32 (t, 4H, *J* = 6.9 Hz), 1.73 (m, 4H), 1.42 (m, 4H), 0.97 (t, 6H, *J* = 7.5 Hz); ^{13}C-NMR ($CDCl_3$, 75 MHz) δ (ppm):167.7, 132.3, 130.9, 128.8, 65.6, 30.6, 19.2, 13.7; FTIR (ATR, cm^{-1}): 2959, 1721, 1273, 1118, 1071.

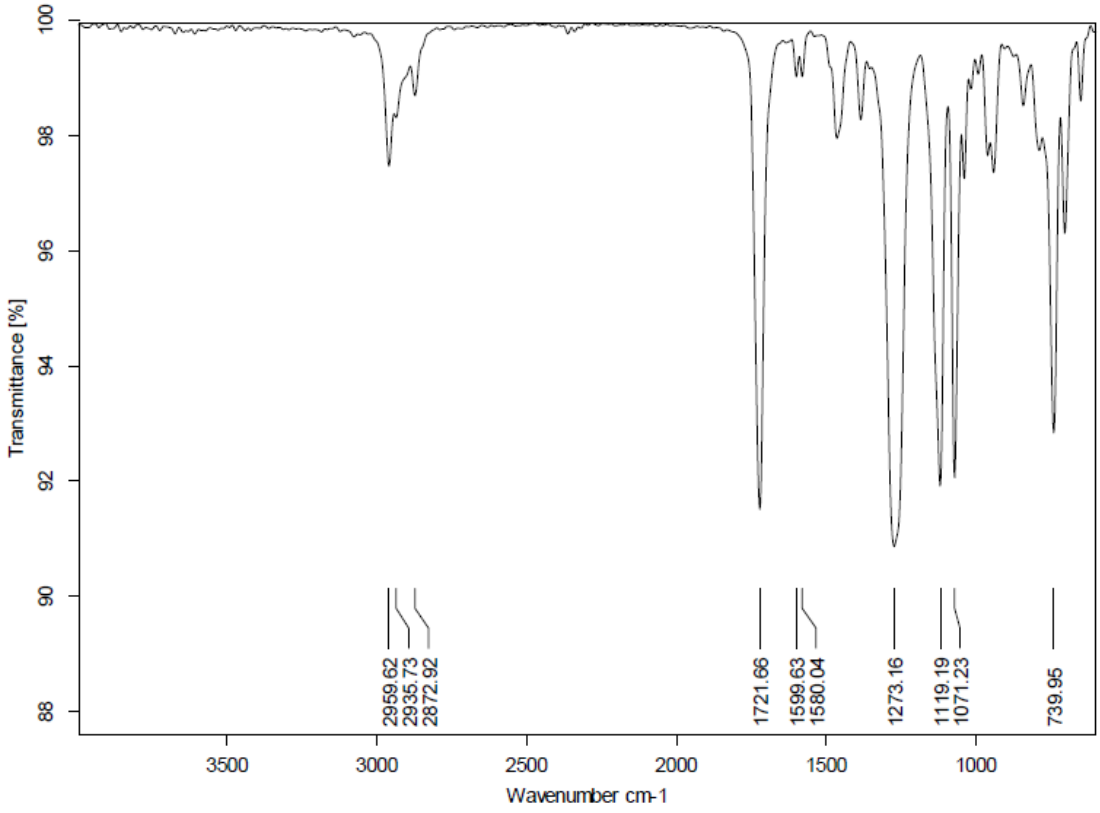

Figure 5.34 FTIR spectrum of dibutyl phthalate **5l**.

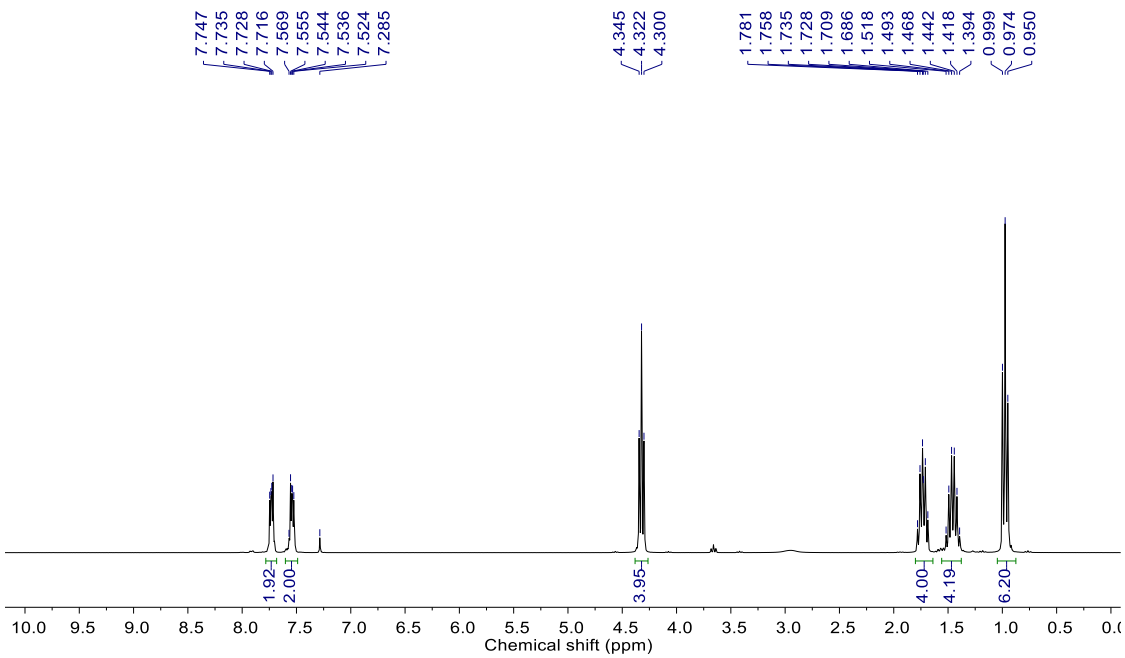

Figure 5.35 ^{1}H-NMR spectrum of dibutyl phthalate **5l**.

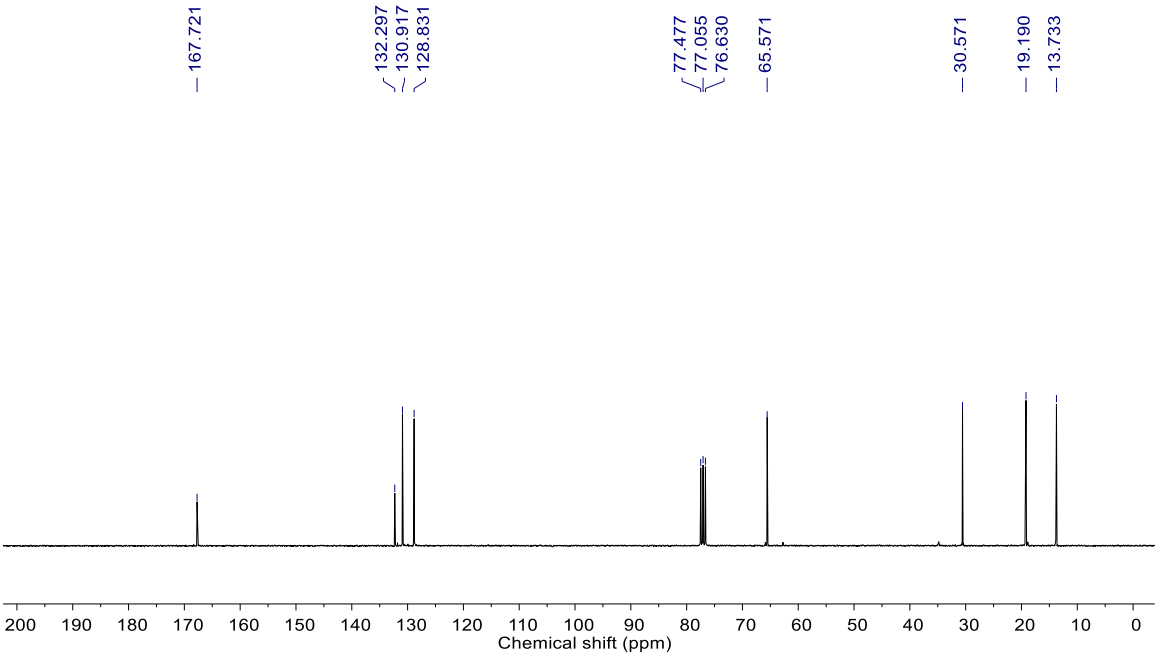

Figure 5.36 ^{13}C-NMR spectrum of dibutyl phthalate **5l**.

5.2.13 FTIR and NMR (^{1}H and ^{13}C) characterization of dibutyl terephthalate 5m

^{1}H-NMR ($CDCl_3$, 300 MHz) δ (ppm): 8.03 (4H, s), 4.28 (t, 4H, J = 6.6 Hz), 1.70 (m, 4H), 1.38 (m, 4H), 0.93 (t, 6H, J = 7.5 Hz); ^{13}C-NMR ($CDCl_3$, 75 MHz) δ (ppm):165.9, 134.2, 129.5, 65.3, 30.7, 19.3, 13.7; FTIR (ATR, cm^{-1}): 2959, 1719, 1267, 1101.

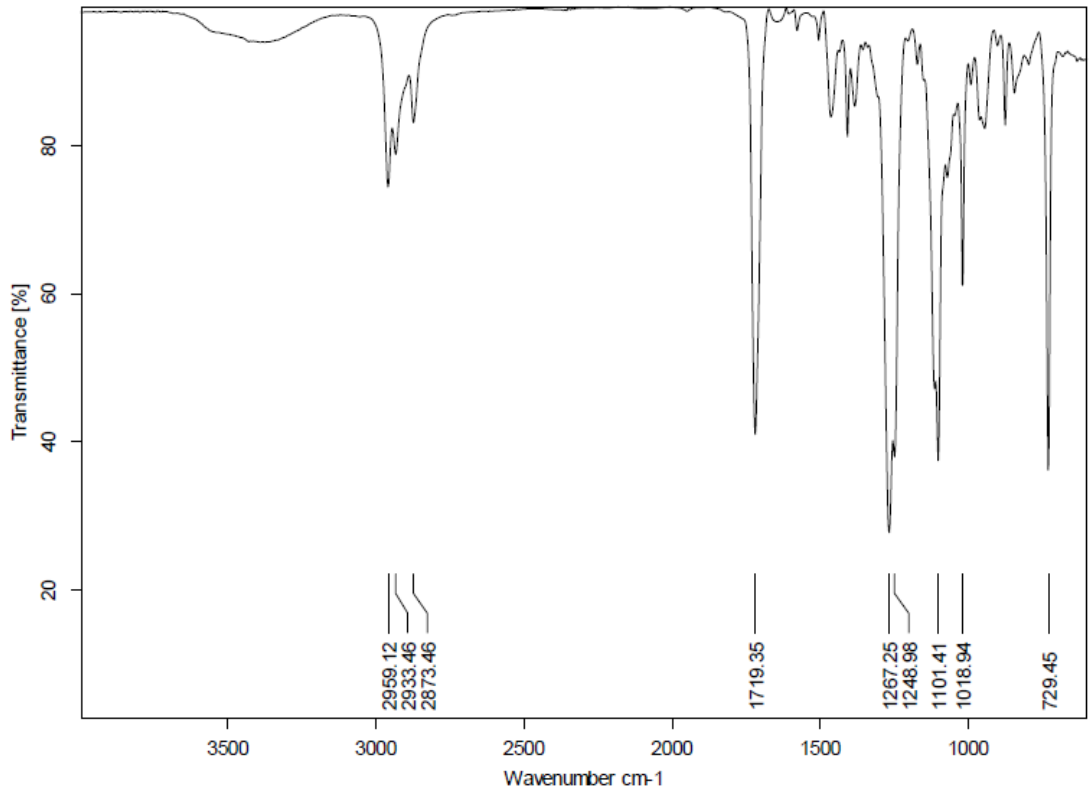

Figure 5.37 FTIR spectrum of dibutyl terephthalate **5m**.

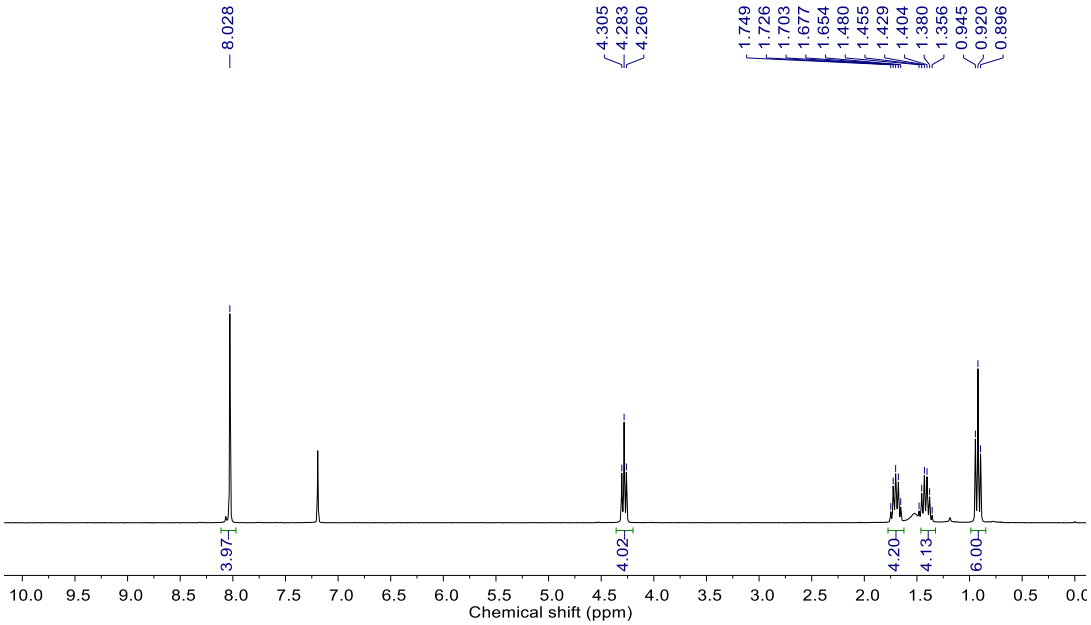

Figure 5.38 ^{1}H-NMR spectrum of dibutyl terephthalate **5m**.

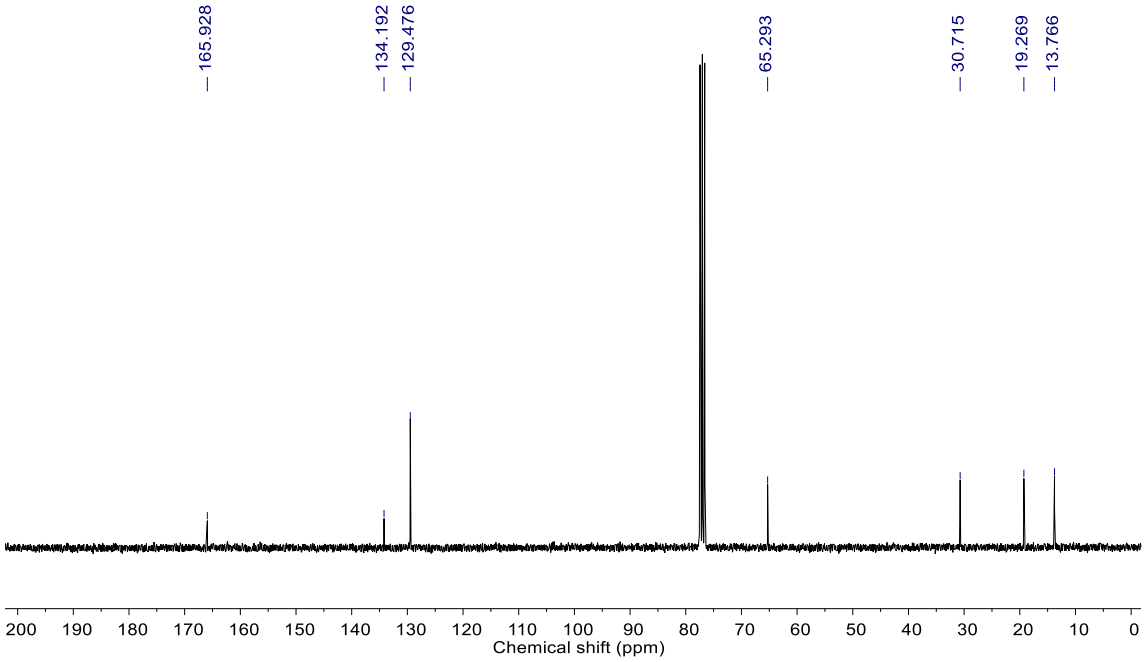

Figure 5.39 ^{13}C-NMR spectrum of dibutyl terephthalate **5m**.

5.2.14 FTIR and NMR (^{1}H and ^{13}C) characterization of butyl trans-cinnamate 5n

^{1}H-NMR ($CDCl_3$, 300 MHz) δ (ppm): 7.73 (d, 1H, *J* = 15.9 Hz), 7.53 (m, 2H), 7.40 (m, 3H), 6.44 (d, 1H, *J* = 15.9 Hz), 4.24 (t, 2H, *J* = 6.6 Hz), 1.72 (m, 2H), 1.45 (m, 2H), 0.99 (t, 3H, *J* = 7.2 Hz); ^{13}C-NMR ($CDCl_3$, 75 MHz) δ (ppm):167.1, 144.5, 134.5, 130.2, 128.9, 128.0, 118.3, 64.4, 30.8, 19.2, 13.8; FTIR (ATR, cm^{-1}): 3061, 2958, 1708, 1165.

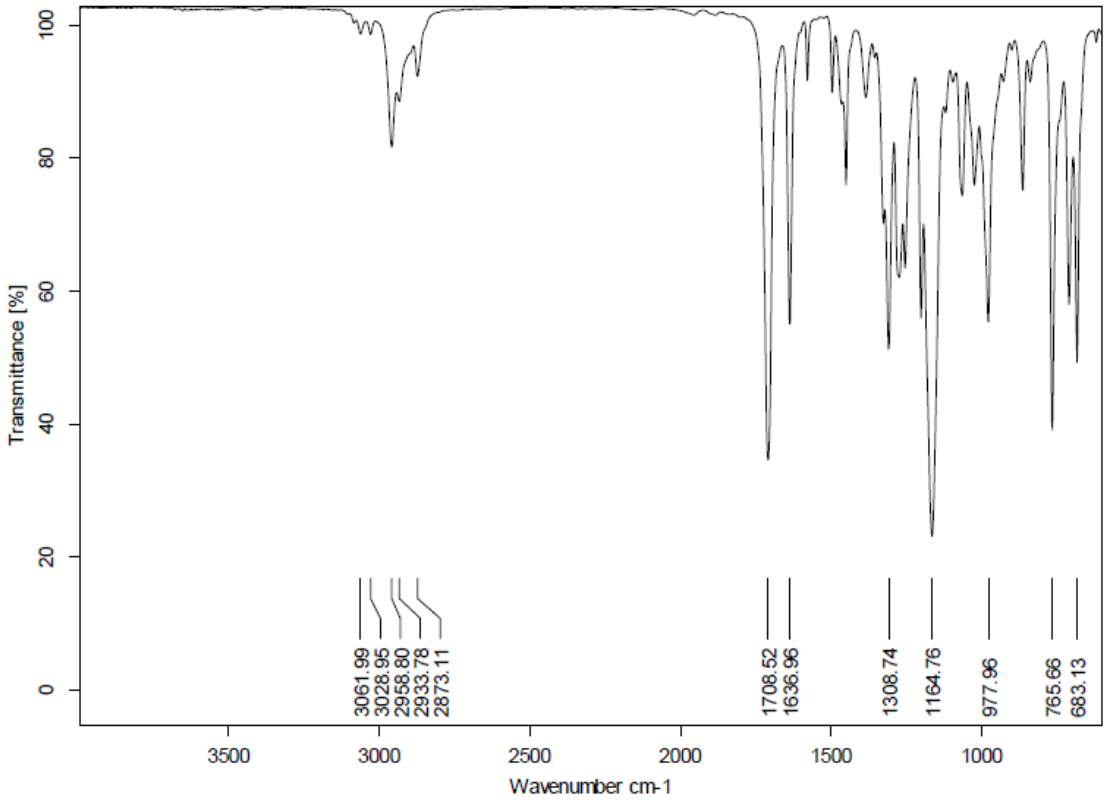

Figure 5.40 FTIR spectrum of butyl trans-cinnamate **5n**.

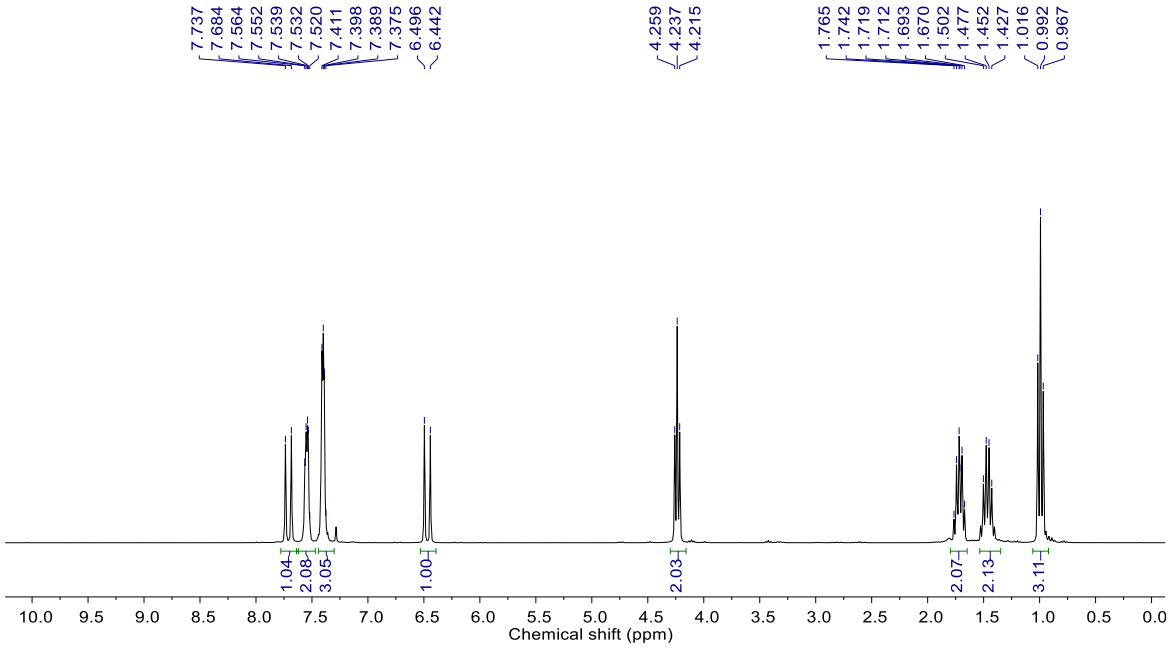

Figure 5.41 ^{1}H-NMR spectrum of butyl trans-cinnamate **5n**.

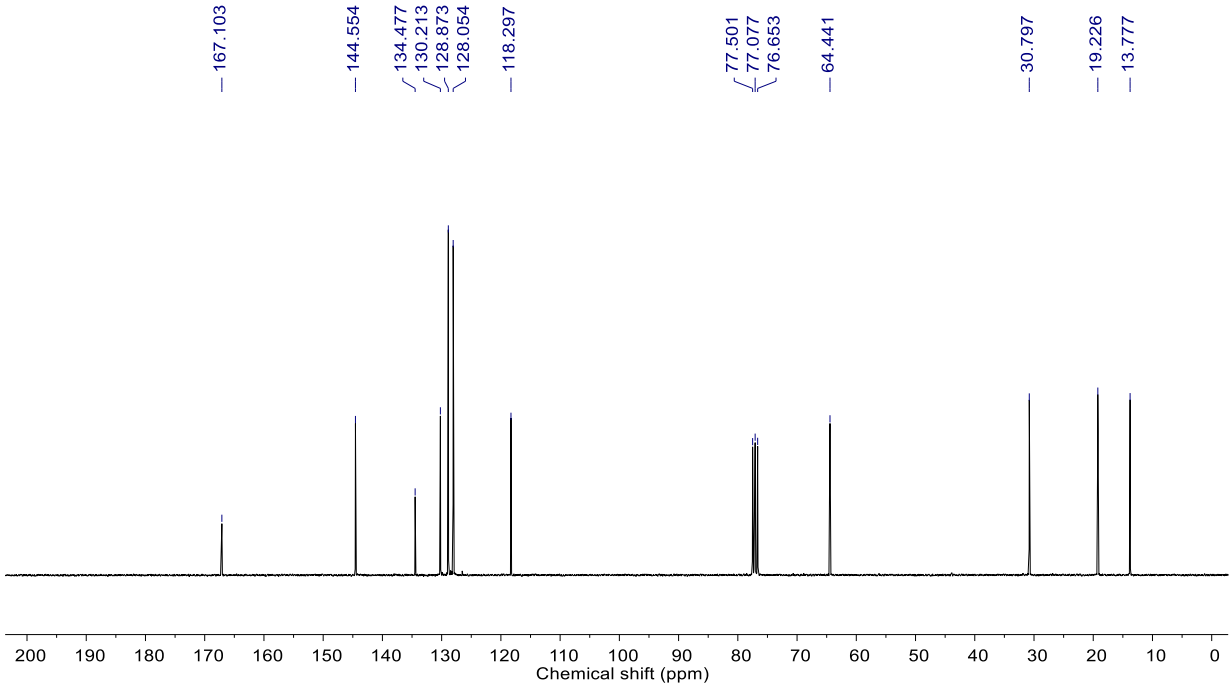

Figure 5.42 ^{13}C-NMR spectrum of butyl trans-cinnamate **5n**.

5.2.15 FTIR and NMR (^{1}H and ^{13}C) characterization of butyl 2-hydroxybenzoate 5o

^{1}H-NMR ($CDCl_3$, 300 MHz) δ (ppm): 10.77 (s, 1H), 7.76 (d, 1H, J = 8.4 Hz), 7.32 (t, 1H, J = 8.4 Hz), 6.89 (d, 1H, J = 8.4 Hz), 6.77 (t, 2H, J = 6.9 Hz), 4.25 (t, 2H, J = 6.3 Hz), 1.67 (m, 2H), 1.39 (m, 2H), 0.89 (t, 3H, J = 7.5 Hz); ^{13}C-NMR ($CDCl_3$, 75 MHz) δ (ppm):170.2, 161.7, 135.5, 129.8, 119.1, 117.5, 112.6, 65.2, 30.6, 19.2, 13.7; FTIR (ATR, cm^{-1}): 3183, 2960, 1671, 1297.

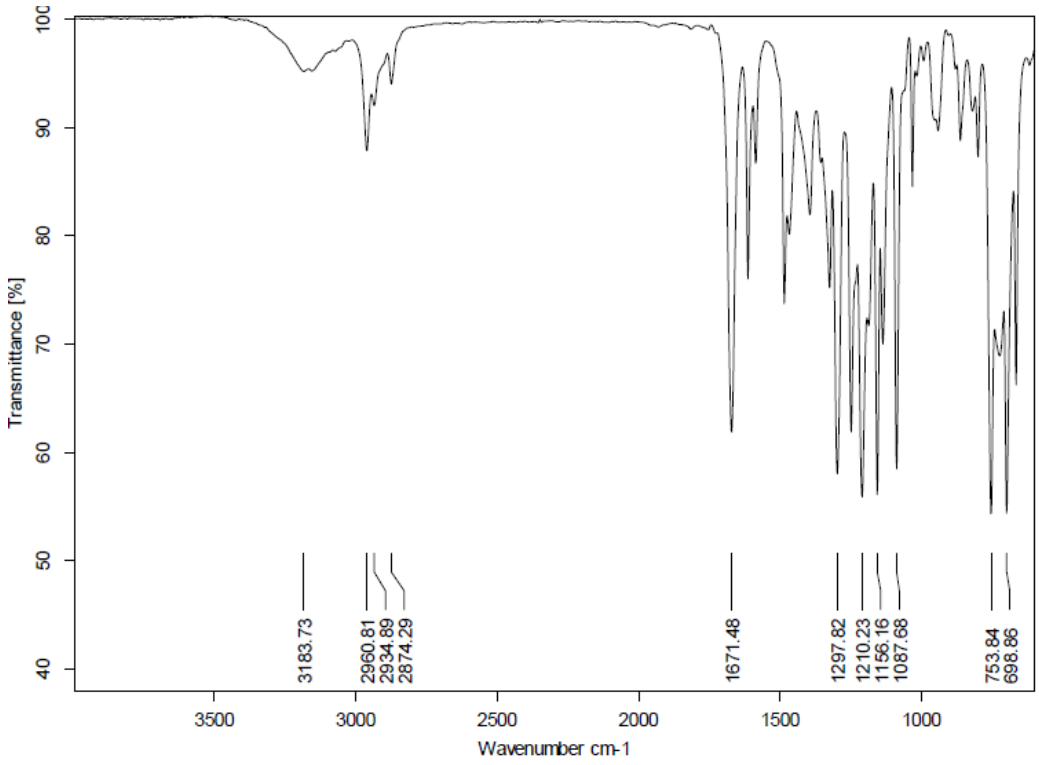

Figure 5.43 FTIR spectrum of butyl 2-hydroxybenzoate **5o**.

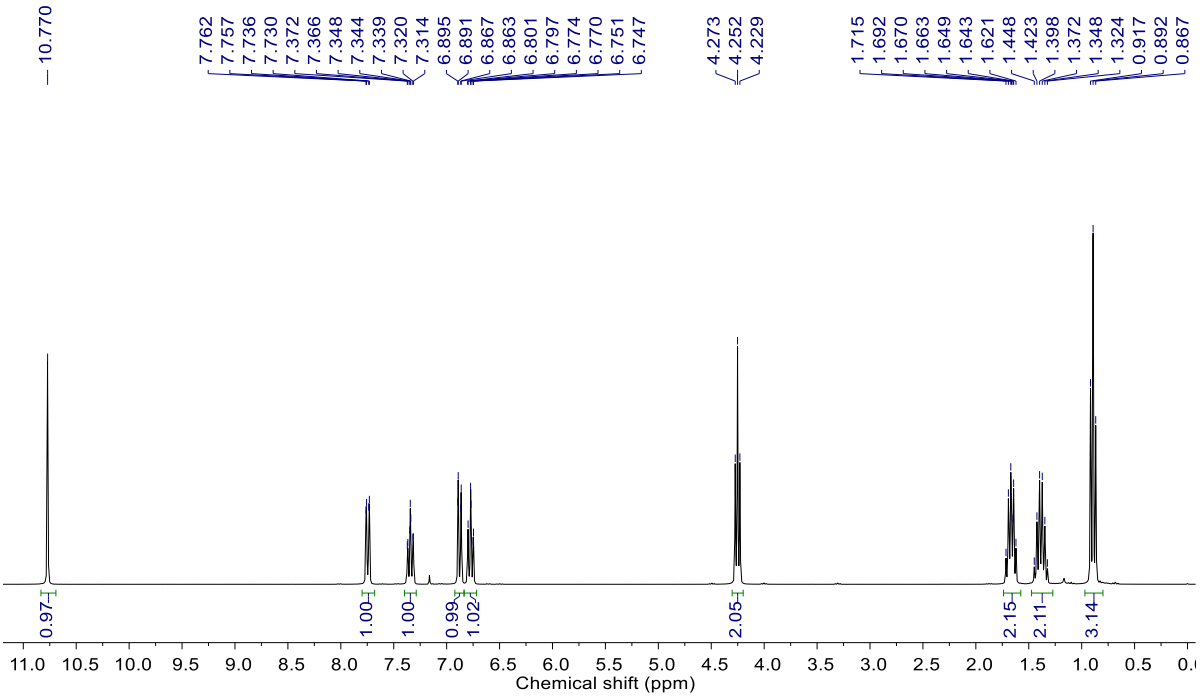

Figure 5.44 ^{1}H-NMR spectrum of butyl 2-hydroxybenzoate **5o**.

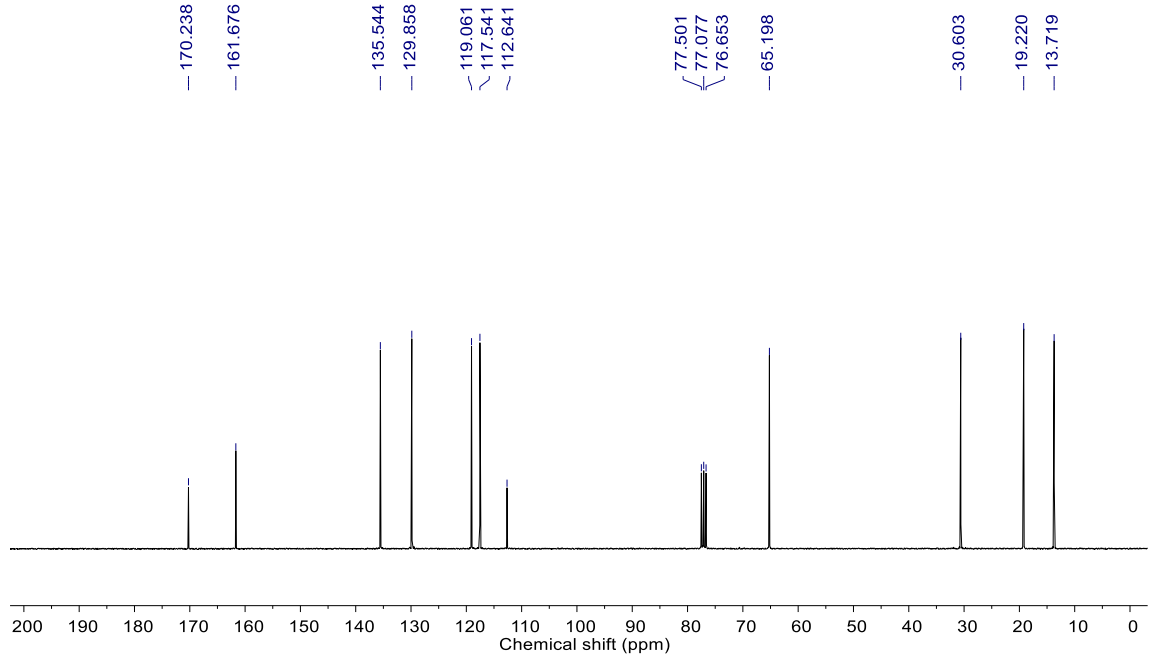

Figure 5.45 ^{13}C-NMR spectrum of butyl 2-hydroxybenzoate **5o**.

5.2.16 FTIR and NMR (^{1}H and ^{13}C) characterization of butyl 2-bromobenzoate 5p

^{1}H-NMR ($CDCl_3$, 300 MHz) δ (ppm): 7.78 (d, 1H, *J* = 9.0 Hz), 7.67 (d, 1H, *J* = 9.0 Hz), 7.38 (m, 2H), 4.37 (t, 2H, *J* = 6.6 Hz), 1.54 (m, 2H), 1.47 (m, 2H), 1.00 (t, 3H, *J* = 7.2 Hz); ^{13}C-NMR ($CDCl_3$, 75 MHz) δ (ppm):166.4, 134.3, 132.6, 132.4, 131.2, 127.1, 121.5, 65.5, 30.6, 19.3, 13.7; FTIR (ATR, cm^{-1}): 3068, 2959, 1728, 1288.

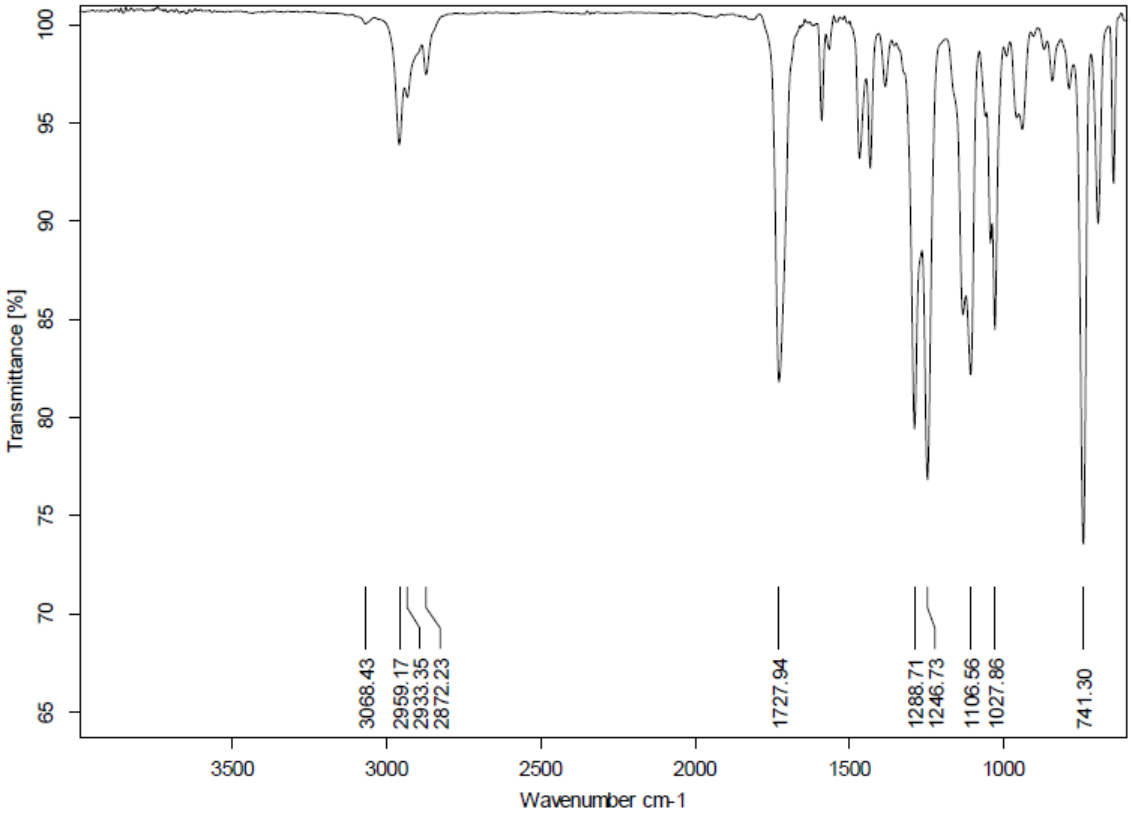

Figure 5.46 FTIR spectrum of butyl 2-bromobenzoate **5p**.

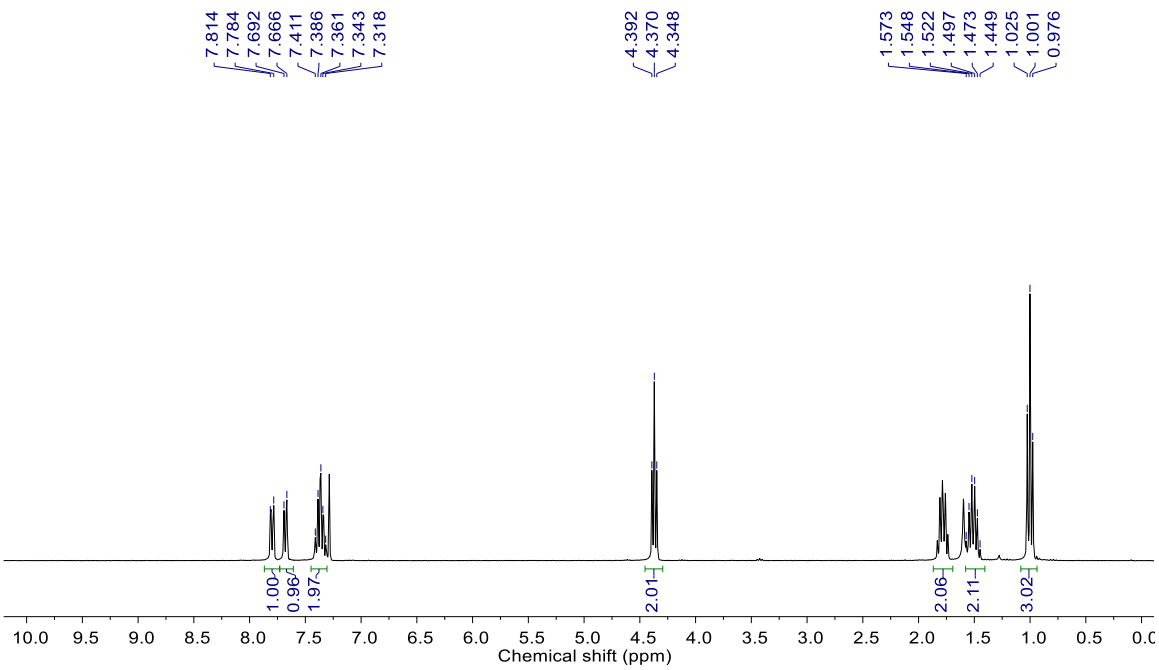

Figure 5.47 ^{1}H-NMR spectrum of butyl 2-bromobenzoate **5p**.

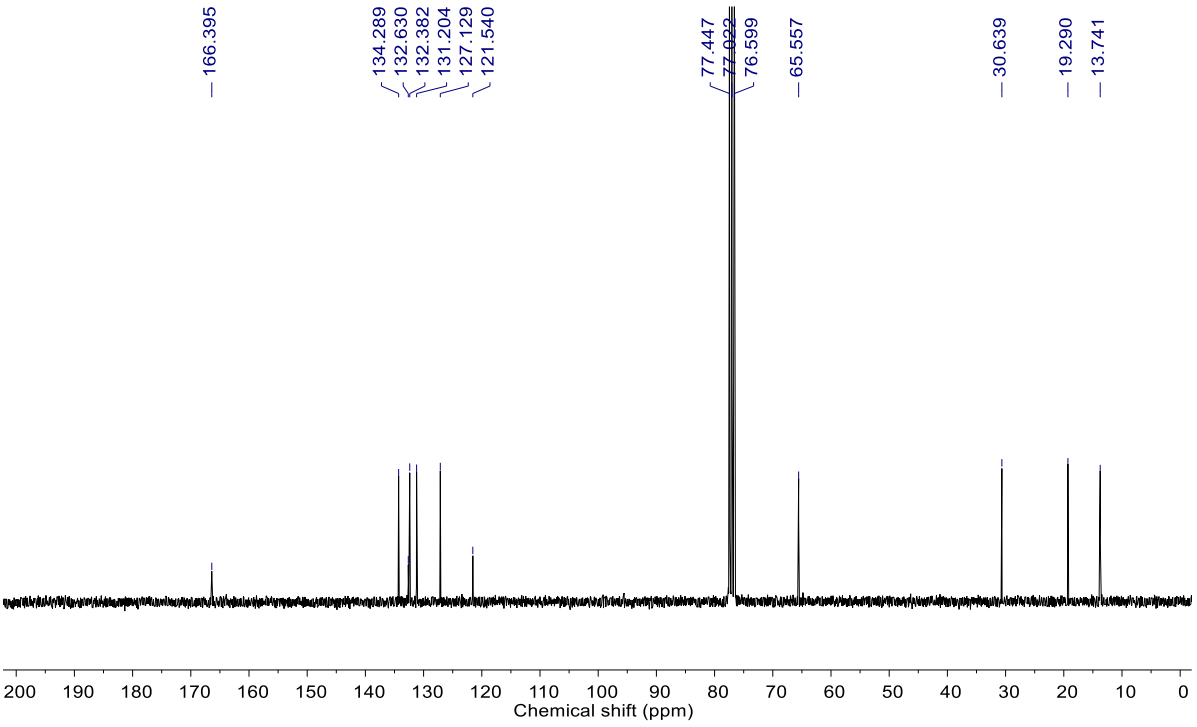

Figure 5.48 ^{13}C-NMR spectrum of butyl 2-bromobenzoate **5p**.

5.2.4 Catalytic reactions (B): Esterification of 2-furoic acid (FA) over HPA catalysts

2-Furoic acid (0.2 g, 1.77 mmol) and 1-butanol (0.264 g, 3.55 mmol, 2 eq.) were charged into a round-bottomed glass pressure reactor (50 mL) fitted with a magnetic stir rod and Teflon screw top. Oven-dried PTA (20 mg, 0.3 mol%) was weighed in air and added to the solution. The reactor was sealed and placed in a pre-heated oil bath and stirred magnetically for 4 h. After reaction, the reactor was cooled to room temperature and opened. Then chloroform (10 mL) was added into mixture and filter or centrifuged, and again dried over anhydrous Na_2SO_4. The chloroform layers were combined, dried over anhydrous Na_2SO_4, and evaporated under reduced pressure in a rotary evaporator to obtain light brown crude mixture. The crude mixture was chromatographed (silica gel, chloroform) and the solvent evaporated to get butyl furoate **5u** (0.276 g, 92%) as a light brown liquid.

5.2.5 Instrument used for the characterization of compounds

FTIR spectra of the samples were collected on a Bruker Alpha FTIR instrument. The FTIR spectrum of samples was collected in the ATR mode and the solid HPA catalysts were collected in the KBr matrix. The ^{1}H-NMR spectra were recorded in a Bruker 300 MHz NMR instrument and the ^{13}C-NMR spectra were recorded in the same instrument in a calculated frequency of 75 MHz.

5.2.5.1 FTIR and NMR (^{1}H and ^{13}C) characterization of methyl 2-furoate 5q

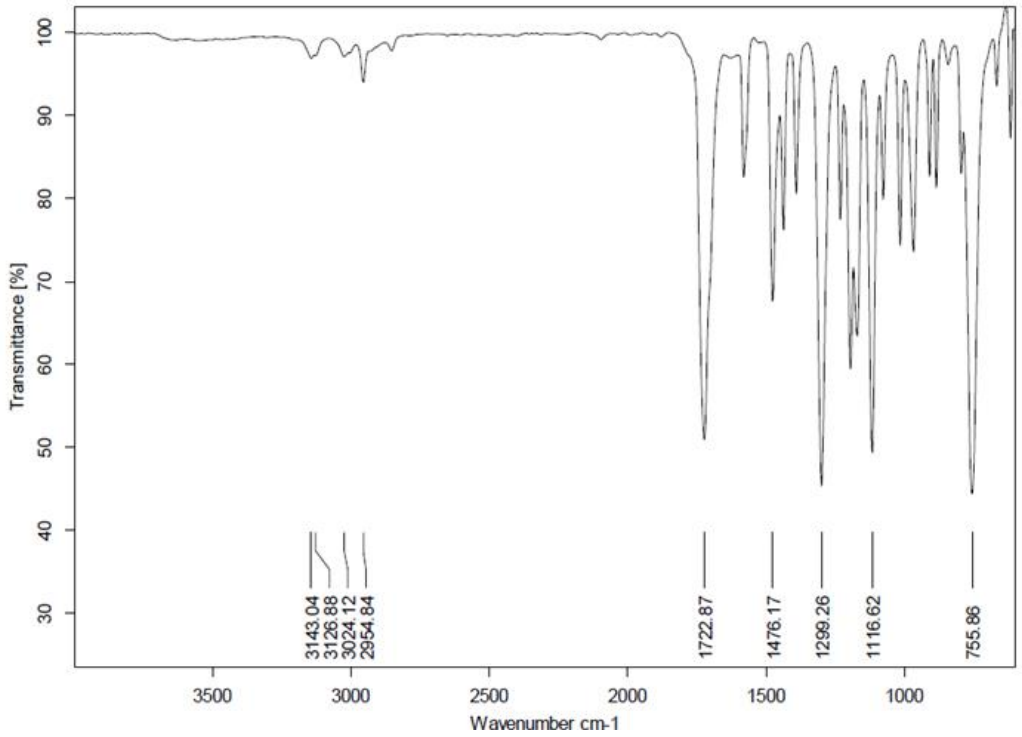

Figure 5.49 FTIR spectrum of methyl 2-furoate **5q**.

The peak at 3143 and 3126 cm^{-1} is due to sp^2 –C-H stretching frequency and the peak at 2954 cm^{-1} is responsible for the sp^3 -C-H stretching frequency. The peak at 1722 cm^{-1} corresponds to the ester C=O stretching frequency and 1299 to 1116 cm^{-1} is due to C-O stretching frequency of ester group.

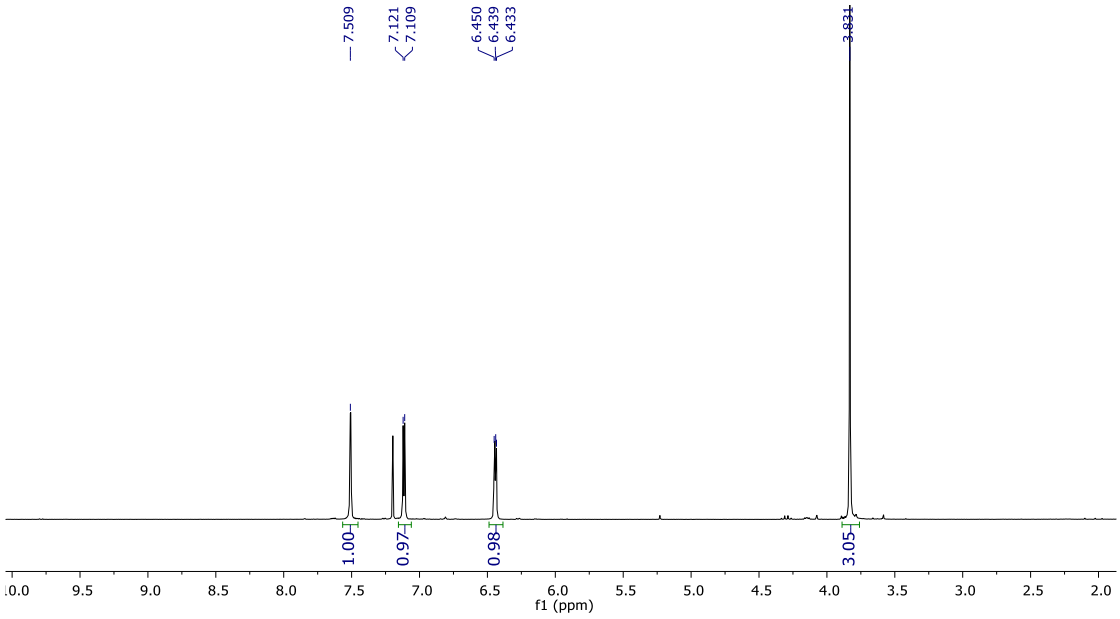

Figure 5.50 ^{1}H-NMR spectrum of methyl 2-furoate **5q**.

^{1}H-NMR of the isolated methyl furoate show the 1H singlet, 1H doublet, and 1H triplet at 7.50 ppm, 7.11 ppm, and 6.43 ppm respectively are due to the furan ring protons. The 3H singlet at 3.83 ppm is due to protons of methoxy (-OCH_3) group.

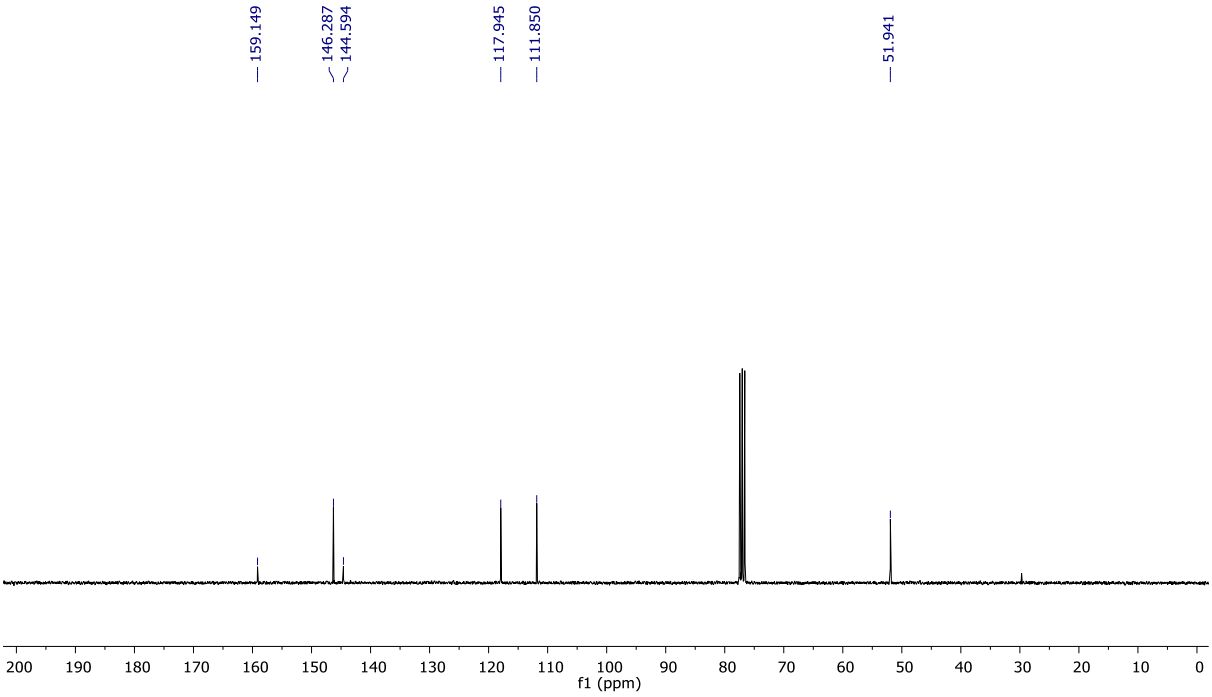

Figure 5.51 ^{13}C-NMR spectrum of methyl 2-furoate **5q**.

^{13}C-NMR of the isolated methyl furoate show the peak at 159.1 ppm is due to the ester carbon (C=O), the four peaks at 146.2 ppm, 144.5 ppm, 117.9 ppm, and 111.85 ppm are due to the carbon atoms of the furan ring. The peak at 51.9 ppm is corresponding to –OCH_3 carbon.

5.2.5.2 FTIR and NMR (^{1}H and ^{13}C) characterization of ethyl 2-furoate 5r

^{1}H-NMR (400 MHz, $CDCl_3$, δ ppm): 7.48 (1H, q), 7.09 (1H, q, Hz), 6.45 (1H, q, Hz), 4.27 (2H, q), 1.28 (3H, t). ^{13}C-NMR (100 MHz, $CDCl_3$, δ ppm): 158.6, 146.1, 144.8, 117.6, 111.7, 60.8, 14.2. FTIR (ATR, cm^{-1}): 3142, 2983, 2874, 1714, 1292, 1177, 1113, 1008.

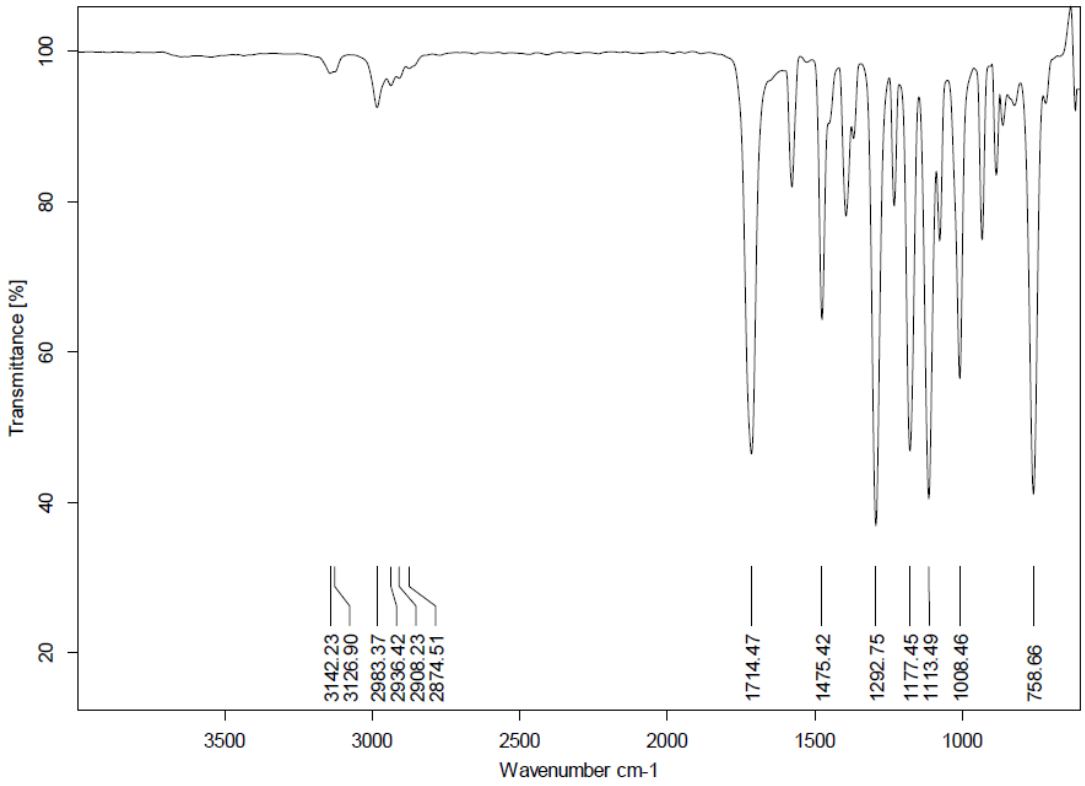

Figure 5.52 FTIR spectrum of ethyl 2-furoate **5r**.

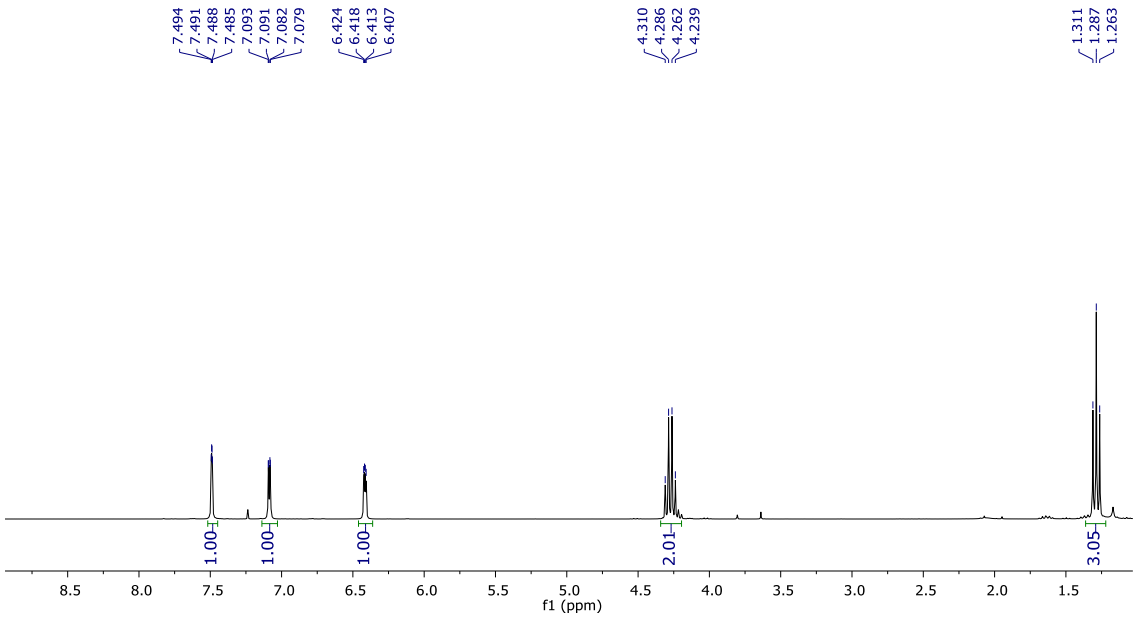

Figure 5.53 ^{13}H-NMR spectrum of ethyl 2-furoate **5r**.

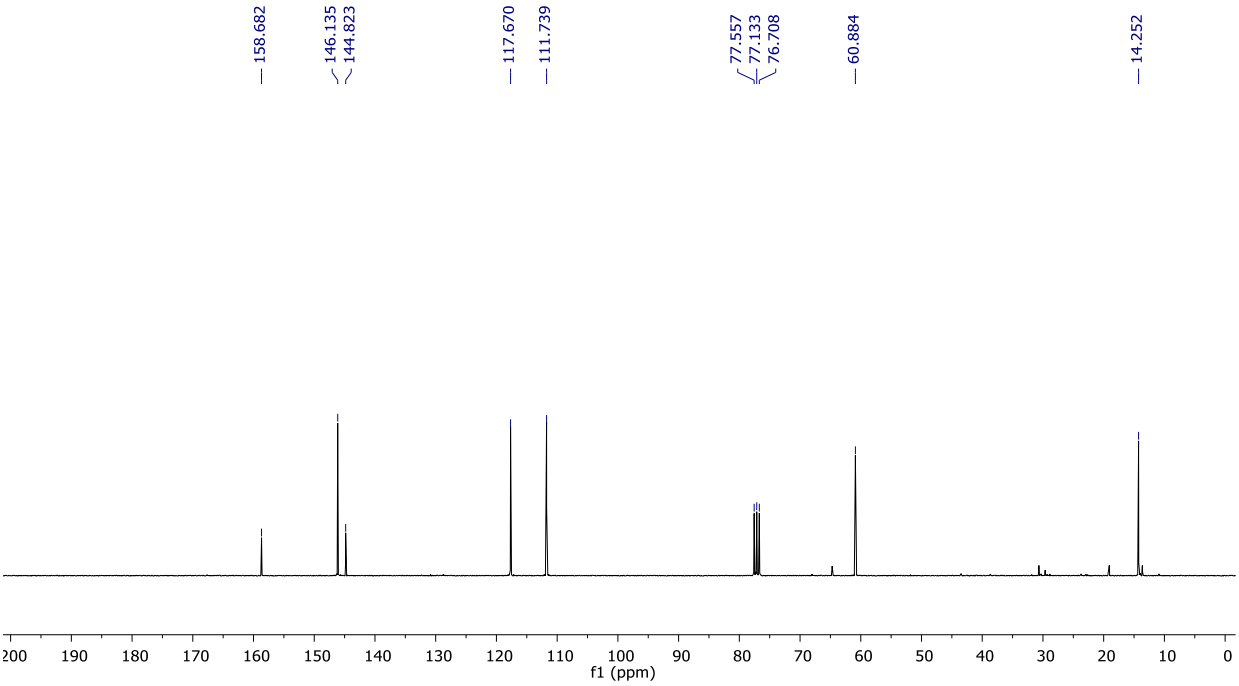

Figure 5.54 ^{13}C-NMR spectrum of ethyl 2-furoate **5r**.

5.2.5.3 FTIR and NMR (^{1}H and ^{13}C) characterization of propyl 2-furoate 5s

^{1}H-NMR (400 MHz, $CDCl_3$, δ ppm): 7.49 (1H, s), 7.08 (1H, s), 6.40 (1H, s), 4.17 (2H, t), 1.67 (2H, m), 0.91 (3H, t). ^{13}C-NMR (100 MHz, $CDCl_3$, δ ppm): 158.6, 146.1, 144.8, 117.6, 111.7, 60.8, 14.2. FTIR (ATR, cm^{-1}): 3142 ,2968, 2856, 1715, 1291, 1175, 1114.

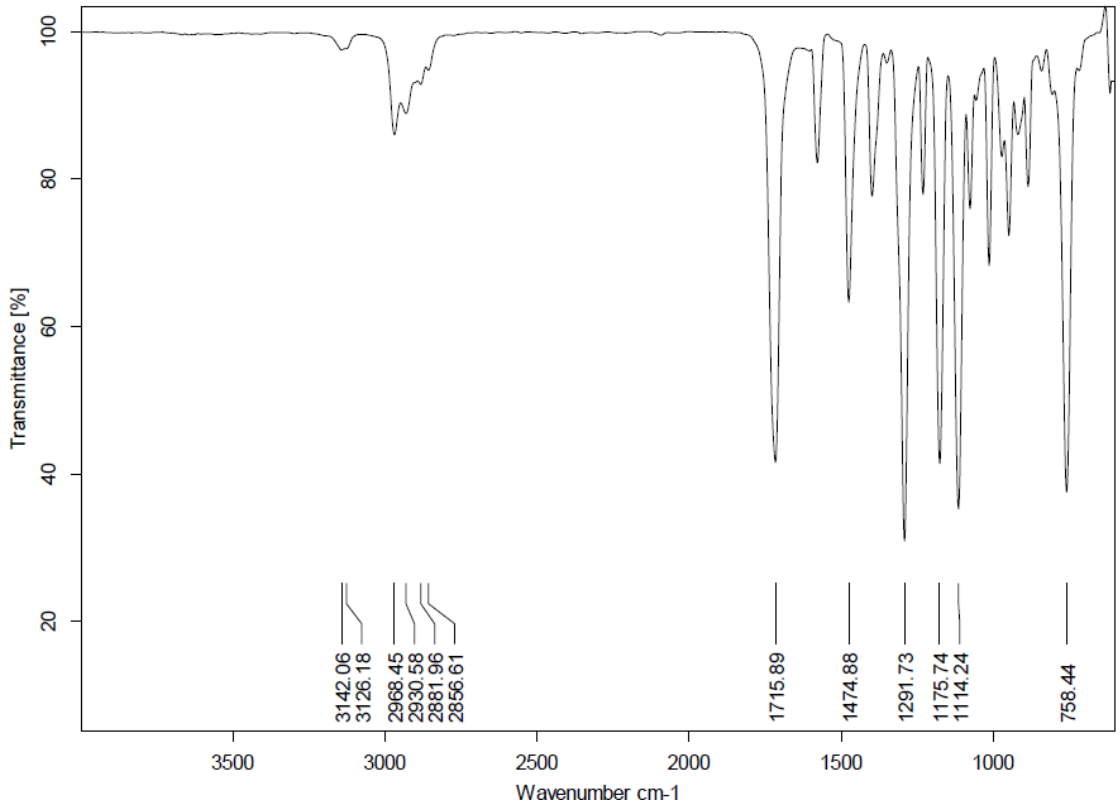

Figure 5.55 FTIR spectrum of propyl 2-furoate **5s**.

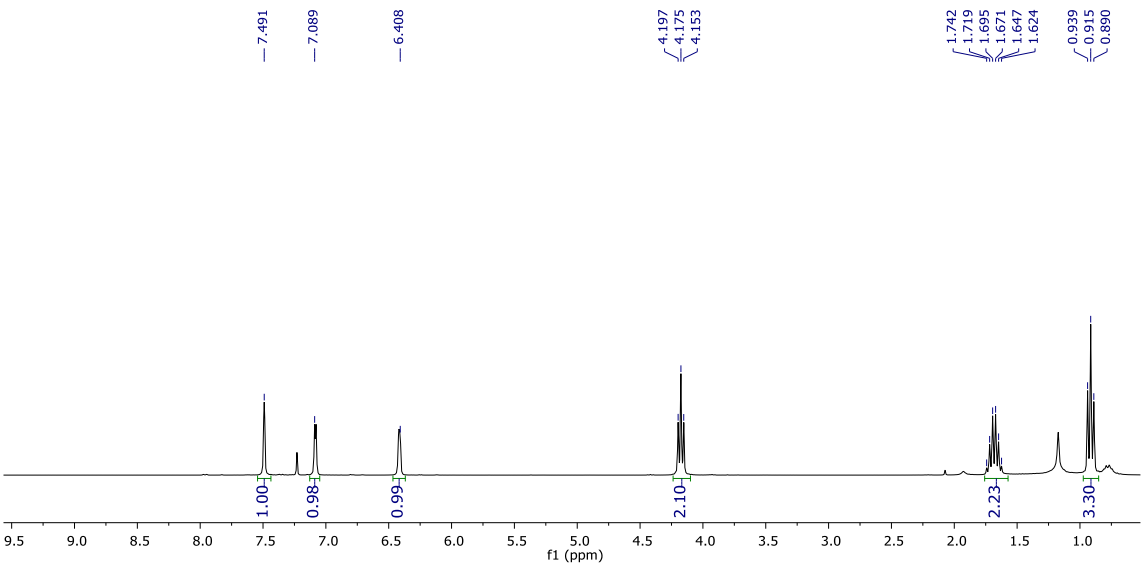

Figure 5.56 ^{1}H-NMR spectrum of propyl 2-furoate **5s**.

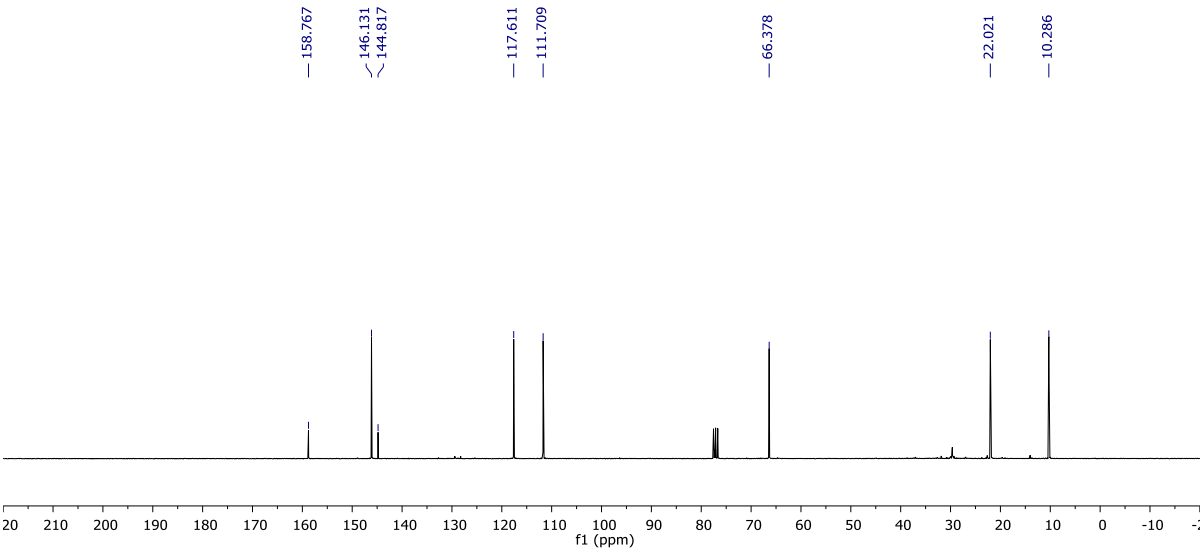

Figure 5.57 ^{13}C-NMR spectrum of propyl 2-furoate **5s**.

5.2.5.4 FTIR and NMR (^{1}H and ^{13}C) characterization of isopropyl 2-furoate 5t

^{1}H-NMR (400 MHz, $CDCl_3$, δ ppm): 7.48 (1H, s), 7.07 (1H, s), 6.41 (1H, s), 5.17 (1H, septet), 1.27 (6H, d). ^{13}C-NMR (100 MHz, $CDCl_3$, δ ppm):158.3, 146.0, 145.1, 117.4, 111.6, 68.5, 21.8. FTIR (ATR, cm^{-1}): 3138, 2982, 2875, 1714, 1293, 1177, 1099.

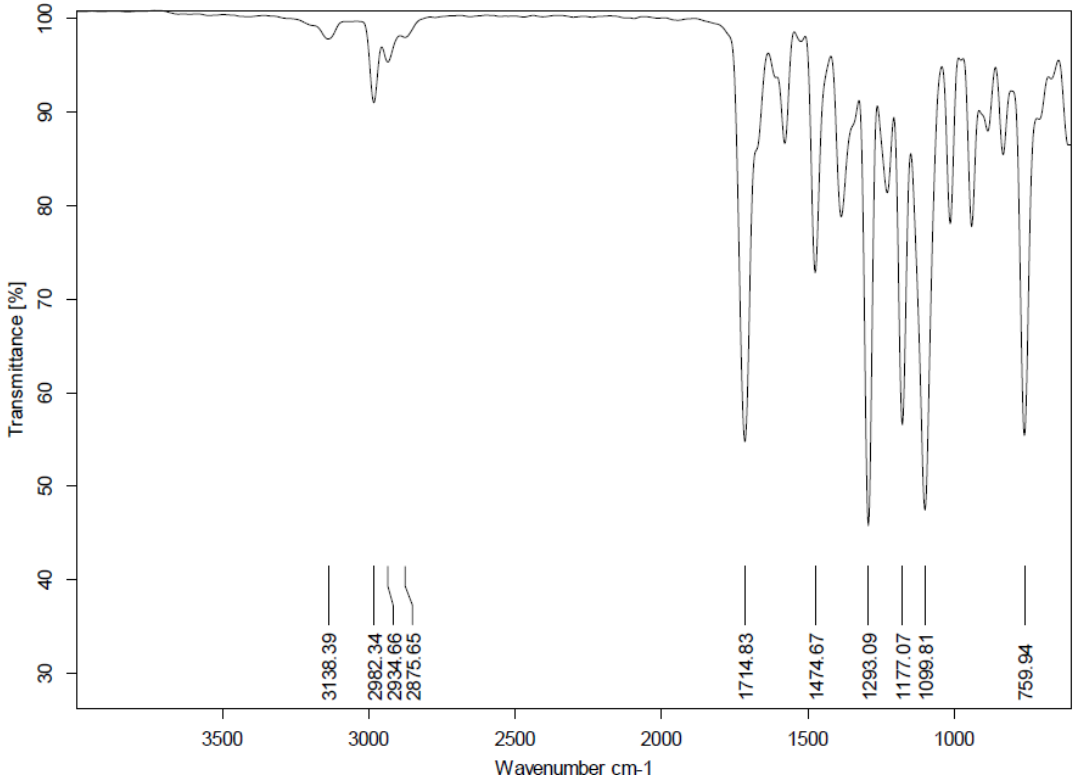

Figure 5.58 FTIR spectrum of isopropyl 2-furoate **5t**.

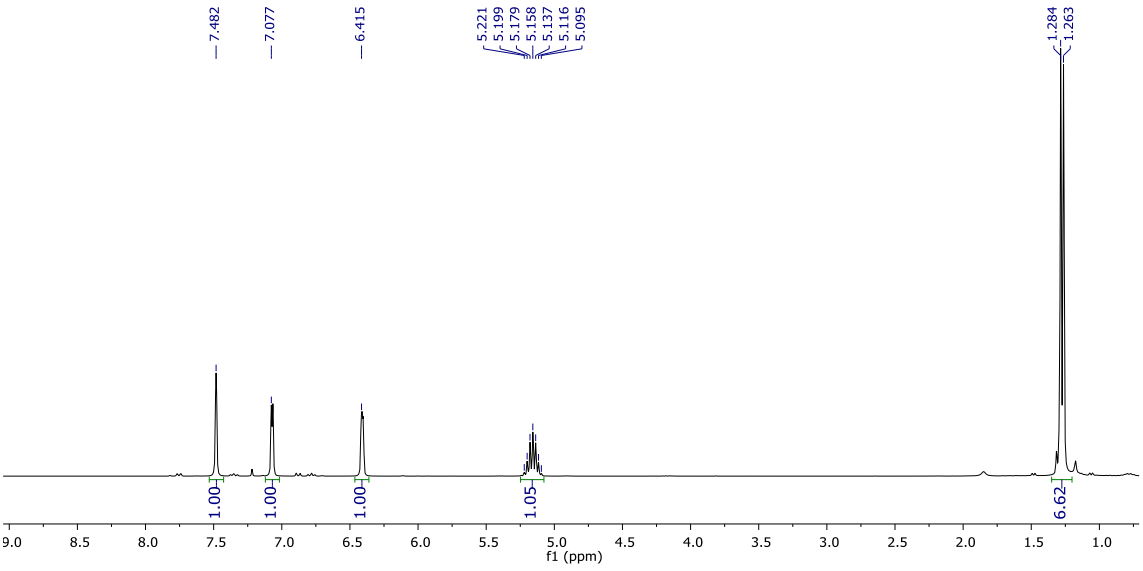

Figure 5.59 ^{1}H-NMR spectrum of isopropyl 2-furoate **5t**.

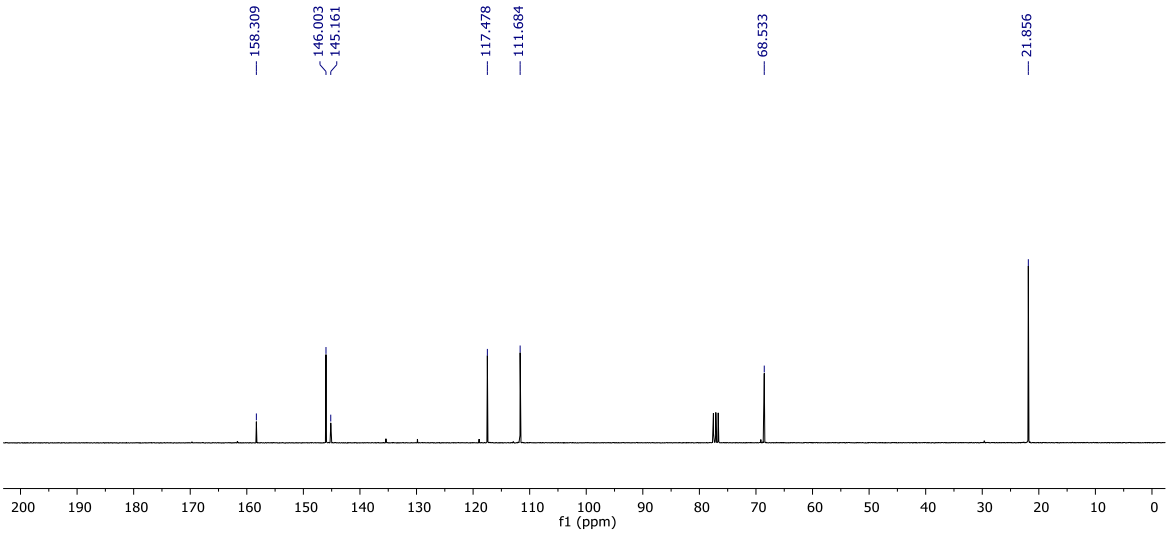

Figure 5.60 ^{13}C-NMR spectrum of isopropyl 2-furoate **5t**.

5.2.5.5 FTIR and NMR (^{1}H and ^{13}C) characterization of butyl 2-furoate 5u

^{1}H-NMR (400 MHz, $CDCl_3$, δ ppm): 7.48 (1H, s), 7.07 (1H, s), 6.40 (1H, s), 4.20 (2H, t), 1.62 (2H, m), 1.34 (2H, m), 0.86 (3H, t). ^{13}C-NMR (100 MHz, $CDCl_3$, δ ppm):168.7, 146.0, 144.8, 117.5, 111.6, 64.6, 30.6, 19.0, 13.5. FTIR (ATR, cm^{-1}): 3142, 2960, 1715, 1292, 1179, 1113, 1011.

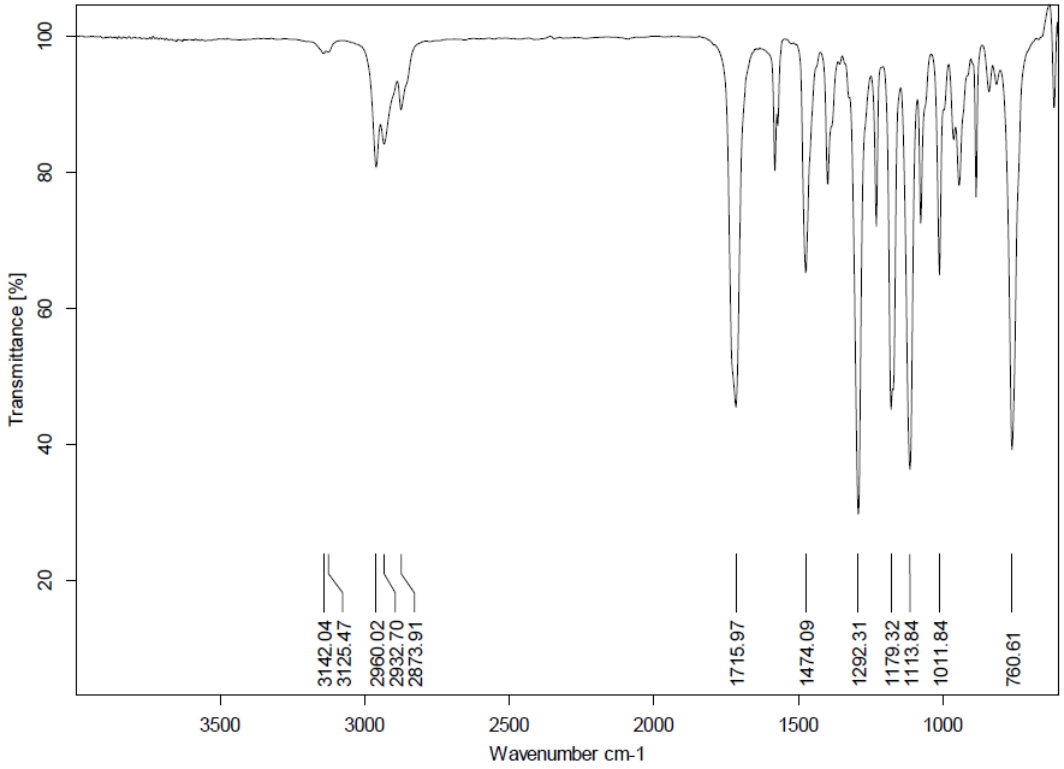

Figure 5.61 FTIR spectrum of butyl 2-furoate **5u**.

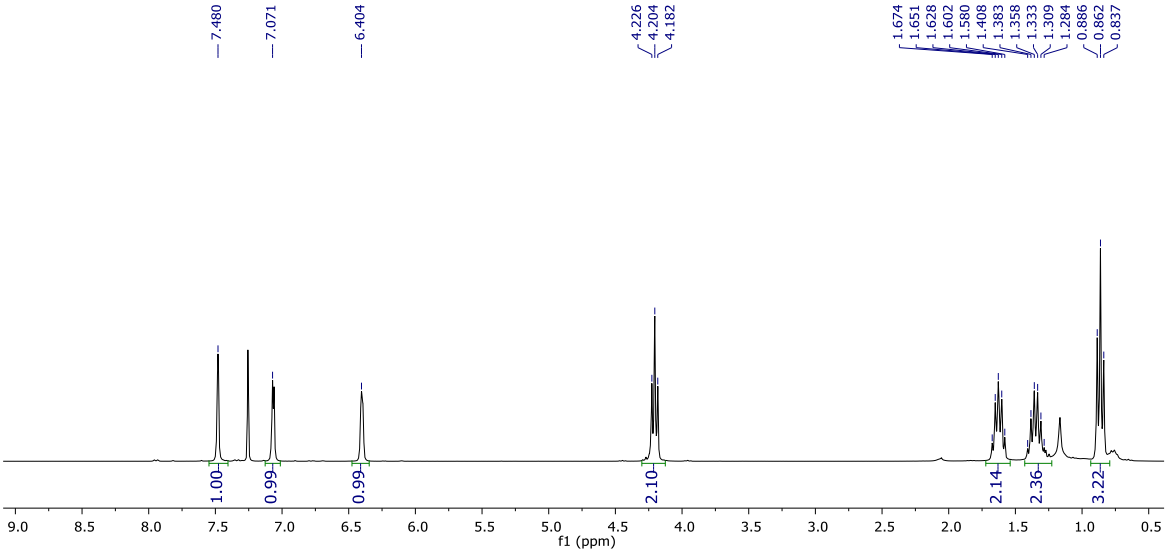

Figure 5.62 ^{1}H-NMR spectrum of butyl 2-furoate **5u**.

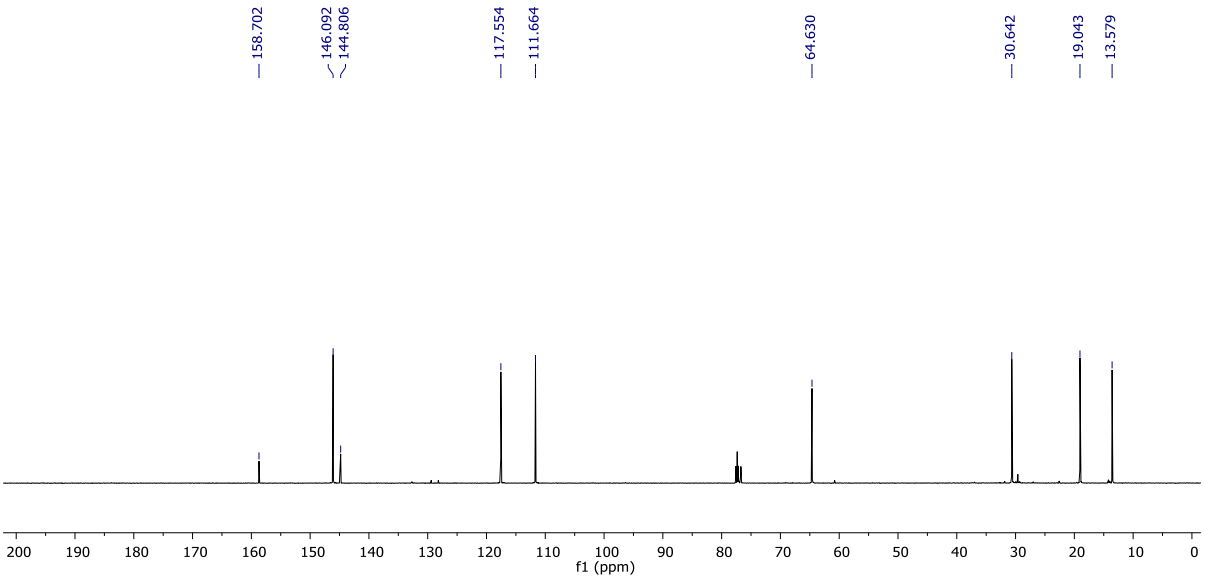

Figure 5.63 ^{13}C-NMR spectrum of butyl 2-furoate **5u**.

5.3 RESULTS AND DISCUSSIONS

5.3.1 Esterification of benzoic acid over HPAs

The esterification of benzoic acid and its derivatives were carried out within a glass pressure reactor fitted with a Teflon screw top. The reactor was heated conventionally in an oil-bath while stirred continuously during the reaction. The HPA catalyst dissolved in the reaction mixture at elevated temperatures and behaved as a homogenous catalyst. However, after the reaction, the catalyst was made heterogeneous by precipitating it from the reaction medium using a non-polar solvent like petroleum ether. The reaction was optimized on the temperature of the reaction, loading of catalyst, molar ratio of reagents, and duration of the reaction. Butyl benzoate **5d** was chosen as the substrate for the optimization. The catalyst was successfully recycled for three consecutive cycles without significant loss in mass or activity of the catalyst.

5.3.2 Efficiency of various HPA catalysts

To investigate the efficiency of various HPA catalysts, the esterification reaction was carried out using commercial PTA, PMA, STA, and SMA catalyst. The catalysts were pre-dried at 110 °C overnight prior use. The esterification of benzoic acid with 1-butanol was carried out at 120 °C for 4 h using 0.4 mol% of HPA catalysts. Among the four HPAs examined, PTA was found to be the most effective catalyst (**Figure 5.64**). Use of PTA as the catalyst afforded butyl benzoate **5d** in 91% isolated yield. STA was found to be nearly as efficient as PTA and provided **5d** in 89% yield. SMA and PMA produced **5d** in 72% and 80% yield, respectively, under identical conditions. The results may be explained by the highest acidity of PTA among the HPA catalysts examined (Timofeeva 2003). Among commercial PTA, PMA, STA, and SMA catalyst, PTA catalyst possess higher acidity and SMA having lower acidity. The pKa value of heteropolyacids are available in literature. PTA showed higher acidity due to its lower pKa value as compared to other heteropolyacids. The pKa value for PTA, STA, PMA, and SMA are 4.70, 4.68, 4.87 and – respectively in acetic acid solvent at 25 °C. Along with dissociation constant it also depends on the composition and structure of HPAs. The acidity decreases with the reduction of HPA and replacement of Mo^{VI} or W^{VI} atom by V^{V} atom and/or the replacement of the central P^{V} atom by Si^{IV}.

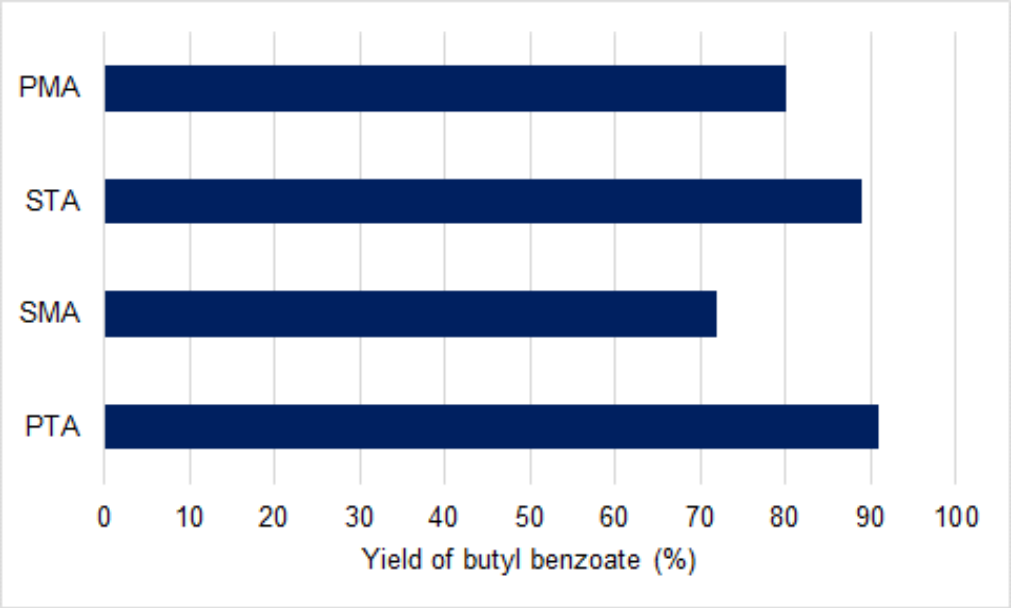

Figure 5.64 The efficiency of various HPAs on the yield of butyl benzoate **5d**.

Reaction conditions: benzoic acid (1.00 g, 8.19 mmol): 1-butanol (0.910 g, 12.30 mmol, 1.5 eq.), 120 °C, 4 h, HPA (0.4 mol%).

5.3.3 Effect of catalyst loading

Since PTA was found to be the most active catalyst, the effect of PTA loading on the isolated yield of **5d** was investigated keeping the other reaction parameters unaltered. When the loading of the PTA catalyst was lowered at 0.2 mol%, the yield of **5d** dropped to 75% (120 °C, 4 h). However, the loading of PTA catalyst more than 0.4 mol% had negligible effect on the yield of **5d** (**Figure 5.65**).

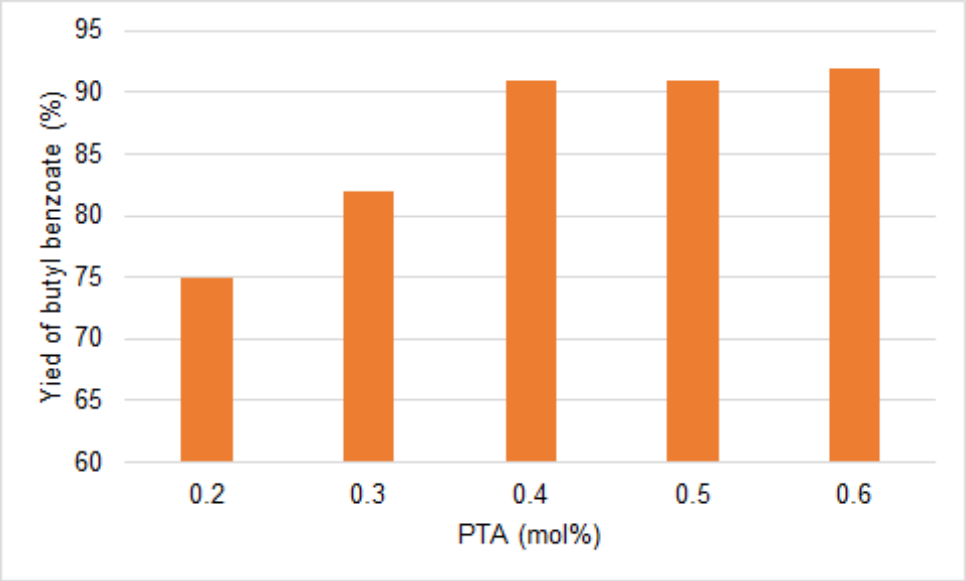

Figure 5.65 The effect of loading of PTA catalyst on the isolated yield of butyl benzoate **5d**.

Reaction conditions: benzoic acid (1.00 g, 8.19 mmol), 1-butanol (0.910 g, 12.30 mmol, 1.5 eq.), 120 °C, 4 h, PTA.

5.3.4 Effect of reaction temperature

The acid-catalyzed esterification of benzoic acid is reversible, and the maximum yield of butyl benzoate **5d** can be obtained if the reaction reaches equilibrium. The effect of reaction temperature on the conversion of benzoic acid and yield of **5d** was studied using PTA as the acid catalyst. The reaction was conducted for 4 h at the chosen temperature using 1.5 equivalent of 1-butanol and 0.4 mol% PTA catalyst. After the reaction, the PTA catalyst was precipitated by adding petroleum ether. The product was purified by column chromatography using silica gel. For 4 h of reaction time, reaction temperatures below 100 °C provided **5d** in poor yields (**Figure 5.66**). When the temperature was increased further, the yield of **5d** increased significantly from 70% at 110 °C to 88% at 110 °C. When the temperature was increased to 120 °C, the yield of **5d** improved marginally to 91%. There was virtually no side product, and the mass balance was essentially the unreacted benzoic acid.

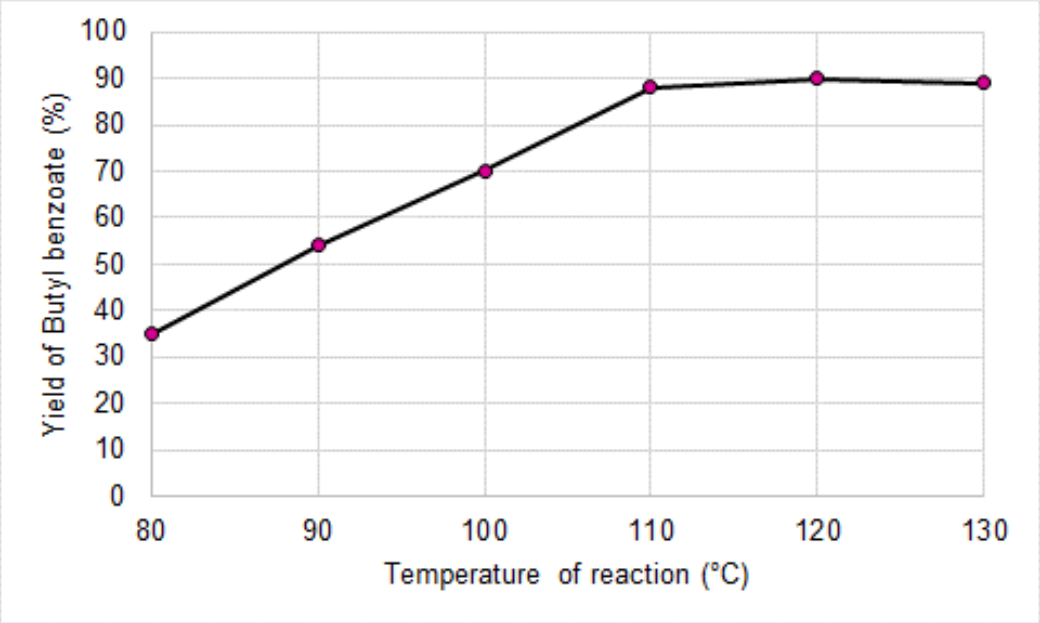

Figure 5.66 Effect of reaction temperature on the yield of butyl benzoate **5d**.

Reaction conditions: benzoic acid (1.00 g, 8.19 mmol), 1-butanol (0.910 g, 12.30 mmol, 1.5 eq.), 4 h, HPA (0.4 mol%).

5.3.5 Effect of mole ratio of benzoic acid to 1-butanol

Synthesis of **5d** was attempted at a temperature of 120 °C, duration of 4 h, and 0.4 mol% of PTA catalyst. The molar ratio of benzoic acid to 1-butanol was varied between 1:1 and 1:2. The results show that the yield of **5d** at ratios above 1:1.5 is nearly constant (**Figure 5.67**). However, using molar ratios lower than 1:1.5 lowered the yield of **5d** due to incomplete reaction and unfavorable equilibrium towards ester formation. However, even with an equivalent amount of 1-butanol, **5d** was isolated in 85% yield. Increasing the equivalence of 1-propanol from 1 to 1.5 (with respect to benzoic acid) increased the yield incrementally and reached 91% at 1.5 equivalent of 1-butanol.

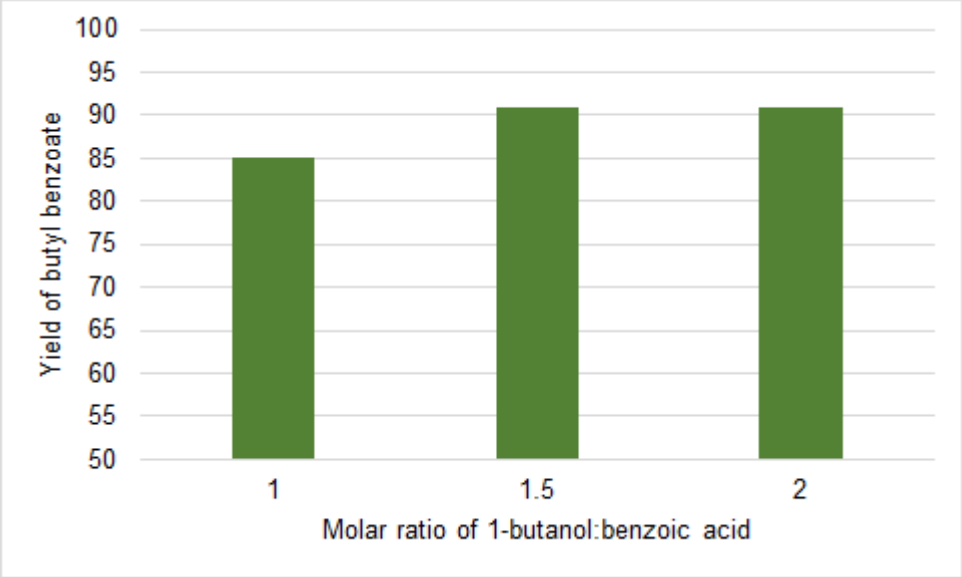

Figure 5.67 Effect of 1-butanol: benzoic acid molar ratio on the isolated yield of butyl benzoate **5d**.

Reaction conditions: benzoic acid (1.00 g, 8.19 mmol), 1-butanol, 120 °C, 4 h, PTA (0.4 mol%).

5.3.6 Effect of different alcohol

The optimized reaction for **5d** was adopted for the production of a homologous series of alkyl benzoates using straight-chain primary alcohols of different alkyl chain length. Methyl- to hexyl benzoates (**5a-5f**) were prepared in excellent isolated yields. In the case of methyl benzoate **5a** and ethyl benzoate **5b**, higher alcohol amount (5 mL) and PTA loading (0.8 mol%) were required to obtain good yields within 4 h of reaction time. Notably, an overnight reaction allowed a lower amount of alcohol and PTA catalyst to be used. The yield of alkyl benzoate was found to increase marginally with increasing alkyl chain length in the alcohol reagent. The result may be explained by a lower rate of hydrolysis of the ester and easier phase separation of the water byproduct. While butyl benzoate 5**d** was isolated in 91% yield, hexyl benzoate **5f** was obtained in 96% yield (**Table 1**, entry 4&6). Use of propane-1,3-diol as the alcohol provided propane-1,3-diyl dibenzoate **5g** in 40% yield. For the synthesis of **5g**, toluene was added as a solvent that

helps to dissolve benzoic acid that otherwise sublimes and collect at the neck of the reactor.

Table 5.1 Esterification of benzoic acid with alkyl alcohols using PTA as the catalyst

Entry	Product	Reaction conditions	Yield (%)[b]
1[a]	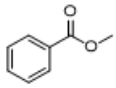 5a	120 °C, 4 h, methanol (5 mL), 0.8 mol% PTA	84
2[a]	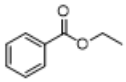 5b	120 °C, 4 h, ethanol (5 mL), 0.8 mol% PTA	86
3	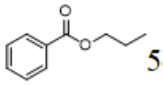 5c	120 °C, 4 h, 1-propanol (1.5 eq.), 0.4 mol% PTA	80
4	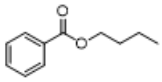 5d	120 °C, 4 h, 1-butanol (1.5 eq.), 0.4 mol% PTA	91
5	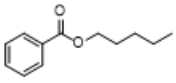 5e	120 °C, 4 h, 1-hexanol (1.5 eq.), 0.4 mol% PTA	94
6	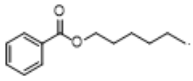 5f	120 °C, 4 h, 1-hexanol (1.5 eq.), 0.4 mol% PTA	96
7	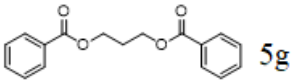 5g	120 °C, 12 h, 1,3-propanediol (0.4 eq.), toluene (5 mL)	40

[a] Excess alcohol and 0.8 mol% PTA was used. [b] Isolated yield.

5.3.7 Effect of different substituted benzoic acid

Butyl ester of various substituted benzoic acid was also synthesized using the PTA catalyst. The electron-donating and electron-withdrawing groups attached to the benzene moiety did not seem to affect the yield of butyl ester. Whereas butyl 4-chlorobenzoate **5h** was obtained in 93% yield, butyl 4-methyl benzoate **5k** was isolated in

89% yield. With strong electron-donating and electron-withdrawing group at the para position, butyl 4-methoxybenzoate **5i** and butyl 4-nitrobenzoate **5j** was isolated in 84% and 86% yield, respectively (**Table 2**, entry 2&3). Dibutyl phthalate **5l** was isolated in 45% yield. The mass balance is the monoester and unreacted phthalic acid. Dibutyl terephthalate **5m** provided a similar yield (40%) under the same reaction condition. Esterification of cinnamic acid afforded butyl cinnamate **5n** in 88% yield. Butyl 2-hydroxybenzoate **5o** was obtained in 83% isolated yield starting from 2-hydroxybenzoic acid or salicylic acid.

Table 5.2 Esterification of various benzoic acid derivatives using PTA catalyst

Entry	Starting material	Product	Yield (%)
1	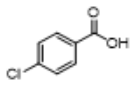	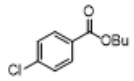 5h	93
2	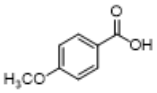	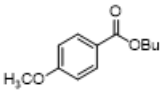 5i	84
3	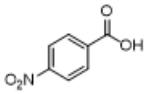	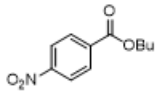 5j	86
4	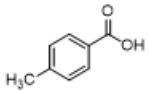	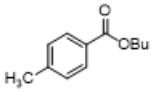 5k	89
5	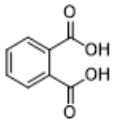	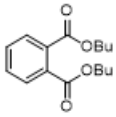 5l	45
6	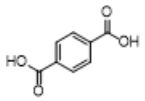	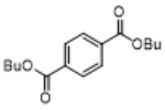 5m	40
7	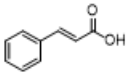	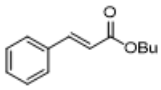 5n	88

8	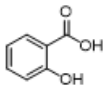	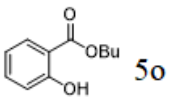 5o	83
9	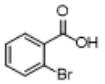	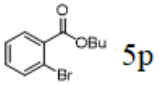 5p	87

The products were purified by column chromatography. Alternatively, the crude reaction mixture (after separating the PTA catalyst) can be washed with saturated sodium bicarbonate solution and dissolve the unreacted benzoic acid.

Optimized conditions: Mole ratio of benzoic acid to alcohol = 1:1.5; catalyst loading = 0.4 mol%, temperature = 120 °C, time = 4 h.

5.3.8 Recycling and regeneration of catalysts

Recyclability of the catalyst is one of the most important parameters for the green indices and process economics. Although the esterification reaction worked with a relatively small quantity of PTA catalyst (i.e., 0.4 mol%), efficient recovery of the PTA catalyst was undertaken. The PTA catalyst used in the preparation of butyl benzoate **5d** was successfully recovered and recycled for three consecutive runs. After the reaction, the crude reaction mixture of **5d** was diluted with petroleum ether, and the precipitated PTA catalyst was separated by decantation or centrifugation. The precipitated recovered catalyst was then dried in a hot-air oven at 110 °C for 12 h before submitting for the subsequent esterification reaction. The mass loss of PTA catalyst was minimized by merely transferring the organic reaction mixture into another flask while drying the catalyst in the reaction vessel itself. A typical mass loss of 1-2% was observed between consecutive runs. The yield of **5d** decreased marginally until the 3rd run (**Figure 5.68**). The amounts of benzoic acid and 1-butanol were adjusted in each trial based on the mass of PTA recovered.

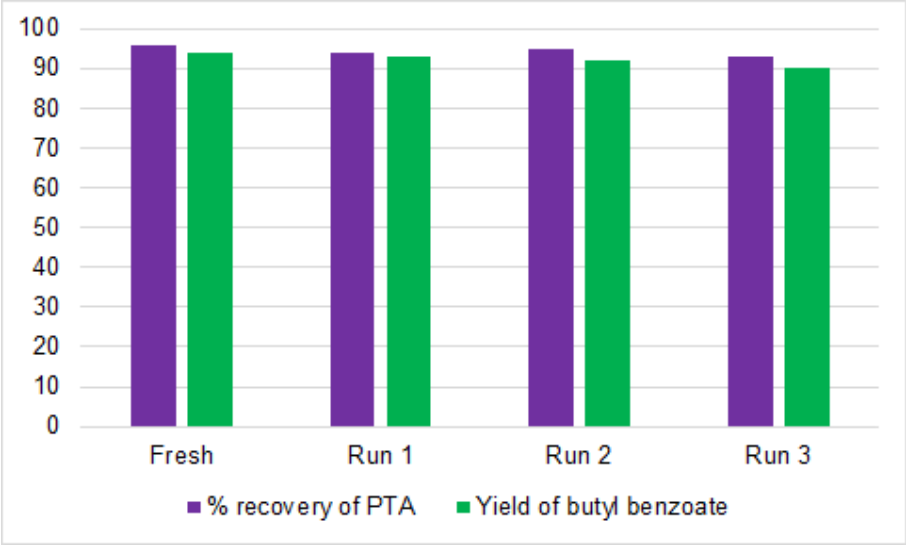

Figure 5.68 Recovery and reuse of PTA catalyst in the preparation of butyl benzoate **5d**.

Reaction conditions: Benzoic acid (1.00 g, 8.19 mmol), 1-butanol (0.910 g, 12.30 mmol, 1.5 eq.), 120 °C, 4 h, HPA (0.4 mol%).

5.3.9 Characterization of recycled catalysts

After each cycle, the dried PTA catalyst was characterized by FTIR spectroscopy to ensure that the structural integrity remained intact. The peak at 1080 cm^{-1} is the characteristic peak for the P-O stretching frequency, whereas the peak at 982 cm^{-1} corresponds to W=O stretching. The peaks at 889 cm^{-1} and 798 cm^{-1} correspond to W-O-W bridges (**Figure 5.69**) (Zhang et al. 2017).

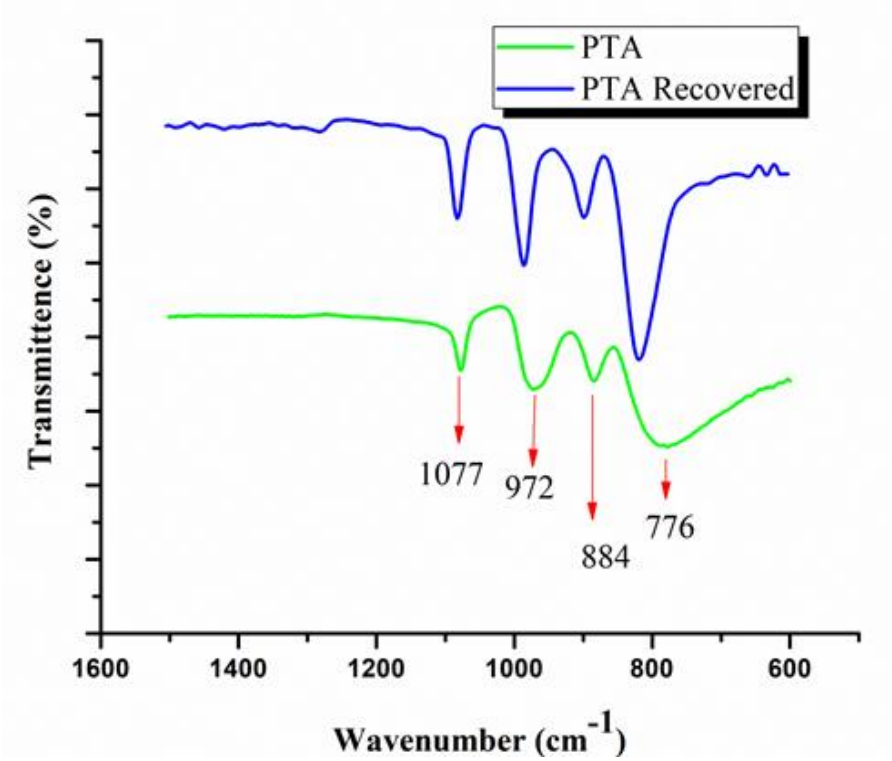

Figure 5.69 FTIR spectra of the fresh PTA (dried) and recycled (3rd cycle) PTA.

In addition, the recovered catalyst after the third cycle was characterized by the ^{31}P-NMR spectroscopy (**Figure 5.70**) and thermogravimetric analysis (TGA) (**Figure 5.71**) to study the structural changes of the catalyst.

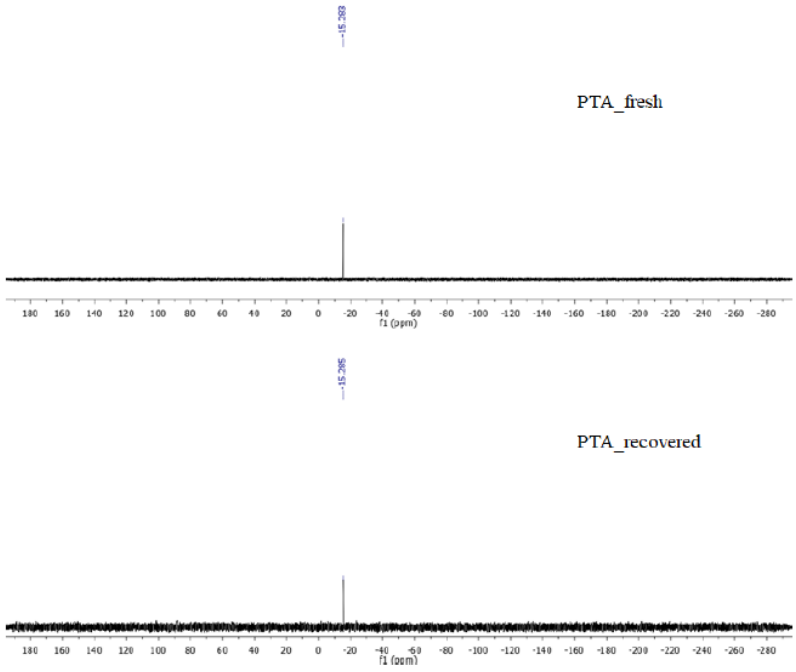

Figure 5.70 The ^{31}P-NMR spectrum of fresh and recovered PTA catalyst.

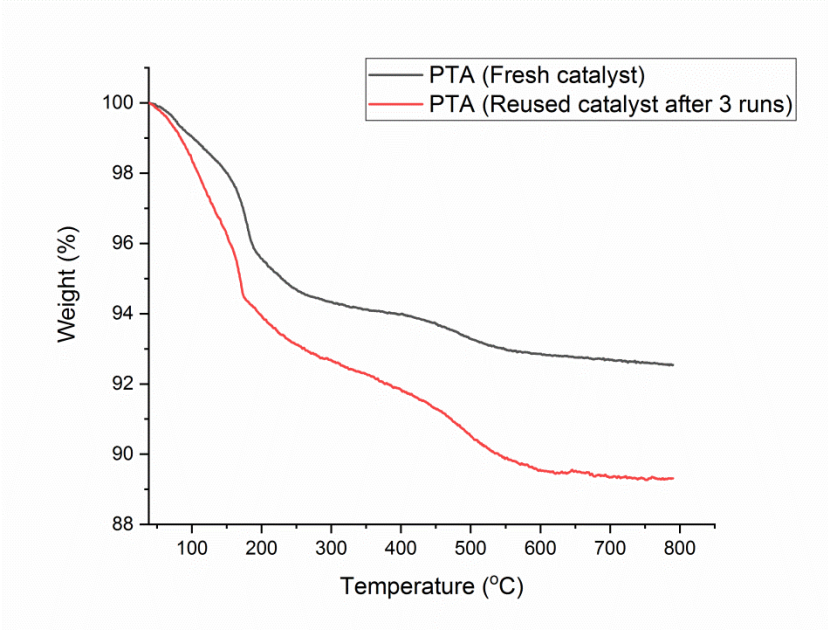

Figure 5.71 The TGA graph of the fresh and recycled PTA catalyst.

5.3.10 Esterification of furoic acid (FA) over HPA catalysts

Similar to the previous section , studies of optimization for maximum conversion were conducted.

In order to find the best reaction conditions, the conversion of furoic acid into alkyl furoates was studied using different HPAs, furoic acid to alcohol ratios, reaction temperature, and catalyst loading. Butyl furoate **5u** has been selected as the model substrate for optimizing the reaction. In a typical reaction, furoic acid, 1-butanol (2 eq.), and PTA (0.3 mol%, with respect to mole of furoic acid used) were taken in a 100 mL glass pressure vessel, sealed, and stirred magnetically during the course of the reaction. After reaction, the PTA catalyst remained suspended in the mixture of reaction and separated from the product. Butyl furoate **5u** was isolated by solubilization in chloroform from the reaction mixture. FTIR and ^{1}H-NMR spectroscopy analyzed the crude product for full conversion and purified through column chromatography (silica gel).

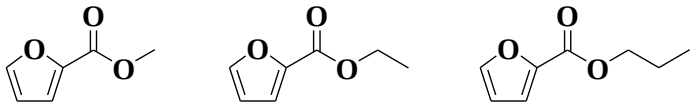

MeFu 5q **EtFu 5r** **PrFu 5s**

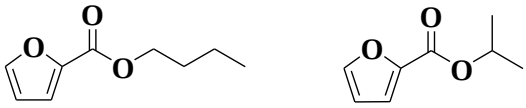

BuFu 5u **IpFu 5t**

Scheme 5.4 Chemical structure of the synthesized alkyl 2-furoates.

5.3.11 Effect of reaction temperature

The effect of reaction temperature on 2-furoic acid conversion and alkyl 2-furoate yield was studied using PTA as the acid catalyst. The reaction even after

stirring at room temperature for 12 h, produced <10% yield of butyl 2-furoate. Increasing the temperature to 80 °C afforded **5u** in 57% isolated yield within 4 h (**Figure 5.72**). Upon increasing the temperature to 90 °C and 100 °C, the yield of **5u** increased to 75% and 82%, respectively. The mass balance was essentially unreacted FA. The yield of **5u** reached 92% after 4 h reaction when the reaction was conducted at 120 °C. The ^{1}H-NMR spectrum of the crude product did not show any unreacted FA certifying its quantitative conversion.

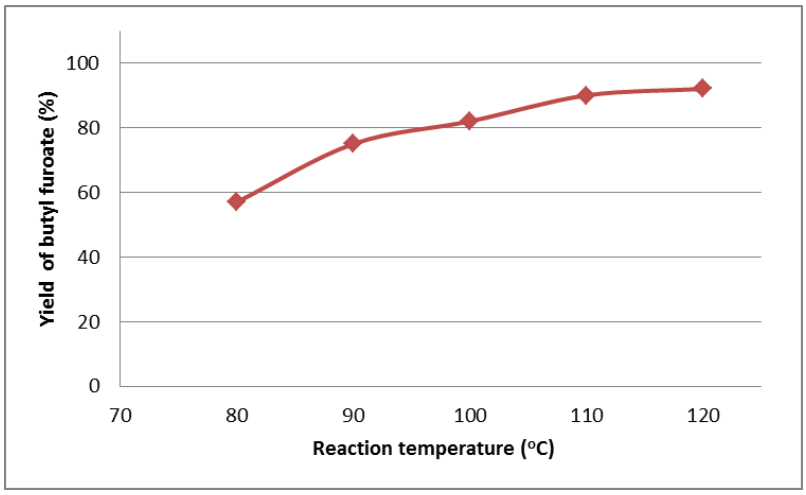

Figure 5.72 Effect of reaction temperature on the yield of butyl furoate **5u**.

Reaction Conditions: FA (1.77 mmol), 1-butanol (3.55 mmol), 4 h, PTA catalyst (0.3 mol%).

5.3.12 Effect of mole ratio of FA to 1-butanol

In order to investigate the effect of molar ratio of FA and 1-butanol on the yield of butyl furoate **5u**, the reaction was carried out at 120 °C for 4 h using 0.3 mol% of PTA as catalyst. The molar ratio of FA to 1-butanol was varied between 1:1 and 1:5. The results show that the yield of **5u** at ratios above 1:1.5 is nearly constant (**Figure 5.73**). However, using ratios lower than 1:1.5 lowered the yield of **5u** due to incomplete reaction. Using equivalent amount of 1-butanol, **5u** was isolated in

65% yield. Increasing the equivalence of 1-butanol from 1 to 2 increased the yield of **5u** incrementally and reached maximum at 92% at 2 equivalent of 1-butanol. Further increase in the equivalence of 1-butanol from 2 to 4 decreases in the yield of butyl furoate. This is attributed due to the additional increase in the 1-butanol quantity causes dilution of the reaction media, act as a solvent, causing a detrimental effect on the contact between the acid and catalyst, reduces the mass transfer and subsequent product yield of the reaction.

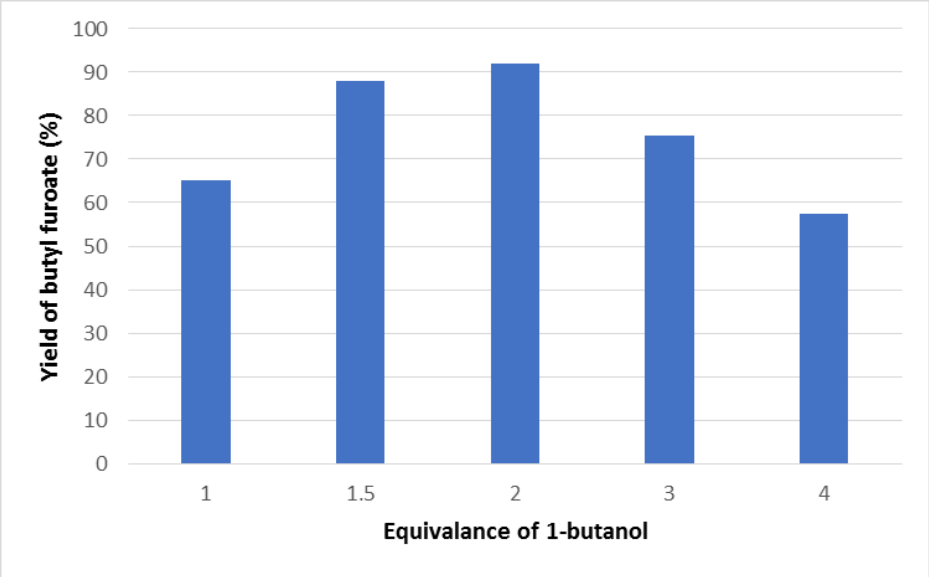

Figure 5.73 Effect of equivalence of 1-butanol with respect to FA on the isolated yield of butyl furoate **5u**.

Reaction conditions: FA (1.77 mmol), 1-butanol, 120 °C, 4 h, PTA catalyst (0.3 mol%).

5.3.13 Efficiency of different HPA in preparing alkyl furoates

To investigate the efficiency of different heteropolyacid (HPA), the esterification reaction was independently carried out using four commercially-

available HPAs, namely, phosphotungstic acid (PTA), phosphomolybdic acid (PMA), silicotungstic acid (STA), and silicomolybdic acid (SMA). The esterification of furoic acid with 1-butanol was carried out at 120 °C for 4 h using 0.3 mol% of HPA catalysts. Among the four HPAs examined, PTA was found to be most effective catalyst. Use of PTA as catalyst afforded butyl furoate **5u** in 92 % yield whereas PMA, STA, and SMA afforded the same in 80.24%, 87%, and 78.16% respectively, under identical conditions (**Figure 5.74**). The results may be explained by the highest acidity of PTA among the HPA catalysts examined.

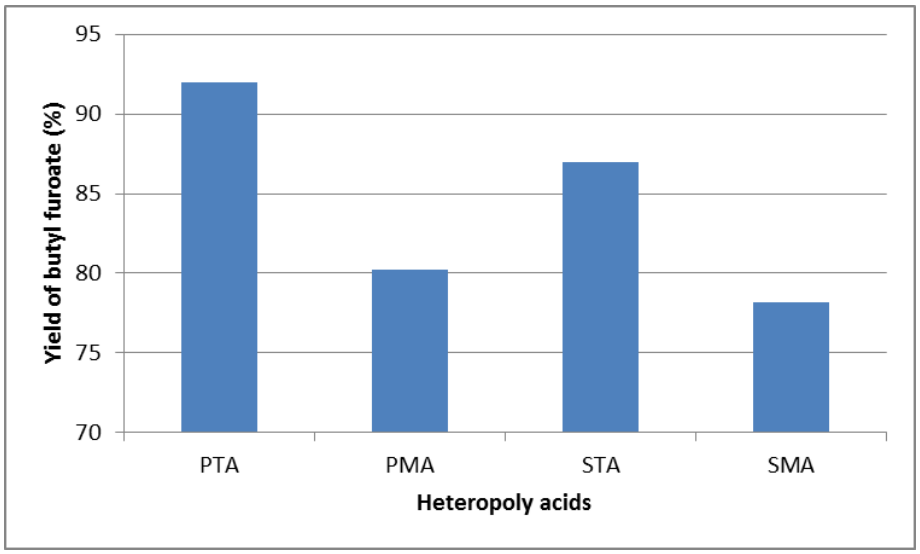

Figure 5.74 Efficiency of various heteropolyacids on the yield of butyl furoate **5u**.

Reaction conditions: FA (1.77 mmol), 1-butanol (3.55 mmol), 120 °C, 4 h, HPAs (0.3 mol%).

Along with HPAs catalyst, salt of phosphotungustic acid and phosphotungustic acid supported over the silica, methyl sulphonic acid and niobium oxide were examined for the esterification of furoic acid. A variety of solid acid catalysts like as Amberlyst-15, $Cs_{2.5}H_{0.5}PW_{12}O_{40}$, $K_{2.2}H_{0.8}PW_{12}O_{40}$, $20\%CH_3SOH/SiO_2$, $20\%PTA/Nb_2O_5$, $25\%PTA/Nb_2O_5$ were used in esterification of furoic acid.

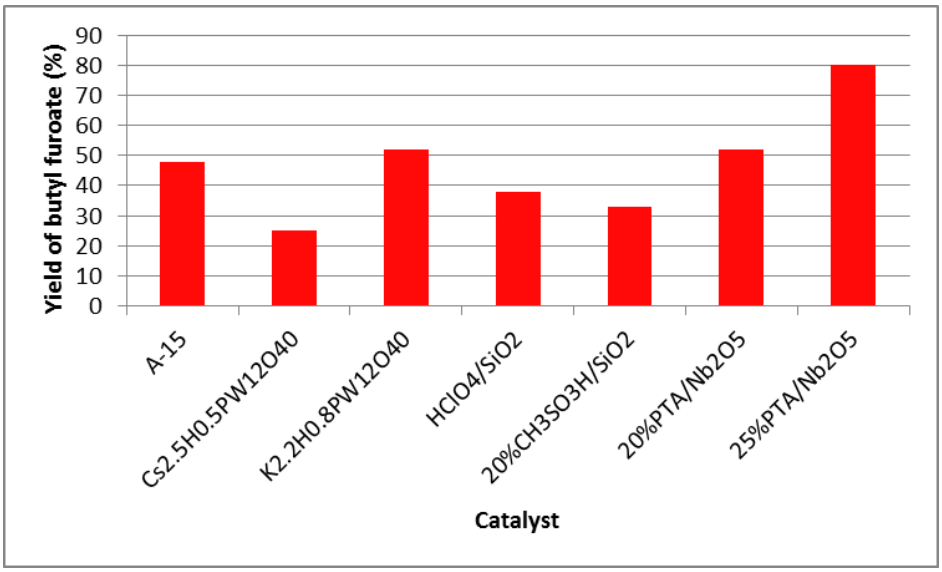

Figure 5.75 The efficiency of various supported HPA catalysts on the yield of butyl furoate **5u**.

Reaction conditions: FA (1.77 mmol), 1-butanol (3.55 mmol), 120 °C, 4 h, catalyst (0.3 mol%).

These supported PTA catalysts have been synthesized by wet impregnation method reported in literature somewhere. Catalytic behaviour was studied for the esterification of furoic acid with 1-butanol at 120 °C for 4 h using 0.3 mol% of supported catalysts. Among the supported catalyst, 25%PTA/Nb_2O_5 was found the most effective catalyst. Use of 25%PTA/Nb_2O_5 catalyst provided butyl furoate **5u** in 80% yield whereas other catalysts afforded less than 50%, under identical conditions (**Figure 5.75**). The results may be explained by the lower number of the acidic sites relative to 25%PTA/Nb_2O_5 among the other solid acid catalysts examined. Among all the examined catalyst PTA catalyst was found most effective compared to other phosphotungustic acid supported catalysts for the esterification of furoic acid.

5.3.14 Effect of catalyst loading

PTA being found to be the most active catalyst, the effect of loading of PTA on the isolated yield of **5u** was investigated keeping the other reaction parameters unaltered (**Figure 5.76**). When the loading of PTA catalyst was lowered to 0.09 mol%, the yield was 55% after 4 h at 120 °C. The yield increased up to 88% after 6 h. The yield increased incrementally up to 0.3mol% and reached maximum of 92% and then decreased to 74% at 0.5 mol%. Lower yield of **5u** at higher loading of PTA catalyst is due to acid-promoted decompositions reactions and ether formation from alcohols and thereby lowering the amount of alcohol available to react with furoic acid.

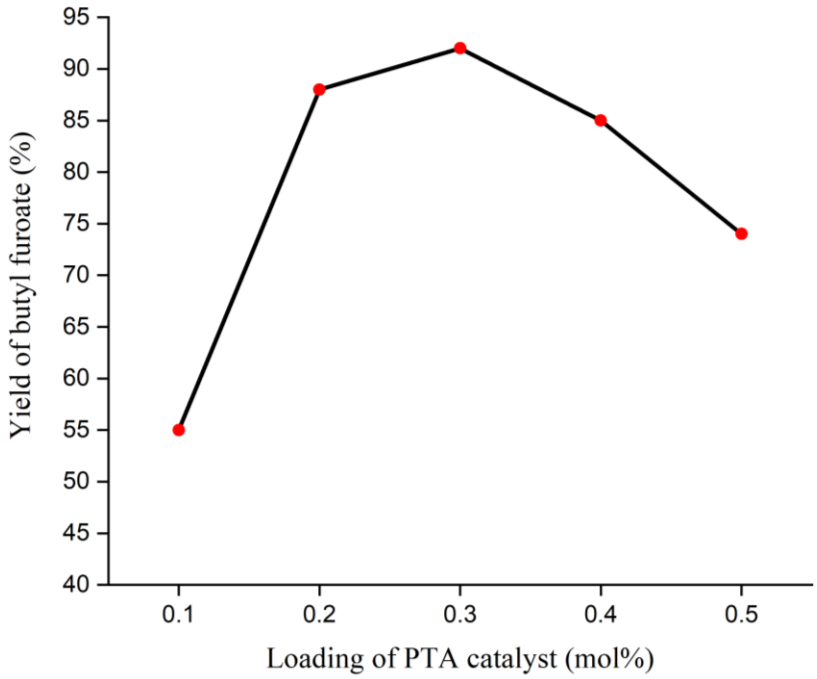

Figure 5.76 Effect of loading of PTA catalyst on the isolated yield of butyl furoate **5u**.

Reaction conditions: FA (1.77 mmol), 1-butanol (3.55 mmol), 120 °C, 4 h.

5.3.15 Effect of different alcohol

The optimized reaction for **5u** was applied for the production of **5q-5u** from FA using 0.3 mol% PTA catalyst. The reactions were performed in a glass pressure tube fitted with a Teflon screw top. The set up allows reaching temperature without evaporative loss of the alcohols during reaction. Where methyl furoate **5q** was isolated in 87% yield, 85% yield ethyl furoate **5r**, 90% yield propyl furoate **5s**, 60% yield isopropyl furoate **5t** and the butyl furoate **5u** was obtained in 92% isolated yield (**Figure 5.77**).

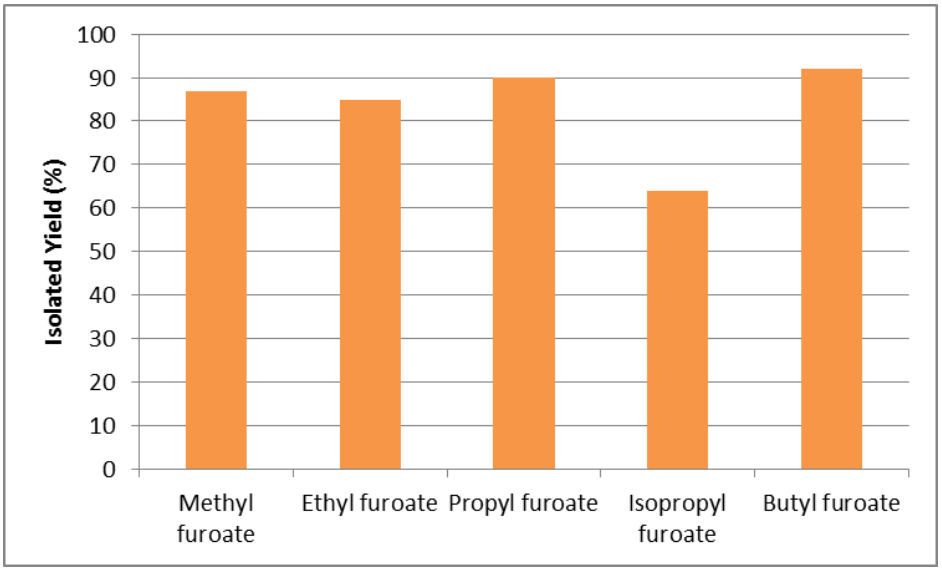

Figure 5.77 Preparation of alkyl furoates (**5q-5u**) from 2-furoic acid.

Reaction Conditions: FA:alcohol (1:2) (molar ratio), 120 °C, 4 h, PTA (0.3 mol%).

Optimized conditions: (85% yield) mole ratio FA to alcohol=1:2, amount of catalyst 0.3 mol%, temperature=120 °C, and time=4 h.

Table 5.3 Esterification of furoic acid using PTA catalyst

Entry	Product	Yield (%)
1	Methyl furoate **5q**	87
2	Ethyl furoate **5r**	85
3	Propyl furoate **5s**	90
4	Isopropyl furoate **5t**	60
5	Butyl furoate **5u**	92
Preparation of alkyl furoates (**5q**-**5u**) from 2-furoic acid. **Reaction Conditions**: FA: alcohol (1:2) (molar ratio), 120 °C, 4 h, PTA (0.3 mol%).		

5.4 CONCLUSION

A solvent-free and gram-scale synthetic protocol for the esterification of benzoic acid and furoic acid (aromatic acid) has been developed using PTA as an efficient and green catalyst. The reactions were performed at 120 °C for 4 h in a glass pressure reactor that provided excellent isolated yields of alkyl benzoates and alkyl furoates using only slight excess of the alcohol reagent and 0.4 mol% and 0.3 mol% of the PTA catalyst respectively. Esterification of several substituted benzoic acid molecules bearing electron-donating and electron-withdrawing groups have been reported. The PTA catalyst was successfully recovered by manipulating the solubility of PTA in the reaction mixture. The physical mass loss of PTA catalyst in subsequent runs was minimal, and the catalyst activity remained nearly the same even after the third run.

CHAPTER 6

SUMMARY AND CONCLUSIONS

Abstract

This chapter includes the summary, conclusions, and scope for future work on the significant research findings discussed in chapter 2 through chapter 5 of this thesis.

6.1 SUMMARY

- The chemocatalytic valorization of biomass requires a new library of robust, selective, inexpensive, recyclable, and environment-friendly catalysts. Heteropolyacids (HPAs) are well-studied compounds, and their applications in catalysis are well documented. The applications of HPA-based catalysts in the chemistry of renewables are relatively new and is being explored over the past few years.
- In the present work, Keggin-type heteropolyacids (HPAs) have been employed for the preparation of 2-(2-Furyl)-1,3-dioxolane by the acetalization of biomass-derived furfural with ethylene glycol. The acetals of furfural are potential fuel oxygenates and renewable chemical intermediate for further value addition.
- HPAs have been used as a catalyst for the esterification of saturated fatty acids like stearic acid and unsaturated fatty acid like oleic acid. Acid-catalyzed esterification of free fatty acid is of immense interest for the preparation of biodiesel from feedstock with significant free fatty acid content. The HPA catalyst was conveniently recovered by precipitating it from the reaction mixture using a non-polar solvent. The catalyst was successfully recycled for several cycles without noticeable loss in mass or activity.
- The selective oxidation of furfural into 2(5H)-furanone was attempted using various HPA-based heterogeneous acid catalysts. Aqueous hydrogen peroxide was used as an inexpensive and environment-friendly oxidant. A series of phosphotungstic acid (PTA) supported on NH_4YZ zeolite catalysts (10-30 wt% PTA-NH_4YZ) were prepared and characterized. The catalysts were characterized by FTIR, PXRD, and SEM analysis. The 20 wt% PTA/NH_4YZ catalyst was found

to be most active that provided 2(5H)-furanone in 40% isolated yield under optimized conditions. Roughly 20% of succinic acid was isolated from the aqueous fraction.

- Solvent-Free and scalable preparation of a series of alkyl benzoates by the HPA-catalyzed esterification of benzoic acid has been reported. The reaction worked equally well for benzoic acid moieties having electron-donating or electron-withdrawing groups attached to it. Post reaction, the HPA catalyst was conveniently recovered from the reaction mixture by precipitation. The esters were purified by simply filtering through a pad of silica gel where the unreacted benzoic acid remained stuck on the silica gel.
- The synthesis of alkyl 2-furoates has been reported by the esterification of biomass-derived furoic acid. The furoates have potential applications as a renewable solvent, fuel oxygenate, perfumes, and chemical feedstock for further value addition pathways. The reaction was performed in a batch-type glass pressure reactor in the presence of an HPA catalyst. The alcohol reagent was used only in slight excess that simplified the product separation and catalyst recovery.

6.2 CONCLUSIONS

The main objective of the thesis was to use HPAs as an efficient and environment-friendly catalyst for converting biomass-derived sugars into fuels and specialty chemicals. The following significant conclusions were drawn on the basis of the experimental results reported in chapter 2 through chapter 5 of this thesis.

2-(furan-2-yl)-1,3-dioxolane was produced in excellent isolated yield by reacting biomass-derived furfural with ethylene glycol using phosphotungstic acid (PTA) as a catalyst. The reaction was conducted in a Dean-Stark apparatus, and benzene was used as the carrier for water removal. The reaction was optimized on parameters such as the type and loading of catalyst, duration of reaction, and the relative ratio of reagents. The cyclic acetal was isolated in 92% yield using a 1:3 molar ratio of furfural and ethylene glycol

and only 2 wt% of the PTA catalyst. The catalyst was conveniently separated from the reaction mixture by exploiting the differential solubility of HPA catalysts.

A high-yielding and scalable synthesis of fatty acid esters were achieved by esterifying free fatty acids like stearic acid and oleic acid with alkyl alcohols within a closed batch reactor using HPA catalysts. The reaction was optimized on temperature, the molar ratio of fatty acid and alkyl alcohol, and the loading of catalyst. The solvent-free, gram-scale reactions afforded >95% yield of alkyl stearates and >85% yield of alkyl oleates under the optimized conditions (1 mol% phosphotungstic acid (PTA) catalyst, 110 °C, 4 h for alkyl stearates and 0.2 mol% PTA catalyst, 120 °C, 4 h for alkyl oleates) by using only slight excess of the alcohol reagent. The PTA catalyst was successfully recovered and reused for five consecutive cycles without significant loss in mass and activity.

The preparation of 2-furanone was achieved by the selective oxidation of biomass-derived furfural using hydrogen peroxide as an inexpensive oxidant and PTA catalyst supported on NH_4YZ zeolite as a catalyst. A series of PTA supported on NH_4YZ zeolite catalysts (10-30 wt% PTA-NH_4YZ) were prepared via the wet impregnation method. The prepared catalysts were characterized by PXRD, FTIR, and TGA. The influences of various reaction parameters such as temperature, duration, loading of catalyst, and furfural to H_2O_2 molar ratio were studied on the conversion of furfural and the yield of 2-furanone. The 20 wt% PTA/NH_4YZ was found to be the most active catalyst for the selective oxidation of furfural. The solvent-free synthesis afforded 2-furanone in 40% isolated yields under optimized conditions, and the reaction was conducted at several grams scale. Around 20% of succinic acid was isolated from the aqueous fraction.

A high-yielding and scalable preparation of alkyl benzoates and alkyl furoates have been achieved from benzoic acid and furoic acid, respectively, using HPA as an efficient and recyclable acid catalyst. A gram-scale synthetic protocol was developed that afforded alkyl benzoates and alkyl furoates in excellent isolated yields (>85%) within 4 h at 120 °C using only slight excess of the alcohol reagent and <1 mol% of the PTA

catalyst under solvent-free conditions. Esterification of several substituted benzoic acid molecules bearing electron-donating and electron-withdrawing groups has been reported with good isolated yield. The PTA catalyst was conveniently recovered and reused for three consecutive cycles without significant loss in mass or activity.

6.3 SCOPE FOR THE FUTURE WORK

In this thesis, the commercial HPAs have been used as efficient, recyclable, and environment-friendly catalysts for the synthetic upgrading of biomass-derived renewable chemical building blocks. In the future, the tailor-made HPAs or polyoxometalates (POMs) can be synthesized with controlled acidity, solubility, and thermal stability for their application in the catalytic upgrading of biomass. Bifunctional catalysts can be prepared by supporting HPAs on noble metal-based catalysts such as Pd/C. The catalysts may be applied for the hydrodeoxygenation of biomass-derived intermediates into fuels and fuel additives. The noble metal would help in the hydrogenation reaction, whereas the HPA would help in the hydrogenolysis and dehydration reactions. For example, the catalyst may be used for the one-pot production of γ-valerolactone from biomass-derived levulinic acid. The HPA catalyst would help in intramolecular lactonization, whereas the Palladium metal would catalyze the hydrogenation of the ketone or olefin. One-Pot preparation of fuel additives like 2-methyl furfural and 2,5-dimethylfuran can also be envisioned by treating biomass-derived sugars like fructose with the bifunctional catalyst. The HPA-based novel ionic liquids may be used as a catalyst or as a green reaction media for various renewable chemistries. The HPA-based catalysts can be used for the acid-catalyzed dehydration of glucose-derived D-sorbitol into isosorbide and the preparation of diphenolic acid by reacting biomass-derived levulinic acid with phenol. The recyclability of the homogeneous and heterogeneous HPA catalysts should be studied in detail.

References

Agirrezabal-Telleria, I., Gandarias, I., and Arias, P. L. (2014). “Heterogeneous acid-catalysts for the production of furan-derived compounds (furfural and hydroxymethylfurfural) from renewable carbohydrates: A review.” *Catal. Today*, 234, 42–58.

Aliyan, H., Fazaeli, R., Massah, A. R., Momeni, A. R., Naghash, H. J., and Moeinifard, B. (2010). “Acetalization of Carbonyl Compounds Catalyzed by Bismuth Triflate Under Solvent-Free Conditions.” *Asian J. Chem.*, 22(2), 873.

Alonso-Fagúndez, N., Agirrezabal-Telleria, I., Arias, P. L., Fierro, J. L. G., Mariscal, R., and Granados, M. L. (2014). “Aqueous-phase catalytic oxidation of furfural with H 2 O 2: high yield of maleic acid by using titanium silicalite-1.” *RSC Adv.*, 4(98), 54960–54972.

Alonso-Fagúndez, N., Granados, M. L., Mariscal, R., and Ojeda, M. (2012). “Selective conversion of furfural to maleic anhydride and furan with VOx/Al2O3 catalysts.” *ChemSusChem*, 5(10), 1984–1990.

Anastas, P. T., and Warner, J. C. (1998). “Green chemistry.” *Front. Chem.*, 640.

Aoshima, H., Miyagisnima, A., Nozawa, Y., Sadzuka, Y., and Sonobe, T. (2005). “Glycerin fatty acid esters as a new lubricant of tablets.” *Int. J. Pharm.*, 293(1–2), 25–34.

Baker, I. J., Matthews, B., Suares, H., Krodkiewska, I., Furlong, D. N., Grieser, F., and Drummond, C. I. (2000). “Sugar fatty acid ester surfactants: structure and ultimate aerobic biodegradability.” *J. Surfactants Deterg.*, 3(1), 1–11.

Baker, L. C., and Glick, D. C. (1998). “Present general status of understanding of heteropoly electrolytes and a tracing of some major highlights in the history of their elucidation.” *Chem. Rev.*, 98(1), 3–50.

Bamoharram, F. F., Heravi, M. M., Roshani, M., Gharib, A., and Jahangir, M. (2007). “Catalytic method for synthesis of aspirin by a green, efficient and recyclable solid acid catalyst (Preyssler’s anion) at room temperature.” *J. Chin. Chem. Soc.*, 54(4), 1017–1020.

Barbosa, S. L., Dabdoub, M. J., Hurtado, G. R., Klein, S. I., Baroni, A. C., and Cunha, C. (2006). “Solvent free esterification reactions using Lewis acids in solid phase catalysis.” *Appl. Catal., A*, 313(2), 146–150.

Bart, J. C., and Cavallaro, S. (2014). “Transiting from adipic acid to bioadipic acid. 1, petroleum-based processes.” *Ind. Eng. Chem. Res*, 54(1), 1–46.

Berzelius, J. (1826). “The preparation of the phosphomolybdate ion [PMo12O40] 3−.” *Pogg Ann*, 6, 369–371.

Blümel, M., Noy, J.-M., Enders, D., Stenzel, M. H., and Nguyen, T. V. (2016). “Development and applications of transesterification reactions catalyzed by N-heterocyclic olefins.” *Org. Lett.*, 18(9), 2208–2211.

Brahmkhatri, V., and Patel, A. (2011). “12-Tungstophosphoric acid anchored to SBA-15: An efficient, environmentally benign reusable catalysts for biodiesel production by esterification of free fatty acids.” *Appl. Catal., A*, 403(1–2), 161–172.

Caetano, C. S., Fonseca, I. M., Ramos, A. M., Vital, J., and Castanheiro, J. E. (2008). “Esterification of free fatty acids with methanol using heteropolyacids immobilized on silica.” *Catal. Commun.*, 9(10), 1996–1999.

Canakci, M. (2007). “The potential of restaurant waste lipids as biodiesel feedstocks.” *Bioresour. Technol.*, 98(1), 183–190.

Cao, R., Liu, C., and Liu, L. (1996). “A convenient synthesis of 2 (5H)-furanone.” *Org. Prep. Proced. Int.*, 28(2), 215–216.

Cardoso, A. L., Augusti, R., and Da Silva, M. J. (2008). “Investigation on the esterification of fatty acids catalyzed by the H3PW12O40 heteropolyacid.” *J AM OIL CHEM SOC.*, 85(6), 555–560.

Castanheiro, J. E., Fonseca, I. M., Ramos, A. M., and Vital, J. (2017). “Tungstophosphoric acid immobilised in SBA-15 as an efficient heterogeneous acid catalyst for the conversion of terpenes and free fatty acids.” *Microporous and Mesoporous Mater.*, 249, 16–24.

Cavalcanti, E. D., Aguieiras, É. C., Silva, P. R. da, Duarte, J. G., Cipolatti, E. P., Fernandez-Lafuente, R., Silva, J. A. C. da, and Freire, D. M. (2018). “Improved

production of biolubricants from soybean oil and different polyols via esterification reaction catalyzed by immobilized lipase from Candida rugosa." *Fuel*, 215, 705–713.

Chakraborti, A. K., Singh, B., Chankeshwara, S. V., and Patel, A. R. (2009). "Protic acid immobilized on solid support as an extremely efficient recyclable catalyst system for a direct and atom economical esterification of carboxylic acids with alcohols." *J. Org. Chem*, 74(16), 5967–5974.

Chang, F., Dutta, S., Becnel, J. J., Estep, A. S., and Mascal, M. (2014). "Synthesis of the insecticide prothrin and its analogues from biomass-derived 5-(chloromethyl) furfural." *J. Agric. Food. Chem.*, 62(2), 476–480.

Choudhary, H., Nishimura, S., and Ebitani, K. (2013). "Metal-free oxidative synthesis of succinic acid from biomass-derived furan compounds using a solid acid catalyst with hydrogen peroxide." *Appl. Catal., A* , 458, 55–62.

D'Oca, M. G. M., Soares, R. M., Moura, R. R. de, and Freitas Granjão, V. de. (2012a). "Sulfamic acid: an efficient acid catalyst for esterification of FFA." *Fuel*, 97, 884–886.

D'Oca, M. G. M., Soares, R. M., Moura, R. R. de, and Freitas Granjão, V. de. (2012b). "Sulfamic acid: an efficient acid catalyst for esterification of FFA." *Fuel*, 97, 884–886.

Engel, C. A. R., Straathof, A. J., Zijlmans, T. W., Gulik, W. M. van, and Wielen, L. A. van der. (2008). "Fumaric acid production by fermentation." *Appl. Microbiol. Biotechnol.*, 78(3), 379–389.

Erythropel, H., Börmann, A., Nicell, J., Leask, R., and Maric, M. (2018). "Designing green plasticizers: Linear alkyl diol dibenzoate plasticizers and a thermally reversible plasticizer." *Polym.*, 10(6), 646.

Escobar, A., Pérez, M., Sathicq, Á., García, M., Paola, A., Romanelli, G., and Blustein, G. (2019). "Alkyl 2-furoates obtained by green chemistry procedures as suitable new antifoulants for marine protective coatings." *J. Coat. Technol. Res.* , 16(1), 159–166.

Escobar, A., Sathicq, Á., Pizzio, L., Blanco, M., and Romanelli, G. (2015). "Biomass valorization derivatives: Clean esterification of 2-furoic acid using tungstophosphoric acid/zirconia composites as recyclable catalyst." *PROCESS SAF ENVIRON.*, 98, 176–186.

Fadhel, A. Z., Pollet, P., Liotta, C. L., and Eckert, C. A. (2010). “Combining the benefits of homogeneous and heterogeneous catalysis with tunable solvents and nearcritical water.” *Molecules*, 15(11), 8400–8424.

Feng, Y., and Zhang, A. (2017). “A floral fragrance, methyl benzoate, is an efficient green pesticide.” *Sci. Rep.*, 7, 42168.

Flores, I., Demarteau, J., Müller, A. J., Etxeberria, A., Irusta, L., Bergman, F., Koning, C., and Sardon, H. (2018). “Screening of different organocatalysts for the sustainable synthesis of PET.” *EUR POLYM J.*, 104, 170–176.

Gallezot, P. (2012). “Conversion of biomass to selected chemical products.” *Chem. Soc. Rev.*, 41(4), 1538–1558.

Garst, J. E., and Schmir, G. L. (1974). “Hydrolysis of 2-methoxyfuran.” *J. Org. Chem.*, 39(19), 2920–2923.

Glattfeld, J. W. E., Leavell, G., Spieth, G. E., and Hutton, D. (1931). “The C4-saccharinic acids. V. The preparation of 2, 3-dihydroxybutyric acid lactone. 3-Hydroxyisocrotonic acid lactone. An attempt to prepare 2, 2′-dihydroxyisobutyric acid.” *J. Am. Chem. Soc.*, 53(8), 3164–3171.

Godói Silva, V. W. de, Laier, L. O., and Da Silva, M. J. (2010). “Novel H 3 PW 12 O 40: catalysed esterification reactions of fatty acids at room temperature for biodiesel production.” *Catal. Lett.*, 135(3–4), 207–211.

Gradzielski, M., Horbaschek, K., and Deme, B. (2019). “Effect of Biocompatible Esters and Alcohols as Cosurfactants on Structure and Solubilization Behavior of the Zwitterionic Surfactant Tetradecyldimethylamine Oxide.” *Ind. Eng. Chem. Res*, 58(7), 2596–2605.

Greenspan, F. P., and Gall, R. J. (1953). “Epoxy fatty acid ester plasticizers.” *Ind. Eng. Chem. Chem. Eng.*, 45(12), 2722–2726.

Grunskaya, E. P., Badovskaya, L. A., Poskonin, V. V., and Yakuba, Y. F. (1998). “Catalytic oxidation of furan and hydrofuran compounds. 4. Oxidation of furfural by hydrogen peroxide in the presence of sodium molybdate.” *Chem. Heterocycl. Compd.*, 34(7), 775–780.

Han, X.-X., Chen, K.-K., Yan, W., Hung, C.-T., Liu, L.-L., Wu, P.-H., Lin, K.-C., and Liu, S.-B. (2016). "Amino acid-functionalized heteropolyacids as efficient and recyclable catalysts for esterification of palmitic acid to biodiesel." *Fuel*, 165, 115–122.

Hanif, M. A., Nisar, S., and Rashid, U. (2017). "Supported solid and heteropoly acid catalysts for production of biodiesel." *Catal. Rev.*, 59(2), 165–188.

Hashem, A., and Kleinpeter, E. (2001). "The chemistry of 2 (5H)-furanones." *Adv. Heterocycl. Chem.*, 81, 107–166.

Hasik, M., Turek, W., Stochmal, E., Lapkowski, M., and Pron, A. (1994). "Conjugated polymer-supported catalysts-polyaniline protonated with 12-tungstophosphoric acid." *J. Catal.*, 147(2), 544–551.

He, L., Qin, S., Chang, T., Sun, Y., and Gao, X. (2013). "Biodiesel synthesis from the esterification of free fatty acids and alcohol catalyzed by long-chain Brønsted acid ionic liquid." *Catal. Sci. Technol.*, 3(4), 1102–1107.

Heravi, M. M., Vazin Fard, M., and Faghihi, Z. (2013). "Heteropoly acids-catalyzed organic reactions in water: doubly green reactions." *Green Chem. Lett. Rev.*, 6(4), 282–300.

Herrmann, S., Margraf, J. T., Clark, T., and Streb, C. (2015). "Thermochromic and solvatochromic properties of Lindqvist polyoxometalates." *Chem. Commun.*, 51(71), 13702–13705.

Horvath, I. T., and Anastas, P. T. (2007). *Innovations and green chemistry*. ACS Publications.

Hosney, H., Nadiem, B., Ashour, I., Mustafa, I., and El-Shibiny, A. (2018). "Epoxidized vegetable oil and bio-based materials as PVC plasticizer." *J. Appl. Polym. Sci.*, 135(20), 46270.

Huber, G. W., Iborra, S., and Corma, A. (2006). "Synthesis of transportation fuels from biomass: chemistry, catalysts, and engineering." *Chem. Rev.*, 106(9), 4044–4098.

Jin, Y., Shi, J., Zhang, F., Zhong, Y., and Zhu, W. (2014). "Synthesis of sulfonic acid-functionalized MIL-101 for acetalization of aldehydes with diols." *J. Mol. Catal. A: Chem.*, 383, 167–171.

Júnior, O. da S. L., Cavalcanti, R. M., Matos, T. M. de, Angélica, R. S., Rocha Filho, G. N. da, and Barros, I. de C. L. (2013). "Esterification of oleic acid using 12-tungstophosphoric supported in flint kaolin of the Amazonia." *Fuel*, 108, 604–611.

Kato, C. N., Hayashi, K., Negishi, S., and Nomiya, K. (2007). "A novel Ti–O–Ti bonding species constructed in a metal-oxide cluster [{Ti (OH2)(ox)} 2 (μ-O)(α-PW11O39)] 5− as a precatalyst: Epoxidation of alkenes with hydrogen peroxide." *J. Mol. Catal. A: Chem.*, 262(1–2), 25–29.

Katsoulis, D. E. (1998). "A survey of applications of polyoxometalates." *Chem. Rev.*, 98(1), 359–388.

Keggin, J. F. (1933). "Structure of the molecule of 12-phosphotungstic acid." *Nature*, 131(3321), 908.

Keggin, J. F. (1934). "The structure and formula of 12-phosphotungstic acid." *Proceedings of the Royal Society of London. Series A, Containing Papers of a Mathematical and Physical Character*, 144(851), 75–100.

Keshavarz, M., Iravani, N., and Parhami, A. (2019). "Novel SO3H-functionalized polyoxometalate-based ionic liquids as highly efficient catalysts for esterification reaction." *J. Mol. Struct.*, 1189, 272–278.

Knothe, G., and Steidley, K. R. (2011). "Fatty acid alkyl esters as solvents: evaluation of the kauri-butanol value. Comparison to hydrocarbons, dimethyl diesters, and other oxygenates." *Ind. Eng. Chem. Res*, 50(7), 4177–4182.

Kochhar, K. S., Bal, B. S., Deshpande, R. P., Rajadhyaksha, S. N., and Pinnick, H. W. (1983). "Protecting groups in organic synthesis. Part 8. Conversion of aldehydes into geminal diacetates." *J. Org. Chem.*, 48(10), 1765–1767.

Kotwal, M., Kumar, A., and Darbha, S. (2013). "Three-dimensional, mesoporous titanosilicates as catalysts for producing biodiesel and biolubricants." *J. Mol. Catal. A: Chem.*, 377, 65–73.

Kozhevnikov, I. V. (1998). "Catalysis by heteropoly acids and multicomponent polyoxometalates in liquid-phase reactions." *Chem. Rev.*, 98(1), 171–198.

Krystof, M., Pérez-Sánchez, M., and Domínguez de María, P. (2013). “Lipase-Mediated Selective Oxidation of Furfural and 5-Hydroxymethylfurfural.” *ChemSusChem*, 6(5), 826–830.

Lan, J., Chen, Z., Lin, J., and Yin, G. (2014). “Catalytic aerobic oxidation of renewable furfural to maleic anhydride and furanone derivatives with their mechanistic studies.” *Green Chem.*, 16(9), 4351–4358.

Lancaster, M. (2016). *Green Chemistry 3rd Edition: An Introductory Text*. Royal society of chemistry.

Lange, J.-P., Van Der Heide, E., Buijtenen, J. van, and Price, R. (2012). “Furfural—a promising platform for lignocellulosic biofuels.” *ChemSusChem*, 5(1), 150–166.

Lee, A. F., Bennett, J. A., Manayil, J. C., & Wilson, K. (2014). "Heterogeneous catalysis for sustainable biodiesel production via esterification and transesterification." *Chem. Soc. Rev.*, 43(22), 7887-7916.

Lefebvre, F. (1992). “31 P MAS NMR study of H 3 PW 12 O 40 supported on silica: formation of ([triple bond, length half m-dash] SiOH 2+)(H 2 PW 12 O 40–).” *J. Chem. Soc., Chem. Commun.*, (10), 756–757.

Leng, Y., Jiang, P., and Wang, J. (2012). “A novel Brønsted acidic heteropolyanion-based polymeric hybrid catalyst for esterification.” *Catal. Commun.*, 25, 41–44.

Leng, Y., Wang, J., Zhu, D., Wu, Y., and Zhao, P. (2009). “Sulfonated organic heteropolyacid salts: Recyclable green solid catalysts for esterifications.” *J. Mol. Catal. A: Chem.*, 313(1–2), 1–6.

Leung, D. Y., Wu, X., and Leung, M. K. H. (2010). “A review on biodiesel production using catalyzed transesterification.” *Appl. Energy*, 87(4), 1083–1095.

Li, H., Yu, S., Liu, F., Xie, C., and Li, L. (2007). “Synthesis of dioctyl phthalate using acid functionalized ionic liquid as catalyst.” *Catal. Commun.*, 8(11), 1759–1762.

Li, R., Song, H., Wang, G., and Chen, J. (2018). “Efficient and reusable SBA-15-immobilized Brønsted acidic ionic liquid for the ketalization of cyclohexanone with glycol.” *RSC Adv.*, 8(13), 7179–7185.

Li, X., Eli, W., and Li, G. (2008). “Solvent-free synthesis of benzoic esters and benzyl esters in novel Brønsted acidic ionic liquids under microwave irradiation.” *Catal. Commun.*, 9(13), 2264–2268.

Li, X., Lan, X., and Wang, T. (2016). “Selective oxidation of furfural in a bi-phasic system with homogeneous acid catalyst.” *Catal. Today*, 276, 97–104.

Lin, C.-Y., and Lin, Y.-W. (2012). “Fuel characteristics of biodiesel produced from a high-acid oil from soybean soapstock by supercritical-methanol transesterification.” *Energies*, 5(7), 2370–2380.

Lotero, E., Liu, Y., Lopez, D. E., Suwannakarn, K., Bruce, D. A., and Goodwin, J. G. (2005). “Synthesis of biodiesel via acid catalysis.” *Ind. Eng. Chem. Res*, 44(14), 5353–5363.

Mäki-Arvela, P., Kubickova, I., Snåre, M., Eränen, K., and Murzin, D. Y. (2007). “Catalytic deoxygenation of fatty acids and their derivatives.” *Energy & Fuels*, 21(1), 30–41.

Mamman, A. S., Lee, J.-M., Kim, Y.-C., Hwang, I. T., Park, N.-J., Hwang, Y. K., Chang, J.-S., and Hwang, J.-S. (2008). “Furfural: Hemicellulose/xylosederived biochemical.” *Biofuels, Bioproducts and Biorefining: Innovation for a sustainable economy*, 2(5), 438–454.

Marchetti, J. M., and Errazu, A. F. (2008). “Esterification of free fatty acids using sulfuric acid as catalyst in the presence of triglycerides.” *Biomass and Bioenergy*, 32(9), 892–895.

Marignac, C. (1862). “CR Acad. SC& 55 (1862) 888.” *Ann. Chim*, 25, 362.

Marino, D., Gallegos, N. G., Bengoa, J. F., Alvarez, A. M., Cagnoli, M. V., Casuscelli, S. G., Herrero, E. R., and Marchetti, S. G. (2008). “Ti-MCM-41 catalysts prepared by post-synthesis methods: Limonene epoxidation with H2O2.” *Catal. Today*, 133, 632–638.

Massart, R., Contant, R., Fruchart, J. M., Ciabrini, J. P., and Fournier, M. (1977). “Phosphorus-31 NMR studies on molybdic and tungstic heteropolyanions. Correlation between structure and chemical shift.” *Inorg. Chem.*, 16(11), 2916–2921.

Meffert, A. (1984). “Technical uses of fatty acid esters.” *J Am Oil Chem Soc.*, 61(2), 255–258.

Meher, L. C., Sagar, D. V., and Naik, S. N. (2006). “Technical aspects of biodiesel production by transesterification—a review.” *Renewable Sustainable Energy Rev.*, 10(3), 248–268.

Mioč, U. B., Dimitrijević, R., Davidović, M., Nedić, Z. P., Mitrović, M. M., and Colomban, P. H. (1994). “Thermally induced phase transformations of 12-tungstophosphoric acid 29-hydrate: synthesis and characterization of PW 8 O 26-type bronzes.” *J. Mater. Sci.*, 29(14), 3705–3718.

Miyake, T., Makino, T., Taniguchi, S., Watanuki, H., Niki, T., Shimizu, S., Kojima, Y., and Sano, M. (2009). “Alcohol synthesis by hydrogenation of fatty acid methyl esters on supported Ru–Sn and Rh–Sn catalysts.” *Appl. Catal., A*, 364(1–2), 108–112.

Mizuno, N., and Misono, M. (1998). “Heterogeneous catalysis.” *Chem. Rev.*, 98(1), 199–218.

Okuhara, T., Mizuno, N., and Misono, M. (2001). “Catalysis by heteropoly compounds—recent developments.” *Appl. Catal., A*, 222(1–2), 63–77.

Oliveira, C. F., Dezaneti, L. M., Garcia, F. A., Macedo, J. L. de, Dias, J. A., Dias, S. C., and Alvim, K. S. (2010). “Esterification of oleic acid with ethanol by 12-tungstophosphoric acid supported on zirconia.” *Appl. Catal., A*, 372(2), 153–161.

Olmo, A. del, Calzada, J., and Nuñez, M. (2017). “Benzoic acid and its derivatives as naturally occurring compounds in foods and as additives: Uses, exposure, and controversy.” *Crit. Rev. Food Sci. Nutr.*, 57(14), 3084–3103.

Onkarappa, S. B., Javoor, M., Mal, S. S., and Dutta, S. (2019). “Efficient and Scalable Production of Alkyl Levulinates from Cellulose-Derived Levulinic Acid Using Heteropolyacid Catalysts.” *ChemistrySelect*, 4(8), 2501–2504.

Otera, J., and Nishikido, J. (2009). *Esterification: methods, reactions, and applications*. John Wiley & Sons.

Othman, I., Mohamed, R. M., Ibrahim, I. A., and Mohamed, M. M. (2006). “Synthesis and modification of ZSM-5 with manganese and lanthanum and their effects on decolorization of indigo carmine dye.” *Appl. Catal., A*, 299, 95–102.

Park, J.-Y., Wang, Z.-M., Kim, D.-K., and Lee, J.-S. (2010). “Effects of water on the esterification of free fatty acids by acid catalysts.” *Renewable Energy*, 35(3), 614–618.

Pires, L. H., Oliveira, A. N. de, Monteiro Jr, O. V., Angélica, R. S., Costa, C. E. da, Zamian, J. R., Nascimento, L. A. do, and Rocha Filho, G. N. (2014). “Esterification of a waste produced from the palm oil industry over 12-tungstophosforic acid supported on kaolin waste and mesoporous materials.” *Appl. Catal., B*, 160, 122–128.

Polucci, P., Magnaghi, P., Angiolini, M., Asa, D., Avanzi, N., Badari, A., Bertrand, J., Casale, E., Cauteruccio, S., and Cirla, A. (2013). “Alkylsulfanyl-1, 2, 4-triazoles, a new class of allosteric valosine containing protein inhibitors. Synthesis and structure–activity relationships.” *J. Med. Chem.*, 56(2), 437–450.

Poskonin, V. V. (2009). “Catalytic oxidation reactions of furan and hydrofuran compounds 9.* characteristics and synthetic possibilities of the reaction of furan with aqueous hydrogen peroxide in the presence of compounds of niobium (ii) and (v).” *Chem. Heterocycl. Compd.*, 45(10), 1177–1183.

Putluru, S. S. R., Jensen, A. D., Riisager, A., & Fehrmann, R. (2011). "Heteropoly acid promoted V 2 O 5/TiO 2 catalysts for NO abatement with ammonia in alkali containing flue gases." *Catal. Sci. Technol.*, 1(4), 631-637.

Rajabi, F., Abdollahi, M., and Luque, R. (2016). “Solvent-free esterification of carboxylic acids using supported iron oxide nanoparticles as an efficient and recoverable catalyst.” *Materials*, 9(7), 557.

Reddy, P. S., Sudarsanam, P., Mallesham, B., Raju, G., and Reddy, B. M. (2011). “Acetalisation of glycerol with acetone over zirconia and promoted zirconia catalysts under mild reaction conditions.” *J. Ind. Eng. Chem.*, 17(3), 377–381.

Ren, Y., Liu, B., Zhang, Z., and Lin, J. (2015). “Silver-exchanged heteropolyacid catalyst (Ag1H2PW): An efficient heterogeneous catalyst for the synthesis of 5-

ethoxymethylfurfural from 5-hydroxymethylfurfural and fructose." *J. Ind. Eng. Chem.*, 21, 1127–1131.

Ren, Y., Yue, B., Gu, M., and He, H. (2010). "Progress of the application of mesoporous silica-supported heteropolyacids in heterogeneous catalysis and preparation of nanostructured metal oxides." *Materials*, 3(2), 764–785.

Rezende, M. J., and Pinto, A. C. (2016). "Esterification of fatty acids using acid-activated Brazilian smectite natural clay as a catalyst." *Renewable energy*, 92, 171–177.

Rieke, R. D., Thakur, D. S., Roberts, B. D., and White, G. T. (1997). "Fatty methyl ester hydrogenation to fatty alcohol part II: process issues." *J Am Oil Chem Soc*, 74(4), 341–345.

Sadaf, S., Iqbal, J., Ullah, I., Bhatti, H. N., Nouren, S., Nisar, J., and Iqbal, M. (2018). "Biodiesel production from waste cooking oil: an efficient technique to convert waste into biodiesel." *SUSTAIN CITIES SOC.*, 41, 220–226.

Santillan-Jimenez, E., Morgan, T., Lacny, J., Mohapatra, S., and Crocker, M. (2013). "Catalytic deoxygenation of triglycerides and fatty acids to hydrocarbons over carbon-supported nickel." *Fuel*, 103, 1010–1017.

Serrano-Ruiz, J. C., Campelo, J. M., Francavilla, M., Romero, A. A., Luque, R., Menendez-Vazquez, C., García, A. B., and García-Suárez, E. J. (2012). "Efficient microwave-assisted production of furfural from C 5 sugars in aqueous media catalysed by Brönsted acidic ionic liquids." *Catal. Sci. Technol.*, 2(9), 1828–1832.

Serrano-Ruiz, J. C., West, R. M., and Dumesic, J. A. (2010). "Catalytic conversion of renewable biomass resources to fuels and chemicals." *Annu. Rev. Chem. Biomol. Eng*, 1, 79–100.

Srikrishna, A., and Viswajanani, R. (1995). "A mild and simple procedure for the reductive cleavage of acetals and ketals." *Tetrahedron*, 51(11), 3339–3344.

Srilakshmi, C., Lingaiah, N., Suryanarayana, I., Prasad, P. S., Ramesh, K., Anderson, B. G., and Niemantsverdriet, J. W. (2005). "In situ synthesis of ammonium salt of 12-molybdophosphoric acid on iron phosphate and the ammoxidation functionality of the

catalyst in the transformation of 2-methylpyrazine to 2-cyanopyrazine." *Appl. Catal., A*, 296(1), 54–62.

Srilatha, K., Issariyakul, T., Lingaiah, N., Sai Prasad, P. S., Kozinski, J., and Dalai, A. K. (2010). "Efficient esterification and transesterification of used cooking oil using 12-tungstophosphoric acid (TPA)/Nb2O5 catalyst." *Energy & Fuels*, 24(9), 4748–4755.

Srilatha, K., Kumar, C. R., Devi, B. P., Prasad, R. B. N., Prasad, P. S., and Lingaiah, N. (2011). "Efficient solid acid catalysts for esterification of free fatty acids with methanol for the production of biodiesel." *Catal. Sci. Technol.*, 1(4), 662–668.

Struve, H. (1854). "Ueber verschiedene Doppelsalze der Molybdänsäure und Wolframsäure." *J. prakt. Chem.*, 61(1), 449–470.

Sun, H.-B., Hua, R., and Yin, Y. (2006). "ZrOCl2· 8H2O: An efficient, cheap and reusable catalyst for the esterification of acrylic acid and other carboxylic acids with equimolar amounts of alcohols." *Molecules*, 11(4), 263–271.

Sun, Z., Duan, X., Zhao, J., Wang, X., and Jiang, Z. (2015). "Homogeneous borotungstic acid and heterogeneous micellar borotungstic acid catalysts for biodiesel production by esterification of free fatty acid." *Biomass and Bioenergy*, 76, 31–42.

Talebian-Kiakalaieh, A., Amin, N. A. S., and Mazaheri, H. (2013). "A review on novel processes of biodiesel production from waste cooking oil." *Appl. Energy*, 104, 683–710.

Thiruvengadaravi, K. V., Nandagopal, J., Baskaralingam, P., Bala, V. S. S., and Sivanesan, S. (2012). "Acid-catalyzed esterification of karanja (Pongamia pinnata) oil with high free fatty acids for biodiesel production." *Fuel*, 98, 1–4.

Timofeeva, M. N. (2003). "Acid catalysis by heteropoly acids." *Appl. Catal., A*, 256(1–2), 19–35.

Tropecêlo, A. I., Casimiro, M. H., Fonseca, I. M., Ramos, A. M., Vital, J., and Castanheiro, J. E. (2010). "Esterification of free fatty acids to biodiesel over heteropolyacids immobilized on mesoporous silica." *Appl. Catal., A*, 390(1–2), 183–189.

Tsigdinos, G. A. (1978). "Heteropoly compounds of molybdenum and tungsten." *TOPICS CURR CHEM*, 1–64.

Vieira, S. S., Magriotis, Z. M., Santos, N. A., Saczk, A. A., Hori, C. E., and Arroyo, P. A. (2013). “Biodiesel production by free fatty acid esterification using lanthanum (La3+) and HZSM-5 based catalysts.” *Bioresour. Technol.*, 133, 248–255.

Wang, H., Liu, L., and Gong, S. (2017). “Esterification of oleic acid to biodiesel over a 12-phosphotungstic acid-based solid catalyst.” *Journal of Fuel Chemistry and Technology*, 45(3), 303–310.

Wang, S.-S., and Yang, G.-Y. (2015). “Recent advances in polyoxometalate-catalyzed reactions.” *Chem. Rev.*, 115(11), 4893–4962.

Wang, Y., Zhao, D., Chen, G., Liu, S., Ji, N., Ding, H., and Fu, J. (2019). “Preparation of phosphotungstic acid based poly (ionic liquid) and its application to esterification of palmitic acid.” *Renewable energy*, 133, 317–324.

Wang, Y., Zhao, D., Wang, L., Wang, X., Li, L., Xing, Z., Ji, N., Liu, S., and Ding, H. (2018). “Immobilized phosphotungstic acid based ionic liquid: Application for heterogeneous esterification of palmitic acid.” *Fuel*, 216, 364–370.

Wilson, W. C., (1926). " 2-Furancarboxylic acid and 2-Furylcarbinol" *Org. Synth.*, 6, 44.

Won, J.-E., Kim, H.-K., Kim, J.-J., Yim, H.-S., Kim, M.-J., Kang, S.-B., Chung, H.-A., Lee, S.-G., and Yoon, Y.-J. (2007). “Effective esterification of carboxylic acids using (6-oxo-6H-pyridazin-1-yl) phosphoric acid diethyl ester as novel coupling agents.” *Tetrahedron*, 63(51), 12720–12730.

Xie, T., Zeng, C., Wang, C., and Zhang, L. (2013). “Preparation of methyl ester sulfonates based on sulfonation in a falling film microreactor from hydrogenated palm oil methyl esters with gaseous SO3.” *Ind. Eng. Chem. Res.*, 52(10), 3714–3722.

Xue, J., Zeng, Z., Xue, W., and Yang, H. (2018). “Kinetics of esterification of benzoic acid and isoamyl alcohol catalyzed by P-toluenesulphonic acid.” *CAN J CHEM ENG.*, 96(11), 2443–2449.

Yadav, J. S., Reddy, B. S., Srinivas, R., and Ramalingam, T. (2000). “Silica gel-supported metallic sulfates catalyzed chemoselective acetalization of aldehydes under microwave irradiation.” *Synlett*, 2000(05), 0701–0703.

Yi, H., Niu, L., Wang, S., Liu, T., Singh, A. K., and Lei, A. (2016). "Visible-Light-Induced Acetalization of Aldehydes with Alcohols." *Org. Lett.*, 19(1), 122–125.

Yu, W.-Y., and Alper, H. (1997). "Palladium-Catalyzed Cyclocarbonylation of Terminal and Internal Alkynols to 2 (5 H)-Furanones." *J. Org. Chem.*, 62(17), 5684–5687.

Zhang, D., Zhang, X., Li, Y., Wang, S., Wang, X., and Jiang, Z. (2018). "Incorporation of Ce3+ ions into dodecatungstophosphoric acid for the production of biodiesel from waste cooking oil." *Mater. Sci. Eng., C*, 92, 922–931.

Zhang, F., Shi, J., Jin, Y., Fu, Y., Zhong, Y., and Zhu, W. (2015). "Facile synthesis of MIL-100 (Fe) under HF-free conditions and its application in the acetalization of aldehydes with diols." *Chem. Eng. J.*, 259, 183–190.

Zhang, J., Bao, S., and Yang, J. (2009). "Synthesis of a novel multi-SO 3 H functionalized strong Brønsted acidic ionic liquid and its catalytic activities for acetalization." *Chin. Sci. Bull.*, 54(21), 3958–3964.

Zhang, J., Cai, D., Wang, S., Tang, Y., Zhang, Z., Liu, Y., and Gao, X. (2014). "Efficient method for the synthesis of fatty acid amide from soybean oil methyl ester catalysed by modified CaO." *CAN J CHEM ENG*, 92(5), 871–875.

Zhang, Q., Wei, F., Li, Q., Huang, J., Feng, Y., and Zhang, Y. (2017). "Mesoporous Ag1 (NH4) 2PW12O40 heteropolyacids as effective catalysts for the esterification of oleic acid to biodiesel." *RSC Adv.*, 7(81), 51090–51095.

Zhang, W.-H., Liu, S.-S., Liu, P., Xu, J., Xue, B., Wei, X.-Y., and Li, Y.-X. (2016a). "Chitosan grafted with a heteropolyanion-based ionic liquid as an effective and reusable catalyst for acetalization." *RSC Adv.*, 6(47), 41404–41409.

Zhang, X., Zhang, D., Sun, Z., Xue, L., Wang, X., and Jiang, Z. (2016b). "Highly efficient preparation of HMF from cellulose using temperature-responsive heteropolyacid catalysts in cascade reaction." *Appl. Catal., B*, 196, 50–56.

Zhang, Z., Song, J., and Han, B. (2016c). "Catalytic transformation of lignocellulose into chemicals and fuel products in ionic liquids." *Chem. Rev.*, 117(10), 6834–6880.

Zhao, J., Guan, H., Shi, W., Cheng, M., Wang, X., and Li, S. (2012). “A Brønsted–Lewis-surfactant-combined heteropolyacid as an environmental benign catalyst for esterification reaction.” *Catal. Commun.*, 20, 103–106.

Zhou, C.-H., Xia, X., Lin, C.-X., Tong, D.-S., and Beltramini, J. (2011). “Catalytic conversion of lignocellulosic biomass to fine chemicals and fuels.” *Chem. Soc. Rev.*, 40(11), 5588–5617.

Zhou, Y., Bao, R., Yue, B., Gu, M., Pei, S., and He, H. (2007). “Synthesis, characterization and catalytic application of SBA-15 immobilized rare earth metal sandwiched polyoxometalates.” *J. Mol. Catal. A: Chem.*, 270(1–2), 50–55.

PUBLICATIONS

Paper published/communicated in international journals

1. **Ritesh Tiwari,** Sib Sankar Mal, and Saikat Dutta (2019). A Scalable and High-Yielding Synthesis of 2-(2-Furyl)-1,3-dioxolane from Biomass Derived Furfural and Ethylene Glycol Using Heteropoly Acids as Green Catalyst. Asian Journal of Chemistry, Vol. 31(7)/pp 1599-1602.
2. **Tiwari, R.,** Rahman, A., Bhat, N. S., Onkarappa, S. B., Mal, S. S., & Dutta, S. (2019). Efficient Preparation of Alkyl Benzoates by Heteropolyacid-Catalysed Esterification of Benzoic Acid under Solvent-Free Condition. ChemistrySelect, 4(31), 9119-9123.
3. Sharath, B. O., **Tiwari, R.,** Mal, S. S., & Dutta, S. (2019). Straightforward synthesis of calcium levulinate from biomass-derived levulinic acid and calcium carbonate in egg-shells. Materials Today: Proceedings, 17, 77-84.
4. Nivedha Vinod, **Ritesh Tiwari**, Navya Subray Bhat, Sib Sankar Mal, and Saikat Dutta (2020). High-yielding Synthesis of Alkyl Stearates from Stearic Acid within a Closed Batch Reactor using Heteropolyacids as Efficient and Recyclable Catalyst. AIP Conference Proceedings 2225, 070004-1-70004-6.
5. **Ritesh Tiwari**, Sib Sankar Mal, and Saikat Dutta. A green and efficient catalyst for the synthesis of Alkyl 2-furoates from biomass-derived furoic acid under solvent-free condition. **(Manuscript under preparation).**

LIST OF CONFERECES AND WORKSHOPS ATTENDED

1. **Best oral presentation award** for the paper titled "Oxidation of biomass-derived furfural to 2-furanone by using heteropolyacids supported molecular sieves" presented at International conference on Energy and Enviromental Technologies for Sustainable Development (Chem-Conflux20) at the Department of Chemical Engineering, Motilal Nehru Institute of Technology Allahabad, Prayagraj, Uttar Pradesh (14^{th}-16^{th} February, 2020).

2. Presented a poster on a research paper titled “Preparation of Alkyl 2-Furoates from Biomass-Derived 2-Furoic Acid using Heteropolyacids as Green Catalyst” at the international conference on Emerging Frontiers in Chemical Sciences at the Department of Chemistry, Farook college, Kozhikode, Kerla (13-15 December, 2019).
3. Presented a poster on a research paper titled “Oxidation of Bio-mass derived 5-Chloromethylfurfural (CMF) to 2,5-Diformylfuran (DFF)” at the international conference on Emerging Trends in Chemical Sciences at the Department of Chemistry, Manipal Institute of Technology, Manipal (14-16 September, 2017).
4. Attended a two day workshop on “High resolution transmission electron microscopy and scanning probe microscopy” at PSG College of Technology, Coimbatore (23-24 November, 2017).
5. Attended a two-day workshop on “Nuclear Magnetic Resonance Spectroscopy (WNMRS-2019)” at The Gandhigram Rural Institute, Coimbatore (22-23 March, 2019).

CIRCULULUM VITE

Present Address

Ritesh Tiwari
Department of Chemistry
National Institute of Technology Karnataka
Surathakal, Mangalore-575025
India
Phone: +91-7409236019
E-mail: riteshnitk.india@gmail.com
riteshcheme@gmail.com

Permanent Address

Ritesh Tiwari
S/O Late Shri D.P.Tiwari
H. No.18,Village Gurgaon
Post MajhaonThana Chhapiya
District: Gonda (U.P.)-271305
India

Research Experience:

July 2016-present

Ph.D. Research Scholar
Department of Chemistry, NITK-Surathkal
Research area: Synthesis of catalyst and Characterization, Biomass conversion into chemical & fuels

April 2012-February 2015

Senior Research Scholar (S.R.F.)
Department of Chemistry, UPES-Dehradun
Research area: Synthesis of catalyst and Characterization, Catalytic conversion of CO_2 into chemical

February 2010-March 2012

Project Assistant (P.A.)
Catalytic Conversion & Process Division (C.C.P.D), C.S.I.R-IIP-Dehradun, Uttarakhand-248001
Research area: Synthesis of metal oxide catalyst and Characterization and its catalytic application in various reactions

Education

July 2016-present	**Ph.D. Research Scholar** Department of Chemistry, NITK-Surathakal Title: Application of polyoxometalates as efficient and green catalyst for catalytic upgrading of cellulosic biomass Supervisor: Dr. Sib Sankar Mal (Guide)
July 2006-June 2008	**M.Sc. (Chemistry)** Department of Chemistry D.A.V. College, Civil Lines Chatrapati Sahu Ji Maharaj University (C.S.J.M.U.), Kanpur, Uttar Pradesh (U.P.)

List of Publications:

1) **Ritesh Tiwari,** Sib Sankar Mal, and Saikat Dutta (2019). A Scalable and High-Yielding Synthesis of 2-(2-Furyl)-1, 3-dioxolane from Biomass Derived Furfural and Ethylene Glycol Using Heteropoly Acids as Green Catalyst. Asian Journal of Chemistry, Vol. 31(7)/pp 1599-1602.
2) **Tiwari, R.,** Rahman, A., Bhat, N. S., Onkarappa, S. B., Mal, S. S., & Dutta, S. (2019). Efficient Preparation of Alkyl Benzoates by Heteropolyacid-Catalysed

Esterification of Benzoic Acid under Solvent-Free Condition. ChemistrySelect, 4(31), 9119-9123.

3) Sharath, B. O., **Tiwari, R.,** Mal, S. S., & Dutta, S. (2019). Straightforward synthesis of calcium levulinate from biomass-derived levulinic acid and calcium carbonate in egg-shells. Materials Today: Proceedings, 17, 77-84.
4) Nivedha Vinod, **Ritesh Tiwari**, Navya Subray Bhat, Sib Sankar Mal, and Saikat Dutta (2020). High-yielding Synthesis of Alkyl Stearates from Stearic Acid within a Closed Batch Reactor using Heteropolyacids as Efficient and Recyclable Catalyst. AIP Conference Proceedings 2225, 070004-1-70004-6.